Proceedings of the workshop

MPI@LHC 2015

The Abdus Salam International Center for Theoretical Physics
ICTP
Trieste, Italy

Editors:
Hannes Jung (DESY)
Daniele Treleani (University of Trieste and INFN)
Mark Strikman (Penn State University)
Nadia van Buuren (ICTP)

April 2016
DESY-PROC-2016-01
ISBN 978-3-945931-01-1
ISSN 1435-8077

Organizing Committee:

Hannes Jung (DESY),
Daniele Treleani (University of Trieste and INFN),
Mark Strikmann (Penn State University),
Nadia van Buuren (ICTP)

Working groups and conveners:

Minimum bias and Underlying event:
Thorsten Kuhl (ATLAS) & Anastasia Grebenyuk (CMS)

Monte Carlo development and tuning:
Andrzej Siódmok (HERWIG) & Tanguy Pierog (EPOS)

Double parton scattering:
Jonathan Gaunt (Theory) & Paolo Gunnellini (CMS)

MPI & small x & diffraction:
Francesco Hautmann (Theory) & Oldrich Kepka (ATLAS)

High multiplicities and interactions with nuclei:
Paolo Bartalini (ALICE) & Boris Blok (Theory)

Advisory Committee:

Paolo Bartalini (China Central Normal University)
Jonathan Butterworth (UC London)
Markus Diehl (DESY)
Livio Fano (University of Perugia, INFN)
Richard Field (University of Florida)
Hannes Jung (DESY, University of Antwerp)
Judith Katzy (DESY)
Frank Krauss (IPPP Durham)
Krzysztof Kutak (IFJ PAN Krakw)
Arthur Moraes (Centro Brasileiro de Pesquisas Fsicas)
Andreas Morsch (CERN)
Giulia Pancheri (INFN Frascati Nat. Lab.)
Michael Schmelling (MPIK Heidelberg)
Torbjörn Sjöstrand (Lund University)
Peter Skands (CERN, Monash University)
Mark Strikman (Pennsylvania State University)
Antoni Szczurek (IFJ PAN Krakw)
Daniele Treleani (University of Trieste, INFN)
Pierre van Mechelen (University of Antwerp)
Nick van Remortel (University of Antwerp)

Supported by:

The Abdus Salam International Center for Theoretical Physics
ICTP, Trieste, Italy

Preface

The workshop *MPI@LHC 2015* was held in a very nice and inspiring atmosphere of the Abdus Salam Institute for Theoretical Physics in Trieste from 23 - 27 November 2015 at Miramare, Trieste, Italy. This workshop was the 7th workshop in a series of workshops on Multiparton Interactions (MPI) which started already in 2006 at DESY [1] and then continues as the MPI@LHC workshops with a kickoff meeting in 2008 in Perugia [2], Italy, and continued with workshops in Glasgow [3] in 2010, DESY [4] in 2011, CERN [6] and Tel Aviv [5] in 2012, in Antwerp [7] in 2013 and in Cracow [8] in 2014.
From the start of the experimental activity of the Large Hadron Collider, Multiple Partonic Interactions (MPI) are experiencing a growing popularity and are widely invoked to account for observations that cannot be explained otherwise. This includes associated hadron production (Underlying Event) in high energy hadronic collisions with jets, the rates for multiple heavy flavor production, the survival probability of large rapidity gaps in hard diffraction, etc. In particular in recent years Double Parton Interactions were observed directly and studied by a number of the FNAL and LHC experiments in different reaction channels.
At the LHC a new QCD regime has now been reached, where MPIs occur with high rates, in particular in central collisions, which give dominant contribution to production of new particles Understanding MPIs is therefore crucial, both for their significant contribution to the background of various processes of interest for the search of new physics and because MPIs are an interesting topic of research by itself, allowing to probe high energy - high density QCD dynamics and, as a consequence of the geometrical characteristics of the interaction, to obtain unprecedented information on the correlated structure of the QCD bound states.
The aim of this workshop is to provide an updated view of MPI studies, both experimental and theoretical, and to foster contacts between theoretical and experimental communities active in the field.
The workshop held in Trieste in 2015 was a special workshop in the sense that many investigations and analyses from LHC run1 were still finalized, presented and compared to model calculations and at the same time the very new first measurements from run2 at the highest center of mass energy of pp collisions of $\sqrt{s} = 13$ TeV were presented.

Daniele Treleani, Hannes Jung, Mark Strikman

MPI workshops

[1] MPI, DESY - Hamburg, 2006, https://www.desy.de/~jung/multiple-interactions/

[2] MPI@LHC, Perugia, 2008 http://www.pg.infn.it/mpi08/
Proceedings: http://inspirehep.net/record/849580?ln=en

[3] MPI@LHC, Glasgow, 2010, http://www.mpi2010.physics.gla.ac.uk/Home.html

[4] MPI@LHC, DESY - Hamburg, 2006 https://indico.desy.de/conferenceDisplay.py?ovw=True&confId=4176
http://www-library.desy.de/preparch/desy/proc/proc12-03.html

[5] Multi partonic interactions at LHC, Tel Aviv, 2012, https://indico.cern.ch/event/194359/

[6] MPI@LHC, CERN - Geneva, 2012, https://indico.cern.ch/event/184925/
http://inspirehep.net/record/1239662?ln=en

[7] MPI@LHC, Antwerp, 2013, https://indico.cern.ch/event/231843/?ovw=True
http://arxiv.org/abs/arXiv:1410.6664

[8] MPI@LHC, Cracow, 2013 https://indico.cern.ch/event/305160/page/0
http://inspirehep.net/record/1377199/

The Abdus Salam International Centre for Theoretical Physics
www.ictp.it

The Abdus Salam International Centre for Theoretical Physics (ICTP), in collaboration with the Italian Institute for Nuclear Physics (INFN), will hold the

7th International Workshop on Multiple Partonic Interactions at the LHC

23 - 27 November 2015

Miramare, Trieste, Italy

From the start of the experimental activity of the Large Hadron Collider, Multiple Partonic Interactions (MPI) are experiencing a growing popularity and are widely invoked to account for observations that cannot be explained otherwise. This includes associated hadron production (Underlying Event) in high energy hadronic collisions with jets, the rates for multiple heavy flavor production, the survival probability of large rapidity gaps in hard diffraction, etc. In particular Double Parton Interactions were observed directly and studied by a number of the FNAL and LHC experiments in different reaction channels.

At the LHC a new QCD regime has now been reached, where MPIs occur with high rates, in particular in central collisions, where the production of new particles is more likely to take place. Understanding MPIs is therefore crucial, both for their significant contribution to the background of various processes of interest for the search of new physics and because MPIs are an interesting topic of research by itself, allowing to probe high energy - high density QCD dynamics and, as a consequence of the geometrical characteristics of the interaction, to obtain unprecedented information on the correlated structure of the QCD bound states.

The aim of this workshop is to provide an updated view of MPI studies, both experimental and theoretical, and to foster contacts between theoretical and experimental communities active in the field.

TOPICS:

- Phenomenology of MPI processes and multiparton distributions
- Considerations for the description of MPI in QCD
- Measuring multiple partonic interactions
- Experimental results on inelastic hadronic collisions: underlying event, minimum bias, forward energy flow
- Monte Carlo development and tuning
- Connections with low x, diffraction, heavy ion physics and cosmic rays

PARTICIPATION

Scientists and students from all countries which are members of the United Nations, UNESCO or IAEA may attend the Workshop. As it will be conducted in English, participants should have an adequate working knowledge of that language.

As a rule, travel and subsistence expenses of the participants should be borne by the home institution. Every effort should be made by candidates to secure support for their fare (or at least half-fare). However, limited funds are available for some participants who are nationals of, and working in, a developing country, and who are not more than 45 years old. Such support is available only for those who attend the entire activity. There is no registration fee.

HOW TO APPLY FOR PARTICIPATION

The application form can be accessed at activity website: **http://indico.ictp.it/event/a14280**. Once in the website, comprehensive instructions will guide you step-by-step, on how to fill out and submit the application form. Please send all file attachments in Word or PDF format.

ACTIVITY SECRETARIAT:

7th International Workshop on Multiple Partonic Interactions at the LHC *(smr2732)*
the Abdus Salam International Centre for Theoretical Physics
Strada Costiera 11, 34151 Trieste, Italy.
Telephone: +39 040 2240 363 - Telefax: +39 040 2240 7363 - E-mail: smr2732@ictp.it
Activity Web Page: http://indico.ictp.it/event/a14280
ICTP Home Page: http://www.ictp.it/

September 2015

INFN Istituto Nazionale di Fisica Nucleare

ORGANIZERS:

H. Jung (DESY)
M. Strikman (Penn State U.)
D. Treleani (U. of Trieste, INFN)

INTERNATIONAL ADVISORY BOARD:

P. Bartalini (China Central Normal U.)
J. Butterworth (UC London)
M. Diehl (DESY)
L. Fanò (U. of Perugia, INFN)
R. Field (U. of Florida)
H. Jung (DESY, U. of Antwerp)
J. Katzy (DESY)
F. Krauss (IPPP Durham)
K. Kutak (IFJ PAN Kraków)
A. Moraes (CBPF Brazil)
A. Morsch (CERN)
G. Pancheri (INFN Frascati Nat. Lab.)
M. Schmelling (MPIK Heidelberg)
T. Sjöstrand (Lund U.)
P. Skands (CERN, Monash U.)
M. Strikman (Pennsylvania State U.)
A. Szczurek (IFJ PAN Kraków)
D. Treleani (U. of Trieste, INFN)
P. van Mechelen (U. of Antwerp)
N. van Remortel (U. of Antwerp)

DEADLINE
for requesting participation
~~**15 September 2015**~~
extended to
15 Ottobre 2015
only for those NOT requesting funding

Contents

Chapter 1

Working Group
Minimum bias and Underlying event

Convenors:

Thorsten Kuhl (ATLAS),
Anastasia Grebenyuk (CMS)

Minimum Bias and Underlying Event session: overview

Anastasia Grebenyuk[1] and Thorsten Kuhl[2]

[1]ULB, Bruxelles, Belgium
[2]DESY, Hamburg, Germany

The start up of the worlds highest energy particle collider, LHC, at the new colliding energy of 13 TeV in spring 2015 opened up a new era at the high energy frontier. LHC's first runs (2010-2012) provided data collected at centre-of-mass energies of 0.9, 2.76, 7 and 8 TeV. After a three-year period that has seen major advances in physics such as the discovery of the H boson in 2012 [1] the LHC was shut down for maintenance in 2013. In spring 2015 LHC restarted and started to operate at a center-of-mass energy of 13 TeV, which is almost its design energy, and expect to deliver about 30 fb^{-1} of integrated luminosity by the end of 2016, and up to 100 fb^{-1} in the end of Run 2 (end 2018). The discovery potential of CMS and ATLAS experiments relies on the level of understanding of the physics of the Standard Model (SM). The interacting constituents are gluons and quarks contained inside the protons of the beams, which only carry a small fraction of the proton momentum and described by parton density functions. Therefor most of the strong interactions between quarks and gluons contained inside the proton are at a very small energy scale, much smaller than the energy of the colliding beams, and events with high mass final state particles, like the production of a H boson, are very rare. Experimentally such soft interaction processes are selected with very inclusive triggers and are called "minimum bias".
An accurate description of these soft strong interaction processes is essential for simulating single pp interactions as well as the effects of multiple pp interactions at high instantaneous luminosity in hadron colliders. This is an important input to the high-p_T physics program in the future, were we expect up to 40 additional soft interactions accompanied the interesting hard interaction.
While every of these 40 interactions contains most time only a small number of low energetic particle, the large number accumulate to a significant number of objects in the detector and dilute properties like the isolation of leptons and the precision of the missing E_T measurement. In addition the higher energetic tail of these interactions can produce additional jets in events.
One of the basic studies to provide insight into the strong interaction in the low-scale, non-perturbative region of quantum chromodynamics (QCD), is the inclusive charged-particle measurement. Particle interactions at these energy scales are typically described by QCD-inspired models implemented in Monte Carlo (MC) event generators with free parameters that can be constrained by such measurements. The Underlying event (UE) is defined as the activity accompanying any hard scattering in a collision event and produce a similar background then the pile-up

interactions, but in the same proton-proton interaction. This includes partons not participating in a hard-scattering process (beam remnants), and additional scatters in the same pp collision, termed multiple parton interactions. Initial and final state gluon radiation also contribute to the UE activity. It is impossible to unambiguously separate the UE from the hard scattering process on an event-by-event basis. However, distributions have been measured that are sensitive to the properties of the UE and used to improve similar models then for the low-energy pp interactions. These additional components are important in very precise measurements like the top-mass measurement.

At this workshop the first results at 13 TeV on the minimum bias and underlying event from LHC were presented. ATLAS, CMS and ALICE have shown recent measurement of underlying events and particle production at the new energy regime [2–6]. To be able to cross check the results from different experiments the discussion on the synchronisation of analysis strategies were discussed [7]. Apart form LHC experiments the latest results on the underlying event by the STAR experiment at RICH were presented [8, 9]. In the forthcoming high-luminosity phase at the LHC many of the most interesting measurements for precision QCD studies are hampered by conditions of large pile-up, particularly at not very high transverse momenta. A novel data-driven approach with a main focus to deal with the presence of high-p_T jets produced from pile-up events, in a region where tracking detectors are not available to identify them was discussed [10]. In content of the phenomenology, the new development on the underlying events and flow in EPOS was reported [11]. Other topics related to the MC generators were developed in the "Monte Carlo development and tuning" session.

The status of the measurements for low-scale QCD events and the UE can be summarized in following: The comparison plots from the LHC wide working group show that the experimental results for the common phase spaces agree within the uncertainties. This shows that experimental issues seems to be understood and well under control.
The interpolation between different center-of-mass energy works. Most of the tunes developed using 7 TeV data agree similar good with data taken at a center-of-mass energy of 13 TeV. Still there are some discrepancies between the data and the model. Most tunes describe the physics best they are tuned to. Underlying event tunes are good in underlying event distributions, astropaticle generators in inclusive single particle distributions and minimum bias tunes in particle distribution for the bulk of the pile up events. There is still some room for the development of models but also for additional measurements, which are still very inclusive, but concentrate only on part of the phase space. These could resolve the situation that tuning can describe some distribution, but not all because of different correlations in the models then in the data.

References

[1] CMS Collaboration, "Observation of a new boson at a mass of 125 GeV with the CMS experiment at the LHC," *Phys. Lett.*, **B716**(2012), 30.

[2] R. Iuppa on behalf of the ATLAS Collaboration, "Charged-particle multiplicities at different pp interaction centre-of-mass energies measured with the ATLAS detector at the LHC", contribution to the workshop, http://indico.ictp.it/event/a14280/session/265/contribution/1032/material/slides/.

[3] J. Robinson on behalf of the ATLAS Collaboration, "Studies of the underlying event and particle production with the ATLAS detector", contribution to the current proceedings.

[4] W.Y. Wang on behalf of the CMS Collaboration, "Recent measurement of underlying events", contribution to the workshop, http://indico.ictp.it/event/a14280/session/265/contribution/1031/material/slides/.

[5] J.M. Grados Luyando on behalf of the CMS Collaboration, "Particle Spectra in Minimum Bias events at 8 TeV and 13 TeV", contribution to the current proceedings.

[6] P. Palni on behalf of the ALICE Collaboration, "Charged particle production in proton-proton collisions at $\sqrt{s}$ = 13 TeV, with ALICE at the LHC", contribution to the current proceedings.

[7] D. Kar, "Review of LPCC MB& UE Working Group Activities", contribution to the current proceedings.

[8] B. Page on behalf of the STAR Collaboration, "Exploring the Underlying Event and Hadronization using Di-jets at STAR", contribution to the current proceedings.

[9] G. Webb on behalf of the STAR Collaboration, "The Underlying Event at $\sqrt{s} = 500$ GeV at STAR", contribution to the current proceedings.

[10] H. Van Haevermaet, "Treating jet correlations in high pile-up at hadron colliders", contribution to the current proceedings.

[11] T. Pierog, "Underlying events and flow in EPOS 3", contribution to the current proceedings.

A data-driven approach to treat jet correlations in high pile-up at hadron colliders

H. Van Haevermaet[1]

[1]University of Antwerp

April 14, 2016

1 Introduction

Experiments at hadron colliders operating at a very high luminosity face the challenge of high pile-up conditions, which create a high probability that the final state of a particular process drowns in pile-up activity. Advanced vertex techniques have been developed to deal with this inside regions covered by tracking detectors, but outside, experiments rely on Monte Carlo simulations to model pile-up effects. This, however, introduces a significant model dependence, especially in more forward regions where currently less precise measurements are available to constrain Monte Carlo models.

We propose a novel data-driven approach with a main focus to deal with the presence of high-p_{T} jets produced from pile-up events, in a region where tracking detectors are not available to identify them. An example would be Higgs production through vector boson fusion, with associated jets produced outside tracking detector acceptances, e.g. $|\eta| > 3$. This is a different issue than what most of the existing pile-up correction methods treat, which are the jet p_{T} pedestal, due to the bias in the jet p_{T} from added pile-up particles in the jet cone, and the clustering of overlapping soft particles from multiple collisions into jets.

We will therefore use an existing method to remove the contribution of soft pile-up particles in the event, and introduce a new approach to treat the misidentification of high-p_{T} jets in regions where no track and vertex information is available. The aim is to look for a method that can restore correlations between final state particles or jets, can be used without track information, and without a Monte Carlo model. To achieve this we propose to use a minimum bias data sample recorded during high pile-up runs, and apply an event-mixing technique with this sample, to retrieve the true signal from the measured one in high pile-up. One of the features of the method is that it does not require any dedicated data-taking at low pile-up conditions, since the required data can be recorded at the same time as the signal events at high pile-up, so there is no loss in luminosity. We will illustrate this using Drell-Yan with associated jet production as a case study, and discuss the main consequences of additional pile-up collisions.

2 Drell-Yan with associated jet production at high pile-up

Consider the production of a Drell-Yan lepton pair via Z-boson exchange with an associated jet, at a centre-of-mass energy of $\sqrt{s} = 13$ TeV. We require the jet transverse momentum and rapidity to be $p_{\mathrm{T}}^{(\mathrm{jet})} > 30$ GeV, $|\eta^{(\mathrm{jet})}| < 4.5$, and the boson invariant mass and rapidity to be 60 GeV $< m^{(\mathrm{boson})} <$ 120 GeV, $|\eta^{(\mathrm{boson})}| < 2$. Event samples are generated by PYTHIA8 with the 4C tune, and jets are reconstructed with the anti-k_T algorithm with distance parameter $R = 0.5$.

Fig. 1 shows the leading jet p_{T} (left) and Drell-Yan p_{T} (right) spectra with and without pile-up. In addition a curve is present that shows the result of applying a SoftKiller (SK) [5] correction to the pile-up distributions. This method (like others [1–4]) can correct quite well for the presence of a large amount of soft pile-up particles in the event, which leads to a bias (jet pedestal) in jet p_{T} due to added pile-up particles in the jet cone or can make fake jets when these soft particles are clustered together; but it is clear that it can not treat the contribution from genuine high-p_{T} jets that come from independent pile-up events.

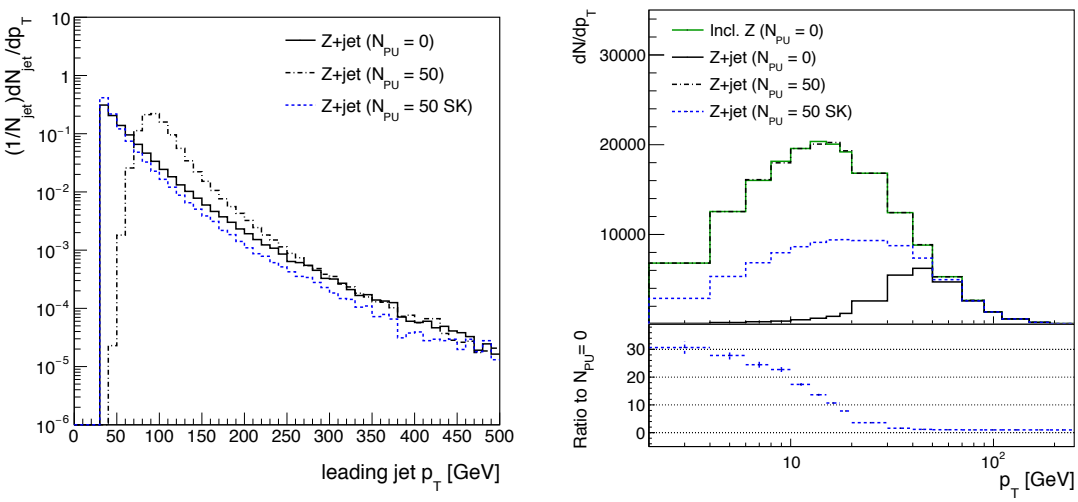

Figure 1: Application of SoftKiller [5] to Z+jet production. Left: (a) the leading jet p_{T} spectrum; right: (b) the Z-boson p_{T} spectrum.

In the higher p_{T} part of the Drell-Yan p_{T} spectrum there is no need for any correction, but at low p_{T} values significant contributions are still present from misidentified pile-up jets. These need to be properly treated, particularly in regions outside tracker acceptances where vertex information is not available.

3 Uncorrelated event samples and the jet-mixing method

To treat the remaining contributions, beyond soft particles and the jet p_{T} pedestal, we propose to apply jet mixing techniques [6–9] using uncorrelated samples. The main idea is that the signal

at high pile-up is obtained by mixing the signal without pile-up with a minimum bias sample of data at high pile-up. Thus to identify the contribution of high-p_{T} jets coming from independent pile-up events, we construct a "signal + pile-up" scenario in a data-driven way, where physics objects from pile-up background are added to the event before selection criteria are applied. The technique is designed to treat the region of high $\mathrm{N_{PU}}$, where $(\mathrm{N_{PU}}+1)/\mathrm{N_{PU}} \approx 1$.

We use the Drell-Yan + jets example to illustrate the method by taking a sample (Monte Carlo in this exercise) containing $\mathrm{N_{PU}}$ minimum bias events, apply a SoftKiller subtraction to it, and mix it with the signal at zero pile-up, to then perform the same event selection requiring a jet with $p_T^{(\mathrm{jet})} > 30$ GeV and $|\eta^{(\mathrm{jet})}| < 4.5$.

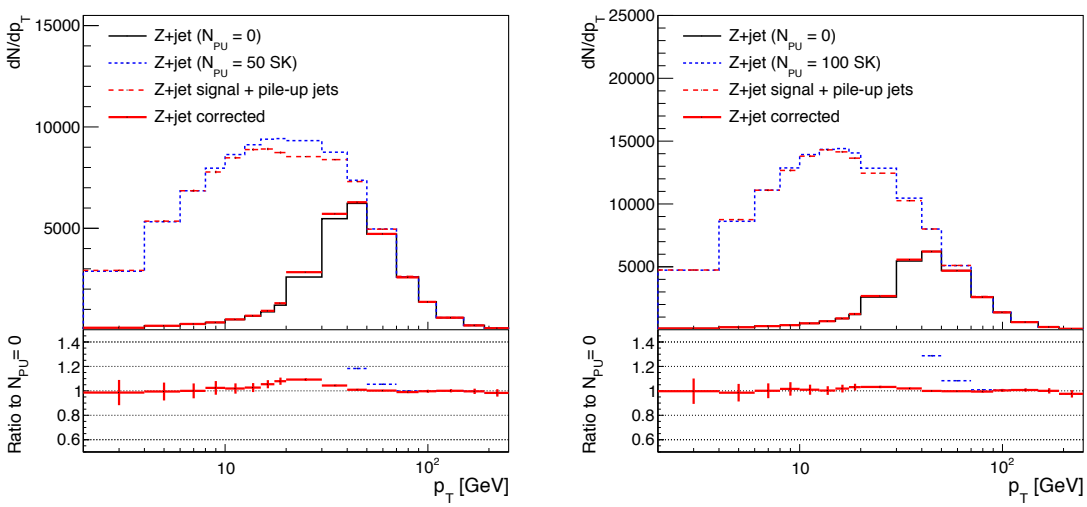

Figure 2: The Z-boson p_{T} spectrum in Z+jet production corrected with the jet-mixing method. Left: (a) $\mathrm{N_{PU}} = 50$; right: (b) $\mathrm{N_{PU}} = 100$.

The results are presented in Fig. 2 for $\mathrm{N_{PU}} = 50$ and $\mathrm{N_{PU}} = 100$. The solid black curve is the "true" Z+jet signal, the dashed blue curve is the high pile-up SoftKiller-corrected result, and the solid red curve is the high pile-up SoftKiller + jet-mixing corrected result. We regard the dashed blue curve as pseudodata in high pile-up, and the long-dashed red curve is the jet-mixed curve, obtained as described above. The result of the mixing method (solid red curve) is then obtained by an unfolding, here defined by multiplying the signal at zero pile-up by the ratio of the pseudodata (dashed blue) curve to the jet-mixed (long-dashed red) curve. Without using any Monte Carlo method, the true signal is extracted nearly perfectly from the jet-mixed sample.

In addition to the closure test shown above, we have checked the model dependence by applying the jet-mixing technique to different starting distributions, and checked the performance of the jet-mixing method as function of $\mathrm{N_{PU}}$. We also performed checks by looking at the jet resolution after the jet-mixing method is applied, and see that the features of the signal distributions at zero pile-up are well reproduced. The aforementioned results can be found in [10].

4 Conclusions

Existing methods designed to treat pile-up at the LHC can use precise vertex and track information to remove all pile-up particles and correct the jet p_{T}, but are limited to the phase space where tracking detectors are available. Hence outside this region one has to rely on Monte Carlo simulations to model pile-up effects, which can lead to significant model dependences.

We proposed a new data-driven approach to treat pile-up, which is model independent, and is able to restore final state correlations without the use of track or vertex information. In particular it is designed to correct for the misidentification of high-p_{T} jets from independent pile-up events, a contribution that is not treated in existing methods outside tracking detector regions.

The main ingredient is a minimum bias data sample recorded during high pile-up runs, which is used to construct a jet-mixing method. Using Z+jet processes as example, we demonstrated that one can successfully extract true signal distributions from the mixed sample, removing any model dependence implied by the use of Monte Carlo event generators.

It is a general technique that can be used in any measurement to restore correlations between final-state particles, and does not require special runs at low pile-up. The method thus implies good prospects both for precision Standard Model studies, and for searches for beyond Standard Model physics in high pile-up regimes.

Acknowledgements

The results in these proceedings have been obtained in collaboration with F. Hautmann and H. Jung. Many thanks to the organizers and conveners of the MPI@LHC 2015 conference for giving us the opportunity to present these studies.

References

[1] ATLAS Collaboration, ATLAS-CONF-2013-083.

[2] CMS Collaboration, CMS-PAS-JME-14-001.

[3] H. Kirschenmann [CMS Collaboration], PoS EPS-HEP2013 (2013) 433.

[4] D. Bertolini, P. Harris, M. Low and N. Tran, JHEP **1410** (2014) 59.

[5] M. Cacciari, G. P. Salam and G. Soyez, Eur. Phys. J. C **75** (2015) 59.

[6] D. Drijard, H. G. Fischer and T. Nakada, Nucl. Instrum. Meth. A **225** (1984) 367.

[7] S. Schael *et al.* [ALEPH Collaboration], Phys. Lett. B **606** (2005) 265.

[8] H. Schettler, DESY-THESIS-2013-036, CERN-THESIS-2013-265.

[9] B. Dutta, T. Kamon, N. Kolev and A. Krislock, Phys. Lett. B **703** (2011) 475.

[10] F. Hautmann, H. Jung and H. Van Haevermaet, Phys. Lett. B **754** (2016) 260.

Review of LPCC MB&UE Working Group Activities

Deepak Kar, on behalf of the members of the working group [1]

[1]University of Witwatersrand

1 A Brief History

On 14th August, 2009, just before LHC Run 1 started, Rick Field (CMS), Arthur Moraes (then ATLAS, now CMS) and D.K (ATLAS) got together and organised a meeting [1] between different LHC collaborations to discuss plans about early minimum-bias (MB) and underlying event (UE) measurements. Not only it started a cross-collaboration dialogue between the people involved in such measurements, it also started the idea of efficiently comparing the results from different collaborations.

Subsequently, Michelangelo Mangano formalised the effort under the banner of the newly formed LHC Physics Center at CERN (LPCC), and the LPCC Minimum-bias and underlying event WG [2] started to exist in the current form. Initially, with early LHC measurements, there were more frequent meetings (thrice on 2010, twice in 2011), and the latest one [3] was held on 19th November, 2015 to start the discussion about Run 2 results.

2 Outputs

The major outcome of the group has been the so called common plots, *i.e* minimum bias and underlying event distributions from different collaborations prepared with:

- common (fiducial) phase space, with same transverse momentum, p_{T} of charged particles, within same psuedorapidity, η range, and requiring the same minimum number of charged particles. For example, ATLAS and CMS can measure tracks within $|\eta| < 2.5$, while ALICE can go only upto $|\eta| < 0.8$, so a version of the common selection was proposed with the more restricted range,
- common binning, which enabled direct overlaying of data points from different collaborations, and
- comparing to at least one common Monte Carlo model prediction, which enabled indirectly comparing the results from different collaboration even before putting them in the common plots.

Although it took a bit of time for experiments to fully come on board with the idea of producing a separate set of results from the nominal published ones, currently these are considered almost an essential part of such an analysis.

Simultaneously, the discussions led to harmonising analysis strategies between different collaborations. For example, the first CMS Run 1 results were corrected back to model dependent non-single-diffractive phase space and used only charged hadrons, which were later changed. ATLAS in Run 2 excluded strange Baryons and their decays products from the fiducial definition, but agreed to provide results without this as well.

In Fig.1 and Fig.2, the MB charged particle multiplicity as function of η is compared between ALICE [4], ATLAS [5], and CMS [6] results at centre-of-mass energy, $\sqrt{s}$ of 900 GeV and 7 TeV. Finally, in Fig.3, the average charged particle multiplicity around $\eta \approx 0$ as function of $\sqrt{s}$ are compared. Overall the comparisons these MB plots showed remarkable consistency between the results. The situation was similar for UE activity measured as a function of leading charged particle p_{T}. This was critical in the early days of the LHC.

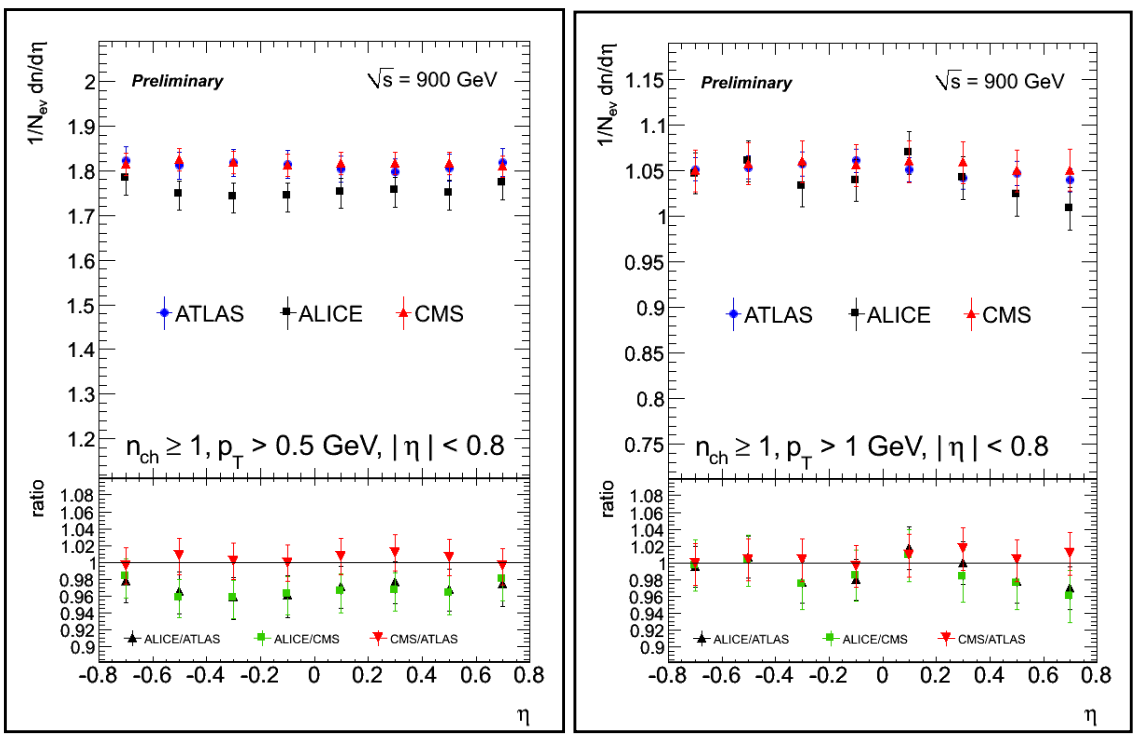

Figure 1: Comparisons of charged particle distributions as a function of pseudorapidity, η, for charged particle transverse momentum p_{T} threshold of 0.5 GeV (left) and 1.0 GeV (right) at 900 GeV pp collisions from ALICE, ATLAS and CMS.

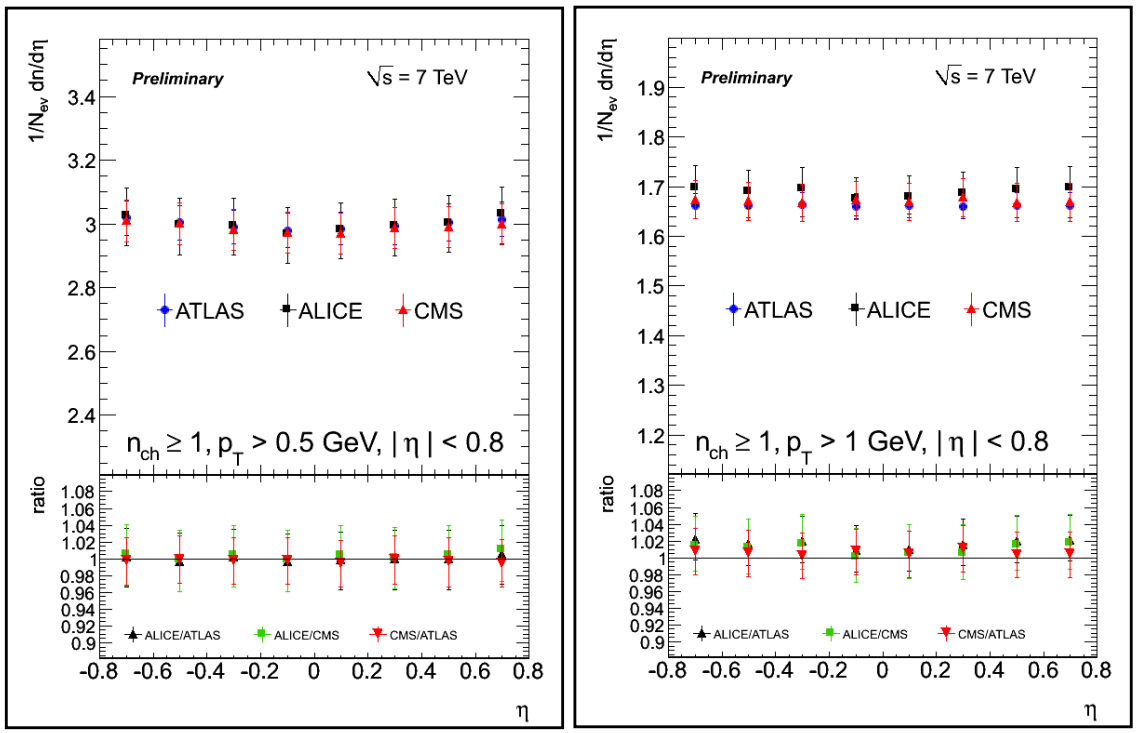

Figure 2: Comparisons of charged particle distributions as a function of pseudorapidity, η, for charged particle transverse momentum p_{T} threshold of 0.5 GeV (left) and 1.0 GeV (right) at 7 TeV pp collisions from ALICE, ATLAS and CMS.

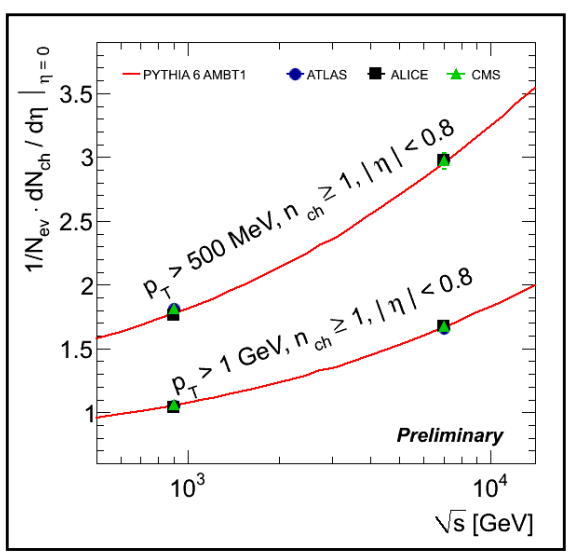

Figure 3: Comparisons of average number of charged particles at $|\eta| \approx 0$ as a function of center-of-mass energy, $\sqrt{s}$ from ALICE, ATLAS and CMS.

3 Outlook

The common plots for Run 2 results are currently under preparation. However, there have been ongoing discussions about how to keep the working group active, possibly expanding it to include other related topics. Among the options are the characterisation of large-multiplicity events, which is closely connected the activities in heavy ion community as well. Another area of potential interest is the connection between central and forward particle production. The previous meetings often included discussion about strange particle production, and in light of observations [7] that most current Monte Carlo generators poorly describe the strange fraction in data, this is of renewed interest as well.

Acknowledgements

The author thanks the ICTP, Trieste for generous travel support enabling him to attend this very useful workshop. He further thanks the organisers and sessions conveners for inviting him to present this talk.

References

[1] "First WG Meeting," http://indico.cern.ch/event/65178/, 2009, [Online; accessed 28-January-2016].

[2] "WG webpage," https://lpcc.web.cern.ch/lpcc/index.php?page=mb_ue_wg/, 2015, [Online; accessed 28-January-2016].

[3] "Latest WG Meeting," http://indico.cern.ch/event/393716/, 2015, [Online; accessed 28-January-2016].

[4] "ALICE Common Plots," http://indico.cern.ch/event/87648/contribution/3/attachments/1083875/1545976/CZampolli_MBUE.pdf, 2010, [Online; accessed 28-January-2016].

[5] "Central charged-particle multiplicities in pp interactions with $|\eta| < 0.8$ and $p_{\mathrm{T}} > 0.5$ and 1 GeV measured with the ATLAS detector at the LHC," Technical Report ATLAS-CONF-2010-101, CERN, Geneva, 2010, URL https://cds.cern.ch/record/1317333.

[6] "Pseudorapidity distributions of charged particles in pp collisions at $\sqrt(s) = 7$ TeV with at least one central charged particles," Technical Report CMS-PAS-QCD-10-024, CERN, Geneva, 2010, URL https://cds.cern.ch/record/1341853.

[7] "Multi-strange baryon production in pp collisions at $\sqrt{s} = 7$ TeV with ALICE," *Phys. Lett.*, **B712**(2012), 309, 1204.0282.

Particle Spectra in Minimum Bias events at 8TeV and 13 TeV

Juan Manuel Grados Luyando
on behalf of the CMS Collaboration

Deutsches Elektronen-Synchrotron

1 Introduction

The measurement of particle production without a bias of a hard scattering is one of the very first and basic measurements in hadron–hadron colliders at high-energies. Unbiased particle production is of great interest. Minimum Bias events are produced by strong interactions of hadrons and/or partons inside the hadrons. Most of these events are produced in a region where predictions of Quantum Chromodynamics (QCD) cannot be obtained perturbatively and where soft to semi-hard multiple partonic interactions (MPI), soft diffractive and non-diffractive processes are involved. The theoretical description of those components of particle production is extremely difficult and up to now, no unified and consistent description in terms of partonic processes exists, and one has to rely on phenomenological models of these components. However, when a hard scale is involved, predictions obtained from perturbative QCD are in many cases in good agreement with the measurements. An interesting and not yet answered question is to determine the transition region characterized by the interplay between hard processes calculable with perturbative techniques and soft processes described by non-perturbative models. Here are described measurements which could help to better understand this transition region and constrain the modelling of the different components of particle production. Apart from these considerations, the understanding of particle production is crucial when the collider is operated at high intensities since many hadron–hadron collisions are overlaid (pileup) and form a background to all other measurements. The measurements of particle production are often used to adjust (tune) free parameters in the models which simulate hadron–hadron interactions. Since these are used to simulate the pileup contribution, the measurements of particle production are important to achieve precise predictions and search for new physics.

Inclusive measurements of charged-particle pseudorapidity distributions, $dN_{\mathrm{ch}}/d\eta$, and transverse momentum distributions, dN_{ch}/dp_T, have previously been performed in pp and $p\bar{p}$ collisions for different centre-of-mass energies and phase space regions [1–10], where η is defined as $\eta = -\ln[\tan(\theta/2)]$, with θ being the polar angle of the particle trajectory with respect to the anticlockwise-beam direction. Here, charged-particle pseudorapidity distribution, also referred to as charged-particle pseudorapidity density, measured with the CMS detector in pp collisions at

a centre-of-mass energy of 13 TeV at 0 Tesla for long-lived charged-hadrons in the range $|\eta| < 1.8$ is discussed [1]. In addition predictions obtained from Monte Carlo (MC) event generators at 3.8 Tesla of pseudorapidity and integrated p_T-leading distributions for different event topologies corresponding to an inelastic enhanced event sample (INEL), a sample dominated by non-single diffractive dissociation (NSD) and a sample enriched by single diffractive dissociative events (SD) are discussed. The Monte Carlo (MC) event generators used were tuned to describe the underlying event (UE) properties at $\sqrt{s} = 7 - 8$ TeV [11] and to predictions from an event generator used in high-energy cosmic ray hadronic interactions.

2 Pseudorapidity distribution measurement by CMS detector at $\sqrt{s}$ =13 TeV

The first measurement of pp collisions at $\sqrt{s}$ =13 TeV was the pseudorapidity distribution of long-lived charged hadrons in the range $|\eta| < 1.8$ as shown in Fig. 1 left [1]. This measurement was presented for inelastic events without minimum transverse momentum requirement. A good agreement of the measurement with the MC predictions within the experimental uncertainties is found, with EPOS agreeing slightly better with the measurement.

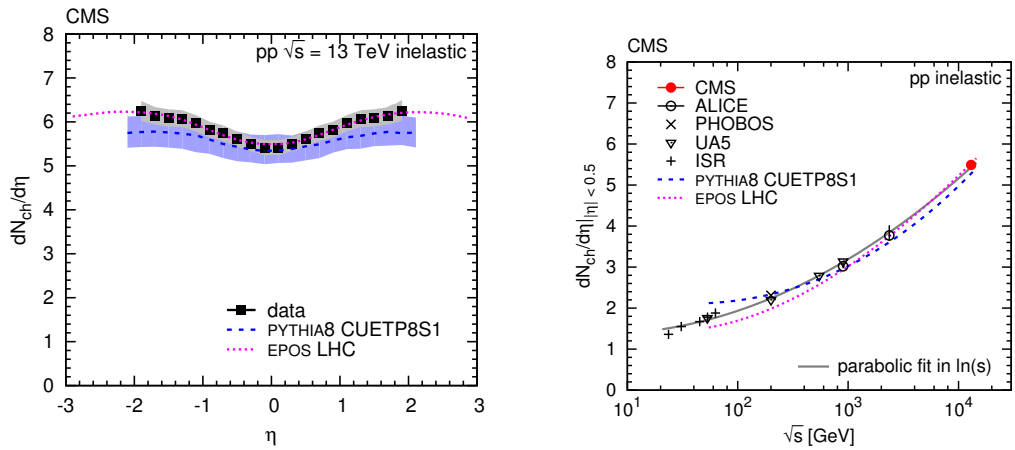

Figure 1: Left: Pseudorapidity distribution measured by CMS at $\sqrt{s}$ =13 TeV working at 0T. Right: Average number of hadrons in the central region as function of the center of mass energy.

On the right side of Fig. 1 is shown the average number of long-lived charged hadrons in the region $|\eta| < 0.5$ as a function of the energy of the center of mass compared with two MC predictions. One can notice that both MC predictions give a reasonable description.

3 Particle spectra

3.1 Pseudorapidity in diffractive events

In previous charged particle pseudorapidity measurements done by the CMS experiment a selection of different diffractive events was performed with the help of the TOTEM calorimeters ($5.3 < |\eta| < 6.4$) [3] according to the activity on the forward regions; an inclusive event sample, a sample dominated by non-single diffractive dissociation (NSD) and a sample enriched by single diffractive dissociative events (SD) by requiring activity or lack of activity on either T2 TOTEM telescopes, activity on both sides simultaneously, and activity in one side only, respectively. In Fig. 2 these distributions for three different event topologies at $\sqrt{s}$ =8 TeV are shown. In them it can be noticed a different behaviour between the most inclusive selections (inclusive and NSD-enhanced) and the SD-enhanced selection, being the latest more flat along the full eta range. The measurements are compared with different MC predictions being PYTHIA6 Z2* the only one to described the central η region of all of them.

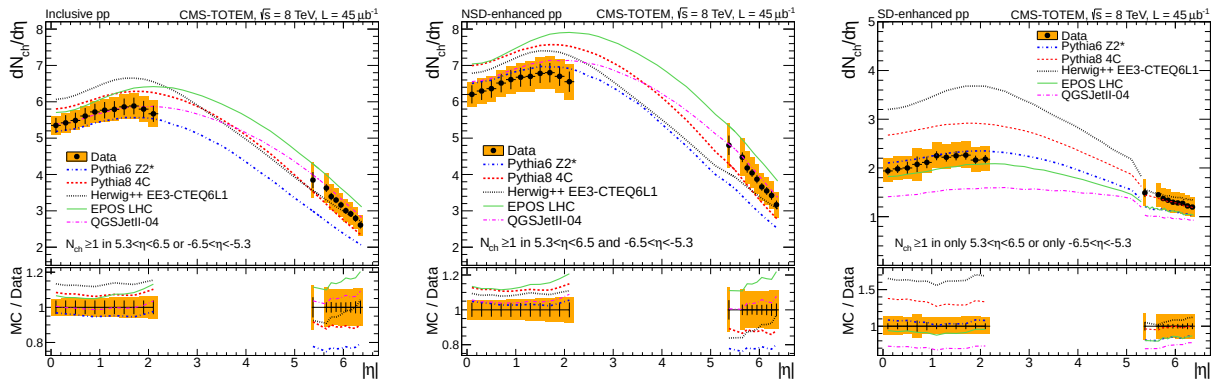

Figure 2: Pseudorapidity distributions measured by CMS experiment at $\sqrt{s}$ =8 TeV for inclusive(left), NonSingle Diffractive(center) and Single Diffractive(right) selections.

3.2 Integrated $\mathbf{p_{T-leading}}$

The total $2 \to 2$ partonic cross section diverges towards small p_T

$$\sigma(p_T) \propto \frac{1}{p_T^2} \tag{1}$$

and eventually becomes bigger than the total inelastic cross section. To deal with it a phenomenological factor $p_{T,0}$ is introduced in order to tame the divergent behaviour at small p_T. This turnover region is considered as the transition between perturbative QCD and non perturbative QCD. This region was investigated for minimum bias events (mostly inelastic events) [12], in Fig. 3 is shown the measurement compared to multiple MC predictions. On the left side of Fig. 3 the effect of MPI and the saturation $p_{T,0}$ taming factor are shown. It is immediately noticed

the importance of the taming factor to describe the data and how MPI has a small effect in this measurement. On the right side of the figure different MC generators are compared.

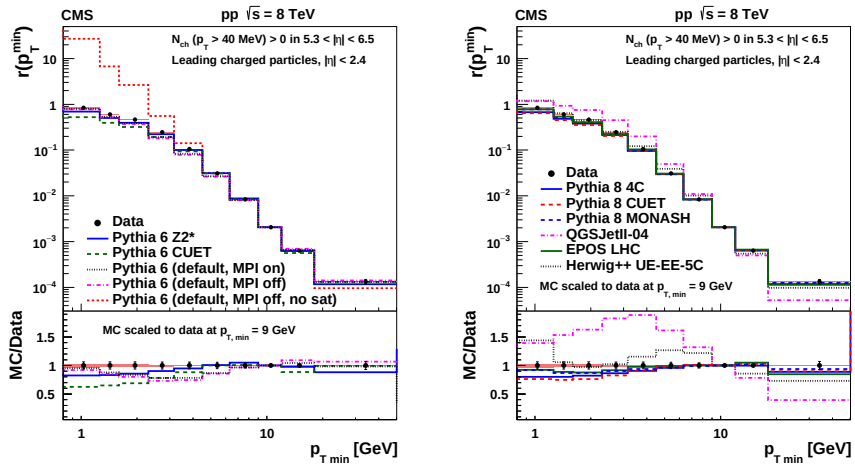

Figure 3: Integrated $p_{T-leading}$ distribution measured by CMS experiment at $\sqrt{s}$ =8 TeV

Acknowledgements

To Hannes Jung and Benoit Roland for all the help and support. To the MPI@LHC organisers for all the hard work to make this conference possible.

References

[1] V. Khachatryan *et al.* (CMS), "Pseudorapidity distribution of charged hadrons in proton-proton collisions at sqrt(s) = 13 TeV," *Phys. Lett.*, **B751**(2015).

[2] Jaroslav Adam *et al.* (ALICE), "Pseudorapidity and transverse-momentum distributions of charged particles in proton-proton collisions at $\sqrt{s}$ = 13 TeV," *Phys. Lett. B.*, **753**(2015).

[3] S. Chatrchyan *et al.* (CMS), "Measurement of pseudorapidity distributions of charged particles in proton-proton collisions at $\sqrt{s} = 8$ TeV by the CMS and TOTEM experiments," *Eur. Phys. J. C*, **74**(2014).

[4] V. Khachatryan *et al.* (CMS), "Transverse momentum and pseudorapidity distributions of charged hadrons in pp collisions at $\sqrt{s}$ = 0.9 and 2.36 TeV," *JHEP*, **02**(2010).

[5] V. Khachatryan *et al.* (CMS), "Transverse-momentum and pseudorapidity distributions of charged hadrons in pp collisions at $\sqrt{s}$ = 7 TeV," *Phys. Rev. Lett.*, **105**(2010).

[6] G. Aad *et al.* (ATLAS), "Charged-particle multiplicities in pp interactions measured with the ATLAS detector at the LHC," *New J. Phys.*, **13**(2011).

[7] K. Aamodt *et al.* (ALICE), "Charged-particle multiplicity measurement in proton-proton collisions at $\sqrt{s}$ = 0.9 and 2.36 TeV with ALICE at LHC," *Eur. Phys. J. C*, **68**(2010).

[8] K. Aamodt *et al.* (ALICE), "Charged-particle multiplicity measurement in proton–proton collisions at $\sqrt{s}$ = 7 TeV with ALICE at LHC," *Eur. Phys. J. C*, **68**(2010).

[9] R. Aaij *et al.* (LHCb), "Measurement of charged particle multiplicities in pp collisions at $\sqrt{s}$ = 7 TeV in the forward region," *Eur. Phys. J. C*, **72**(2012).

[10] G. Antchev *et al.* (TOTEM), "Measurement of the forward charged-particle pseudorapidity density in pp collisions at $\sqrt{s}$ = 7 TeV with the TOTEM experiment," *Europhys. Lett.*, **98**(2012).

[11] V. Khachatryan *et al.* (CMS), "Underlying Event Tunes and Double Parton Scattering," *CMS Physics Analysis Summary*, **CMS-PAS-GEN-14-001**(2014).

[12] V. Khachatryan *et al.* (CMS), "Production of leading charged particles and leading charged-particle jets at small transverse momenta in pp collisions at sqrt(s) = 8 TeV," *Phys. Rev. D*, **92**(2015).

Studies of the underlying event and particle production with the ATLAS detector

James Robinson[1], on behalf of the ATLAS Collaboration

[1]Deutsches Elektronen-Synchrotron, Notkestraße 85, 22607 Hamburg, Germany

1 Introduction

Studies of underlying event and particle production allow tuning and validation of models while helping describe pile-up and soft backgrounds to other processes. Such measurements in ATLAS [1] at the LHC use the inner tracking detectors, sensitive to charged particles with transverse momentum $p_{\mathrm{T}} > 100$ MeV and pseudorapidity $|\eta| < 2.5$, and the electromagnetic and hadronic calorimeters, sensitive to electrons, photons and hadrons that have transverse energy E_{T} greater than a few hundred MeV and $|\eta| < 4.9$. Often "Minimum Bias" events are used: inclusive collisions triggered by scintillators located at $2.1 < |\eta| < 4.9$.

2 Underlying event

Underlying event (UE) is any hadronic activity not associated with the hard scatter; an unavoidable background to collisions. UE is modelled with multiple parton interactions (MPI), initial- and final-state QCD radiation and colour-reconnection to the beam remnants. A reference object is identified in each event, such as the highest-p_{T} jet, track or Z-boson. For each particle, the azimuthal distance to the reference, $\Delta\phi$, is used to assign it to one of several regions: "towards" ($|\Delta\phi| \leq \pi/3$), "away" ($|\Delta\phi| \geq 2\pi/3$) and "transverse" ($\pi/3 < |\Delta\phi| \leq 2\pi/3$); "trans-max" and "trans-min" are subdivisions of the transverse region. UE is characterised in each region using calorimeter deposits and charged tracks.

Using a leading jet reference [2], the differential p_{T} sum of charged particles is shown for inclusive (Fig. 1a) and exclusive events (Fig. 1b). The roughly flat trans-min activity shows UE can be treated as constant at hard scales. Inclusively, activity increases in the trans-max region, showing colour connection to the jets. For exclusive events, vetoing extra jets lessens sensitivity to perturbative QCD. Another measurement at 7 TeV used a Z-boson as the reference [3], for which the towards region has a smaller amount of hard QCD activity. UE is compared for different reference objects in Fig. 2a; agreement between jet and Z-boson references supports the model of universal MPI, as does Fig. 2a showing 13 TeV data [4]. In all cases the data are used to constrain state-of-the-art theoretical predictions.

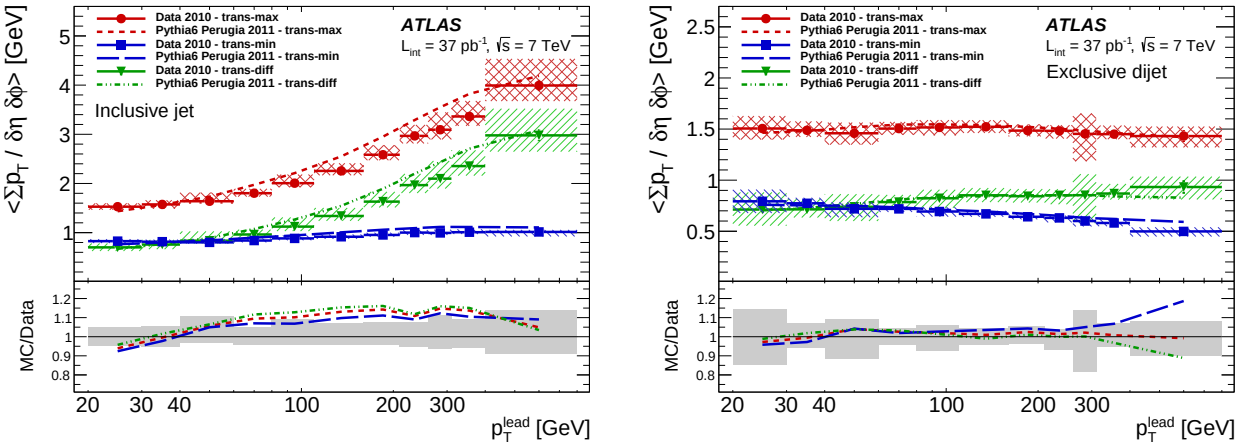

(a) Inclusive: ≥ 1 jet

(b) Exclusive: exactly two jets

Figure 1: Average scalar p_{T} sum of charged particles using a highest-p_{T} jet reference object [2].

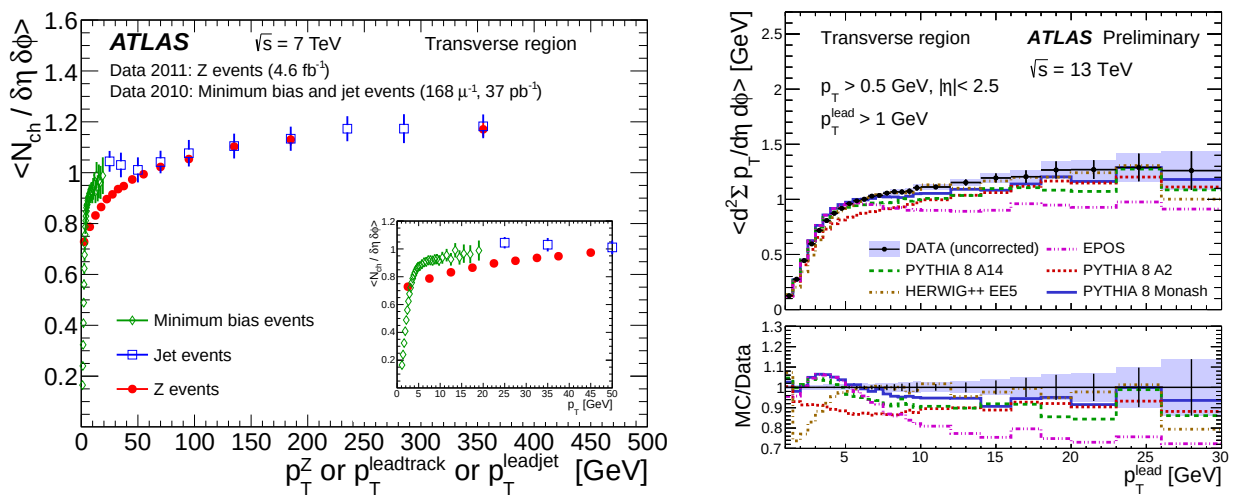

(a) Charged particle density as a function of reference object p_{T}

(b) Scalar transverse momentum density at 13 TeV with reference to the leading track

Figure 2: UE measurements using track, jet and Z-boson reference objects [3, 4].

3 Diffractive dijet production with rapidity gaps

Diffractive dijet production is analysed in terms of $\Delta\eta^F$, the largest forward pseudorapidity region devoid of hadronic activity and of $\tilde{\xi}$, an estimator of the fractional momentum loss in single diffractive dissociation [5]. Differential cross-sections (Fig. 3) show the non-diffractive component dominates at low $\Delta\eta^F$, but diffractive components are significant at higher $\Delta\eta^F$ and low $\tilde{\xi}$.

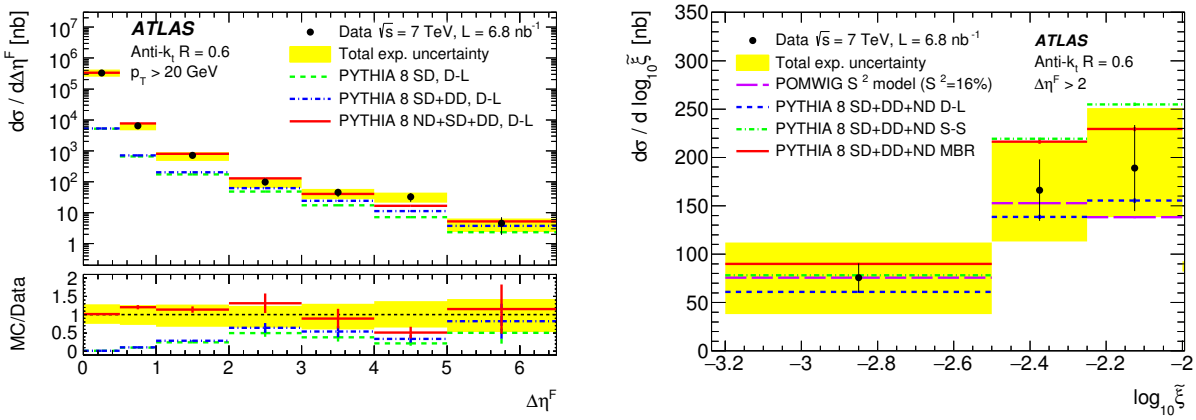

(a) As a function of $\Delta\eta^F$

(b) As a function of $\tilde{\xi}$

Figure 3: Diffractive dijet cross-sections [5].

4 Exclusive photoproduction of dileptons

The cross-section of exclusive $\gamma\gamma \to l^+l^-$ production was measured using 7 TeV data [6]. For electron or muon pairs passing a strict selection, the fiducial cross-section is extracted by fitting the dilepton acoplanarity distribution, shown in Fig. 4a. When the Equivalent Photon Approximation (EPA), which corrects for the finite proton size, is taken into account then the extracted cross-sections are found to be consistent with theoretical expectations, shown in Fig. 4b.

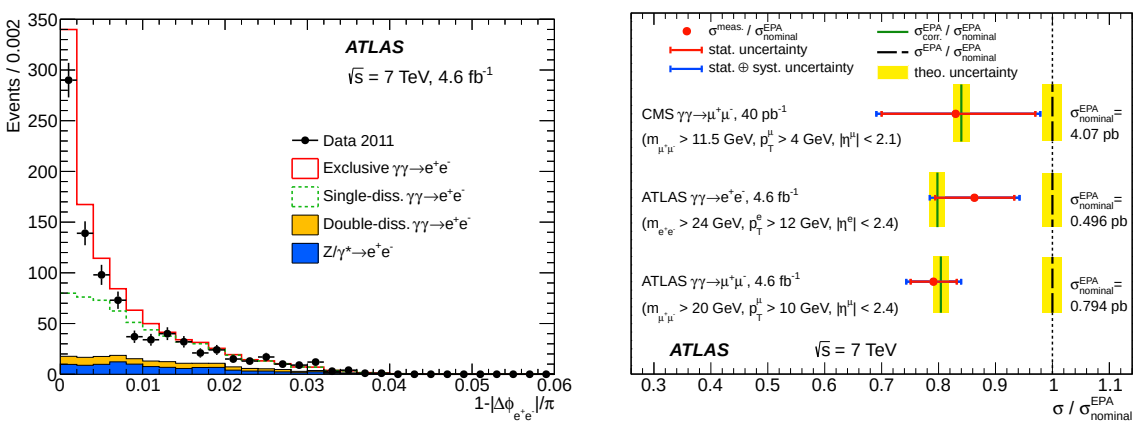

(a) Template fit to acoplanarity distribution

(b) EPA-corrected cross-section

Figure 4: Extraction of single dissociative fraction and comparison to theoretical predictions [6].

5 Transverse polarisation of Λ and $\bar{\Lambda}$ hyperons

The transverse polarisation of Λ and $\bar{\Lambda}$ hyperons was measured as a function of Feynman x_F [7]. Large polarisation of Λ hyperons was observed by previous experiments, while $\bar{\Lambda}$ was consistently

compatible with zero. Fig. 5a shows no significant dependence on x_F, and compatibility with zero in both cases. Fig. 5b demonstrates that the ATLAS results are compatible with an extrapolation from fixed-target experiments to the x_F range accessible in this measurement.

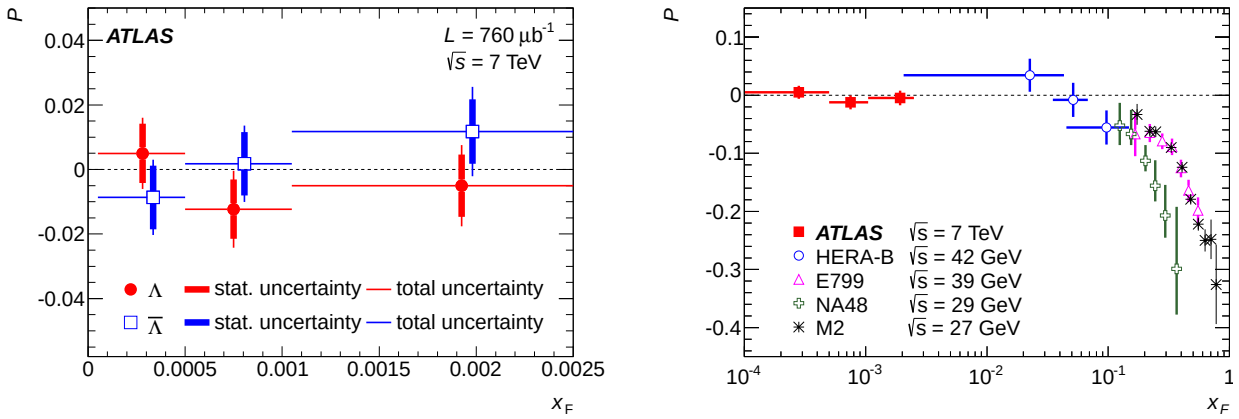

(a) Extracted polarisations for Λ and $\bar{\Lambda}$

(b) ATLAS measurement compared to measurements from lower centre-of-mass energy experiments

Figure 5: Extracted $\Lambda/\bar{\Lambda}$ polarisations as a function of x_F; comparison to other measurements [7].

6 Conclusion

The ATLAS collaboration has measured underlying event with different references, diffractive dijet and dilepton production and Λ polarisation. Such measurements are helpful for the development and tuning of models of soft particle production.

References

[1] ATLAS Collaboration, *JINST*, **3**(2008), S08003.

[2] ATLAS Collaboration, *Eur. Phys. J.*, **C74**(2014), 2965, 1406.0392.

[3] ATLAS Collaboration, *Eur. Phys. J.*, **C74**(2014), 3195, 1409.3433.

[4] ATLAS Collaboration, Technical Report ATL-PHYS-PUB-2015-019, 2015.

[5] ATLAS Collaboration, *Phys. Lett.*, **B754**(2016), 214, 1511.00502.

[6] ATLAS Collaboration, *Phys. Lett.*, **B749**(2015), 242, 1506.07098.

[7] ATLAS Collaboration, *Phys. Rev.*, **D91**(2015) (3), 032004, 1412.1692.

The Underlying Event at $\sqrt{s}$ = 500 GeV at STAR

Grant Webb, for the STAR Collaboration[1]

[1]Brookhaven National Laboratory

1 Introduction

The Relativistic Heavy Ion Collider (RHIC) is the world's first and only polarized proton beam collider. It allows for the measurement of spin dependent observables, which are crucial to resolve the elusive pieces of the proton spin puzzle. The underlying event (UE) is often interpreted as the set of all final state particles not associated with the initial hard-parton interaction. This is a combination of the beam remnants, the multiple parton interactions, and the initial and final state interactions [1]. It is vital to determine the effect these soft processes have in the measurements of hard interactions, which are theoretically calculable by perturbative QCD.

The underlying event may be characterized experimentally on an event-by-event basis by defining regions based upon the azimuthal angle difference between the leading jet and outgoing particle $\Delta\phi = \phi_{jet} - \phi_{particle}$. In this study the *toward* region is defined as $|\Delta\phi| < 60^\circ$, the *away* region $|\Delta\phi| > 120^\circ$, and the *transverse* region $60^\circ < |\Delta\phi| < 120^\circ$. The transverse region is also separated into two regions called transMax and transMin, which may provide insight on the initial and final state radiation contributions [1]. A schematic is shown in Fig. 1. The main observables for the charged particles are the transverse momentum sum and track multiplicity in each region. Likewise, for the neutral particles the main observables are the transverse energy sum and tower multiplicity in each region. These proceedings will focus on the charge track multiplicity as an example.

In 2009 approximately 8.7 pb^{-1} of RHIC data from proton-proton collisions were taken at the Solenoid Tracker at RHIC (STAR) using for the first time, center of mass energies of 500 GeV. The STAR detector's large acceptance in rapidity and full azimuthal coverage allows jet reconstruction using the Time Projection Chamber (TPC), Barrel (BEMC) and Endcap (EEMC) electromagnetic calorimeters [2] . Jets were constructed from the four-momenta of the charged particle tracks detected in the TPC ($-1.3 < \eta < 1.3$) and the electromagnetic energy deposits in the BEMC ($-1.0 < \eta < 1.0$). To prevent an overestimation of the jet energy a 100% subtraction scheme was implemented. This approach subtracts the track four-momentum from the four-momentum of the tower it struck. This avoids double-counting of energy from both hadronic showers and electrons in the jet. Simulations of this effect in PYTHIA/GEANT [3] [4] suggest that double-counting of energy is reduced from 20% to 5% for jets with transverse momentum in the range $5 < p_T < 60$

GeV/c. The same method was implemented for the UE region observables. Events were selected that satisfied the jet patch (JP) trigger, which required ∼13 GeV of energy to be deposited into a 1.0×1.0 region of $\Delta\eta - \Delta\phi$ space in the BEMC and/or EEMC.

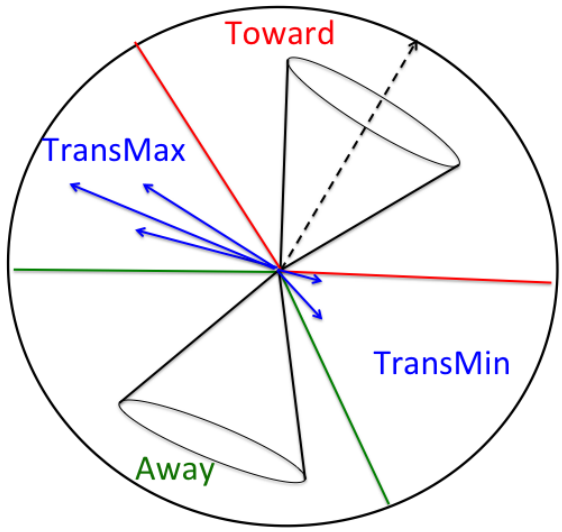

Figure 1: Diagram of the UE regions defined based upon the leading jet position with respect to the azimuthal angle. The toward region contains the leading jet, while the away region contains the away side jet. The transverse region, perpendicular to the hard 2-to-2 interaction, is sensitive to the underlying event. The transMax (transMin) is the region with the higher (lower) "activity".

2 Analysis and Results

The anti-k_T algorithm with a radius of 0.6 as implemented in FastJet [5] was used for jet reconstruction. The data are compared to an embedding Monte-Carlo sample of 4M events. The embedding sample takes zero-bias data, events randomly selected throughout the run, and embeds simulated events generated using PYTHIA version 6.4 [3] with Tune 320 (Perugia 0) [6]. The STAR detector response was simulated using the GEANT 3 package [4]. This procedure incorporates features of the STAR event, such as pile-up tracks and background, that cannot be easily simulated. The charged particle distribution of the multiplicity and sum transverse momenta in the embedding over-predict the data by ∼8% in the transverse region. An example of this is shown in Fig. 2. The opposite behavior is observed when comparing the neutral particle distributions. The embedding under-predicts the data by ∼5%.

In addition, a comparison of tunes between the Perugia 0 and Tune 100 (Pythia Tune A) [7] was discussed in the presentation. The underlying event analysis was performed with 1M events each. The particle multiplicity and particle p_T sum as a function of the leading jet p_T were examined. It

showed that the Perugia 0 tune over-predicted the Tune 100 simulation by 10% in the transverse region. This indicates Tune 100 better simulates the underlying event in proton-proton collisions at $\sqrt{s}$ = 500 GeV. To probe if the UE has an spin dependences, which could contaminate the measured asymmetries, we performed an analysis as a function of the beam polarization as shown in Fig. 3. Unfortunately, the polarization in the Run 9 pp 500 GeV data was very poor (∼30%) and does not allow for a definitive conclusion on the spin dependence of the underlying event. However, from this first glance there doesn't seem to be a large dependence on the different beam polarizations. Improvements in the polarization, reaching close to $\sim$ 60% polarization, were achieved in recent years can further confirm any dependence.

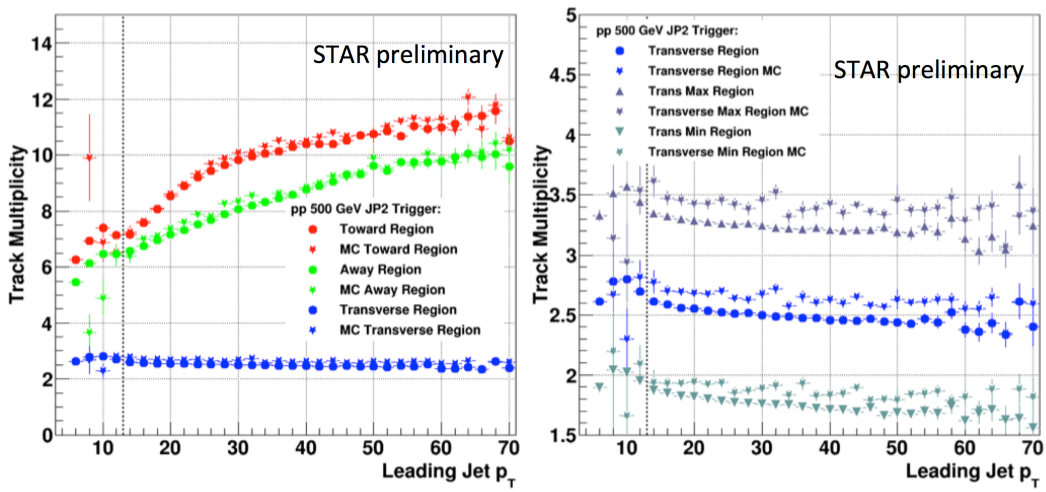

Figure 2: Data (solid circles) and Perugia 0 MC (solid stars) comparison of the track multiplicity as a function of leading jet p_T at the detector level. Left: Toward (red), Away (green), Transverse (blue) Regions. Right: Transverse, TransMax and TransMin Regions.

3 Conclusions

The underlying event of proton-proton collisions at $\sqrt{s}$ = 500 GeV has been accessed at STAR by studying the transverse region. The theoretical simulations are systematically higher (∼8%) than the charged particle distributions experimentally measured in data. The opposite behavior is observed in the neutral particle distributions, a systematic ∼5% decrease. In addition, data for future analyses are on tape to determine if the UE has any spin dependence utilizing RHIC's unique capabilities to provide polarized proton beams.

References

[1] Rick D. Field (CDF), "The Underlying event in hard scattering processes," *eConf*, **C010630**(2001), P501, hep-ph/0201192.

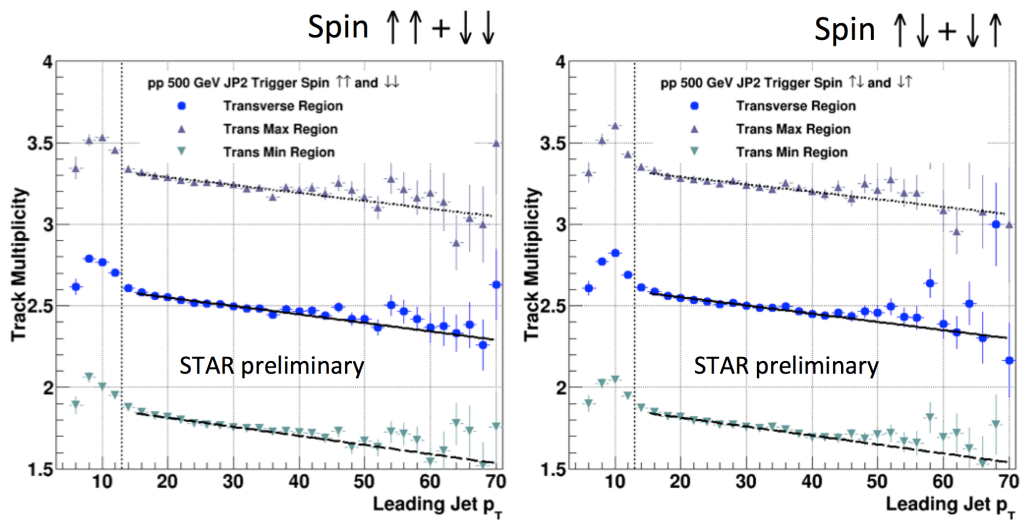

Figure 3: The track multiplicity distribution as a function of the leading jet p_T. Left: proton spin aligned. Right: proton spin anti-aligned.

[2] K. H. Ackermann *et al.* (STAR), "STAR detector overview," *Nucl. Instrum. Meth.*, **A499**(2003), 624.

[3] Torbjorn Sjostrand, Stephen Mrenna, and Peter Z. Skands, "PYTHIA 6.4 Physics and Manual," *JHEP*, **05**(2006), 026, hep-ph/0603175.

[4] Rene Brun, Federico Carminati, and Simone Giani, "GEANT Detector Description and Simulation Tool," (1994).

[5] G. P. Salam M. Cacciari and G. Soyez, *Eur. Phys. J.*, **C 72**(2012).

[6] Peter Zeiler Skands, "Tuning Monte Carlo Generators: The Perugia Tunes," *Phys. Rev.*, **D82**(2010), 074018, 1005.3457.

[7] Rick Field and R. Craig Group (CDF), "PYTHIA tune A, HERWIG, and JIMMY in Run 2 at CDF," (2005), hep-ph/0510198.

Exploring the Underlying Event and Hadronization using Di-jets at STAR

Brian Page[1]

[1]Brookhaven National Laboratory , Upton, NY 11973 USA

1 Introduction

As the world's first and only polarized proton-proton collider, the Relativistic Heavy Ion Collider (RHIC) is a unique platform for the study of the spin structure of the proton. Despite many years of experimental and theoretical effort, a detailed understanding of how the intrinsic and angular momenta of the quarks and gluons contribute to the overall proton spin budget is still lacking. Recent measurements of the longitudinal double helicity asymmetry A_{LL} [1,2] from the two major experiments at RHIC, STAR and PHENIX, have begun to place constraints on the contribution due to the intrinsic gluon spin, ΔG. These data have been incorporated into next to leading order global analyses by both the DSSV and NNPDF groups which, for the first time, find non-zero gluon polarization values for momentum fractions greater than 0.05 [3,4].

To date, the most precise A_{LL} measurements from STAR have been made using inclusive jet final states, however, extensions to correlated di-jet measurements are being pursued in the hope that they will place better constraints on the behavior of ΔG as a function of gluon momentum fraction. In addition to the asymmetry, the measurement of the unpolarized di-jet cross section at $\sqrt{s} = 200$ GeV should help constrain parton distribution functions (PDFs) at high momentum fractions and comparison to theory will demonstrate that di-jet reconstruction is well understood at STAR. The remainder of this note will discuss the issue of properly accounting for underlying event and hadronization effects when comparing theoretical and experimental di-jet cross sections.

2 Underlying Event and Hadronization Corrections

The extraction of a cross section from raw data requires corrections for detector resolution, efficiency, and acceptance effects. To this end, simulated events were created using PYTHIA 6.425 [5] with the Perugia 0 [6] tune and run through a STAR detector response package. An unfolding was performed using the SVD method [7] and corrections for trigger efficiency and detector acceptance were made. The unfolding and efficiency corrections were all done to particle level in

the simulation, where the input to the jet maker was all stable particles arising from the hard scattering as well as underlying event sources such as multiple partonic interactions, beam remnants, etc.

While the experimental cross section is corrected to particle level, many theoretical calculations do not take into account these non-perturbative effects, meaning a correction to the theory must be applied before a faithful comparison between the two can be made. This correction was found by taking the ratio of the raw particle over parton level di-jet yield from simulation. Here, parton level refers to jets whose constituents are pre-hadronization partons arising from the hard scattering as well as initial and final state radiation, but not underlying event.

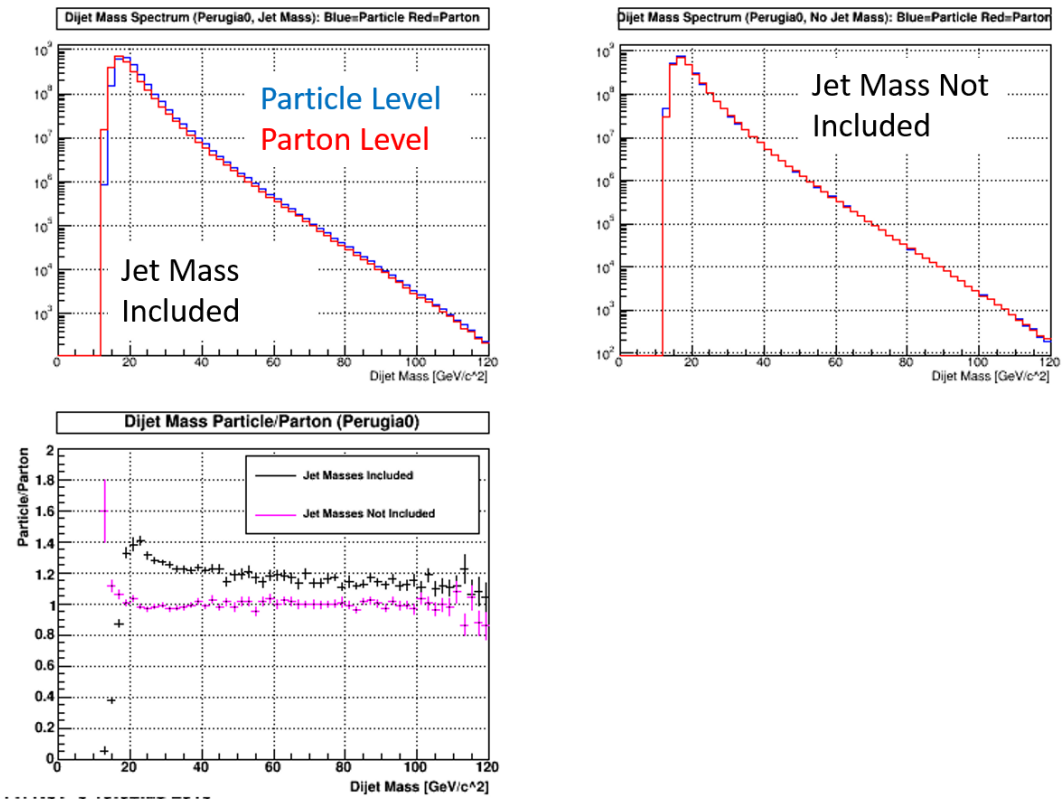

Figure 1: Comparison of particle (blue curve) vs parton (red curve) level di-jet mass. The spectra in the upper left panel were constructed with the jet masses included while those in the upper right do not include the jet masses. The bottom panel shows the particle over parton level ratio for the two cases. The Perugia 0 tune is used.

Figure 1 shows the particle and parton level spectra, as well as their ratio, for two di-jet invariant mass determinations using the Perugia 0 tune. The di-jet invariant mass is found by adding the four-momenta of the two constituent jets and can be expressed in terms of the masses, transverse momenta, rapidity difference and azimuthal angle difference of the two jets as shown in equation 1. Typical values of jet mass range from 3 to 6 GeV/c^2 although masses can extend to 15

GeV/c^2. Equation 1 was used to produce the 'Jet Mass Included' curves shown in the figures. If the individual jet masses are neglected, as is often done in theoretical calculations, the mass terms in equation 1 are set to zero and a simplified expression is obtained which is used in the 'Jet Mass Not Included curves'.

$$M = \sqrt{m_1^2 + m_2^2 + 2\sqrt{m_1^2 + p_{T1}^2}\sqrt{m_2^2 + p_{T2}^2}\cosh(\Delta y) - 2p_{T1}p_{T2}\cos(\Delta\phi)} \quad (1)$$

As can be seen in the upper left panel of figure 1, the particle and parton level spectra are shifted in mass with respect to one another in the case where jet mass terms are included. This leads to a particle over parton level ratio which stays significantly above unity for the entire measured mass range which is somewhat against expectation as underlying event and hadronization effects should contribute predominantly at low mass. When the jet mass terms are excluded from the di-jet mass calculation however, the particle and parton spectra align, resulting in a ratio which is unity over nearly the full mass range.

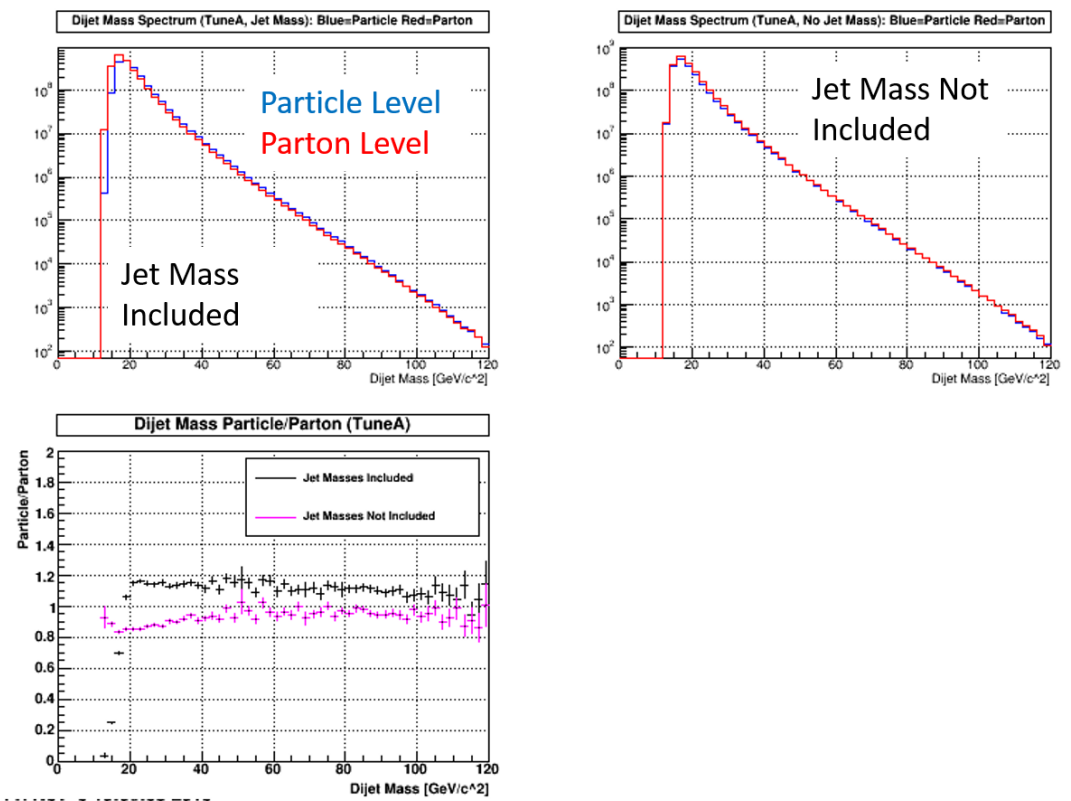

Figure 2: Same format as figure 1, but the CDF Tune A parameters are used.

Figure 2 has the same layout as figure 1, but now the simulation was run with CDF Tune A parameters [8]. As with the Perugia 0 simulations, the particle and parton spectra are shifted with respect to one another when jet masses are included but align when they are neglected.

However, the relative amounts of di-jets are different resulting in particle over parton ratios which are significantly different than the Perugia 0 case.

3 Conclusion

The extracted cross section should be relatively insensitive to the choice of tune, but the large differences seen in the particle over parton level di-jet yield shows that the underlying event and hadronization correction is quite sensitive to the modeling of the soft physics. In addition, it appears that the choice of mass definition can affect the size of the correction. While these effects need to be studied with more modern tunes, the large variation in correction factor between tunes which describe STAR data well [1, 9] points to the need for better classification of the underlying event at STAR. As tuning Monte Carlo generators can be resource intensive, future measurements may also benefit from techniques designed to remove contributions from the underlying event.

References

[1] L. Adamczyk *et al.* (STAR), *Phys. Rev. Lett.*, **115**(2015) (9), 092002, 1405.5134.

[2] A. Adare *et al.* (PHENIX), *Phys. Rev.*, **D90**(2014) (1), 012007, 1402.6296.

[3] Daniel de Florian, Rodolfo Sassot, Marco Stratmann, and Werner Vogelsang, *Phys. Rev. Lett.*, **113**(2014), 012001, URL http://link.aps.org/doi/10.1103/PhysRevLett.113.012001.

[4] Emanuele R. Nocera, Richard D. Ball, Stefano Forte, Giovanni Ridolfi, and Juan Rojo, *Nuclear Physics B*, **887**(2014), 276 , URL http://www.sciencedirect.com/science/article/pii/S0550321314002636.

[5] T. Sjostrand, S. Mrenna, P. Skands, *JHEP*, **05**((2006)), 026.

[6] P. Skands, *Phys. Rev. D*, **82**((2010)), 074018.

[7] A. Hoecker, V. Kartvelishvili, *Nucl. Instrum. Meth A*, **372**((1996)), 469.

[8] R.D. Field et al, hep-ph/0510198.

[9] B. I. Abelev *et al.* (STAR), *Phys. Rev. Lett.*, **100**(2008), 232003, 0710.2048.

Underlying Events and Flow in EPOS 3

T. Pierog[1], B. Guiot[2,3], Iu. Karpenko[4,5,6], and K. Werner[2]

[1]Karlsruhe Inst. of Technology, KIT, Campus North, Inst. f. Kernphysik, Germany
[2]SUBATECH, University of Nantes,IN2P3/CNRS,EMN, Nantes, France
[3]Universidad Tcnica Federico Santa Mara, Valparaiso , Chile
[4]FIAS, Johann Wolfgang Goethe Universitaet, Frankfurt am Main, Germany
[5]Bogolyubov Institute for TheoreticalPhysics, Kiev 143, 03680, Ukraine
[6]INFN - Sezione di Firenze, Via G. Sansone 1, I-50019 Sesto Fiorentino (Firenze), Italy

In this paper we will present a new approach to calculate the saturation scale in EPOS which allows better initial conditions to test the effect of collective hadronization on underlying event analysis in proton-proton (pp) interactions. We will demonstrate that this effect which was attributed to heavy ion collisions only is very important to describe pp data in particular for strange particle production.

1 Initial Conditions: EPOS 3

In order to make a hydrodynamical evolution calculation, proper initial conditions are needed. In our approach the EPOS 3 [1] model is used to determine the energy density tensor and flavor content of the thermalized matter and to solve the differential equations of the hydrodynamical calculation.

EPOS 3 is a minimum bias monte-carlo hadronic generator used for heavy ion interactions. It is the last generation of a long development of the EPOS model [2–6]. It is the only hadronic model which has a consistent treatment of cross-section calculation and particle production taking into account energy conservation in both cases thanks to the parton-based Gribov-Regge theory [7]. In this approach, the basic ingredient is the purely imaginary amplitude of a single Pomeron exchange which is the sum of a (parametrized) soft contribution (Regge-like after Fourier transformation from t space to impact parameter b space) $G_0(\hat{s},b) = \alpha_0(b)\hat{s}^{\beta_0}$ and a semi-hard contribution based on the convolution of a soft pre-evolution, a DGLAP [8] based hard evolution and a standard leading order QCD 2→2 cross-section (mini-jet). The latter (called $\hat{G}$) needs complex calculations but can be fitted to a simple Regge-like term: $G_1(\hat{s},b) = \alpha_1(b)\hat{s}^{\beta_1}$. $\hat{s} = sx^+x^-$ is the fraction of the center-of-mass energy squared (mass) carried by the Pomeron and b the impact parameter of the nucleon-nucleon collision. Details can be found in [7].

Both cross-sections and particle production are based on the total amplitude $G = \sum_i G_i$ via a complex Markov-Chain monte-carlo. The particle production has two main components: the

strings composed from the Pomerons (2 strings per Pomeron (Initial State Radiation and Final State Radiation and the soft contribution from the non-perturbative pre-evolution (below the fixed scale Q_0^2) are included) and at high energy many Pomerons can happen in parallel for each event (multiple parton interaction (MPI))) which cover the mid-rapidity part and the remnants which carry the remaining energy and quarks and cover mostly the fragmentation region. A remnant can be as simple as a resonance or a string elongated along beam axis if its mass is too high and is treated the same way for both diffractive and non-diffractive events.

The string fragments are then used to compute the energy density tensor on an even-by-event basis. If the energy density is higher than some threshold, string segments are merged locally into the so-called "core" to solve hydrodynamical differential equation with an equation of state based on lattice QCD. Details can be found in [4].

2 Saturation scale

To correct the limitation observed for instance in EPOS LHC [2] for high transverse momentum (pt) particles in particular in proton-nucleus (pA), a new saturation scale has been introduced which can be different for each Pomeron. In EPOS LHC and previous versions, non-linear effects due to Pomeron-Pomeron interactions were treated by a simple correction on the β_i exponent of the G_i contributions of the Pomeron amplitude [6]. But this approach was changing both soft (multiplicity) and hard component (high pt) the same way. Since strong nuclear effects are needed to reproduce both cross-section and multiplicity of pA interactions leading to a strong correction on β, a strong suppression of high pt particles was observed in EPOS simulations.

Instead of applying the correction on β to the real Pomeron amplitude $\hat{G}$, it is possible to change $\hat{G}$ itself to reproduce the modified G (called $\tilde{G}$) simply by changing the scale at which the perturbative calculation is done: Q_0^2. Q_0^2 is replaced by $Q_s^2(x, x, s, b)$ to calculate each Pomeron amplitude. It is in fact possible to calculate Q_s^2 by the generation of Pomeron using the effective $\tilde{G}$ which reproduce the cross-section and the multiplicity observed in the data. Since by definition we want to recover a perfect binary scaling at high pt we can use $N_{bin}\hat{G}(Q_s^2) = N_{col}\tilde{G}(x, x, s, b)$ to compute Q_s^2 Pomeron-by-Pomeron. N_{bin} is the number of binary collisions based on the Glauber model for a particular event while N_{col} is the real number of colliding pairs of nucleon in the model (using $\tilde{G}$).

To illustrate the fact that a change of Q_s^2 is a way to reduce soft parton production without changing the hard ones (above Q_s^2), the deviation between EPOS 3.2 calculation of the jet transverse momentum distribution rescaled by the number of binary collisions and a pure pQCD calculation using Cteq6 [9] parton distribution functions can be observed in Fig. 1 for central pPb collisions at 5 TeV. The high pt part is in perfect agreement while a strong suppression is observed at low pt.

The same scheme to compute Q_s^2 is of course used for pp interactions and with enough MPI it solves the problem observed in EPOS LHC [2] with high pt leading particles.

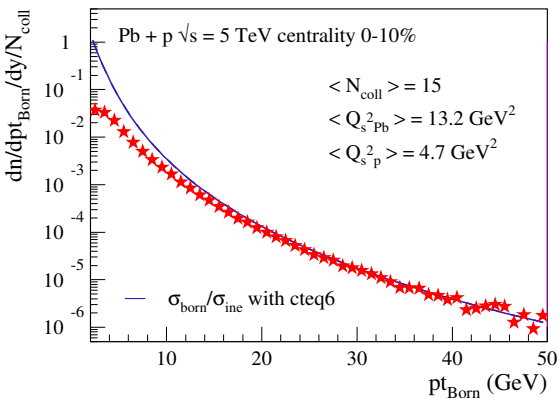

Figure 1: Born parton pt distribution normalized by the Glauber number of binary collisions from pPb collisions at 5.02 TeV for 0-10% centrality bin. EPOS 3.2 simulations are shown with stars and compared to the normalized inclusive cross-section (full line).

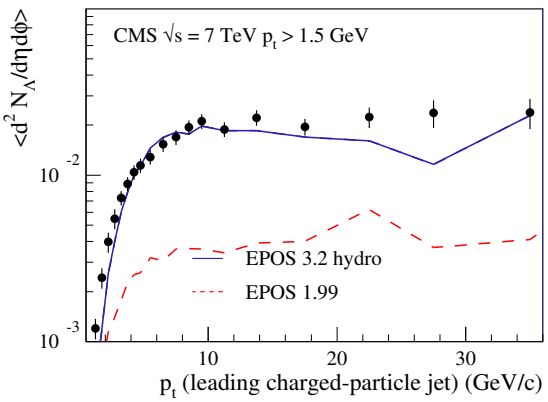

Figure 2: CMS measurement [10] of the number of λ particles with $p_{\rm t} \geq 1.5$ GeV produced in the underlying event, i.e. a region of $60° \leq |\Delta\phi| \leq 120°$ around the leading particle as a function of the leading charged-particle jet transverse momentum. EPOS 3.2 simulations are shown with a full line with collective hadronization and with a dashed line otherwise.

3 Collective hadronization and underlying events

With hard scatterings being properly described, it is possible to test underlying event activity. The measurement of this activity has been initiated by the CDF collaboration more than ten years ago [11] to understand multiple parton interaction and test the capability of the event generators to reproduce real events. This analysis has been generalized to more recent collider data including the main LHC experiment ATLAS [12] and CMS [13]. Another analysis is of particular interest when focusing on the effect of collective hadronization since it is based on strange particle production [10]. Indeed the strange particles and in particular strange baryons are more sensitive to hydrodynamical effects since statistical hadronization which occur at the surface of the fluid leads to an increase of strangeness production compared to usual string fragmentation and the transverse momentum flow due to the fluid evolution is larger for heavier particles.

In Fig. 2 we can compare the λ production in underlying event activity in EPOS 3 with (full line) or without (dashed-line) collective hadronization. Without this effect the strange baryon production is clearly underestimated as observed for other monte-carlo generator in [10] while the data can be nicely reproduced if the formation of a core which hadronizes statistically is taken into account. The effect is relatively important since underlying activity is measured in events whose multiplicity is higher than the average, increasing the probability to have core formation. We can conclude that underlying event activity measurements, and in particular whose related to strange particles, can be used to test collective hadronization effects in proton-proton collisions.

References

[1] K. Werner and B. Guiot, and I. Karpenko and T. Pierog , "Analysing radial flow features in p-Pb and p-p collisions at several TeV by studying identified particle production in EPOS3," *Phys.Rev.*, **C89**(2014) (6), 064903.

[2] T. Pierog, Iu. Karpenko, J. M. Katzy, E. Yatsenko, and K. Werner, "EPOS LHC: Test of collective hadronization with data measured at the CERN Large Hadron Collider," *Phys. Rev.*, **C92**(2015) (3), 034906, 1306.0121.

[3] K. Werner, Iu. Karpenko, M. Bleicher, T. Pierog, and S. Porteboeuf-Houssais, "Jets, Bulk Matter, and their Interaction in Heavy Ion Collisions at Several TeV," *Phys.Rev.*, **C85**(2012), 064907.

[4] K. Werner, Iu. Karpenko, T. Pierog, M. Bleicher, and K. Mikhailov, "Event-by-Event Simulation of the Three-Dimensional Hydrodynamic Evolution from Flux Tube Initial Conditions in Ultrarelativistic Heavy Ion Collisions," *Phys.Rev.*, **C82**(2010), 044904.

[5] T. Pierog and K. Werner, "EPOS Model and Ultra High Energy Cosmic Rays," *Nucl.Phys.Proc.Suppl.*, **196**(2009), 102.

[6] Klaus Werner, Fu-Ming Liu, and Tanguy Pierog, "Parton ladder splitting and the rapidity dependence of transverse momentum spectra in deuteron-gold collisions at RHIC," *Phys. Rev.*, **C74**(2006), 044902.

[7] H. J. Drescher, M. Hladik, S. Ostapchenko, T. Pierog, and K. Werner, "Parton based Gribov-Regge theory," *Phys. Rept.*, **350**(2001), 93.

[8] Guido Altarelli and G. Parisi, "Asymptotic Freedom in Parton Language," *Nucl. Phys.*, **B126**(1977), 298.

[9] J. Pumplin *et al.*, "New generation of parton distributions with uncertainties from global QCD analysis," *JHEP*, **07**(2002), 012.

[10] Serguei Chatrchyan *et al.* (CMS), "Measurement of neutral strange particle production in the underlying event in proton-proton collisions at sqrt(s) = 7 TeV," *Phys. Rev.*, **D88**(2013), 052001, 1305.6016.

[11] Anthony Allen Affolder *et al.* (CDF), "Charged jet evolution and the underlying event in $p\bar{p}$ collisions at 1.8 TeV," *Phys.Rev.*, **D65**(2002), 092002.

[12] Georges Aad *et al.* (Atlas Collaboration), "Measurement of underlying event characteristics using charged particles in pp collisions at $\sqrt{s} = 900GeV$ and 7 TeV with the ATLAS detector," *Phys.Rev.*, **D83**(2011), 112001.

[13] Serguei Chatrchyan *et al.* (CMS), "Measurement of the Underlying Event Activity at the LHC with $\sqrt{s} = 7$ TeV and Comparison with $\sqrt{s} = 0.9$ TeV," *JHEP*, **09**(2011), 109, 1107.0330.

Charged Particle Production in Proton-Proton Collisions at $\sqrt{s}$ = 13 TeV with ALICE at the LHC

Prabhakar Palni (for the ALICE Collaboration)[1]

[1] Institute of Particle Physics, Central China Normal University, Wuhan

1 Introduction

The Run II of the Large Hadron Collider (LHC) at the CERN laboratory started mid 2015, with proton-proton collisions at the unprecedented center-of-mass energy of $\sqrt{s}$ = 13 TeV. At the Run II start-up it is crucial to measure the general properties of these collisions starting from those observables that require a minimal integrated luminosity such as the average pseudorapidity density distribution $\langle \mathrm{d}N_{\mathrm{ch}}/\mathrm{d}\eta \rangle$ and the transverse-momentum (p_{T}) spectrum of charged particles.

The experimental measurement of these inclusive charged hadron observables provide an essential input for the tuning of the general purpose perturbative QCD models, in particular for what concerns the constraints to the parameters handling the Multiple-Parton Interactions (MPI) that are expected to play a significant role in particle production at the LHC energies [1]. The non-perturbative parameters, in particular those dealing with fragmentation and hadronization, are also affecting the $\langle \mathrm{d}N_{\mathrm{ch}}/\mathrm{d}\eta \rangle$ and p_{T} distribution predictions of these models. Models adopting alternative descriptions can also be tuned and tested against the data [2]. Moreover, these measurements serve as a reference data to study nuclear effects such as the nuclear modification factors R_{AA} and R_{pA}, of the transverse-momentum spectra of inclusive charged hadrons in Pb-Pb and p-Pb collisions, respectively [3]. The details of the analysis discussed here are reported in reference [4].

2 Data sample and analysis details

The measurements presented here rely on the data collected with the ALICE detector [5, 6] at the beginning of the LHC Run II (in June 2015). These data were collected using a minimum-bias trigger that requires at least one hit in either the V0 plastic scintillator arrays (V0A and V0C) or in the newly installed ALICE Diffractive detector arrays (ADA and ADC). The data sample consists of about 1.5 million minimum-bias events at a center-of-mass energy of $\sqrt{s}$ = 13 TeV passing the trigger selection criteria. The measurement of the pseudorapidity density distribution of charged-particles at mid-rapidity is based on the short track segments (or tracklets) reconstructed using the position of the reconstructed primary vertex and one hit on each of the two innermost layers

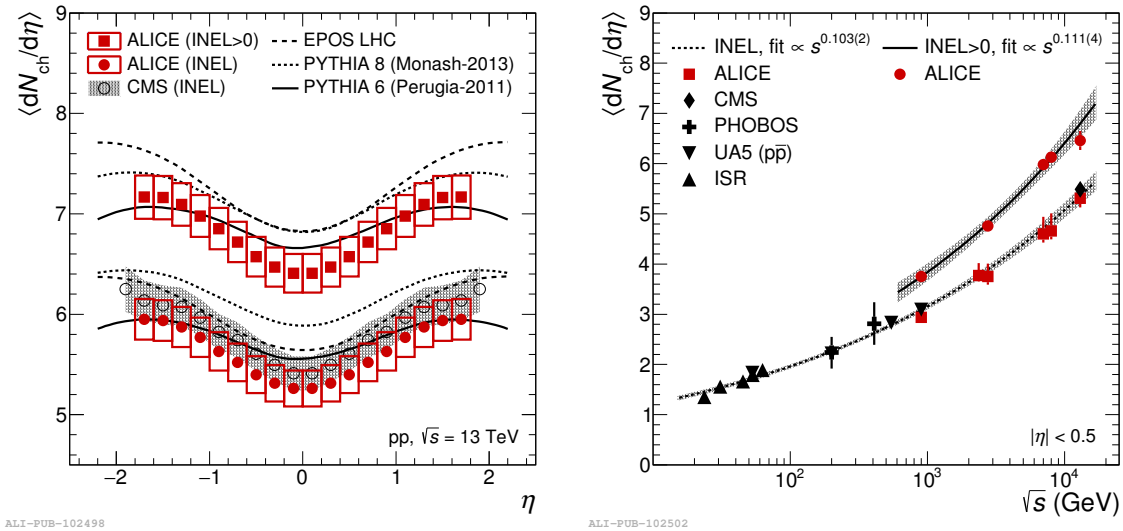

(a) (b)

Figure 1: Average pseudorapidity density distribution of charged-particles as a function of η. Charged-particle pseudorapidity density measured as a function of colliding center-of-mass energy for INEL and INEL>0. Figures are taken from [4].

of the Inner Tracking System (ITS), and on the tracks reconstructed using also the Time Projection Chamber (TPC) and additional hits in the ITS.

The efficiency of charged-hadron reconstruction and all the corrections accounting for the background contamination are estimated from a Monte Carlo simulation using the PYTHIA 6 generator adopting the Perugia-2011 tune. The simulation of the particle transport in the ALICE detector relies on the GEANT3 simulation package.

3 Results

The pseudorapidity distribution in $|\eta| < 1.8$ is reported in Fig. 1a for inelastic (INEL) events and for events with at least one charged particle in $|\eta| < 1$ (the so called INEL>0 sample). The charged-particle pseudorapidity density distribution is computed as $\mathrm{d}N_{\mathrm{ch}}/\mathrm{d}\eta = \alpha(1-\beta)\,\mathrm{d}N_{\mathrm{tracklets}}/\mathrm{d}\eta$, where α is the acceptance times the efficiency for a primary charged-particle to produce a tracklet, β is the contamination of reconstructed tracklets from combinatorial background, and $\mathrm{d}N_{\mathrm{tracklets}}/\mathrm{d}\eta$ is the pseudorapidity density distribution of tracklets. The primary charged-particles are defined as prompt particles produced in the proton-proton collision, including all the decay products, except those from weak decays of strange hadrons.

The transverse-momentum distribution is measured in the range $0.15 < p_{\mathrm{T}} < 20$ GeV/c and $|\eta| < 0.8$ for events with at least one charged particle in $|\eta| < 1$. Track candidates are selected with requirements on the number of space points in TPC used for tracking and on the quality of the track fit, as well as on the distance of closest approach to the reconstructed vertex.

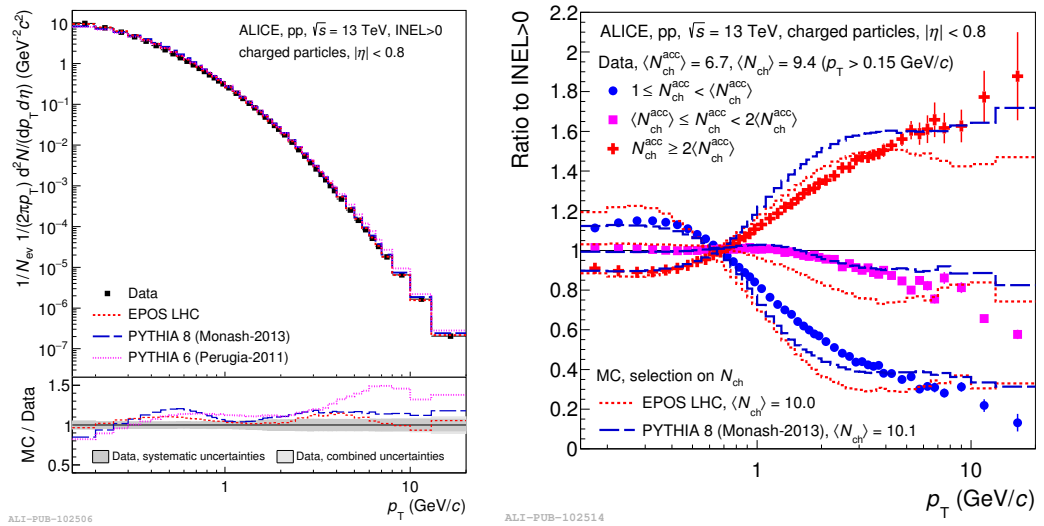

(a) (b)

Figure 2: Invariant charged-particle yield in the central pseudorapidity region $|\eta| < 0.8$ as a function of p_{T} normalised to INEL>0 events. Ratios of transverse-momentum distributions of charged particles in three intervals of multiplicities to the respective one for inclusive (INEL>0) collisions in the central pseudorapidity region $|\eta| < 0.8$. Figures are taken from [4].

A comprehensive summary of the contributions to the relative systematic uncertainties of the charged-particle pseudorapidity and transverse-momentum distributions can be found in [4]. The major contribution to the systematic uncertainties is due to the normalization to the physical event classes of INEL and INEL>0. In the case of the transverse-momentum distribution the primary contribution to the systematic uncertainties comes from the contamination of weak decays of strange hadrons at low momenta and from the detector acceptance and efficiency at higher momenta.

The average pseudorapidity densities shown in Fig. 1a, are 5.31 ± 0.18 and 6.46 ± 0.19, for the INEL and INEL>0 event classes, respectively. The result for INEL events is compared to the measurements in $|\eta| < 0.5$ by CMS Collaboration for inelastic collisions [8], which is in agreement with our measurement within the uncertainties. The average pseudorapidity density measured for the INEL>0 events in $|\eta| < 1$ is 6.61 ± 0.20, which is directly compared with the previously obtained INEL>0 results by ALICE at 7 TeV [7]. The results are also compared to the predictions of three different Monte Carlo generators: PYTHIA 6 (Perugia-2011 tune), PYTHIA 8 (Monash-2013 tune) and EPOS LHC for both the INEL and INEL>0 event classes. Overall, PYTHIA 6 provides the best predictions at 13 TeV both for what concerns the INEL and INEL>0 event classes. The charged-particle pseudorapidity density in $|\eta| < 0.5$ as a function of the centre-of-mass energy is shown in Fig. 1b for both the INEL and INEL>0 event classes, along with the lower energies results from other experiments. The energy dependence of $\langle \mathrm{d}N_{\mathrm{ch}}/\mathrm{d}\eta \rangle$ is parametrised by the power law as^b and fitted to data, where a and b are fit parameters: the best fit is obtained for $b = 0.103 \pm 0.002$

and $b = 0.111 \pm 0.004$ for the INEL and the INEL>0 event class, respectively.

The measured charged-particle p_{T} spectrum and its comparison to predictions from PYTHIA 6, PYTHIA 8 and EPOS LHC simulations are shown in Fig. 2a. All these event generators describes the p_{T} spectrum reasonably well. Both PYTHIA 8 and EPOS LHC models calculations show a similar pattern in the ratio to data, with discrepancies up to 15-20% while PYTHIA 6 turns out to overestimate particle production at high p_{T} (above 3 GeV/c). The ratio of p_{T} spectra to the inclusive (INEL>0) p_{T} spectrum is reported in Fig. 2b for three multiplicity intervals. The charged multiplicity is quoted in the same kinematic region as the spectrum, $|\eta| < 0.8$ and $0.15 < p_{\mathrm{T}} < 20$ GeV/c, using the measured track multiplicity $N_{\mathrm{ch}}^{\mathrm{acc}}$ for the data and the true multiplicity value N_{ch} known for the Monte Carlo events (PYTHIA 8 and EPOS LHC). The correlation of the spectrum with multiplicity is prominent over the whole p_{T} range and it becomes stronger at high p_{T}.

4 Conclusions

This contribution summarizes the first measurements of inclusive charged-particle production in proton-proton collisions at $\sqrt{s}$ = 13 TeV with the ALICE detector at LHC [4]. The pseudorapidity density distribution is measured for inelastic events (INEL) and events having at least one charged particle in the pseudorapidity interval $|\eta| < 1$ (INEL>0). The transverse-momentum distribution is measured in the range $0.15 < p_{\mathrm{T}} < 20$ GeV/c and in the central pseudorapidity region $|\eta| < 0.8$ for INEL>0 events. As expected the spectrum is significantly harder at $\sqrt{s}$ = 13 TeV than at $\sqrt{s}$ = 7 TeV; the hardness does also turn out to be correlated to the charged-particle multiplicity. In general the models tuned on the older LHC data provide a good predictivity for the $\langle \mathrm{d}N_{\mathrm{ch}}/\mathrm{d}\eta \rangle$ and p_{T} distribution measurements of charged particles at 13 TeV, the best tested model being PYTHIA 6 using the Perugia-2011 tune.

References

[1] I. M. Dremin and V. A. Nechitailo, *Phys. Rev. D* **84** (2011) 034026.

[2] D. d'Enterria *et al.*, *Astropart. Phys.* **35** (2011) 98–113.

[3] **ALICE** Collaboration, B. Abelev *et al.*, *Phys. Rev. Lett.* **110** no. 8, (2013) 082302.

[4] **ALICE** Collaboration, B. Abelev *et al.*, *Phys. Lett. B* **753** (2016) 319–329.

[5] **ALICE** Collaboration, K. Aamodt *et al.*, *JINST* **3** (2008) S08002.

[6] **ALICE** Collaboration, B. Abelev *et al.*, *Int. J. Mod. Phys.* **A29** (2014) 1430044.

[7] **ALICE** Collaboration, K. Aamodt *et al.*, *Eur. Phys. J.* **C68** (2010) 345–354.

[8] **CMS** Collaboration, V. Khachatryan *et al.*, `arXiv:1507.05915 [hep-ex]`.

[9] **ALICE** Collaboration, B. Abelev *et al.*, *Eur. Phys. J.* **C73** no. 12, (2013) 2662.

Recent measurement of underlying events

W.Y.Wang[1]

[1]Physics Department , Faculty of Science ,
National University of Singapore, Singapore
On behalf of the CMS Collaboration

A measurement of the underlying event (UE) activity is performed in proton-proton collisions at the centre-of-mass energy of 13 TeV . The measurement is performed using leading charged-particles as well as leading charged-particle jets as reference objects. A leading charged-particle or charged-particle jet is required to be produced in the central pseudorapidity region ($|\eta| < 2$) and with transverse momentum $p_t \geq 0.5$ ($p_t^{jet} \geq 1$) GeV for leading charged-particle (charged-particle jet) [1].

The data used in this analysis are selected from an unbiased sample of events whenever there is a beam crossing in the CMS detector. This corresponds to an integrated luminosity of 281 nb^{-1}. Events with exactly 1 primary vertex within 10 cm of the beamspot in the z-direction, 2 cm in the xy-plane ($\rho \leq 2$ cm), and at least 5 degrees of freedom ($dof > 4$) are chosen. Fake tracks from mis-reconstruction and secondary decays are removed by requiring the tracks to pass a selection based on a minimum fraction of consecutive hits and by requiring the impact parameter significance d_0/σ_{d_0} and the significance in the z-direction d_z/σ_{d_z} to each be less than 3. Only tracks with a relative uncertainty of $\sigma_{p_t}/p_t < 0.05$ are selected.

Jets are constructed by clustering reconstructed tracks/particles within the interval of $|\eta| < 2.5$ and with $p_t > 0.5$ GeV using the Seedless Infrared-Safe Cone (SISCone) jet algorithm [2] with a distance parameter of 0.5.

The UE activity is quantified in terms of the average multiplicity and scalar transverse momentum sum (Σp_t) densities of charged-particles (with $|\eta| < 2$ and $p_t \geq 0.5$ GeV) in the region orthogonal to the azimuthal direction of the leading charged-particle or jet, referred to as the transverse region. The densities of particles within an azimuthal opening angle of $60^\circ < |\Delta\phi| < 120^\circ$ with respect to the leading jet are defined as the transAVE densities.

The transverse region can be split into 2 halves depending on the sign of $\Delta\phi$. The transMAX (transMIN) densities are then defined as the densities in the transverse half with a higher (lower) activity. The transDIF density is then defined as the difference of transMAX and transMIN densities. The average Σp_t and particle densities are measured as function of the p_t of the leading particles and jets.

The measurement of the UE activity in terms of the transMAX, transMIN, and transDIF densities improves the differential power in the quantification of the activity coming from MPI. The transMIN activity is expected to largely contain radiation coming from MPI and the transDIF activity is more sensitive to initial- and final-state radiation. This differential power allows for improvements in the tuning of the model parameters describing the MPI.

Data correction is performed using a Bayesian unfolding method [3] which properly accounts for bin migration effects. The systematic uncertainty due to the model dependency (up to 8% in the lowest few bins in p_t^{jet}) of the correction method contributes the most to the total systematic uncertainty. The rest of the uncertainties come from PU (4%), fake mis-modelling (2%), impact parameter significance (0.8%), and vertex degree of freedom (1.5%). In general, the systematic uncertainties vary between the densities in the different regions (transAVE/transDIF/transMAX/transMIN), and as a function of p_t and p_t^{jet}.

The corrected distributions of the average particle and Σp_t densities as a function of the p_t of the leading jet/particle are compared with predictions by the Monte Carlo generator tunes PYTHIA8 (version 8.153) [4] CUETP8M1 and Monash [5], HERWIG++ (version 2.7.0) [6] CUETHS1, and EPOS (version 1.99) [7]. Generated events are passed through detector simulation using GEANT [8]. These various event generators differ in the treatment of initial- and final-state radiation, hadronisation, colour reconnections, and the regularisation of the infrared cross-section divergence (including that for MPI). PYTHIA uses the Lund string hadronisation model [9], EPOS uses a similar string fragmentation hadronisation model [10], while HERWIG uses a cluster hadronisation model [11]. Models for MPI are implemented assuming a Poissonian distribution of elementary partonic interactions, with an average number depending on the impact parameter of the hadronic collision [12, 13].

The transMAX and transMIN particle densities are shown in figure 1 as a function of p_t and p_t^{jet}. The transAVE and transDIF distributions are not shown as they can be obtained from the transMAX and transMIN densities. The agreement between the measurements and the simulations is quantified by the ratio plots shown in the bottom panels. The measurements are better described by the Monash tune of PYTHIA8. The PYTHIA8 CUETP8M1 describe the measurements within 10–20%. The predictions by the CUETHS1 tune of HERWIG fails in the low p_t region. EPOS describes the low p_t rising region well but fails to describe the plateau region by 20%. The amount of agreement between the simulations and the measured transAVE and transDIF densities, is similar to that of the average particle densities as described above. Distributions for the average Σp_t densities (not shown) also reveal similar behaviour.

In all plots, the densities increase sharply up to 5 (12–15) GeV and then rise slowly with increasing p_t (p_t^{jet}). The transMIN densities are flatter compared to the transMAX and transDIF (not shown) densities, whereas the transMAX and transDIF densities show a similar trend in the plateau region. Simulations describe the qualitative behavior of the measurements, i.e. the sharp rise and the flattening of the UE activity, and a larger rise in transMAX and transDIF in the plateau region. The level of agreement between simulations and the measurements falls within 10–20% in the plateau region but differs in the low p_t region. The sharp rise with p_t is interpreted in the MC models as due to an increase in the MPI contribution which reaches a plateau at high

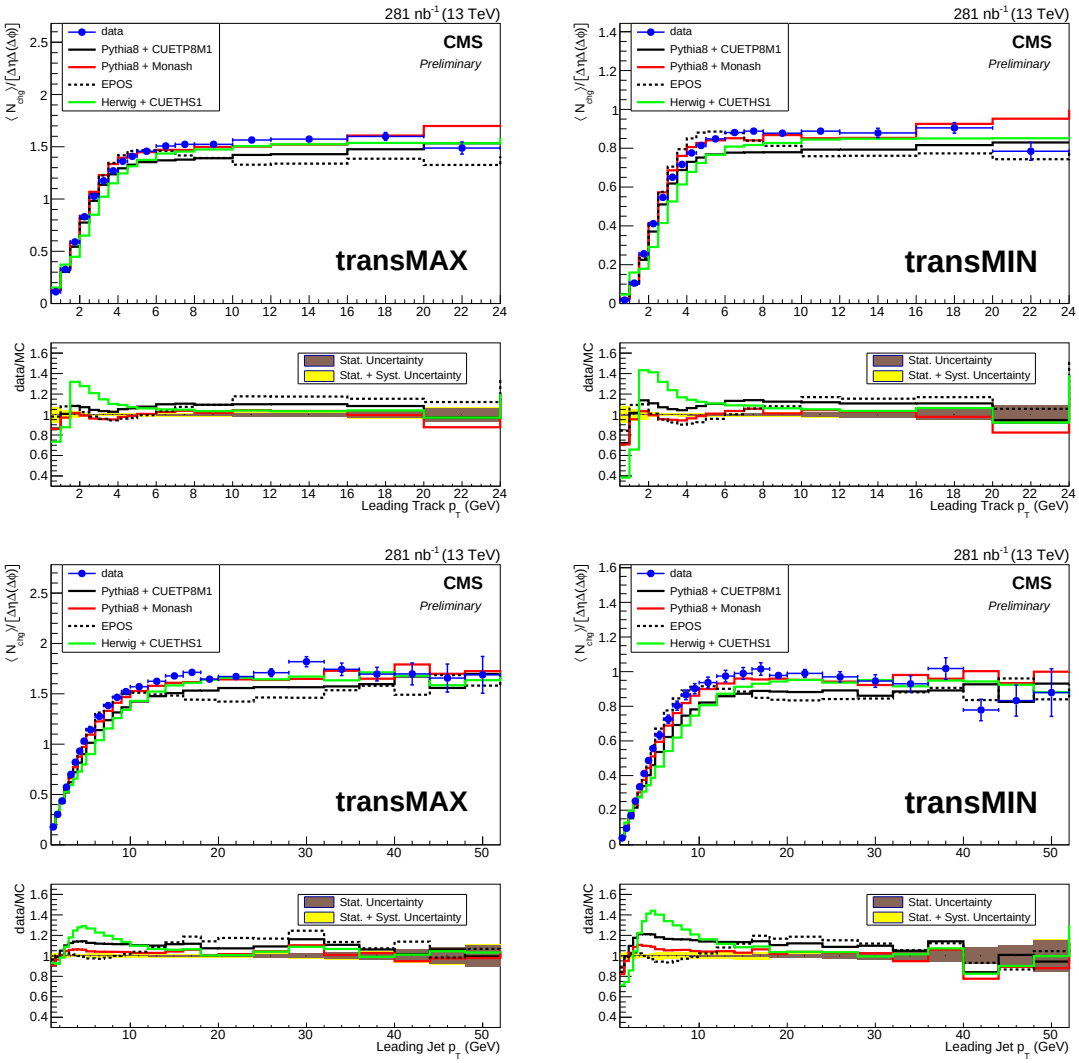

Figure 1: Comparisons of corrected (left column) transMAX and (right column) transMIN average particle densities with the various simulations as a function of (top row) p_t and (bottom row) p_t^{jet}. The error bar represents the statistical and systematic uncertainties added in quadrature. Bottom panels show the ratio of the simulation with the measurements. The brown band in the bottom plot represents the statistical uncertainty in the corrected data whereas the total uncertainty is shown in the yellow band.

p_t. A slow increase in large p_t region is mainly due to the increase in the initial- and final- state radiation contribution. As MPI activity is expected to be uniform in the whole phase-space, the transMIN densities capture mainly the activity coming from MPI whereas transDIF densities give the evolution of the radiation with p_t of the reference object.

Comparisons between various MC simulated samples and data across centre-of-mass energies of 0.9, 2.76, 7, and 13 TeV are made for transAVE as a function of p_t^{jet} as shown in figure 2. There is a strong rise in the UE activity as a function of the centre-of-mass energy as predicted by the MC tunes. This is attributed to an increase in the of number partons with smaller fractional momenta $x \sim 2p_t/\sqrt{s}$. The transMIN (not shown) densities exhibit a stronger $\sqrt{s}$ dependence than the transDIF (not shown) density, indicating that the activity coming from MPI grows more with $\sqrt{s}$ than that from ISR and FSR.

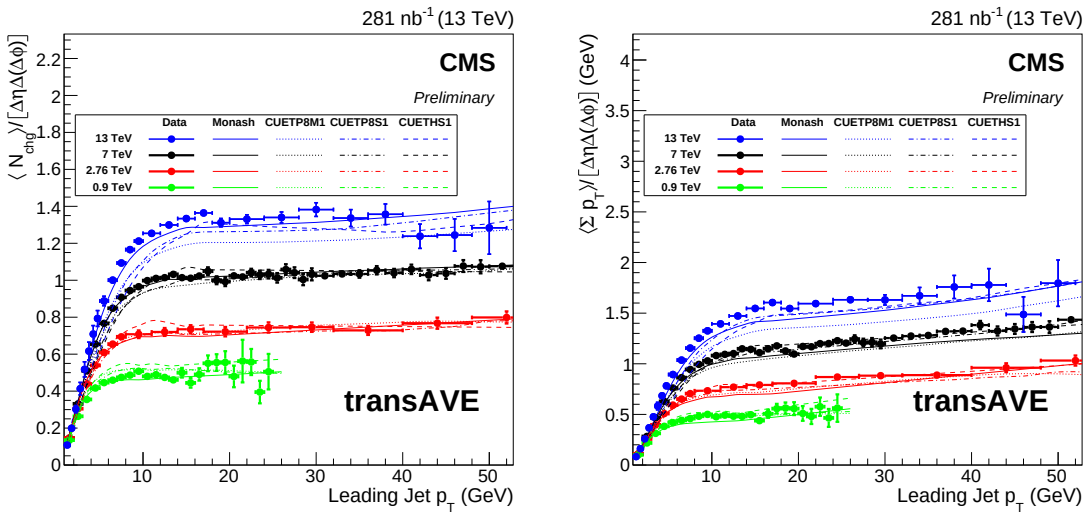

Figure 2: Comparisons of corrected transAVE (left) particle and (right) Σp_t densities with various simulations at $\sqrt{s} = 0.9$, 2.76, 7, and 13 TeV as a function of p_t^{jet}.

Acknowledgements

The author is grateful for the efforts by the analysis team, convenors, review commitee, the CMS Collaboration, and everyone else who had contributed to the analysis. Special thanks to Prof. A.H.Chan and Prof. C.H.Oh for their patient guidance and support.

References

[1] "Underlying Event Measurements with Leading Particles and Jets in pp collisions at $\sqrt{s} = 13$ TeV," *CMS Physics Analysis Summary*, **CMS-PAS-FSQ-15-007**(2015), URL https://cds.cern.ch/record/2104473/files/FSQ-15-007-pas.pdf.

[2] Gavin P. Salam and Grgory Soyez, "A practical seedless infrared-safe cone jet algorithm," *JHEP*, **05**(2007), 086, URL http://stacks.iop.org/1126-6708/2007/i=05/a=086.

[3] G. D'Agostini, "A multidimensional unfolding method based on Bayes' theorem," *Nucl. Instrum. Meth. A*, **362**(1995), 487, URL http://www.sciencedirect.com/science/article/pii/016890029500274X.

[4] Torbjorn Sjöstrand, Stephen Mrenna, and Peter Z. Skands, "A Brief Introduction to PYTHIA 8.1," *Comput. Phys. Commun.*, **178**(2008), 852, 0710.3820.

[5] P. Skands, S. Carrazza, and J. Rojo, "Tuning PYTHIA 8.1: the Monash 2013 tune," *Eur. Phys. J. C*, **74**(2014) (8), 3024, 1404.5630, URL http://dx.doi.org/10.1140/epjc/s10052-014-3024-y.

[6] M. Bähr, *et al.*, "Herwig++ physics and manual," *Eur. Phys. J. C*, **58**(2008), 639.

[7] T. Pierog and K. Werner, "EPOS Model and Ultra High Energy Cosmic Rays," *Proceedings of the XV International Symposium on Very High Energy Cosmic Ray Interactions (ISVHECRI 2008)*, **196**(2009), 102, 0905.1198.

[8] S. Agostinelli *et al.* (GEANT4), "GEANT4—a simulation toolkit," *Nucl. Instrum. Meth. A*, **506**(2003), 250.

[9] B. Andersson, G. Gustafson, G. Ingelman, and T. Sjöstrand, "Parton fragmentation and string dynamics," *Phys. Rept.*, **97**(1983), 31.

[10] H. J. Drescher and others, "Parton-based Gribov-Regge theory," *Phys. Rept.*, **350**(2001), 93, hep-ph/0007198.

[11] B. R. Webber, "A QCD model for jet fragmentation including soft gluon interference," *Nucl. Phys. B*, **238**(1984), 492.

[12] Torbjorn Sjöstrand and Maria Van Zijl, "Multiple parton-parton interactions in an impact parameter picture," *Phys. Lett. B*, **188**(1987), 149, URL http://www.sciencedirect.com/science/article/pii/0370269387907222.

[13] L. Frankfurt, M. Strikman, and C. Weiss, "Transverse nucleon structure and diagnostics of hard parton-parton processes at LHC," *Phys. Rev. D*, **83**(2011), 054012, URL http://link.aps.org/doi/10.1103/PhysRevD.83.054012.

Chapter 2

Working Group
Monte Carlo development and tuning

Convenors:

Andrzej Siódmok (HERWIG),
Tanguy Pierog (EPOS)

Recent PYTHIA 8 developments: Hard diffraction, Colour reconnection and $\gamma\gamma$ collisions

Ilkka Helenius, Jesper R. Christiansen, and Christine O. Rasmussen

Department of Astronomy and Theoretical Physics, Lund University, Sölvegatan 14A, SE-223 62 Lund, Sweden

1 Introduction

An overview of recent developments in PYTHIA 8 is given. First the new hard diffraction model, which is implemented as a part of the multiparton interactions (MPI) framework, is discussed. Then the new colour reconnection model, which includes beyond leading colour effects that can become important when MPI are present, is briefly reviewed. As a last topic an introduction is given to our implementation of photon-photon collisions. In particular photon PDFs, required modifications for the initial state radiation algorithm and beam remnant handling with photon beams is discussed.

2 Hard Diffraction

A model for soft diffraction has long been available in PYTHIA 8 and earlier versions [1, 2]. This model allows for $2 \to 2$ QCD processes at all $p_\perp$ scales, but is primarily intended for lower values of $p_\perp$. For truly hard diffractive processes, the new model for hard diffraction [3] was developed, not only for high-$p_\perp$ jets, but also allowing for $W^\pm, Z^0, H$ etc.

The model is based on the assumption that the proton PDF can be split into a diffractive and a nondiffractive part,

$$f_{i/\mathrm{p}}(x,Q^2) = f^{\mathrm{ND}}_{i/\mathrm{p}}(x,Q^2) + f^{\mathrm{D}}_{i/\mathrm{p}}(x,Q^2) \ \text{ with} \tag{1}$$

$$f^{\mathrm{D}}_{i/\mathrm{p}}(x,Q^2) = \int_x^1 \frac{\mathrm{d}x_{\mathbb{P}}}{x_{\mathbb{P}}}\, f_{\mathbb{P}/\mathrm{p}}(x_{\mathbb{P}})\, f_{i/\mathbb{P}}\left(\frac{x}{x_{\mathbb{P}}}, Q^2\right) \ , \tag{2}$$

with x and Q^2 the momentum fraction and virtuality of parton i, $x_{\mathbb{P}}$ and t the momentum fraction and virtuality of the Pomeron, and where the Pomeron flux $f_{\mathbb{P}/\mathrm{p}}(x_{\mathbb{P}}) = \int_{t_{\min}}^{t_{\max}} \mathrm{d}t\, f_{\mathbb{P}/\mathrm{p}}(x_{\mathbb{P}}, t)$, as t for the most part is not needed. The tentative probability for side A to be diffractive is then given by the ratio of diffractive to inclusive PDFs,

$$\mathcal{P}^{\mathrm{D}}_A = \frac{f^{\mathrm{D}}_{i/B}(x_B,Q^2)}{f_{i/B}(x_B,Q^2)} \quad \text{for} \quad AB \to XB \tag{3}$$

with a similar equation for side B. The model further implements a dynamical rapidity gap survival, cf. Fig. 1. On an event-by-event basis the possibility for additional MPIs in the pp system is evaluated, and if no such MPIs are found, then the event is diffractive. Only then is the $\mathbb{P}\mathrm{p}$ system set up and a full evolution is performed in this subsystem, along with the hadronization of the colour strings in the event.

The dynamical gap survival introduces an additional suppression of the diffractive events, such that the total probability for hard diffraction drops from $\sim 10\%$ to $\sim 1\%$, exact numbers depending on parametrization of $\mathbb{P}$ flux and PDF as well as the free parameters of the MPI framework in PYTHIA 8. The new model is compatible with suppression factors measured at the LHC.

3 Colour Reconnection

The colour reconnection (CR) refers to a phenomenon where the colour strings formed during the hard process and parton shower generation can reconnect and form a different configuration prior to hadronization. A new model for CR in PYTHIA 8 was introduced in Ref. [4]. The model is based on three main principles: use of SU(3) colour rules to determine if the strings are colour compatible, a simplistic space-time picture to check whether the two colour strings can be causally connected, and minimization of string length measure λ to find which colour configurations are preferred. In addition to simple colour strings between a quark and an antiquark, the new model includes also junction structures which can connect three (anti)quarks together. As the junction structures are related to baryons, an enhanced baryon production can be expected.

Natural observables to study the CR effects are baryon-to-meson ratios. The parameters related to the new CR model was fixed using the CMS data for the rapidity dependence of the Λ/K^0_S ratio, while keeping the rate in $\mathrm{e^+e^-}$ collisions unaffected. Without further tuning also the $p_\perp$ dependence of this ratio can be described more accurately than with the old PYTHIA model, although there still exists some discrepancy for $p_\perp > 5$ GeV/c.

A novel way to constrain different CR models is to study the multiplicity dependence of the baryon-to-meson ratios [5]. The old PYTHIA model is more or less flat with multiplicity but – due to the junction structures – the new model predicts an enhancement for baryon production with higher multiplicities. A very interesting observable is the $p_\perp$ dependence of Λ/K ratio in different multiplicities, shown in Fig. 2. In the lowest multiplicity bin the ratio is flat above $p_\perp = 2$ GeV/c, but with higher multiplicities there is a growing enhancement at intermediate $p_\perp$, flattening again at $p_\perp \gtrsim 8$ GeV/c. Also, the peak of the ratio shifts towards higher values of $p_\perp$ with higher multiplicities – a behaviour that is typically connected to collective flow in heavy-ion collisions. To sort out the physical origin of these kind of observations, further studies are of great interest.

4 Photon-photon Collisions

The $\gamma\gamma$ collisions give access to several interesting hard processes and provide an additional test of QCD factorization. A further motivation to study these collisions is provided by the future $\mathrm{e^+e^-}$ experiments, where the $\gamma\gamma$ interactions will generate background processes that influence to the physics potential of future measurements.

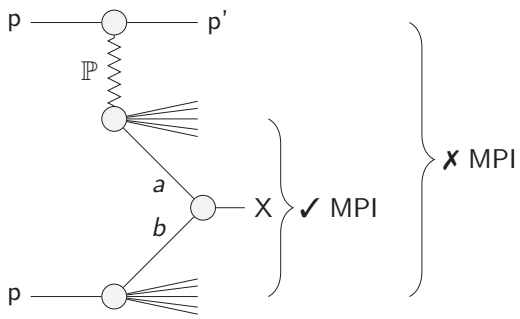

Figure 1: The dynamical gap survival implemented in PYTHIA 8. The model does not allow for MPIs in the pp system, but allows for additional MPIs in the ℙp system.

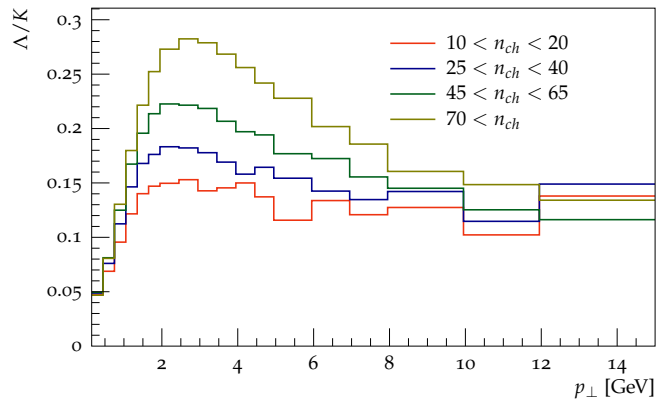

Figure 2: Transverse momentum dependence of the Λ/K ratio for different multiplicities in p+p collisions.

An option to simulate $\gamma\gamma$ collisions with PYTHIA 8 have been added with the 8.215 release. The new implementation is not just a repetition of the framework included in PYTHIA 6 [1] but a new – more robust – machinery has been under development [6]. Currently hard processes with parton showers and hadronization of resolved $\gamma\gamma$ interactions can be generated for real photons, but MPIs and soft processes are not included. Here the key differences to the hadronic collisions are briefly described.

4.1 Evolution equations and parton showers

The partonic structure of resolved photons is described by the PDFs in a similar manner as for hadrons. The scale evolution of the photon PDFs is given by

$$\frac{\partial f_i^\gamma(x,Q^2)}{\partial \log(Q^2)} = \frac{\alpha_{\mathrm{EM}}}{2\pi} e_i^2 P_{i\gamma}(x) + \frac{\alpha_s(Q^2)}{2\pi} \sum_j \int_x^1 \frac{\mathrm{d}z}{z} P_{ij}(z)\, f_j(x/z, Q^2), \tag{4}$$

where the first term on the right hand side corresponds to the $\gamma \to q\bar{q}$ splitting of the beam photon and the second to the usual partonic splittings. Due to the first term, the scale evolution increases the quark PDFs over the whole x region and thus increases the large-x quark PDFs in photons compared to quark PDFs in hadrons.

As the parton shower is generated using the DGLAP equations, the PYTHIA algorithm [7] must be extended accordingly by including a possibility to find the original beam photon during the generation of the initial state radiation (ISR). If the beam photon is found, no further ISR evolution is allowed for the beam.

4.2 Beam remnants

The beam remnants describe the leftovers of the beam particle after the interaction, for details of PYTHIA 8 implementation see Ref. [8]. Unlike in the case of protons, the valence content of photons

is not known beforehand. To fix for the valence content the PDFs are decomposed into sea and valence contributions. These are then used to decide whether the parton taken from the beam was a valence parton or not. If it was a valence quark, the remnant is simply the corresponding (anti)quark and if not, the valence content is sampled according to the PDFs. After the valence content is fixed, a minimal number of partons are added to make sure that the flavour and colour are preserved in an event. If the ISR algorithm ends up at the beam photon, there is no need to add any remnant partons for the given beam.

As the quark PDFs for photons have a large contribution also from large values of x, it may happen that there is no room to add the beam remnants with non-zero masses. Also the parton shower can lead to a situation where the remnants can not be constructed due to the lack of invariant mass available for the remnants. These cases are rejected during the event generation to make sure that only events with appropriate remnants are generated.

Acknowledgements

Work has been supported by the MCnetITN FP7 Marie Curie Initial Training Network, contract PITN-GA-2012-315877 and has received funding from the European Research Council (ERC) under the European Union's Horizon 2020 research and innovation programme (grant agreement No 668679).

References

[1] Torbjörn Sjöstrand, Stephen Mrenna, and Peter Z. Skands, "PYTHIA 6.4 Physics and Manual," *JHEP*, **05**(2006), 026, hep-ph/0603175.

[2] Torbjörn Sjöstrand, *et al.*, "An Introduction to PYTHIA 8.2," *Comput. Phys. Commun.*, **191**(2015), 159, arXiv:1410.3012.

[3] Christine O. Rasmussen and Torbjörn Sjöstrand, "Hard Diffraction with Dynamic Gap Survival," *JHEP*, **02**(2016), 142, 1512.05525.

[4] Jesper R. Christiansen and Peter Z. Skands, "String Formation Beyond Leading Colour," *JHEP*, **08**(2015), 003, arXiv:1505.01681.

[5] Christian Bierlich and Jesper Roy Christiansen, "Effects of color reconnection on hadron flavor observables," *Phys. Rev.*, **D92**(2015) (9), 094010, arXiv:1507.02091.

[6] Ilkka Helenius and Torbjörn Sjöstrand, *Work in progress*, (2016).

[7] Torbjörn. Sjöstrand and Peter Z. Skands, "Transverse-momentum-ordered showers and interleaved multiple interactions," *Eur. Phys. J.*, **C39**(2005), 129, hep-ph/0408302.

[8] Torbjörn. Sjöstrand and Peter Z. Skands, "Multiple interactions and the structure of beam remnants," *JHEP*, **03**(2004), 053, hep-ph/0402078.

On the impact of nonperturbative parton correlations on the rate of double parton scattering

Sergey Ostapchenko[1,2]

[1]Frankfurt Institute for Advanced Studies, 60438 Frankfurt am Main, Germany
[2]D.V. Skobeltsyn Institute of Nuclear Physics, Moscow State University, 119992 Moscow, Russia

1 Introduction

The relative rate of double parton scattering (DPS) may be quantified by the so-called effective cross section defined (here, for the production of two dijets in proton-proton collisions) as

$$\sigma_{pp}^{\rm eff}(s,p_{\rm t}^{\rm cut}) = \frac{1}{2}\,\frac{\left[\sigma_{pp}^{\rm 2jet}(s,p_{\rm t}^{\rm cut})\right]^2}{\sigma_{pp}^{\rm 4jet(DPS)}(s,p_{\rm t}^{\rm cut})}\,, \tag{1}$$

where $\sigma_{pp}^{\rm 2jet}(s,p_{\rm t}^{\rm cut})$ is the inclusive cross section for the production of a pair of jets of transverse momentum $p_{\rm t} > p_{\rm t}^{\rm cut}$, $\sigma_{pp}^{\rm 4jet(DPS)}(s,p_{\rm t}^{\rm cut})$ is the cross section for DPS production of two dijets of $p_{\rm t} > p_{\rm t}^{\rm cut}$, (1/2) is a symmetry factor, and s is the center-of-mass energy squared.

While $\sigma_{pp}^{\rm 2jet}(s,p_{\rm t}^{\rm cut})$ depends on the usual parton momentum distribution functions (PDFs), $\sigma_{pp}^{\rm 4jet(DPS)}$ involves generalized 2-parton distributions ($_2$GPDs) [1–3]. In impact parameter representation, $_2$GPD $F^{(2)}_{I_1I_2}(x_1,x_2,q_1^2,q_2^2,\Delta b)$ describes the momentum distribution of a pair of partons I_1 and I_2 probed at the virtuality scales q_1^2 and q_2^2, separated by the transverse distance Δb.

In the simplest approach, one neglects multi-parton correlations and expresses $_2$GPDs as a convolution of generalized parton distributions (GPDs) $G_I(x,q^2,b)$ for two independent partons. In particular, assuming the b-dependence to factorize, for the respective DPS cross section one has $\sigma_{pp}^{\rm 4jet(2v2)}(s,p_{\rm t}^{\rm cut}) \propto \left[\sigma_{pp}^{\rm 2jet}(s,p_{\rm t}^{\rm cut})\right]^2$ and the corresponding effective cross section $\sigma_{pp}^{\rm eff(2v2)}$ appears to be a universal constant which characterizes spacial distribution of partons in the proton.

In reality, one has to take into consideration Gribov's transverse diffusion which produces a larger transverse spread for partons at smaller x [4]. Moreover, the rate of the diffusion is slower for partons of larger virtuality [5]. Thus, one expects $\sigma_{pp}^{\rm eff(2v2)}$ to increase with s due to the longer rapidity range available for the parton evolution, resulting in a larger transverse spread, and to decrease with $p_t^{\rm cut}$ - due to a smaller part of the parton cascade developing in the low q^2 region.

Recently, it has been demonstrated that substantial corrections to this simple picture arise from parton correlations induced by a perturbative parton splitting [1–3,6,7]. In the latter case, two (say, projectile) partons participating in the two hard processes are no longer independent but emerge from the same "parent" parton of relatively high virtuality $|q^2| > Q_0^2 \gg \Lambda^2_{\rm QCD}$ and are close to each other in the transverse plane. The respective "$(2{\rm v}1)_{\rm h}$" contribution to $\sigma_{pp}^{4{\rm jet}({\rm DPS})}$, while being suppressed by an additional power of $\alpha_{\rm s}$, receives strong collinear enhancements [1] and, for sufficiently high $p_{\rm t}^{\rm cut}$ and $Q_0 \sim 1$ GeV, $\sigma_{pp}^{4{\rm jet}(2{\rm v}1)_{\rm h}}$ appears to be comparable to $\sigma_{pp}^{4{\rm jet}(2{\rm v}2)}$, thus reducing the effective cross section [Eq. (1)] by a factor of two [2,8].

For decreasing $p_{\rm t}^{\rm cut}$, the contribution of the perturbative parton splitting goes down due to the reduced kinematic space for the parton evolution. However, as suggested in [2,9], additional important corrections to the DPS cross section should arise from nonperturbative parton correlations, e.g. ones related to nonperturbative parton splitting at $|q^2| < Q_0^2$. In the following, we estimate this "soft splitting" contribution, $\sigma_{pp}^{4{\rm jet}(2{\rm v}1)_{\rm s}}$, in the Reggeon Field Theory framework [10], as implemented in the QGSJET-II-04 model [11]. Treating soft parton evolution at $|q^2| < Q_0^2$ as a phenomenological soft Pomeron emission, this soft parton splitting is described as a triple-Pomeron interaction, as discussed in more detail in [12]. In numerical calculations we use the default parameters of QGSJET-II-04, in particular, for the "soft-hard" separation scale we have $Q_0^2 = 3\,{\rm GeV}^2$.

2 Results and discussion

In Fig. 1 (left), we plot by solid lines $\sigma_{pp}^{\rm eff}$ for the production of two dijets of transverse momenta $p_{\rm t}^{\rm jet} > p_{\rm t}^{\rm cut}$ for two choices of $p_{\rm t}^{\rm cut}$, integrated over the phase space. More specifically, $\sigma_{pp}^{\rm eff}$ is calculated according to Eq. (1), taking into account all the discussed contributions to $\sigma_{pp}^{4{\rm jet}({\rm DPS})}$, i.e. $\sigma_{pp}^{4{\rm jet}({\rm DPS})} = \sum_\alpha \sigma_{pp}^{4{\rm jet}(\alpha)}$, where $\alpha = (2{\rm v}2), (2{\rm v}1)_{\rm s}, (2{\rm v}1)_{\rm h}$. In addition, we show by dashed lines the effective cross section as obtained by considering the simplest (2v2) DPS configuration only, $\sigma_{pp}^{{\rm eff}(2{\rm v}2)} = \frac{1}{2}\left[\sigma_{pp}^{2{\rm jet}}\right]^2 / \sigma_{pp}^{4{\rm jet}(2{\rm v}2)}$. For comparison with earlier studies, we repeat the above calculations for the case of central ($\eta = 0$) production of a pair of dijets of fixed transverse momentum $p_{\rm t}^{\rm jet}$, the results being plotted in Fig. 1 (right). Looking first at $\sigma_{pp}^{{\rm eff}(2{\rm v}2)}$ shown by the dashed lines in Fig. 1, we clearly see the trends discussed in the Introduction and already observed in previous studies [2,8]: the respective effective cross section increases with $\sqrt{s}$ and decreases with jet $p_{\rm t}$. The energy rise is due to the increasing rapidity interval for the parton evolution, hence, also an extended rapidity range for the soft ($|q^2| < Q_0^2$) evolution, which results in a larger parton transverse spread. The decrease of $\sigma_{pp}^{\rm eff}$ with increasing jet $p_{\rm t}$ for the same $\sqrt{s}$ is caused by a reduction of the soft part of the parton evolution. In turn, shorter soft evolution produces a smaller transverse spread of partons and leads to a smaller effective cross section. Taking into account the contributions of the soft and hard parton splitting substantially reduces the energy and $p_{\rm t}^{\rm jet}$ dependencies of $\sigma_{pp}^{\rm eff}$ in the very high energy limit, as shown by the solid lines in Fig. 1.

In Fig. 2, we plot the calculated $p_{\rm t}^{\rm cut}$ dependence (at $\sqrt{s} = 13$ TeV) and the energy dependence (for $p_{\rm t}^{\rm cut} = 50\,{\rm GeV/c}$) of the ratio of the (2v1) to (2v2) contributions to the DPS cross section

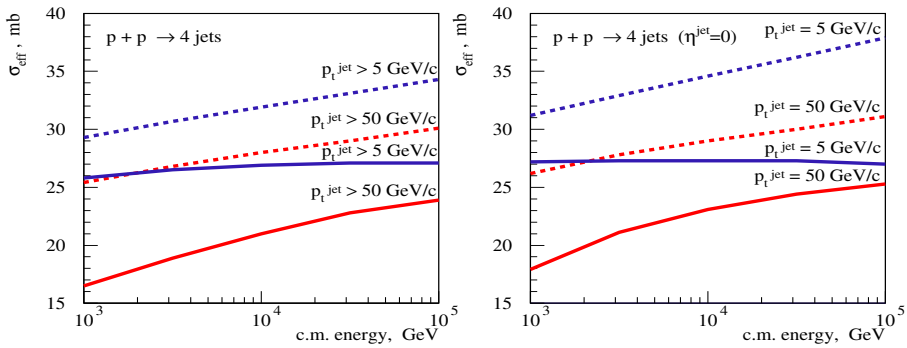

Figure 1: Energy dependence of the effective cross section for the production of two dijets in double parton scattering. Left: for jet transverse momenta $p_{\rm t}^{\rm jet} > 5$ GeV/c and $p_{\rm t}^{\rm jet} > 50$ GeV/c (as indicated in the plots), integrated over the phase space. Right: for fixed $p_{\rm t}^{\rm jet} = 5$ and 50 GeV/c and $\eta^{\rm jet} = 0$. Solid lines - both the $(2{\rm v}2)$ and $(2{\rm v}1)$ contributions to DPS taken into account, dashed lines - only the $(2{\rm v}2)$ contribution considered.

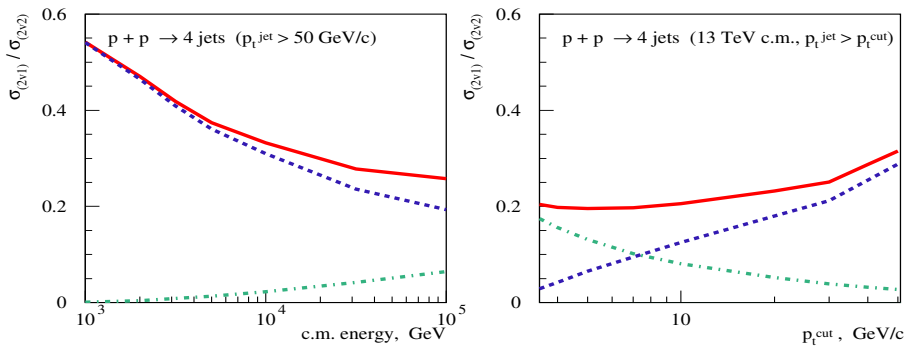

Figure 2: Energy dependence for $p_{\rm t}^{\rm cut} = 50$ GeV/c (left) and $p_{\rm t}^{\rm cut}$ dependence for $\sqrt{s} = 13$ TeV (right) of the ratio of the (2v1) to (2v2) contributions to the DPS cross section for double dijet ($p_{\rm t}^{\rm jet} > p_{\rm t}^{\rm cut}$) production (solid) and partial contributions to this ratio from hard (dashed) and soft (dot-dashed) parton splitting mechanisms.

for the production of two dijets of $p_{\rm t}^{\rm jet} > p_{\rm t}^{\rm cut}$, $R_{(2{\rm v}1)} = \left[\sigma_{pp}^{4{\rm jet}(2{\rm v}1)_{\rm s}} + \sigma_{pp}^{4{\rm jet}(2{\rm v}1)_{\rm h}}\right] / \sigma_{pp}^{4{\rm jet}(2{\rm v}2)}$. The partial contributions to this ratio from soft, $R_{(2{\rm v}1)_{\rm s}} = \sigma_{pp}^{4{\rm jet}(2{\rm v}1)_{\rm s}} / \sigma_{pp}^{4{\rm jet}(2{\rm v}2)}$, and hard, $R_{(2{\rm v}1)_{\rm h}} = \sigma_{pp}^{4{\rm jet}(2{\rm v}1)_{\rm h}} / \sigma_{pp}^{4{\rm jet}(2{\rm v}2)}$, parton splitting are shown as well. The plot in Fig. 2 (right) clearly demonstrates the increasing importance of the contribution of the nonperturbative parton splitting when jet $p_{\rm t}$ decreases. In turn, Fig. 2 (left) reveals the different energy behavior of $R_{(2{\rm v}1)_{\rm s}}$ and $R_{(2{\rm v}1)_{\rm h}}$. Indeed, $R_{(2{\rm v}1)_{\rm s}}$ exhibits a noticeable energy rise, which is mostly due to the increasing rapidity range available for parton evolution. In contrast, $R_{(2{\rm v}1)_{\rm h}}$ is gradually reduced with increasing energy. This is mainly because the contribution of the perturbative parton splitting to ${}_2$GPDs of gluons is effectively one $\ln x$ short in the low x limit, compared to the case of two independent parton

cascades,[1] as discussed previously in Refs. [2, 9] (see e.g. Fig. 2 in [9]). An additional reduction arises due to color fluctuations in the interacting protons and partons' transverse diffusion [12].

It is noteworthy that a number of other effects contribute to the uncertainty of the hard splitting contribution and are partly responsible for the much smaller values of our $R_{(2v1)_h}$, compared to previous calculations [2, 8]. For example, our choice of the factorization scale, $M_F^2 = p_t^2/4$, shortens somewhat the kinematic range available for the perturbative parton evolution, compared to the standard choice ($M_F^2 = p_t^2$), which reduces the respective collinear enhancements. Another effect is the sensitivity of $R_{(2v1)_h}$ to the chosen functional form for the two-gluon form factor: replacing the dipole ansatz used in [2] by a Gaussian reduces $R_{(2v1)_h}$ by $\simeq 17\%$ [see their Eqs. (19-21)]. Additionally, the relative importance of the perturbative parton splitting for DPS depends noticeably on both the large and small x behavior of gluon PDF, $g(x, Q_0^2)$. A steeper low x rise of $g(x, Q_0^2)$ would enhance the (2v2) contribution, compared to $(2v1)_h$, and thus reduce $R_{(2v1)_h}$ (see Eq. (5) of Ref. [2]). On the other hand, a harder large x shape of the gluon PDF would enhance the hard splitting contribution, while leaving the (2v2) contribution practically unchanged.

Acknowledgements

The author acknowledges useful discussions with B. Blok, M. Strikman, and other participants of MPI-2015. This work was supported by Deutsche Forschungsgemeinschaft (project OS 481/1).

References

[1] B. Blok, Yu. Dokshitzer, L. Frankfurt, and M. Strikman, *Phys. Rev.*, **D83**(2011), 071501.

[2] B. Blok, Yu. Dokshitzer, L. Frankfurt, and M. Strikman, *Eur. Phys. J.*, **C74**(2014), 2926.

[3] J. R. Gaunt, *JHEP*, **1301**(2013), 042.

[4] L. Frankfurt and M. Strikman, *Phys. Rev.*, **D66**(2002), 031502(R).

[5] L. Frankfurt, M. Strikman and C. Weiss, *Phys. Rev.*, **D69**(2004), 114010.

[6] A. M. Snigirev, *Phys. Rev.*, **D81**(2010), 065014.

[7] M. G. Ryskin and A. M. Snigirev, *Phys. Rev.*, **D83**(2011), 114047.

[8] J. R. Gaunt, R. Maciula and A. Szczurek, *Phys. Rev.*, **D90**(2014), 054017.

[9] B. Blok, Yu. Dokshitzer, L. Frankfurt, and M. Strikman, arXiv:1206.5594 [hep-ph].

[10] V. N. Gribov, *Sov. Phys. JETP*, **26**(1968), 414.

[11] S. Ostapchenko, *Phys. Rev.*, **D83**(2011), 014018.

[12] S. Ostapchenko and M. Bleicher, arXiv:1511.06784 [hep-ph].

[1] *In the case of the hard parton splitting, there is a single convolution with the gluon PDF at the initial scale Q_0^2.*

Towards Diffraction in Herwig

Stefan Gieseke[1], Frashër Loshaj[1], and Miroslav Myska[2]

[1]Institute for Theoretical Physics, Karlsruhe Institute of Technology
[2]Czech Technical University in Prague, FNSPE, Brehova 7, Prague

The multiple parton interactions (MPI) models in Monte Carlo generators are crucial in explaining many observables in hadron collisions. For a recent review of Monte Carlo generators see [1]. One can view the incoming hadrons as bunches of incoming partons, where many scatterings between them can take place. One of the motivations for considering the MPI is the fact that the inclusive jet cross section, calculated in the usual perturbative QCD formalism, exceeds the total cross section at moderate values of the center of mass energy (see for example [2]). A resolution to this problem is to use MPI, where one considers the luminosity of collided particles [3, 4] to factorize in an impact parameter dependent factor and the usual PDFs. One can parametrize the average multiplicity of multiple hard scatterings as a function of the cross section and an impact parameter dependent function - the overlap function. One can then use the eikonal model to parametrize the amplitude of multiple scattering as is done in Herwig [5].

Soft MPI in Herwig is simulated using the eikonal model as well. The kinematics of the outgoing soft partons is implemented by generic two-to-two processes with colour connections between them and the rest of the process explicitly specified. The purpose of this model was to describe minimum bias data at central pseudorapidity and small pseudorapidity gaps. Although the model was not expected to describe events with large pseudorapidity gaps, it was surprising to see that it gives an enhancement, rather than a depletion of those events. This can be seen in a recent measurement by ATLAS [6], shown in Fig. 1, where the differential cross section versus the forward pseudorapidity is shown. The forward pseudorapidity gap is defined as the larger of two pseudorapidities from the last particle to the edge of the detector.

The enhancement seems to be larger when the colour reconnection model is switched on. The colour reconnection model in Herwig creates different cluster configurations from the original colour topology in order to minimize the sum of the cluster masses [7]. This procedure seems to produce large pseudorapidity gaps, partly due to the splitting of large clusters into smaller ones, which end up being too forward in pseudorapidity.

In what follows we will address this issue. It is well known that the large pseudorapidity gaps should come from diffractive events. The differential cross section in $\Delta\eta^F$, using Regge phenomenology, should behave like $\sim\ e^{\Delta\eta^F(\alpha_{\mathbb{P}}(0)-1)}$ (see [8] for a review), where $\alpha_{\mathbb{P}}(0)$ is the

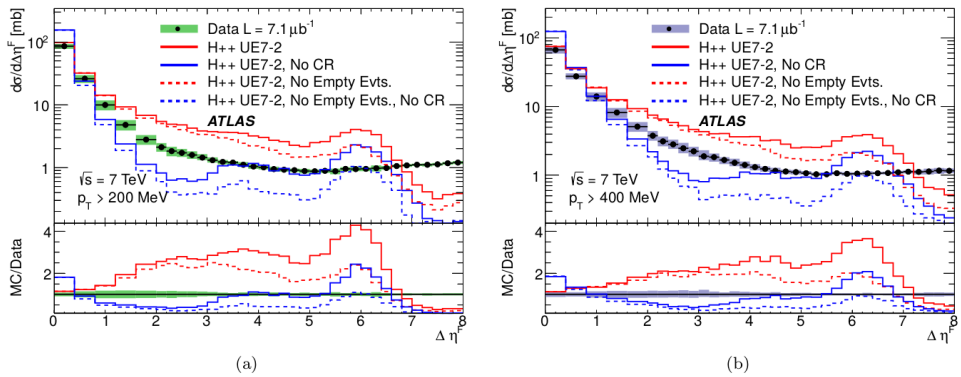

Figure 1: Inelastic differential cross section versus forward pseudorapidity gap $\Delta\eta^F$ taken from [6].

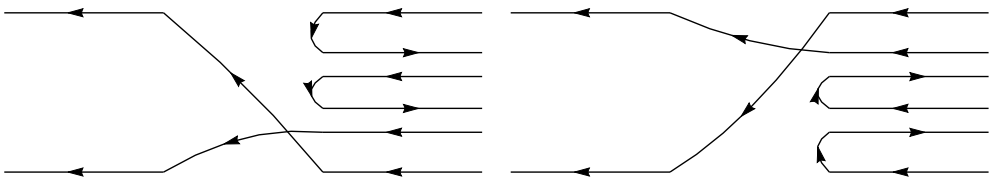

Figure 2: Colour connection topologies with small pseudorapidity gaps.

pomeron intercept and its value is close to 1. This explains the almost constant value at large $\Delta\eta^F$. The differential cross section for nondiffractive events (at small $\Delta\eta^F$) behaves like $\sim e^{-\Delta\eta^F}$.

In order to get the proper behaviour of the cross section we have to consider separately the non-diffractive and diffractive parts. To get the correct non-diffractive cross section, we have to modify the existing colour connections between the soft partons and proton remnants in the soft MPI model. An example of a topology giving the required suppression of large gaps is given in Fig. 2.

Arrows pointing to the (left) right, represent an outgoing (anti) colour line. The top and bottom lines represent proton remnants which are connected to either soft partons or the other remnant. Contributions from different classes of colour topologies denoted by letters A,H, etc, are shown in Fig. 3. We notice that none of the topologies gives the required exponential fall off. This behaviour may be obtained by changes in the colour reconnection model in restricting reconnection of forward clusters, but also more work is needed to understand better the colour connections themselves. This concludes our discussion of the non-diffractive cross section.

We next move to the generation of diffractive events. Diffraction is implemented using the results from Regge theory and the cross sections are given in the familiar form, for single diffraction

$$\frac{d^2\sigma^{SD}}{dM^2dt} = \frac{1}{16\pi^2 s}|g_{\mathbb{P}}(t)|^2 g_{\mathbb{P}}(0) g_{\mathbb{P}\mathbb{P}\mathbb{P}}(0) \left(\frac{s}{M^2}\right)^{2\alpha_{\mathbb{P}}(t)-1} \left(M^2\right)^{\alpha_{\mathbb{P}}(0)-1}, \quad (1)$$

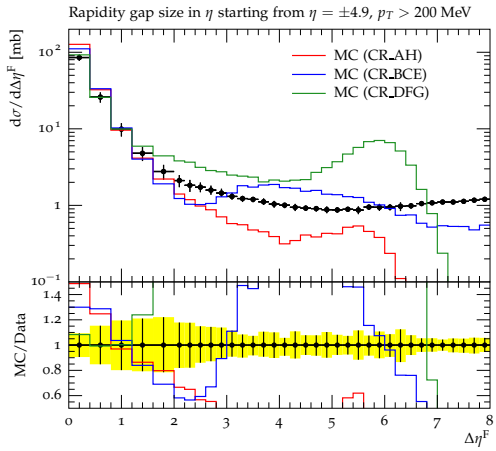

Figure 3: Differential cross section in forward pseudorapidity gap $\Delta\eta^F$ in Herwig using different topologies of colour.

and double diffraction

$$\frac{d^3\sigma^{DD}}{dM_1^2 dM_2^2 dt} = \frac{1}{16\pi^3 s} g_{\mathbb{P}}^2(0) g_{\mathbb{P}\mathbb{P}\mathbb{P}}^2(0) \left(\frac{s}{M_1^2 M_2^2}\right)^{2\alpha_{\mathbb{P}}(t)-1} \left(M_1^2\right)^{\alpha_{\mathbb{P}}(0)-1} \left(M_2^2\right)^{\alpha_{\mathbb{P}}(0)-1}, \tag{2}$$

(for an extensive review see [8]) where $\alpha_{\mathbb{P}}(t) = \alpha_{\mathbb{P}}(0) + \alpha' t$ with $\alpha_{\mathbb{P}}(0)$ and α' being the pomeron intercept and slope respectively, $g_{\mathbb{P}} = g_{p\mathbb{P}}$ is the proton pomeron coupling and $g_{\mathbb{P}\mathbb{P}\mathbb{P}}$ is the triple-pomeron coupling. The events are generated using a matrix element which implements the two-to-two body kinematics from the cross sections above. Namely, we implement processes $pp \to p^* p$, $pp \to pp^*$ and $pp \to p^* p^*$, where p^* is the dissociated proton. The dissociation is simulated by a cluster made up of a quark and a diquark. We first consider an isotropic decay of the dissociated proton into quark and diquark. The preliminary result is shown in Fig. 4, left. In this case we notice a quick fall off of the cross section for small $\Delta\eta^F$, which should be constant for a significant range. We also consider the case when the quark is collinear with the outgoing dissociated proton. In this case the hadronization effects populate the region of small forward pseudorapidity gap as shown in Fig. 4, right. The cluster hadronization seems to give better results in this case, but not exactly as expected, since the constant behaviour of the cross section doesn't extend to low values of $\Delta\eta^F$ and hadronization effects start at very high $\Delta\eta^F$. An improvement could come from considering the dissociation into quark, diquark and gluon, since this scenario allows for more isotropic distribution of final state particles and it could shift hadronization effects at very low $\Delta\eta^F$ as expected.

In conclusion, we have shown that large pseudorapidity gaps appearing in minimum bias results in Herwig can be tamed by introducing new colour connection topologies for soft interactions and modifying the colour reconnection model. Events with final state particles in the forward pseudorapidity region should be described properly using diffraction. We have shown how one can implement diffraction in Herwig and some preliminary results.

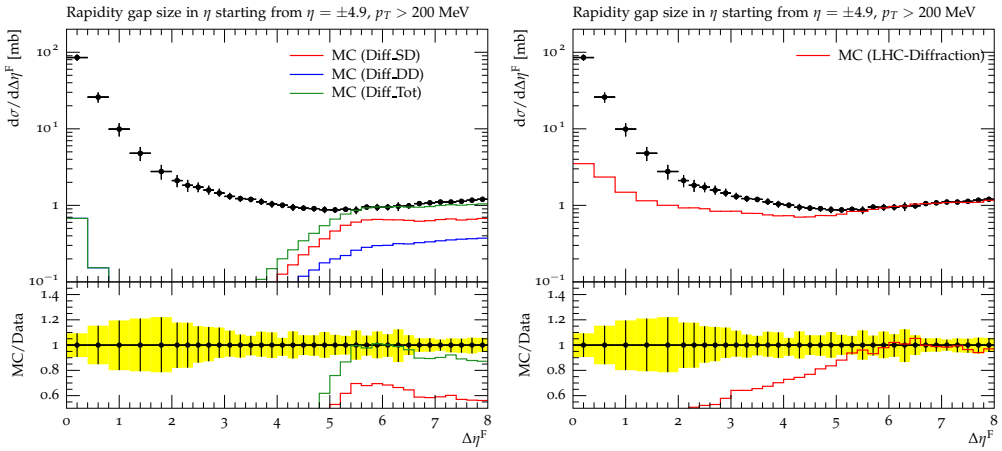

Figure 4: Single and double diffractive contribution to differential cross section in forward pseudorapidity gap compared to the measurement taken from [6]. Left: diffraction with isotropic decay of dissociated proton. Single and double diffraction shown separately. Right: sum of single and double diffractive events in the case when quark and diquark are collinear with outgoing dissociated proton.

Acknowledgements

The authors are grateful to A. Siodmok and M. Seymour for useful discussions. This work was supported in part by the European Union as part of the FP7 Marie Curie Initial Training Network MCnetITN (PITN-GA-2012-315877).

References

[1] Andy Buckley *et al.*, "General-purpose event generators for LHC physics," *Phys. Rept.*, **504**(2011), 145, 1101.2599.

[2] Manuel Bahr, Jonathan M. Butterworth, Stefan Gieseke, and Michael H. Seymour, "Soft interactions in Herwig++," in "Proceedings, 1st International Workshop on Multiple Partonic Interactions at the LHC (MPI08)," 239–248, 2009, 0905.4671.

[3] I. Borozan and M. H. Seymour, "An Eikonal model for multiparticle production in hadron hadron interactions," *JHEP*, **09**(2002), 015, hep-ph/0207283.

[4] Manuel Bahr, Jonathan M. Butterworth, and Michael H. Seymour, "The Underlying Event and the Total Cross Section from Tevatron to the LHC," *JHEP*, **01**(2009), 065, 0806.2949.

[5] Manuel Bahr, Stefan Gieseke, and Michael H. Seymour, "Simulation of multiple partonic interactions in Herwig++," *JHEP*, **07**(2008), 076, 0803.3633.

[6] Georges Aad *et al.* (ATLAS), "Rapidity gap cross sections measured with the ATLAS detector in pp collisions at $\sqrt{s} = 7$ TeV," *Eur. Phys. J.*, **C72**(2012), 1926, 1201.2808.

[7] Stefan Gieseke, Christian Rohr, and Andrzej Siodmok, "Colour reconnections in Herwig++," *Eur. Phys. J.*, **C72**(2012), 2225, 1206.0041.

[8] Vincenzo Barone and Enrico Predazzi, High-Energy Particle Diffraction, volume v.565 of *Texts and Monographs in Physics*, Springer-Verlag, Berlin Heidelberg, 2002, ISBN 3540421076, URL http://www-spires.fnal.gov/spires/find/books/www?cl=QC794.6.C6B37::2002.

SHRiMPS — Status of soft interactions in SHERPA

Holger Schulz for the SHERPA collaboration[1]

[1]IPPP, Durham

1 Status of SHRiMPS

SHRiMPS is a Monte-Carlo implementation of the Khoze-Martin-Ryskin model [1] within the event generator SHERPA [2]. It aims to describe Minimum-Bias and Underlying Event observables with similar precision. Ultimately, SHRiMPS will replace the default model for multiple parton interactions in SHERPA. Despite exhaustive tuning studies the predictive power of SHRiMPS is currently not entirely satisfactory. This report contains the parameter settings the authors find best suited to get a fair assessment of the capabilities of SHRiMPS (Table 1).

2 Tuning

The release of SHERPA version 2.2 necessitated a re-tuning of the parameters of the dynamical part of SHRiMPS. The tuning was done to ATLAS data at $\sqrt{s} = 7$ TeV. We included minimum bias [3], underlying event [4] and rapidity gap [5] data. The tuning aimed at a balanced description of that data as the model is not yet able to reproduce all observables equally well.

The SHRiMPS predictions suitable for comparison with data were obtained with Rivet [6] while the tuning itself was carried out using version 2 of the Professor [7] tool. Figure 1 shows an encouraging prediction of SHRiMPS for the $\sqrt{s} = 13$ TeV minimum bias data recorded with CMS [8].

A summary of the tuning effort is given in Figures 2 and 3 for a selection of typical observables. A discussion can be found in the respective captions.

Parameter	Tuned value
`Q_0^2`	3.02
`Chi_S`	0.65
`Shower_Min_KT2`	1.19
`KT2_Factor`	3.48
`RescProb`	1.01
`RescProb1`	0.18
`Q_RC^2`	0.50
`ReconnProb`	-15.30

Table 1: Tuned SHRiMPS parameter for usage with with Sherpa 2.2.

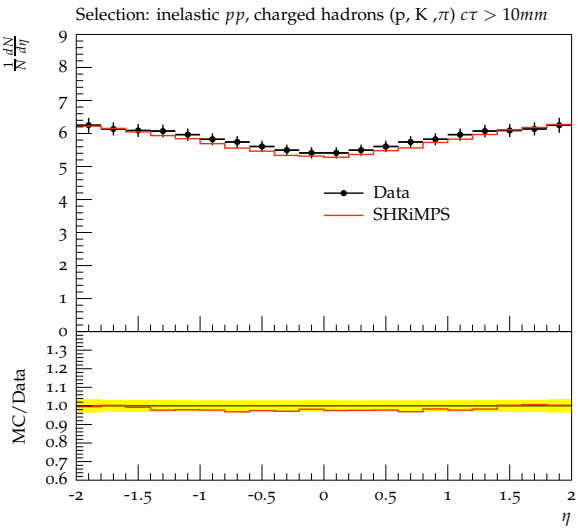

Figure 1: Comparison of 13 TeV CMS data [8] with SHRiMPS prediction.

References

[1] M. G. Ryskin, A. D. Martin, and V. A. Khoze, "Soft processes at the LHC. I. Multi-component model," *Eur. Phys. J.*, **C60**(2009), 249, 0812.2407.

[2] T. Gleisberg, *et al.*, "Event generation with SHERPA 1.1," *JHEP*, **02**(2009), 007, 0811.4622.

[3] G. Aad *et al.* (ATLAS), "Charged-particle multiplicities in pp interactions measured with the ATLAS detector at the LHC," *New J. Phys.*, **13**(2011), 053033, 1012.5104.

[4] Georges Aad *et al.* (ATLAS), "Measurements of underlying-event properties using neutral and charged particles in pp collisions at 900 GeV and 7 TeV with the ATLAS detector at the LHC," *Eur. Phys. J.*, **C71**(2011), 1636, 1103.1816.

[5] Georges Aad *et al.* (ATLAS), "Rapidity gap cross sections measured with the ATLAS detector in pp collisions at $\sqrt{s} = 7$ TeV," *Eur. Phys. J.*, **C72**(2012), 1926, 1201.2808.

[6] Andy Buckley, *et al.*, "Rivet user manual," *Comput. Phys. Commun.*, **184**(2013), 2803, 1003.0694.

[7] Andy Buckley, Hendrik Hoeth, Heiko Lacker, Holger Schulz, and Jan Eike von Seggern, "Systematic event generator tuning for the LHC," *Eur. Phys. J.*, **C65**(2010), 331, 0907.2973.

[8] Vardan Khachatryan *et al.* (CMS), "Pseudorapidity distribution of charged hadrons in proton-proton collisions at $\sqrt{s}$ = 13 TeV," *Phys. Lett.*, **B751**(2015), 143, 1507.05915.

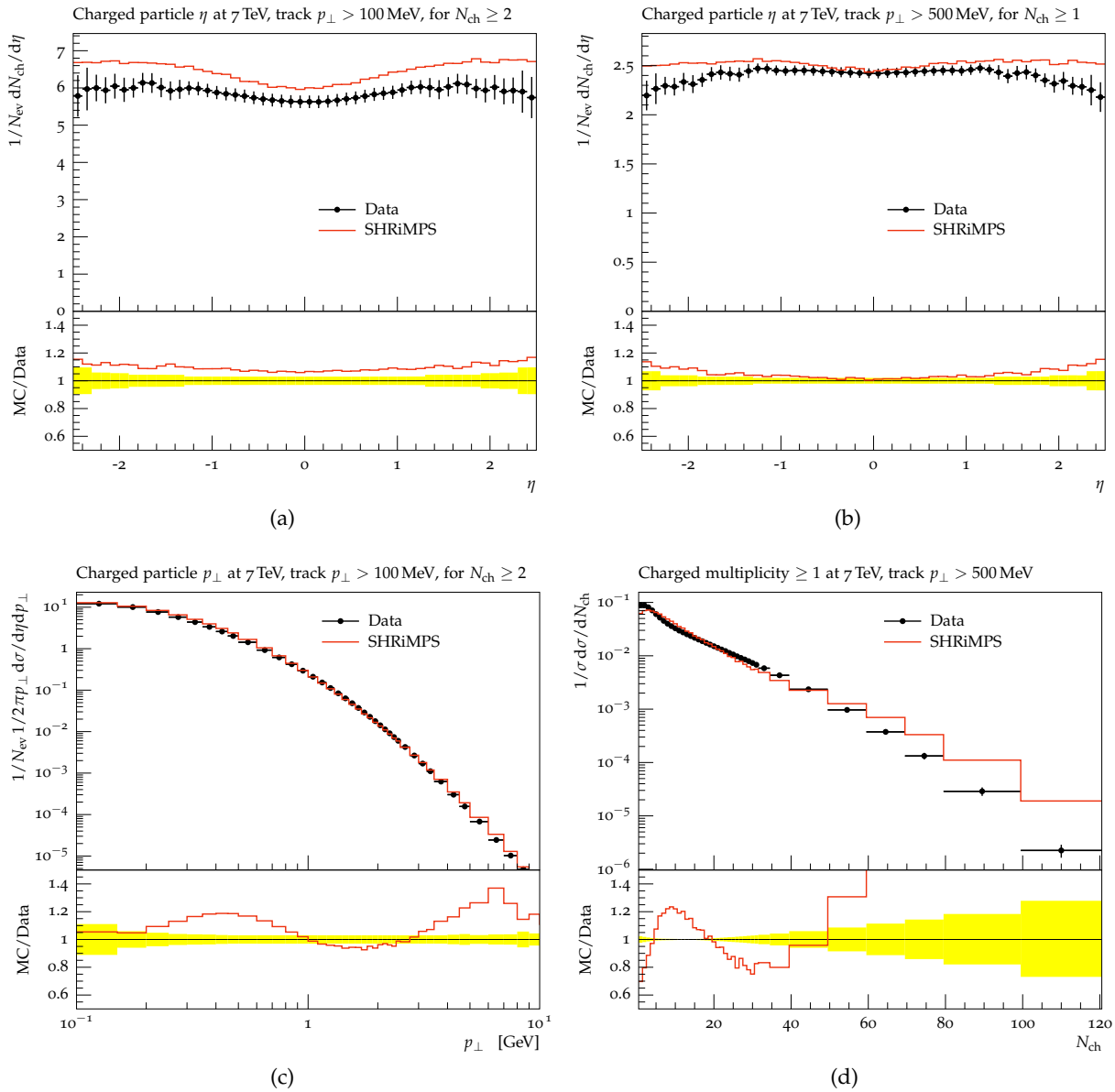

Figure 2: SHRiMPS predictions for minimum bias distributions at $\sqrt{s} = 7$ TeV [3].
(a) and (b) show that on average SHRiMPS produces too many particles at high rapidities.
In (c) a modulation of the prediction of generated particle transverse momenta with respect to the data can be seen although the overall shape is satisfying.
The plot in (d) again shows and issue with the generated multiplicity i.e. events with more than 50 particles are generated far too frequently.

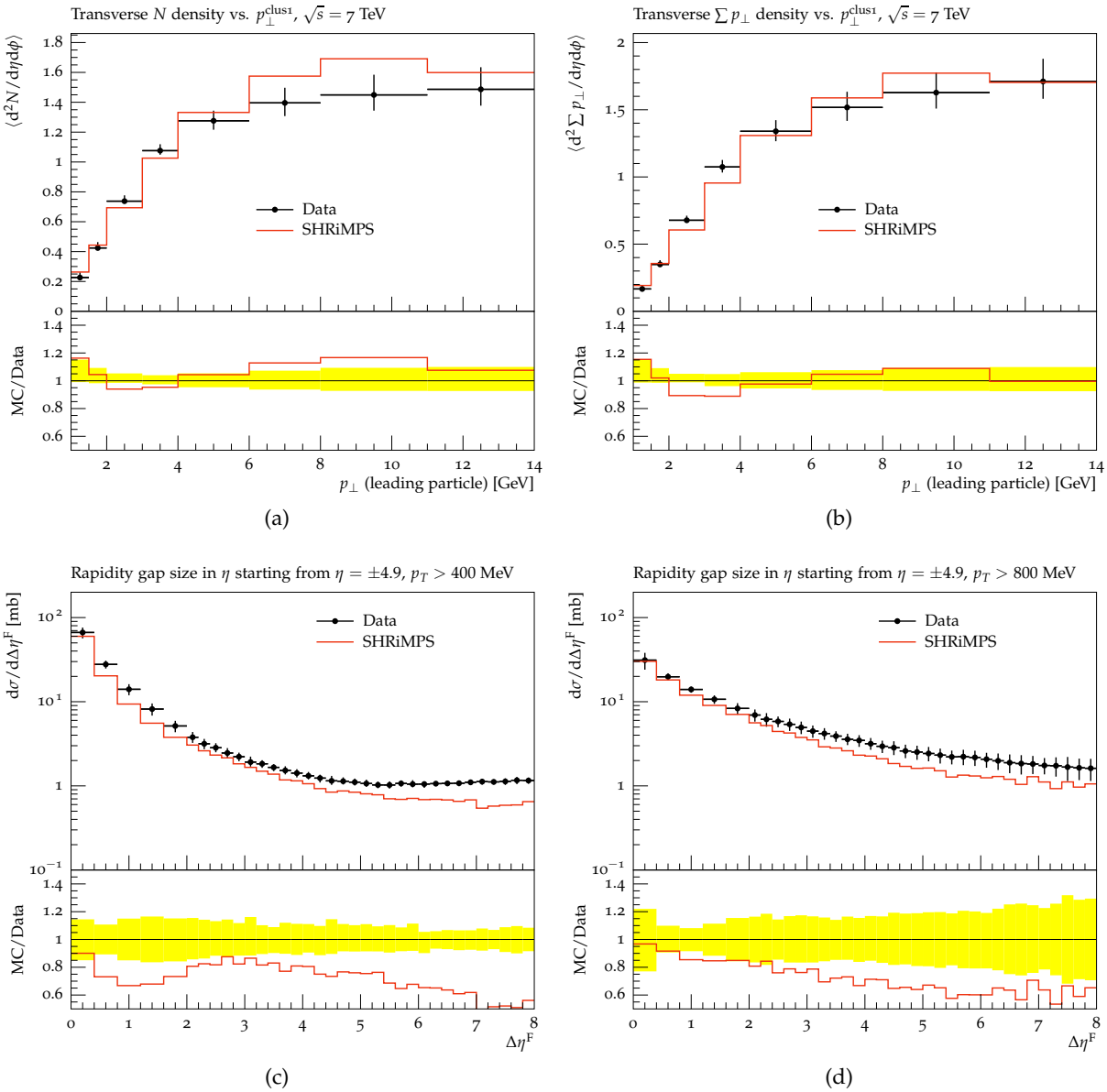

Figure 3: SHRiMPS predictions for underlying event [4] and rapidity gap distributions at $\sqrt{s} = 7$ TeV [5].
The plots in (a) and (b) show a satisfying prediction of SHRiMPS for typical underlying event observables. The plateau region is compatible with the data if measurement uncertainties are taken into account.
Similarly, the prediction of rapidity gaps ((c) and (d)) can be considered satisfying.

CMS Underlying Event and Double Parton Scattering Monte Carlo Tunes

Deniz Sunar Cerci (for the CMS collaboration)[1]

[1]Adiyaman University, Faculty of Arts and Sciences, Department of Physics, 02040 Adiyaman, Turkey.

1 Introduction

It is essential to have reliable predictions for the completely new and unexplored energy scenario of which LHC recently reaches up to 13 TeV center-of-mass energy. The underlying event, consisting of beam-beam remnants as well as the particles coming from the multiple partonic interactions (MPI), in a hadron-hadron collision is simulated in QCD Monte Carlo models. The partonic cross section of the hard scatterings can be perturbatively calculable. The non-perturbative interactions are modeled with the use of experimental data. Double parton scattering (DPS) [1–3] where two hard scattering partons can occur within the same hadron-hadron collision is described with an effective cross section parameter, σ_{eff}, which is a non-directly observed parton level quantity. Measurements of σ_{eff} were performed in pp collision at $\sqrt{s} = 7$ TeV, by the CMS [4] and ATLAS [5] collaborations in a W+dijet final state. Although various experimental measurements were performed, no evidence of an energy dependence of σ_{eff} has been observed yet.

2 CMS underlying event tunes

The charged particle with largest transverse momentum p_T^{max} in the event is selected and named as the "leading object". In order to characterize the UE activity, the charged particles with $p_T > 0.5$ GeV and $|\eta| < 0.8$ are used. The transverse plane is divided in different regions by taking into account the azimuthal angle ϕ and pseudorapidty η of the leading jet. The regions are called "toward" ($|\Delta\phi| < \pi/3$, $|\eta| < 0.8$) and "away" ($\Delta\phi < 2\pi/3$, $|\eta| < 0.8$). The charged-particle density and the scalar transverse momentum p_T sum density in the transverse region are evaluated as the sum of the contribution in the two regions: "Transverse-1" ($\pi/3 < -\Delta\phi < 2\pi/3$, $|\eta| < 0.8$) and "Transverse-2" ($\pi/3 < \Delta\phi < 2\pi/3$, $|\eta| < 0.8$). Further separation is used for the transverse region. The one with bigger activity in terms of p_T of the charged particles is defined as "TransMAX" region whereas the "TransMIN" region is the one with less activity. The average of the TransMIN and TransMAX regions are labelled "TransAVE". This additional subdivision of the transverse region allows a better separation of the MPI and PS components. The TransMAX region might

contain a third jet which can be produced by PS. However, TransMIN region does not contain the third jet but can have contribution from MPI. The TransMIN region has sensitivity to the components of the UE such as beam-beam remnants and MPI.

The software tool, Robust Independent Validation of Experiment and Theory (RIVET) [6], is used for generating MC predictions with a different choice of parameters related to the UE simulation. The PROFESSOR [7] framework which provided the generator response parameters and set of tuned parameters best fits to the measurement is then utilized to include the MC predictions.

CDF data at $\sqrt{s} = 0.9$ and 1.96 TeV [8] for charged-particle density in the TransMIN region as a function of p_T^{max} is shown in Figure 1. The data are compared to predictions obtained with the PYTHIA 8 Tune 4C and with the new CMS tunes: CUETP8S1-CTEQ6L1, CUETP8S1-HERAPDF1.5LO, and CUETP8M1 [9]. Predictions from the new CMS tunes describe CDF data. The new CMS tunes significantly provides a better description than the PYTHIA 8 Tune 4C. This can be explained with the better choice of parameters used in the MPI energy dependence and the obtaining of the color reconnection in the retuning.

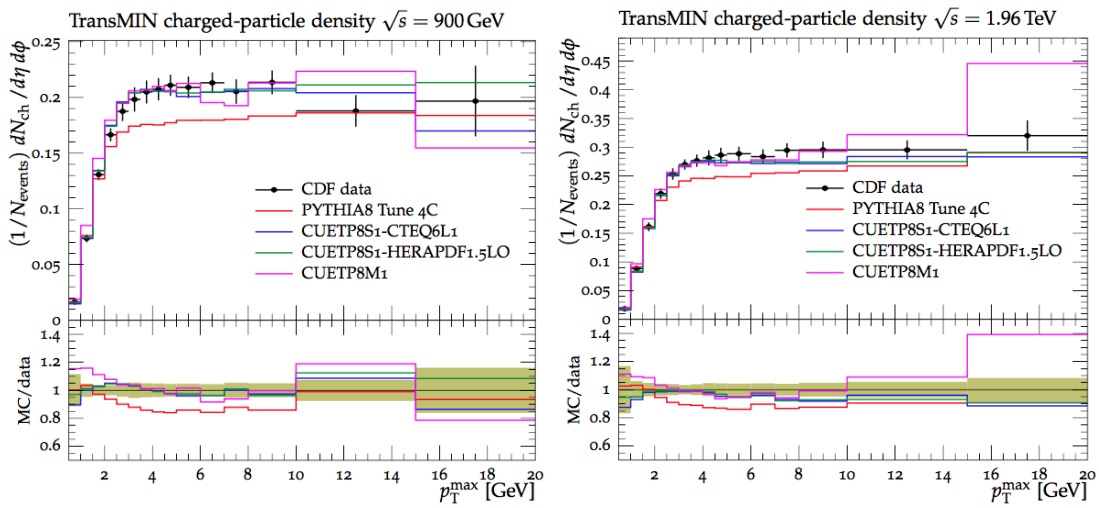

Figure 1: The particle density for charged particles with $p_T > 0.5$ GeV and $|\eta| < 0.8$ in the TransMIN region as a function of the transverse momentum of the leading charged particle p_T^{max} shown for CDF data $\sqrt{s} = 0.9$ TeV (left) and for $\sqrt{s} = 1.96$ TeV (right). The ratio of MC to CDF data is given at the bottom panel of each figure. Total experimental uncertainty is represented with green band.

DPS-sensitive observable, the azimuthal angle between the two selected pairs of hard probes, ΔS, is mesured in four-jet production at $\sqrt{s} = 7$ TeV with the CMS detector [10]. The comparison of CMS data and predictions using CUETP8M1 and CUETHppS1 is shown in Figure 2 (left). Figure 2 (right) shows the comparison of predictions and the charged particle density with $p_T > 0.5$ GeV and $|\eta| < 2$ in the TransAVE region measured by ATLAS at $\sqrt{s} = 7$ TeV [11]. CUETP8M1 reproduces reasonably well the DPS-sensitive observable, ΔS, but prediction using CDPSTP8S2-4j does not describe the UE data.

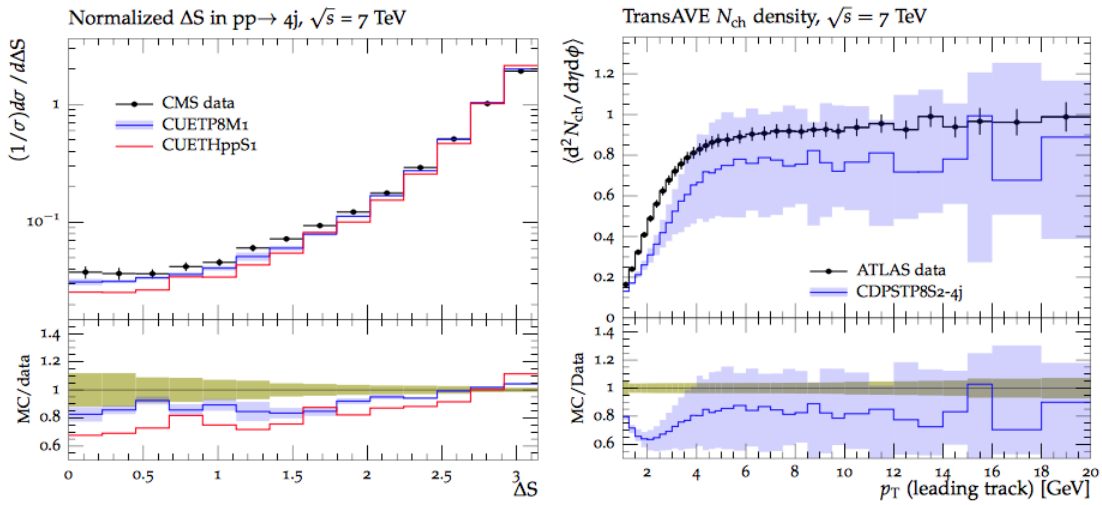

Figure 2: Comparison of ΔS observable measured in CMS with predictions of PYTHIA8 using CUETP8M1 and HERWIG++ with CUETHppS1 (left), the charged particle density with $p_T > 0.5$ GeV and $|\eta| < 2$ in the TransAVE region measured by ATLAS at $\sqrt{s} = 7$ TeV (right).

3 Conclusion

In conclusion, CMS has produced new tunes of PYTHIA 6 [12], PYTHIA 8 [13] and HERWIG++ [14] event generators by using the UE data measured at various centre-of-mass energies by the CDF and CMS experiments. The UE parameters were constrained by testing the UE models. The new CMS tunes at different collision energies provide an improved description of UE data. The new DPS-based tunes, two W+dijet DPS tunes and two four-jet DPS tunes, were constructed for testing the dependence of the DPS-sensitive observables on the MPI parameter. Predictions of the new CMS tunes were also compared to several other data distributions, such as the energy flow and charged particle spectra in the toward and the away regions measured by various experiments and results were found to be very accurate. The new CMS tunes will have an important role on the new LHC data as well as the predictions at the higher collision energies such as 13 or 14 TeV.

Acknowledgements

The author is grateful to ICTP for providing the partial financial support to present this talk during the Workshop.

References

[1] Aneesh V. Manohar and Wouter J. Waalewijn, "What is Double Parton Scattering?" *Phys. Lett.*, **B713**(2012), 196, [arXiV:hep-ph/1202.5034].

[2] B. Blok, Y. Dokshitser, L. Frankfurt, and M. Strikman, "pQCD physics of multiparton interactions," *Eur.Phys.J.*, **C72**(2012), 1963, [arXiV:hep-ph/1106.5533].

[3] A. Del Fabbro and D. Treleani, "Double parton scatterings at the CERN LHC," in "Multiparticle production: New frontiers in soft physics and correlations on the threshold of the third millennium. Proceedings, 9th International Workshop, Torino, Italy, June 12-17, 2000," volume 92, 130, 2001.

[4] S. Chatrchyan *et al.* (CMS), "Study of double parton scattering using W + 2-jet events in proton-proton collisions at 7 TeV," *JHEP*, **03**(2014), 032, [arXiV:hep-ex/1312.5729].

[5] G. Aad *et al.* (ATLAS), "Measurement of hard double-parton interactions in W+ 2 jet events at sqrt(s)=7 TeV with the ATLAS detector," *New J.Phys.*, **15**(2013), 033038, [arXiv:hep-ex/1301.6872].

[6] A. Buckley, *et al.*, "Rivet user manual," *Comput. Phys. Commun.*, **184**(2013), 2803, [arXiv:hep-ph/1003.0694].

[7] A. Buckley, H. Hoeth, H. Lacker, H. Schulz, and J. E. von Seggern, "Systematic event generator tuning for the LHC," *Eur. Phys. J. C*, **65**(2010), 331, [arXiv:hep-ph/0907.2973].

[8] T. Aaltonen *et al.* (CDF), "A study of the energy dependence of the underlying event in proton-antiproton collisions," *Phys. Rev. D*, **92**(2015) (9), 092009, [arXiv:hep-ex/1508.05340].

[9] V. Khachatryan *et al.* (CMS), "Event generator tunes obtained from underlying event and multiparton scattering measurements," *submitted to EPJ C*, (2015), [arXiv:hep-ex/1512.00815].

[10] S. Chatrchyan *et al.* (CMS), "Measurement of four-jet production in proton-proton collisions at $\sqrt{s} = 7$ TeV," *Phys. Rev.*, **D89**(2014) (9), 092010, [arXiv:hep-ex/1312.6440].

[11] G. Aad *et al.* (ATLAS), "Measurement of underlying event characteristics using charged particles in pp collisions at $\sqrt{s} = 900$ GeV and 7 TeV with the ATLAS detector," *Phys. Rev.*, **D83**(2011), 112001, [arXiv:hep-ex/1012.0791].

[12] T. Sjostrand, S. Mrenna, and P. Z. Skands, "PYTHIA 6.4 Physics and Manual," *JHEP*, **05**(2006), 026, [arXiV:hep-ph/0603175].

[13] T. Sjostrand, S. Mrenna, and P. Z. Skands, "A Brief Introduction to PYTHIA 8.1," *Comput.Phys.Commun.*, **178**(2008), 852, [arXiV:hep-ph/0710.3820].

[14] M. Bahr *et al.*, "Herwig++ Physics and Manual," *Eur. Phys. J.*, **C58**(2008), 639, [arXiv:hep-ph/0803.0883].

Charm production in high multiplicity pp events

K. Werner[1], B. Guiot [1,2], Iu. Karpenko [3,4,5], T. Pierog [6], and G. Sophys [1]

[1]SUBATECH, University of Nantes – IN2P3/CNRS– EMN, Nantes, France, [2]Universidad Tcnica Federico Santa Mara, Valparaiso , Chile [3]FIAS, Johann Wolfgang Goethe Universitaet, Frankfurt am Main, Germany [4]Bogolyubov Institute for Theoretical Physics, Kiev 143, 03680, Ukraine [5]INFN - Sezione di Firenze, Via G. Sansone 1, I-50019 Sesto Fiorentino (Firenze), Italy [6]Karlsruhe Inst. of Technology, KIT, Campus North, Inst. f. Kernphysik, Germany

Studying proton-proton scattering at 7 TeV, the ALICE collaboration found the unexpected result that the D meson multiplicity increases more than linear as a function of the charged particle multiplicity. We try to understand this behavior using the EPOS3 approach. Two issues play an important role in this context: multiple scattering, in particular its impact on multiplicity fluctuations, and the collective hydrodynamic expansion. These data contain therefore valuable information about very basic features of the reaction mechanism in proton-proton collisions.

Recently, several experimental groups investigated the dependence of heavy quark production on the event activity, both for open and hidden charm or bottom, in high energy proton-proton collisions. We will focus here on D meson production, where the term "D meson multiplicity" refers in the following to the average multiplicity of D^+, D^0 and D^{*+}. The ALICE collaboration found a quite unexpected result [1]: When plotting the D meson multiplicity versus the charged particle multiplicity, both divided by the corresponding minimum bias mean values, one obtains a dependence which is very significantly more than linear (where "linear" means $N_D/\langle N_D\rangle = N_{\rm ch}/\langle N_{\rm ch}\rangle$). The effect seems to be bigger for larger transverse momentum (p_t). Both D meson and charged particle multiplicity refer to central rapidities.

It is clear that the experimental observations are very interesting, and provide valuable insight into the very nature of the reaction mechanism in pp scattering, in particular in case of high event activity. So we try in this paper to provide an analysis of the phenomenon in the EPOS3 framework. Two key aspects are: Multiple scattering and collectivity.

EPOS3 [2] is a universal model in the sense that for pp, pA, and AA collisions, the same procedure applies, based on several stages:

Initial conditions. A Gribov-Regge multiple scattering approach is employed ("Parton-Based Gribov-Regge Theory" PBGRT [3]), where the elementary object (by definition called Pomeron) is a DGLAP parton ladder, using in addition a CGC motivated saturation scale [4] for each

Pomeron, of the form $Q_s \propto N_{\rm part}\,\hat{s}^{\lambda}$, where $N_{\rm part}$ is the number of nucleons connected the Pomeron in question, and $\hat{s}$ its energy. The parton ladders are treated as classical relativistic (kinky) strings.

Core-corona approach. At some early proper time τ_0, one separates fluid (core) and escaping hadrons, including jet hadrons (corona), based on the momenta and the density of string segments (First described in [5], a more recent discussion in [2]). The corresponding energy-momentum tensor of the core part is transformed into an equilibrium one, needed to start the hydrodynamical evolution. This is based on the hypothesis that equilibration happens rapidly and affects essentially the space components of the energy-momentum tensor.

Viscous hydrodynamic expansion. Starting from the initial proper time τ_0, the core part of the system evolves according to the equations of relativistic viscous hydrodynamics [2,6], where we use presently $\eta/s = 0.08$. A cross-over equation-of-state is used, compatible with lattice QCD [7, 8]. The "core-matter" hadronizes on some hyper-surface defined by a constant temperature T_H, where a so-called Cooper-Frye procedure is employed, using equilibrium hadron distributions, see [8]. After hadronization, there occur still hadron-hadron rescatterings, realized via UrQMD [9].

The above procedure is employed for each event (event-by-event procedure).

Heavy quarks (Q) are produced during the initial stage, in the PBGRT formalism, in the same way as light quarks. We have several parton ladders, each one composed of two space-like parton cascades (SLC) and a Born process. The time-like partons emitted in the SLC or the Born process are in general starting points of time like cascades (TLC). In all these processes, whenever quark–antiquark production is possible, heavy quarks may be produced. We take of course into account the modified kinematics in case of non-zero quark masses (we use $m_c = 1.3$, $m_b = 4.2$). D meson production in the EPOS3 framework has been studied extensively, comparing to data and other calculation, in ref. [10].

We try to understand the dependence of the D meson multiplicity on the charged particle multiplicity, first for EPOS basic (without hydro). We study the case, where both multiplicities refer to central rapidities ($|y| \leq 0.5$ for the D mesons, and $|\eta| \leq 1$ for the charged particles). We use the variables $N_{\rm ch}$ for the charged particle multiplicity, and N_{Di} for the D meson multiplicities for different p_t ranges (N_{D1} for $1 < p_t[{\rm GeV/c}] < 2$, and N_{D8} for $8 < p_t[{\rm GeV/c}] < 12$).

In EPOS3, we have in each individual event a certain number of parton ladders (cut Pomerons). Each ladder contributes (roughly, on the average) the same to both charged particle and charm production, so both corresponding multiplicities are proportional to the number $N_{\rm Pom}$ of cut Pomerons: $N_{Di} \propto N_{\rm ch} \propto N_{\rm Pom}$, which leads to a "natural" linear relation between the charged particle multiplicity $N_{\rm ch}$ and the D meson multiplicities N_{Di} (to first approximation).

We define normalized multiplicities, $n = N/\langle N\rangle$, both for charged particles ($n_{\rm ch}$) and D meson multiplicities (n_{Di}). In the following, we consider fixed values $n^*_{\rm ch}$ of normalized charged multiplicities.

We will study the average normalized D meson multiplicity for the largest p_t range, for some given $n^*_{\rm ch}$, which may be expressed in terms of the Pomeron number distribution ${\rm prob}(N_{\rm Pom}, {n_{\rm ch}}^*)$

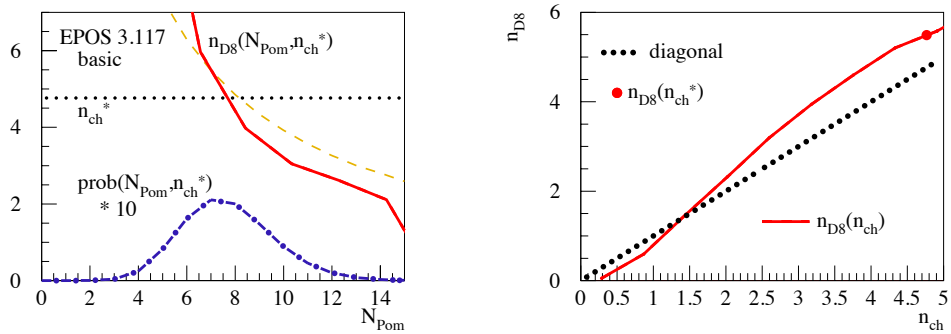

Figure 1: (Color online) Left: Pomeron number distribution at fixed charged multiplicity, $\mathrm{prob}(N_{\mathrm{Pom}}, n_{\mathrm{ch}}{}^*)$ (blue line), and number $n_{D8}(N_{\mathrm{Pom}}, n_{\mathrm{ch}}{}^*)$ of D mesons (large p_t) for fixed N_{Pom} and $n_{\mathrm{ch}}{}^*$ as a function of the Pomeron number N_{Pom} (red line). The dotted line represents the constant value $n_{\mathrm{ch}}{}^*$.
Right: Average multiplicity $n_{D8}(n_{\mathrm{ch}})$ of D mesons (large p_t) as a function of n_{ch} (red line) and the diagonal ($n_{D1} = n_{\mathrm{ch}}$, dotted line). The red point refers to $n_{D8}(n^*_{\mathrm{ch}})$ for the particular value of $n_{\mathrm{ch}}{}^*$ used in eq. (1).

at fixed n^*_{ch} and the number $n_{D8}(N_{\mathrm{Pom}}, n_{\mathrm{ch}}{}^*)$ of D mesons for fixed N_{Pom} and $n_{\mathrm{ch}}{}^*$, as

$$n_{D8}(n^*_{\mathrm{ch}}) = \sum_{N_{\mathrm{Pom}}} \mathrm{prob}(N_{\mathrm{Pom}}, n_{\mathrm{ch}}{}^*) \times n_{D8}(N_{\mathrm{Pom}}, n_{\mathrm{ch}}{}^*) \quad . \tag{1}$$

The two curves representing $\mathrm{prob}(N_{\mathrm{Pom}}, n_{\mathrm{ch}}{}^*)$ and $n_{D8}(N_{\mathrm{Pom}}, n_{\mathrm{ch}}{}^*)$ are shown in fig. 1 (left). We see in the figure that $n_{D8}(N_{\mathrm{Pom}}, n_{\mathrm{ch}}{}^*)$ increases strongly towards small N_{Pom} with an increasing slope. Let us compare the expression of eq. (1) with the corresponding sum (as a reference) where we use $n_{D8}(N_{\mathrm{Pom}}, n_{\mathrm{ch}}{}^*) = n_{\mathrm{ch}}{}^*$, which would lead to $n_{D8}(n^*_{\mathrm{ch}}) = n^*_{\mathrm{ch}}$. For large N_{Pom}, the contribution to the sum in eq. (1) will be less than the reference case, but this is more than compensated at small N_{Pom}. Therefore, we have $n_{D8}(n^*_{\mathrm{ch}}) > n_{\mathrm{ch}}{}^*$, which is confirmed by the precise calculation shown in fig. 1 (right) as red point. Also shown is the complete curve $n_{D8}(n_{\mathrm{ch}})$ as obtained from EPOS basic. Indeed, we get a more than linear increase.

The results of our calculation agree qualitatively with the trend in the data, namely a more than linear increase, in particular for high transverse momentum D mesons. But the effect is actually too small, as seen in fig. 2 (left), where we plot the D meson multiplicities versus the charged particle multiplicity, both for our calculation and data from ALICE [1].

But anyhow, EPOS basic (w/o hydro) reproduces neither spectra nor correlations, we have to consider the full approach, i.e. EPOS with hydrodynamical evolution (with or without hadronic cascade makes no difference). In fig. 2 (right), we plot again the D meson multiplicities versus the charged particle, EPOS3 compared to data, but here we refer to the calculations based on the full EPOS model (with hydro). We see a significant non-linear increase, much more pronounced as in the case of EPOS basic (without hydro), mainly due to the fact that the multiplicities from

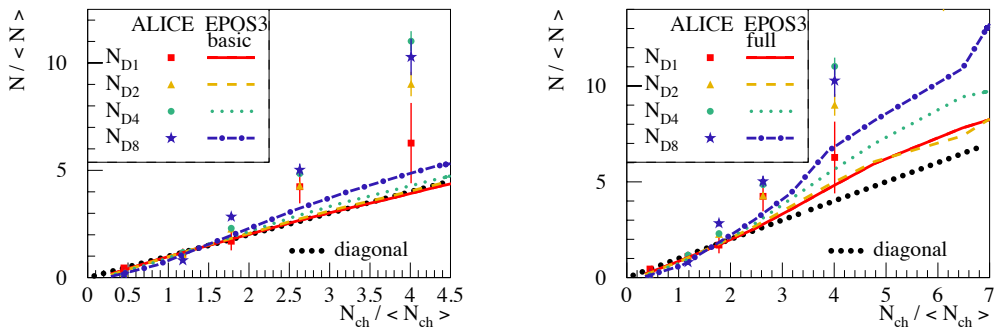

Figure 2: (Color online) D meson multiplicities versus the charged particle multiplicity, both divided by the corresponding minimum bias mean values. The different symbols and the notations N_{D1}, N_{D2}, N_{D4}, N_{D8} refer to different p_t ranges: 1-2, 2-4, 4-8, 8-12 (in GeV), $N_{\rm ch}$ refers to the charged particle multiplicity. We compare our calculations (lines) to ALICE data (points). Left plot : EPOS basic. Right plot : full EPOS.

full EPOS are considerably below the results from EPOS basic. A much more detailed discussion will be provided in a separate publication.

To summarize: We analyzed the dependence of D meson multiplicities (in different p_t ranges) on the charged particle multiplicity in proton-proton collisions at 7 TeV, using the EPOS3 approach. We find a non-linear increase. Two issues play an important role: Multiplicity fluctuations due to multiple scattering (realized via multiple Pomerons), and the collective hydrodynamic expansion. Multiplicity fluctuations are important since in particular high p_t D meson production at given (large) charged particle multiplicity is very much favored for small Pomeron numbers, which is responsible for the strong increase of the D meson production with multiplicity. In addition, the effect is amplified when turning on the hydrodynamical expansion, due to a reduction of the charged particle multiplicity with respect to the model without hydro.

Acknowlegments

This research was carried out within the scope of the GDRE (European Research Group) "Heavy ions at ultrarelativistic energies". B.G. acknowledges the financial support by the TOGETHER project of the Region of "Pays de la Loire". B. G. gratefully acknowledges generous support from Chilean FONDECYT grants 3160493.

References

[1] ALICE collaboration, arXiv:1505.00664v1

[2] K. Werner, B. Guiot, I. Karpenko, and T. Pierog, Phys.Rev. C89 (2014) 064903, arXiv:1312.1233.

[3] H. J. Drescher, M. Hladik, S. Ostapchenko, T. Pierog and K. Werner, Phys. Rept. 350, 93, 2001

[4] L. McLerran, R. Venugopalan, Phys. Rev. D 49 (1994) 2233; L. McLerran, R. Venugopalan, Phys. Rev. D 49 (1994) 3352; L. McLerran, R. Venugopalan, Phys. Rev. D 50 (1994) 2225.

[5] K. Werner, Phys. Rev. Lett. 98, 152301 (2007)

[6] Iu. Karpenko, P. Huovinen, M. Bleicher, arXiv:1312.4160

[7] S. Borsanyi et al., JHEP 1011 (2010) 077, arXiv:1007.2580

[8] K. Werner, Iu. Karpenko, T. Pierog, M. Bleicher, K. Mikhailov, arXiv:1010.0400, Phys. Rev. C 83, 044915 (2011)

[9] M. Bleicher et al., J. Phys. G25 (1999) 1859; H. Petersen, J. Steinheimer, G. Burau, M. Bleicher and H. Stocker, Phys. Rev. C78 (2008) 044901

[10] B. Guiot, Ph.D. Thesis, University of Nantes, 2014

Quark/gluon jet tagging and colour reconnection

Andrzej Siódmok*[1]

[1]CERN, Theory Division, Geneva, Switzerland
[2]Institute of Nuclear Physics, Polish Academy of Sciences, Krakw, Poland

1 Introduction

Colour reconnection (one of the primary, yet least understood, building blocks of MPI models) and quark/gluon jet tagging (relevant for searches for physics beyond the Standard Model[1]), two seemingly very different problems, turn out to be very closely related. This interesting observation is an outcome from the "Les Houches 2015 quark/gluon jet tagging" working group. This working group aimed to better understand the experimental observation [1,2] that PYTHIA [3,4] predicts greater quark/gluon jet discrimination and Herwig [5,6] predicts lower quark/gluon discrimination than is seen in data.

2 Les Houches study on quark and gluon jets

The working group in Les Houches 2015 [7] for quark/gluon discriminants considered the generalized angularities λ_β^κ [8]:

$$\lambda_\beta^\kappa = \sum_{i \in \text{jet}} z_i^\kappa \theta_i^\beta, \tag{1}$$

where i runs over the jet constituents, $z_i \in [0,1]$ is a momentum fraction, and $\theta_i \in [0,1]$ is a (normalized) angle to the jet axis. The parameters $\kappa \geq 0$ and $\beta \geq 0$ determine the momentum and angle weighting respectively. We consider five different (κ, β) working points, which roughly map onto five variables in common use in the literature:

$$\begin{array}{ccccc} (0,0) & (2,0) & (1,0.5) & (1,1) & (1,2) \\ \text{multiplicity} & p_T^D & \text{LHA} & \text{width} & \text{mass}, \end{array} \tag{2}$$

where multiplicity is the hadron multiplicity within the jet, p_T^D was defined in Refs. [9,10], LHA refers to the "Les Houches Angularity" (named after the venue of this workshop), width is closely

*On behalf of the "Les Houches 2015 Quark/Gluon tagging jet" working group: M. Freytsis, P. Gras, D. Kar, L. Lönnblad, S, Plätzer, G. Soyez, P. Skands, D. Soper and J. Thaler.

[1]Where signals are often dominated by quarks while backgrounds are dominated by gluons.

related to jet broadening [11–13], and mass is closely related to jet thrust [14]. To quantify discrimination performance, we focus on classifier separation:

$$\Delta = \frac{1}{2}\int \mathrm{d}\lambda \, \frac{\big(p_q(\lambda) - p_g(\lambda)\big)^2}{p_q(\lambda) + p_g(\lambda)}, \tag{3}$$

where p_q (p_g) is the probability distribution for λ in a generated quark jet (gluon jet) sample. We consider parton shower generator predictions for quark/gluon discrimination using an idealized setup with e^+e^- collisions. We can use the following processes as proxies for quark and gluon jets:

$$\text{“quark jets”}: \quad e^+e^- \to (\gamma/Z)^* \to u\overline{u}, \tag{4}$$

$$\text{“gluon jets”}: \quad e^+e^- \to h^* \to gg, \tag{5}$$

where h is the Higgs boson.

3 Results

In this short section we focus only on one effect influencing the quark/gluon tagging, namely colour reconnection(CR), and show results of only two generators Herwig++ [15] and PYTHIA [4]. For detailed information on other effects and generators [16–18] studied in Les Houches 2015 we refer the reader to [7].

Our Herwig++ baseline uses version 2.7.1, with improved modeling of underlying event [19] and the most recent UE-EE-5-MRST tune [20], which is able to describe the double-parton scattering cross section [21] and underlying event data from $\sqrt{s} = 300$ GeV to $\sqrt{s} = 7$ TeV. Our PYTHIA baseline uses version 8.205 and is based on the Monash 2013 tune, with parameters described in Ref. [22].

In Fig. 1 we show some predictions for the five observables defined in the previous section obtained with Herwig and PYTHIA. It is evident, from comparison of the relevant lines, labelled “Herwig: no CR” and “PYTHIA: CR1”, to their respective baselines, that there is a strong influence from CR. One thinks of colour reconnection as being primarily important for hadron collider, but even at a lepton collider colour reconnection may change the Lund strings or clusters used for hadronization. The presented Pythia variation uses an alternative “SU(3)”- based colour reconnection model [23]. No attempts were made to retune any of the other hadronization parameters (as would normally be mandated in a tuning context). This change simply illustrates the effects of switching on this reconnection model with all other model parameters kept at their default values. This variation considerably decreases quark/gluon separation compared to the baseline. This is the most surprising effect in PYTHIA and it is also important for the Herwig generator described next. In Herwig, CR is switched on by default and we denote by “Herwig: no CR” the variation which turns off colour reconnections. This has no effect at parton level, as expected. At hadron level, this variation for Herwig gives a rather dramatic improvement in quark/gluon discrimination power. We think this arises because colour reconnection in Herwig allows any colour-anticolour pair to reconnect, even if they arose from an initially colour octet configuration.

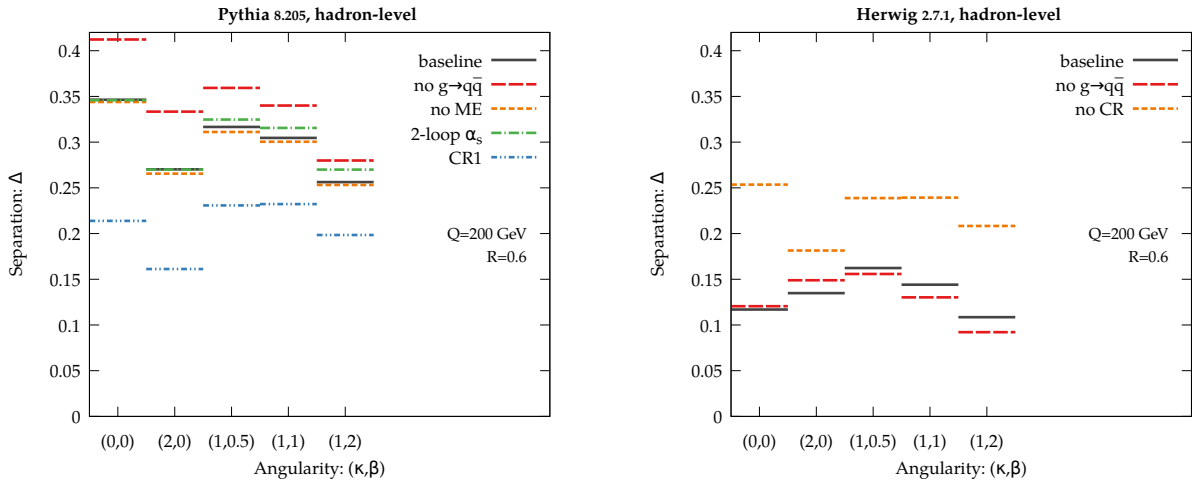

(a) (b)

Figure 1: Settings variations for PYTHIA 8.205 and Herwig 2.7.1. Hadron-level results are shown for the classifier separation, Δ, derived from the five benchmark angularities.

Turning off colour reconnection causes the gluons look more octet-like, explaining the improvement seen. This observation is a big surprise from this study, motivating future detailed studies on colour reconnection models. Finally, it is worth mentioning that modern CR models were validated against existing data from lepton colliders and they showed little effect there. Therefore, it is quite surprising to see their significant effect in our idealized setup of e^+e^- collisions. The main reason for this is that we have extensive information about quark jet radiation patterns from LEP event shapes, however gluon jet radiation patterns are largely unconstrained. Therefore, it is extremely important to find a way to constrain gluon jet radiation patterns using past or future experimental data.

Acknowledgements

The author is grateful to all of the members of the quark/gluon LH working group 2015: Andy Buckley, Jon Butterworth, Mario Campanelli, Marat Freytsis, Peter Loch, Philippe Gras, Deepak Kar, Simon Pleatzer, Peter Skands, Dave Soper, Gregory Soyez, Frank Tackmann, Jesse Thaler, on behalf which the studies were presented. We thank S. Webster for his critical reading of the manuscript. The author is also grateful for the long discussions during the MPI workshop which took place in Via Torino.

References

[1] Georges Aad *et al.* (ATLAS), "Light-quark and gluon jet discrimination in pp collisions at $\sqrt{s} = 7$ TeV with the ATLAS detector," *Eur. Phys. J.*, **C74**(2014) (8), 3023, 1405.6583.

[2] Tom Cornelis (CMS), "Quark-gluon Jet Discrimination At CMS," in "Proceedings, 2nd Conference on Large Hadron Collider Physics Conference (LHCP 2014)," 2014, 1409.3072, URL https://inspirehep.net/record/1315816/files/arXiv:1409.3072.pdf.

[3] Torbjorn Sjostrand, Stephen Mrenna, and Peter Z. Skands, "PYTHIA 6.4 Physics and Manual," *JHEP*, **05**(2006), 026, hep-ph/0603175.

[4] Torbjrn Sjstrand, *et al.*, "An Introduction to PYTHIA 8.2," *Comput. Phys. Commun.*, **191**(2015), 159, 1410.3012.

[5] M. Bahr *et al.*, "Herwig++ Physics and Manual," *Eur. Phys. J.*, **C58**(2008), 639, 0803.0883.

[6] Johannes Bellm *et al.*, "Herwig 7.0 / Herwig++ 3.0 Release Note," (2015), 1512.01178.

[7] M Freytsis, *et al.*, "Les Houches 2015 proceedings: SYSTEMATICS OF QUARK/GLUON TAGGING," *In preparation*.

[8] Andrew J. Larkoski, Jesse Thaler, and Wouter J. Waalewijn, "Gaining (Mutual) Information about Quark/Gluon Discrimination," *JHEP*, **11**(2014), 129, 1408.3122.

[9] Francesco Pandolfi and Daniele Del Re, "Search for the Standard Model Higgs Boson in the $H \to ZZ \to llqq$ Decay Channel at CMS," Ph.D. thesis, Zurich, ETH, 2012.

[10] Serguei Chatrchyan *et al.* (CMS), "Search for a Higgs boson in the decay channel H to ZZ(*) to q qbar ℓ^- l+ in pp collisions at $\sqrt{s} = 7$ TeV," *JHEP*, **04**(2012), 036, 1202.1416.

[11] S. Catani, G. Turnock, and B. R. Webber, "Jet broadening measures in e^+e^- annihilation," *Phys. Lett.*, **B295**(1992), 269.

[12] Paul E. L. Rakow and B. R. Webber, "Transverse Momentum Moments of Hadron Distributions in QCD Jets," *Nucl. Phys.*, **B191**(1981), 63.

[13] R. Keith Ellis and B. R. Webber, "QCD Jet Broadening in Hadron Hadron Collisions," *Conf. Proc.*, **C860623**(1986), 74.

[14] Edward Farhi, "A QCD Test for Jets," *Phys. Rev. Lett.*, **39**(1977), 1587.

[15] J. Bellm *et al.*, "Herwig++ 2.7 Release Note," (2013), 1310.6877.

[16] T. Gleisberg, *et al.*, "Event generation with SHERPA 1.1," *JHEP*, **02**(2009), 007, 0811.4622.

[17] Leif Lonnblad, "ARIADNE version 4: A Program for simulation of QCD cascades implementing the color dipole model," *Comput. Phys. Commun.*, **71**(1992), 15.

[18] Zoltan Nagy and Davison E. Soper, "A parton shower based on factorization of the quantum density matrix," *JHEP*, **06**(2014), 097, 1401.6364.

[19] Stefan Gieseke, Christian Rohr, and Andrzej Siodmok, "Colour reconnections in Herwig++," *Eur.Phys.J.*, **C72**(2012), 2225, 1206.0041.

[20] Michael H. Seymour and Andrzej Siodmok, "Constraining MPI models using σ_{eff} and recent Tevatron and LHC Underlying Event data," *JHEP*, **10**(2013), 113, 1307.5015.

[21] Manuel Bähr, Miroslav Myska, Michael H. Seymour, and Andrzej Siodmok, "Extracting σ_{eff} from the CDF $\gamma + 3$ jets measurement," *JHEP*, **1303**(2013), 129, 1302.4325.

[22] Peter Skands, Stefano Carrazza, and Juan Rojo, "Tuning PYTHIA 8.1: the Monash 2013 Tune," *Eur. Phys. J.*, **C74**(2014) (8), 3024, 1404.5630.

[23] Jesper R. Christiansen and Peter Z. Skands, "String Formation Beyond Leading Colour," *JHEP*, **08**(2015), 003, 1505.01681.

Chapter 3

Working Group
Double parton scattering

Convenors:

Jonathan Gaunt (Theory),
Paolo Gunnellini (CMS)

Introduction: Double Parton Scattering from an experimental point of view

Paolo Gunnellini[1]

[1]Deutsches Elektronen-Synchrotron (DESY), Hamburg

1 Current state of the art

In the DPS experimental session, results from various active experiments at the LHC have been presented:

- Experimental review from CMS;
- Measurement of same-sign W pairs at the CMS experiment;
- Experimental review from ATLAS;
- Experimental review from LHCb;

Published results show a very detailed investigation of various final states in a wide region of phase space. The general strategy for experimental analyses aiming for measuring the DPS signal is based on the following points:

- Identification of a physics channel and observables sensitive to a DPS contribution;
- Measurements of distributions of DPS-sensitive variables corrected at the stable-particle level;
- Interpretation and unambiguous definition of the SPS and DPS contributions;
- Extraction of the DPS fraction, study of the process dependence and possible tests of different DPS models.

So far, a quantitative measurement of the DPS signal contributing to a considered final state has been provided by means of σ_{eff}, which appears in the so-called "pocket formula", based on very basic assumptions of complete factorization of the two scatterings. Current values of σ_{eff} are shown in Figure 1.

From the current picture of available DPS measurements, some interesting questions arise:

- Is a value of σ_{eff} a useful input for the theory or is it just a parameter of the simulation or of a simplistic model?
- How can one reduce the experimental uncertainty of DPS measurements?
- Should one try also a global extraction of σ_{eff} from the different final states?

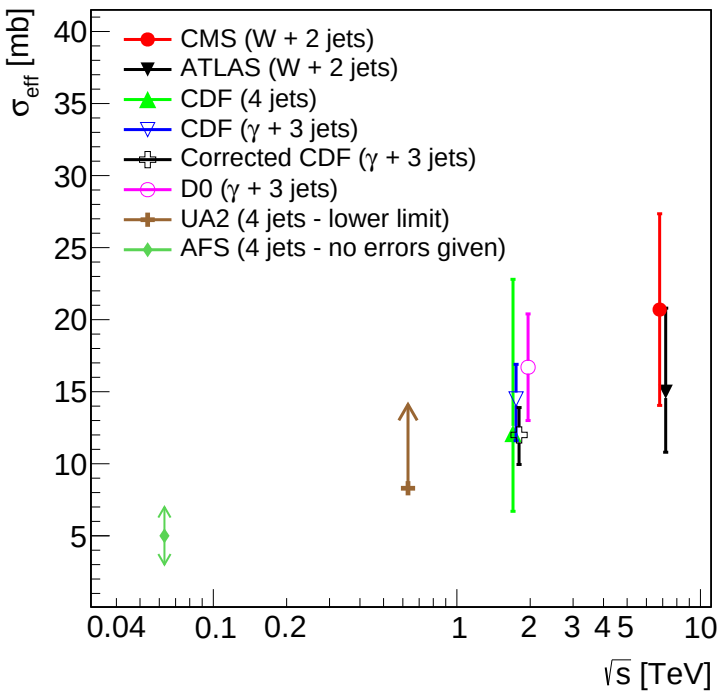

Figure 1: Values of σ_{eff} as a function of the centre-of-mass energy measured in hadronic collisions for several final states.

Moreover, with the new phase of the LHC run, experimental research looking for DPS signals is going to face new challenges for the near future, such as the measurement of the energy dependence of DPS contributions, the identification of new sensitive observables, physics channels or phase space. A dialogue between the experimental and theoretical community will be necessary and fruitful for addressing and developing these points.

Constraining the double gluon distribution

Krzysztof Golec-Biernat[1]

[1]Institute of Nuclear Physics PAS, Cracow and Rzeszów University, Rzeszów, Poland

1 Introduction

Multiparton interactions play an important role in the hadronic collisions at high energies, see e.g. [1–5]. A theoretical description of such interactions within perturbative QCD is possible in the presence of hard scales, e.g. two such scales in the case of a double parton scattering (DPS). In the latter case, the DPS cross sections in the collinear framework make use of the double parton distribution functions (DPDFs), see e.g. [6], which obey QCD evolution equations, see e.g. [7,8], similar to the Dokshitzer-Gribov-Lipatov-Altarelli-Parisi (DGLAP) equations for single parton distribution functions (PDFs). The evolution equations for DPDFs conserve new sum rules which relate the double and single parton distributions once they are imposed on initial conditions for the evolution equations. All the attempts up till now to construct the DPDFs which satisfy these sum rules were moderately successful, see e.g. [8–11]. In this contribution, we present a construction of DPDFs in a pure gluonic case which gives the known single gluon distribution in the MSTW parameterization [12], using the momentum sum rule. For a full presentation, see [13].

2 The sum rules

The evolution equations for DPDFs , see e.g. [8], conserve the following sum rules imposed at some initial scale Q_0, the momentum sum rule

$$\sum_{f_1} \int_0^{1-x_2} dx_1\, x_1 D_{f_1 f_2}(x_1, x_2, Q_0, Q_0) = (1-x_2) D_{f_2}(x_2, Q_0)\,, \tag{1}$$

where $f_{1,2}$ denote both quark flavors and gluon, and the valence quark number sum rule

$$\int_0^{1-x_2} dx_1 \{D_{q f_2}(x_1, x_2) - D_{\bar{q} f_2}(x_1, x_2, Q_0, Q_0)\} = (N_q - \delta_{f_2 q} + \delta_{f_2 \bar{q}}) D_{f_2}(x_2, Q_0)\,, \tag{2}$$

where $q = u, d, s$ and $N_u = 2, N_d = 1, N_s = 0$ are the valence quark numbers. The same relations hold true with respect to the second parton. If the initial DPDFs are parton exchange symmetric,

$$D_{f_1 f_2}(x_1, x_2, Q_0, Q_0) = D_{f_2 f_1}(x_2, x_1, Q_0, Q_0)\,, \tag{3}$$

the evolution equations guarantee that the sum rules with respect to the first parton imply the sum rules with respect to the second one. The above sum rules relate the double and single parton distribution functions, which reflects the common origin of those distributions, the Fock expansion of the nucleon state in light-cone partonic components. In addition, the momentum and valence quark number sum rules for initial single PDFs are also satisfied, respectively,

$$\sum_f \int_0^1 dx\, x D_f(x,Q_0) = 1\,, \qquad \int_0^1 dx\, \{D_q(x,Q_0) - D_{\overline{q}}(x,Q_0)\} = N_q\,. \tag{4}$$

We will present the construction of the double gluon distribution function, $D_{gg}(x_1,x_2)$, in the case when only gluons are present, using the rule (1) reduced to such a case. The key idea is to obtain the known single gluon distribution, $D_g(x_2)$, after performing the integration in the sum rule (1). The full case with quarks has to be postponed to further studies.

3 The pure gluon case

The single gluon distribution at the scale $Q_0 = 1$ GeV in the LO MSTW parameterization [12] is given by

$$D_g(x) = A_g\, x^{\delta_g - 1}(1-x)^{\eta_g}(1 + \epsilon_g \sqrt{x} + \gamma_g\, x) \tag{5}$$

where $A_g = 0.0012216, \delta_g = -0.83657, \eta_g = 2.3882, \epsilon_g = -38.997$ and $\gamma_g = 1445.5$. This can be written in a general form

$$D_g(x) \;=\; \sum_{k=1}^{3} N_g^k\, x^{\alpha_g^k}\,(1-x)^{\beta_g^k} \tag{6}$$

where the parameters N_g^k, α_g^k and β_g^k can easily be found by the comparison with eq. (5). Let us assume the parton exchange symmetric double gluon distribution in the form

$$D_{gg}(x_1,x_2) \;=\; \sum_{k=1}^{3} \bar{N}_{gg}^k\,(x_1 x_2)^{\bar{\alpha}_g^k}\,(1-x_1-x_2)^{\bar{\beta}_g^k} \tag{7}$$

where $\bar{N}_{gg}^k, \bar{\alpha}_g^k$ and $\bar{\beta}_g^k$ are the parameters to be determined. Substituting the above on the l.h.s. of the momentum sum rule (1) in the pure gluonic case, we find

$$\int_0^{1-x_2} dx_1 x_1 D_{gg}(x_1,x_2) = (1-x_2)\sum_{k=1}^{3} \bar{N}_{gg}^k\, \frac{\Gamma(\bar{\alpha}_g^k+2)\Gamma(\bar{\beta}_g^k+1)}{\Gamma(\bar{\alpha}_g^k+\bar{\beta}_g^k+3)}\, x_2^{\bar{\alpha}_g^k}\,(1-x_2)^{\bar{\alpha}_g^k+\bar{\beta}_g^k+1}\,. \tag{8}$$

By the comparison with the known distribution (6), we find for the sought parameters

$$\bar{\alpha}_g^k = \alpha_g^k\,, \qquad \bar{\beta}_g^k = \beta_g^k - \alpha_g^k - 1\,, \qquad \bar{N}_{gg}^k = N_g^k\, \frac{\Gamma(\beta_g^k+2)}{\Gamma(\alpha_g^k+2)\Gamma(\beta_g^k-\alpha_g^k)}\,. \tag{9}$$

Notice that even for small momentum fractions, $x_{1,2} \ll 1$, the resulting double gluon distribution is not factorizable, i.e. $D_{gg}(x_1,x_2) \neq D_g(x_1)D_g(x_2)$.

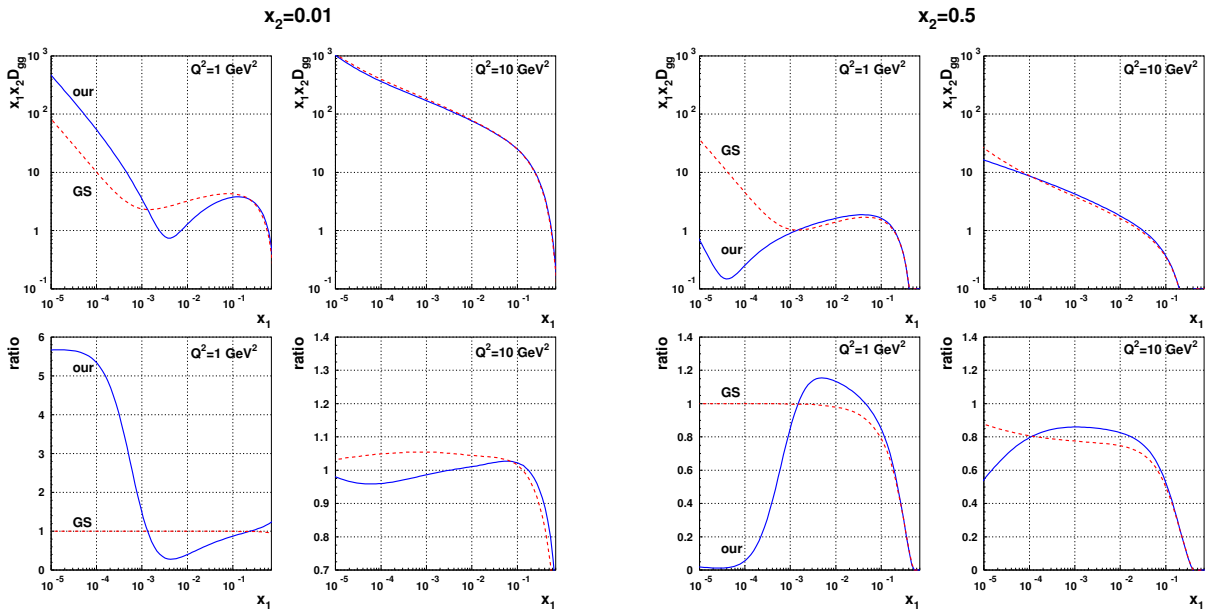

Figure 1: $D_{gg}(x_1, x_2)$ (multiplied by $x_1 x_2$) as a function of x_1 for fixed $x_2 = 0.01,\ 0.5$ at the scales $Q^2 = 1,\ 10\ \mathrm{GeV}^2$ (upper plots) and the ratio $D_{gg}(x_1, x_2)/(D_g(x_1)D_g(x_2))$ (lower plots).

4 Numerical results

Using our numerical program, we solve the evolution equations for the double gluon distribution for the initial condition (7) with the parameters (9) (our-solid lines). In Fig. 1 we compare our results for $D_{gg}(x_1, x_2)$ with those obtained from initial conditions from Ref. [8] (GS-dashed lines),

$$D_{gg}(x_1, x_2) = D_g(x_1) D_g(x_2)\, \frac{(1 - x_1 - x_2)^2}{(1 - x_1)^2 (1 - x_2)^2}\,. \tag{10}$$

In the lower panels we plot the ratio indicated in the caption which characterizes factorizability of the double gluon distribution into a product of two single gluon distributions. At the initial scale, $Q^2 = 1\ \mathrm{GeV}^2$, the two double gluon distributions differ significantly in the small x_1 region, however, the evolution equations erase this difference already at the scale $Q^2 = 10\ \mathrm{GeV}^2$.

The initial double gluon distribution (7) is not factorizable for any values of x_1 and x_2. However, if both x_1 and x_2 are small, D_{gg} becomes factorizable with good accuracy after evolution to the shown value of Q^2 (see lower panels). A small breaking of the factorization can be attributed to the non-homogeneous terms in the evolution equations. If one of the two momentum fractions is large, e.g. $x_2 = 0.5$, the factorization is significantly broken for all values of x_1 and any evolution scale. We have to remember, however, that the large x domain has to be supplemented by quarks.

In conclusion, the found initial double gluon distribution (7) is very different from those proposed so far. However, the QCD evolution equations significantly reduce this difference at rather low values of the evolution scale Q^2.

Acknowledgements

I thank my collaborators, Emilia Lewandowska, Mirko Serino, Zack Snyder and Anna Staśto. The grant of National Science Center, Poland, No. 2015/17/B/ST2/01838 is gratefully acknowledged.

References

[1] T. Akesson *et al.* (Axial Field Spectrometer Collaboration), "Double Parton Scattering in pp Collisions at $\sqrt{s} = 63$-GeV," *Z.Phys.*, **C34**(1987), 163.

[2] F. Abe *et al.* (CDF Collaboration), "Double parton scattering in $\bar{p}p$ collisions at $\sqrt{s} = 1.8$TeV," *Phys.Rev.*, **D56**(1997), 3811.

[3] V.M. Abazov *et al.* (D0 Collaboration), "Double parton interactions in photon+3 jet events in pp^- bar collisions $\sqrt{s} = 1.96$ TeV," *Phys.Rev.*, **D81**(2010), 052012, 0912.5104.

[4] Serguei Chatrchyan *et al.* (CMS Collaboration), "Study of double parton scattering using W + 2-jet events in proton-proton collisions at $\sqrt{s}$ = 7 TeV," *JHEP*, **1403**(2014), 032, 1312.5729.

[5] Georges Aad *et al.* (ATLAS Collaboration), "Measurement of the production cross section of prompt J/ψ mesons in association with a $W^{\pm}$ boson in pp collisions at $\sqrt{s} = 7$ TeV with the ATLAS detector," *JHEP*, **1404**(2014), 172, 1401.2831.

[6] Markus Diehl and Andreas Schafer, "Theoretical considerations on multiparton interactions in QCD," *Phys. Lett.*, **B698**(2011), 389, 1102.3081.

[7] V.P. Shelest, A.M. Snigirev, and G.M. Zinovev, "The Multiparton Distribution Equations in QCD," *Phys.Lett.*, **B113**(1982), 325.

[8] Jonathan R. Gaunt and W. James Stirling, "Double Parton Distributions Incorporating Perturbative QCD Evolution and Momentum and Quark Number Sum Rules," *JHEP*, **03**(2010), 005, 0910.4347.

[9] V. L. Korotkikh and A. M. Snigirev, "Double parton correlations versus factorized distributions," *Phys. Lett.*, **B594**(2004), 171, hep-ph/0404155.

[10] Wojciech Broniowski and Enrique Ruiz Arriola, "Valence double parton distributions of the nucleon in a simple model," *Few Body Syst.*, **55**(2014), 381, 1310.8419.

[11] Krzysztof Golec-Biernat and Emilia Lewandowska, "How to impose initial conditions for QCD evolution of double parton distributions?" *Phys.Rev.*, **D90**(2014), 014032, 1402.4079.

[12] A.D. Martin, W.J. Stirling, R.S. Thorne, and G. Watt, "Parton distributions for the LHC," *Eur.Phys.J.*, **C63**(2009), 189, 0901.0002.

[13] Krzysztof Golec-Biernat, Emilia Lewandowska, Mirko Serino, Zachary Snyder, and Anna M. Stasto, "Constraining the double gluon distribution by the single gluon distribution," *Phys. Lett.*, **B750**(2015), 559, 1507.08583.

Study of high p_T particle production from double parton scatterings at the CMS experiment

Paolo Gunnellini[1]

[1]Deutsches Elektronen Synchrotron (DESY), Hamburg
[1] on behalf of the CMS Collaboration

A wide range of measurements sensitive to DPS contributions has been carried out within the CMS physics program for different physics channels. The investigated channels are characterized by a high number of physics objects in the final state, e.g. jets. Measurements related to the W+two-jet [1], four-jet [2], γ+three-jet [3] and two-b+two-light-jet [4] final states have been released by the CMS experiment. The current strategy for DPS-extraction analyses is based on the association of the selected objects in two pairs and on the measurement of differential cross sections as a function of correlation observables defined by the kinematical topology of the final state. The two pairs can be produced by two independent scatterings in case of a DPS event and the correlation observables are expected to be able to disentangle this occurrence. Studies at generator level have shown that variables which are most sensitive to a DPS contribution are the ones which consider the relative topology of all selected objects, not only of the objects of one of the two pairs [5]. One of such observables is ΔS, which corresponds to the azimuthal angle between the two selected pairs and is defined as:

$$\Delta\mathrm{S} = \arccos\left(\frac{\vec{p}_{\mathrm{T}}(\mathrm{pair}_1)\cdot\vec{p}_{\mathrm{T}}(\mathrm{pair}_2)}{|\vec{p}_{\mathrm{T}}(\mathrm{pair}_1)|\cdot|\vec{p}_{\mathrm{T}}(\mathrm{pair}_2)|}\right) \quad (1)$$

For the W+two-jet channel, pair_1 and pair_2 are, respectively, the reconstructed W and the dijet system, while in the four-jet (two-b+two-light-jet) final state, they correspond to the hard (bottom) and soft (light) dijet systems. In Figure 1, the differential cross section normalized to the number of selected events as a function of the ΔS observable measured by CMS is shown for various final states.

In each of them, the measured cross sections have a similar shape with a falling distribution from correlated configurations at high values, down to uncorrelated jet topologies at low values of ΔS. The measured cross sections have been also compared to predictions obtained with various MC event generators, implementing different matrix elements (ME) interfaced with parton shower (PS) and underlying event (UE) simulation. The PYTHIA 8 [6] and HERWIG++ [7] event

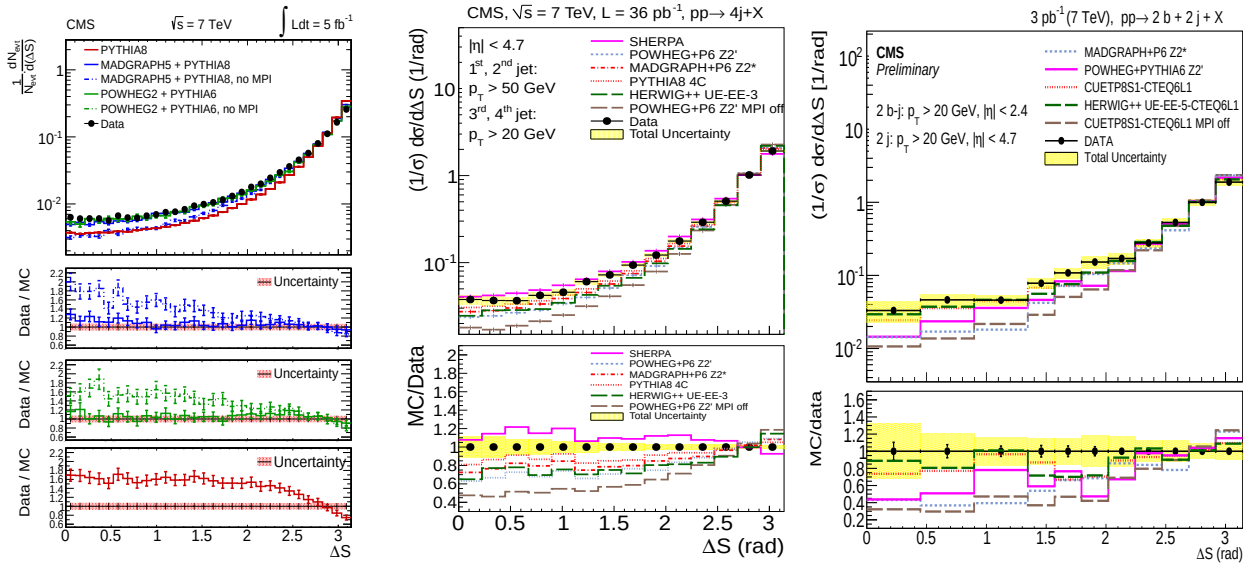

Figure 1: CMS data on the ΔS observable for various measured final states: W+two-jet (left), four-jet (center), γ+three-jet (right) channels.

generators simulate Leading Order (LO) 2→2 processes, SHERPA [8] and MADGRAPH [9] generate LO diagrams with higher number of partons in the final state, while POWHEG [10] produces Next-to-Leading-Order (NLO) processes, with real and virtual corrections included in the ME. Predictions without the contribution of MPI are also considered in the comparison. All predictions include a simulation of parton-shower and underlying-event effects generated according to MC tunes to the data.

In general, for all considered channels, predictions of multileg or NLO event generators are able to reproduce reasonably well the measured distributions. However, some room for improvement is available for the simulation of hard MPI contribution in the current models, in order to achieve a better description of the cross section at low values of ΔS. Predictions from event generators without the simulation of MPI do not reproduce the measured points, mainly in the region at low values of ΔS, where a DPS contribution is expected. This comparison clearly indicates the need for MPI in the current models to achieve a correct description of the DPS-sensitive observables. A quantitative extraction of the DPS contribution necessarily relies on the measurement of correlation observables and can be carried out through the so-called template [1] or the fitting [11] methods.

Moreover, other measurements in double J/ψ final states [12] and vector-boson production associated to b-jets [13, 14], show a clear evidence of need for DPS events in the simulation for a correct description of the sensitive distributions. Nevertheless, no quantitative value of the DPS contribution has been extracted so far for these measurements.

In conclusion, measurements sensitive to hard multiple interactions are available in many different physics channels. Observables investigating correlations in azimuthal angle between the

objects selected in the considered final states can not be described by current models without implementing a simulation of multiple-parton interactions. These measurements can be used in the future to study the dependence of the double parton scattering contribution on the partonic initial state in terms of x and flavour, and on the scale of the process.

References

[1] Serguei Chatrchyan *et al.* (CMS), "Study of double parton scattering using W + 2-jet events in proton-proton collisions at $\sqrt{s}$ = 7 TeV," *JHEP*, **03**(2014), 032, 1312.5729.

[2] Serguei Chatrchyan *et al.* (CMS), "Measurement of four-jet production in proton-proton collisions at $\sqrt{s} = 7$TeV," *Phys. Rev.*, **D89**(2014) (9), 092010, 1312.6440.

[3] CMS Collaboration (CMS), "Study of double parton scattering in photon + 3 jets final state in proton-proton collisions at 7TeV," 2015, CMS-PAS-FSQ-12-017.

[4] CMS Collaboration (CMS), "Studies of 2 b-jet + 2 jet production in proton-proton collisions at 7 TeV," 2015, CMS-PAS-FSQ-13-010.

[5] Paolo Gunnellini, "Study of double parton scattering using four-jet scenarios in proton-proton collisions at $\sqrt{s}$ = 7 TeV with the CMS experiment at the Large Hadron Collider," Ph.D. thesis, U. Hamburg, Dept. Phys., 2014.

[6] Torbjorn Sjostrand, Stephen Mrenna, and Peter Z. Skands, "A Brief Introduction to PYTHIA 8.1," *Comput. Phys. Commun.*, **178**(2008), 852, 0710.3820.

[7] J. Bellm *et al.*, "Herwig++ 2.7 Release Note," (2013), 1310.6877.

[8] T. Gleisberg, *et al.*, "Event generation with SHERPA 1.1," *JHEP*, **02**(2009), 007, 0811.4622.

[9] J. Alwall, *et al.*, "The automated computation of tree-level and next-to-leading order differential cross sections, and their matching to parton shower simulations," *JHEP*, **07**(2014), 079, 1405.0301.

[10] Stefano Frixione, Paolo Nason, and Carlo Oleari, "Matching NLO QCD computations with Parton Shower simulations: the POWHEG method," *JHEP*, **0711**(2007), 070, 0709.2092.

[11] Vardan Khachatryan *et al.* (CMS), "Event generator tunes obtained from underlying event and multiparton scattering measurements," (2015), 1512.00815.

[12] Vardan Khachatryan *et al.* (CMS), "Measurement of prompt J/ψ pair production in pp collisions at $\sqrt{s}$ = 7 Tev," *JHEP*, **09**(2014), 094, 1406.0484.

[13] Serguei Chatrchyan *et al.* (CMS), "Measurement of the production cross section for a W boson and two b jets in pp collisions at $\sqrt{s}$=7 TeV," *Phys. Lett.*, **B735**(2014), 204, 1312.6608.

[14] Serguei Chatrchyan *et al.* (CMS), "Measurement of the cross section and angular correlations for associated production of a Z boson with b hadrons in pp collisions at $\sqrt{s} = 7$ TeV," *JHEP*, **12**(2013), 039, 1310.1349.

Double Parton Scattering effects in kt-factorisation for 4-jet production

Mirko Serino*[1], Krzysztof Kutak[1], and Andreas van Hameren[1]

[1]The Henryk Niewodniczański Institute of Nuclear Physics, Polish Academy of Sciences, Ul. Radzikowskiego 152, 31-342, Cracow, Poland

1 The setup

We present a study of both Single and Double Parton Scattering contributions to the inclusive 4-jet production in the kt-factorisation framework at Leading Order and $E_{CM} = 7\,\text{TeV}$ and compare it to collinear results in the literature for various sets of kinematic cuts.
We use the Kimber-Martin-Ryskin prescription to build Next-to-Leading-Order Transverse Momentum Dependent PDFs and the AVHLIB[1] package to evaluate and perform the numerical Montecarlo integration. When it comes to kt-factorisation, we use fully gauge-invariant amplitudes with both initial state particles off the mass-shell for both Single Parton Scattering and Double Parton Scattering processes, which means that we generate up to six legs amplitudes with two off-shell legs. Techniques to compute such amplitudes in gauge invariant ways are by now well established [1–3].

We employ a running α_s from the MSTW0868cl PDF sets, use a hard scale and renormalisation scale equal to $\mu_R = \mu_F = 1/2 \sum_i p_T^i$, where the sum runs over the final state particles, and work in the $N_f = 5$ and $N_f = 4$ flavour schemes for the collinear and kt factorisation case respectively.

We apply the Kimber-Martin-Ryskin prescription to the MSTW0868cl sets, resumming gluon emissions and thereby obtaining TMD PDFs depending on x, the transverse momentum k_T and the factorization scale μ_F

2 Hard central cuts

In order to test the tools employed for our calculation, we compare our LO results to those reported by the BlackHat and NJET collaborations [4,5]. The cuts on the transverse jet momenta are $p_T > 80\text{GeV}$ for the leading jet, defined as the jet with highest transverse momentum, $p_T > 60\text{GeV}$ for the subleading jets, $|\eta| < 2.8$ for the rapidity and the jet-size parameter is $R = 0.4$. In the

*Presenter

[1]available for download at https://bitbucket.org/hameren/avhlib

collinear case, we find complete agreement with the results presented by BlackHat and NJET. Predictions for the 4-th leading jet are shown in Fig. 1; the deviations from the collinear case found when switching from collinear (left panel) to kt-factorisation (right panel), as well as when including the DPS contributions, are shown to be negligible. In particular, it is expected that the DPS contribution is negligible for hard central jets, as it is really unlikely to have two parton scatterings with high momentum transfer in the same proton-proton collision. Fig. 1 also shows the ATLAS data from [6], showing that they are well described by perturbation theory.

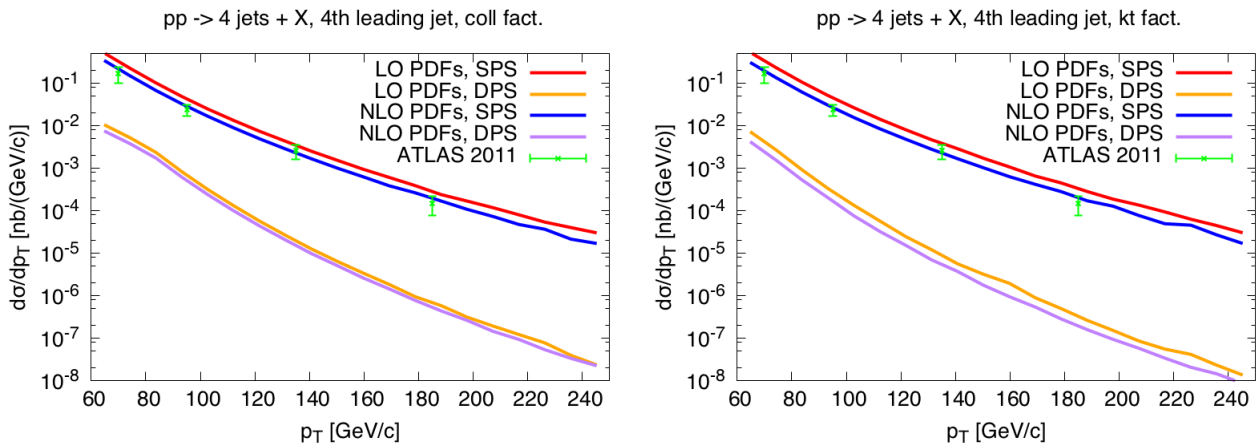

Figure 1: Predictions from LO collinear (left) and kt factorisation (right) calculations for the 4th leading jet spectrum compared to ATLAS data

3 Lower cuts

On the other hand, when we lower the cuts on the transverse momentum of the final state partons, we find that the DPS dominance found in [7] for low transverse momentum in the leading jet p_T spectrum is tamed by kt-factorisation.

We present the leading jet p_T spectrum for the symmetric cuts $35\,\text{GeV} < p_T < 100\,\text{GeV}$, $|\eta| < 4.7$, $R = 0.5$ in Fig. 2. It is striking how, in kt-factorisation, the DPS cross section is suppressed with respect to the collinear case. This is not expected and needs some explanation. The interpretation of this discrepancy is that there is a kinematic effect playing an important role here: kt-factorisation resums gluon emission from initial state partons, which implies that, in the case of $2 \to 2$ scattering, the back-to-back configuration of the final state, which is fine in a pure tree level calculation, is doomed; in this respect symmetric cuts do not do a good job, because they rule out all the configurations in which one transverse momentum is above the lower threshold and the other one is below. We thus propose to impose the following asymmetric cuts, i.e. $35\,\text{GeV} < p_T < 100\,\text{GeV}$ for the leading jet, $20\,\text{GeV} < p_T < 100\,\text{GeV}$ for non leading jets, $|\eta| < 4.7$, $R = 0.5$, thereby observing that the two behaviours still differ, but the strong suppression of DPS observed in kt-factorisation for symmetric cuts is tamed (see Fig. 3).

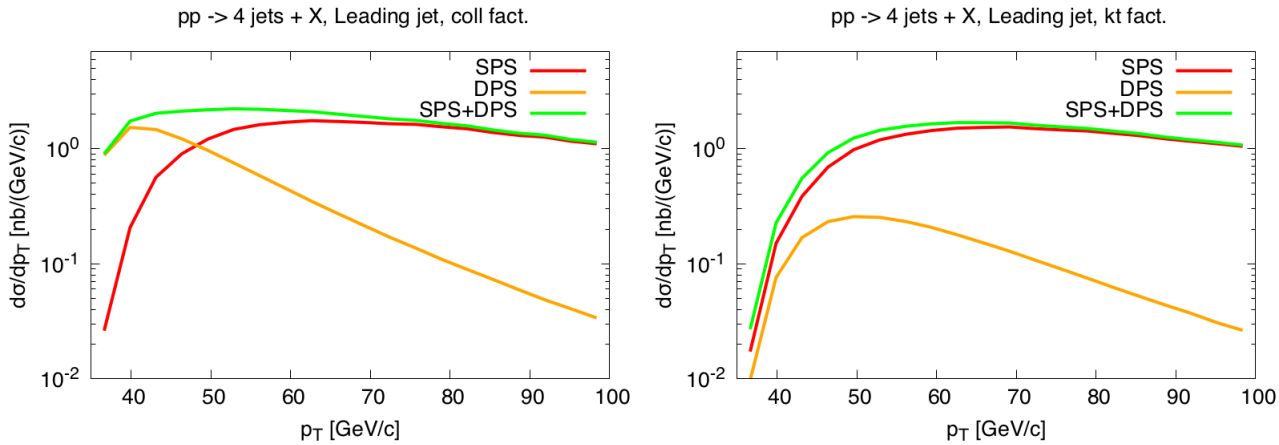

Figure 2: Theoretical predictions for the leadin jet p_T spectrum in collinear (left) and kt (right) factorisation for symmetric cuts.

We thus conclude that kt-factorisation pushes the DPS dominance region for the leading jet p_T differential cross section down to lower values of the transverse momentum cuts. Further improvement of the theoretical predictions can of course be reached by pushing the perturbative computations to NLO. This is already well established in the collinear case, whereas work is in progress for the kt-factorisation approach.

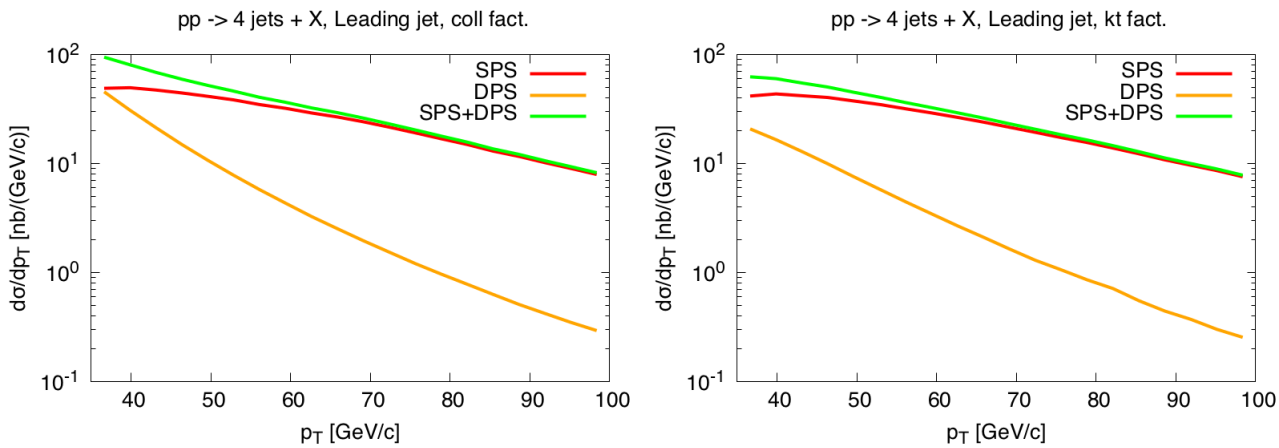

Figure 3: Theoretical predictions for the leadin jet p_T spectrum in collinear (left) and kt (right) factorisation for asymmetric cuts.

Acknowledgements

This work was partially supported by NCN grant DEC-2013/10/E/ST2/00656 and by the "Angelo Della Riccia" foundation.

References

[1] A. van Hameren, "BCFW recursion for off-shell gluons," *JHEP*, **07**(2014), 138, 1404.7818.

[2] M. Bury and A. van Hameren, "Numerical evaluation of multi-gluon amplitudes for High Energy Factorization," *Comput. Phys. Commun.*, **196**(2015), 592, 1503.08612.

[3] Andreas van Hameren and Mirko Serino, "BCFW recursion for TMD parton scattering," *JHEP*, **07**(2015), 010, 1504.00315.

[4] Z. Bern, *et al.*, "Four-Jet Production at the Large Hadron Collider at Next-to-Leading Order in QCD," *Phys. Rev. Lett.*, **109**(2012), 042001, 1112.3940.

[5] Simon Badger, Benedikt Biedermann, Peter Uwer, and Valery Yundin, "NLO QCD corrections to multi-jet production at the LHC with a centre-of-mass energy of $\sqrt{s} = 8$ TeV," *Phys. Lett.*, **B718**(2013), 965, 1209.0098.

[6] Georges Aad *et al.* (ATLAS), "Measurement of multi-jet cross sections in proton-proton collisions at a 7 TeV center-of-mass energy," *Eur. Phys. J.*, **C71**(2011), 1763, 1107.2092.

[7] Rafał Maciuła and Antoni Szczurek, "Searching for and exploring double-parton scattering effects in four-jet production at the LHC," *Phys. Lett.*, **B749**(2015), 57, 1503.08022.

Cancellation of Glauber gluon exchange in the double Drell-Yan process

Markus Diehl[1], Jonathan R. Gaunt[2], Daniel Ostermeier[3], Peter Plößl[3], and Andreas Schäfer[3]

[1]Deutsches Elektronen-Synchroton DESY, 22603 Hamburg, Germany
[2]Nikhef and VU Amsterdam, De Boelelaan 1081, 1081 HV Amsterdam, The Netherlands
[3]Institut für Theoretische Physik, Universität Regensburg, 93040 Regensburg, Germany

Abstract

For any factorisation proof, a crucial step is a demonstration of the cancellation of so-called Glauber gluons. We summarise a recent paper in which we demonstrated this cancellation for double Drell-Yan production (the double parton scattering process in which a pair of electroweak gauge bosons is produced), both for the integrated cross section and for the cross section differential in the boson transverse momenta.

1 Introduction

In order to make predictions at the LHC one relies on factorisation formulae that separate the short distance/high scale dynamics of interest, from the low-scale nonperturbative physics. The short distance physics is encoded in perturbatively-computable partonic cross sections, whilst the infra-red physics is encoded in parton distribution-type objects (and possibly also soft functions). In single parton scattering, factorisation has been rigorously proven for Drell-Yan production (or, more generally, colour-singlet production), for the total cross section and cross section differential in the p_T of the colour singlet system [1–4]. These factorisation formulae are correct at leading power – i.e. up to corrections of order Λ^2_{QCD}/Q^2, with Q the hard scale of the process. For the analogous process in double parton scattering, namely double Drell-Yan (dDY) production, a factorisation formula was written down long ago for the total cross section [5, 6] based on the analysis of the lowest-order Feynman diagrams. A factorisation formula for the cross section differential in the p_Ts of the colour singlet systems has also been written down using the same method [7]. However, serious attempts to rigorously justify these formulae have only begun in recent years [7–10].

One approach to proving factorisation formulae at leading power (and potentially beyond) is the so-called Collins-Soper-Sterman (CSS) approach, which is the one that was employed in [1–4] (there exists an alternative approach that we will not discuss based on effective field theories – see e.g. [11–17]). Let us give a brief review of this method. The first goal is to identify leading infra-red contributions in Feynman graphs contributing to the process of interest –

contributions from small regions around the points at which certain lines go on shell, which despite having a smaller phase space are leading due to propagator denominators blowing up. These infra-red contributions are the ones that will have to be absorbed in the PDF-type objects. To be more precise, one needs to identify regions around pinch singular surfaces (PSSs) – these are points where propagator denominators pinch the contour of the Feynman integral [strictly speaking the singularities only appear in the limit in which parton masses and the boson p_T (if appropriate) are set to zero]. If poles all converge on the Feynman contour from one side, one can perform a contour deformation to avoid them (in that case the contribution originally in the vicinity of the poles is subsumed into another region). The identification of PSSs is facilitated by the Coleman-Norton theorem [18], which states that PSSs in Feynman graphs correspond to classically allowed processes, and the PSSs for single Drell-Yan (sDY) and dDY are known.

The pinch singularity analysis tells us nothing about the strength of the singularities, and so must be complemented with a power counting procedure to identify the leading power regions around the singularities. Doing this, one identifies several types of loop momentum scaling that can give rise to a leading power contribution. These are *collinear* (momentum close to some beam/jet direction), *(central) soft* (all momentum components small and of the same order), *hard* (all momentum components large and of order Q) and *Glauber*. The kinematics of Glauber particles is that of those mediating forward or small-angle scattering – i.e. a Glauber momentum r satisfies $|r^+ r^-| \ll \mathbf{r}^2$, where $r^\pm = (r^0 \pm r^3)/\sqrt{2}$, $\mathbf{r} = (r^1, r^2)$.

Initially, there are many longitudinally-polarised gluon connections between parton lines in the collinear region and the union of the soft and Glauber regions, as well as between lines in the collinear region and the hard region. The next step of the factorisation procedure is to apply approximations appropriate to these momentum regions, followed by Ward identities in the sum over graphs to strip away these multiple attachments, yielding the separate functions that appear in the factorisation formula. Unfortunately, this procedure does not work for the Glauber modes, since the approximations needed to apply the Ward identities may not be made in this case. Thus, to achieve factorisation one must demonstrate that the contribution from the Glauber region cancels for the given observable. Note that by 'cancels' here, we mean that there is no remaining 'distinct' (pinched) Glauber contribution – there can (and will) be remaining contributions associated with the Glauber kinematic region, but these can be absorbed into the collinear or soft functions (this was re-emphasised recently in the effective field theory context in [17]). The cancellation of Glauber exchanges was achieved in sDY (total cross section and cross section differential in colour singlet p_T) by CSS, and recently in dDY (total cross section and cross section differential in colour singlet p_Ts) by us in [10] – here we summarise this latter work. In this short proceedings contribution we mainly limit ourselves to a discussion of the cancellation of Glauber modes at the one-gluon level in section 2 – this is useful to illustrate why the cancellation works for dDY as it does for sDY. We very briefly mention how the all-order proof works in section 3.

2 Glauber cancellation for one-gluon exchange

In order to show the cancellation of Glauber modes at the one-gluon level, we adopt a model in which all partons (except the exchanged Glauber gluon) are scalar (represented by a solid line), and the hadrons are also scalars (represented by a dashed line). These partons may be predominantly collinear to the lower hadron travelling in the plus direction (we colour plus-collinear lines in red), or collinear to the upper hadron travelling in the minus direction (we colour minus-collinear lines in blue). As the Glauber cancellation argument below depends

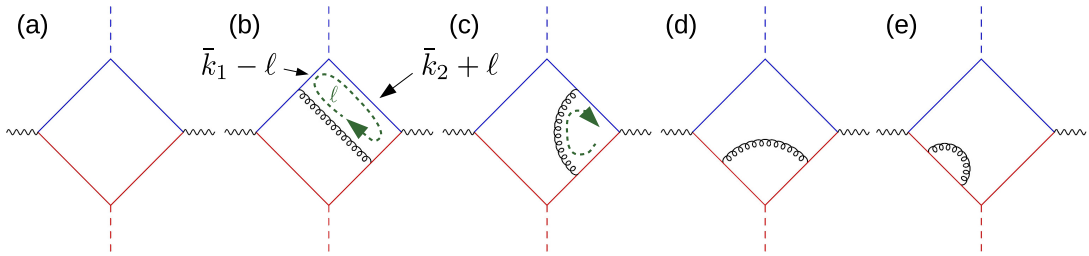

Figure 1: Lowest order diagram contributing to dDY in the model described in the text (a), and the nonzero virtual one-gluon corrections to this (b)-(e).

only on the analyticity properties of the Feynman integrands, which is determined only by the propagator denominators, this argument applies beyond the model, also to diagrams in QCD.

The lowest-order diagram contributing to the dDY amplitude (which one simply squares to get the lowest order contribution to the cross section) is given in figure 1, along with the nonzero virtual one-gluon corrections to this (these are combined with the tree-level amplitude to get the virtual one-gluon corrections to the cross section). The real one-gluon corrections to the tree-level amplitude squared are zero by colour considerations, and anyway can have no contribution associated with the Glauber kinematic region due to the on-shell constraint for the gluon. Let us consider the virtual corrections in turn, starting with the 'double box' graph in figure 1(b). In this graph, the gluon momentum ℓ runs 'against' and 'with' a large minus momentum – this results in ℓ^+ being trapped at small values, as one can see by looking at the propagator denominators associated with these minus-collinear lines:

$$2\ell^+\bar{k}_2^- + ... + i\varepsilon \qquad -2\ell^+\bar{k}_1^- + ... + i\varepsilon \tag{1}$$

The terms indicated by '...' are products of small components only. This is a general principle - to trap the plus/minus component of a soft momentum at small values, the momentum must run both 'against' and 'with' a collinear line (or multiple lines) with large minus/plus momentum. Now, since ℓ in figure 1(b) only runs against a large plus momentum, ℓ^- is not trapped, and we can deform ℓ^- until ℓ is out of the Glauber region (and is in the collinear region). So there is no distinct Glauber contribution associated with figure 1(b).

In the gauge boson vertex correction graph, figure 1(c), neither ℓ^+ nor ℓ^- is trapped, so we can deform the contour out of the Glauber region there too. This leaves us only with the hadron vertex correction and parton self-energy graphs in figures 1(d) and (e), which are topologically factorised already, and thus can present no problem. Thus, for the one-gluon corrections to the tree-level graph, there is no problematic pinched Glauber contribution in the first place.

This kind of consideration can be extended to arbitrarily complex one-gluon diagrams in the model, some of which are sketched in figure 2. For many types of diagram, a routing can be found for the gluon momentum ℓ such that ℓ^+ and/or ℓ^- is not trapped at small values. This is the case for diagrams (a) - (e) in figure 2 – for each of these diagrams a routing for ℓ that leaves one light-cone component untrapped is given by the green dashed arrow. The only graphs for which both ℓ^+ and ℓ^- are always pinched are the ones in which the gluon attaches to spectator partons that either go directly into the final state or only split into partons that go into the final state, both in the upper and lower parts of the graph. An example of this type of graph is given in figure 2(f) (with a routing that gives ℓ^+, ℓ^- trapped denoted by the solid purple arrow). However, these graphs are of essentially the same nature as the Glauber-pinched graphs that appear for sDY (only with the dDY production subgraph, as on the left of figure 2(f), replaced by a simpler sDY production). For these graphs one can use the same unitarity-based argument as was used by CSS for sDY (reviewed in e.g. [19]), to cancel the Glauber contribution after the

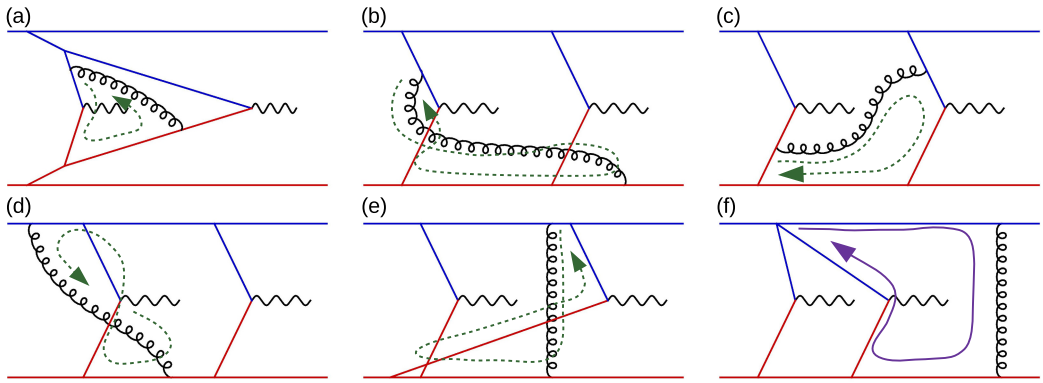

Figure 2: Example graphs for the dDY amplitude within the model described in the text. The incoming lines on the left of each graph could represent the proton, or partons emerging from the proton.

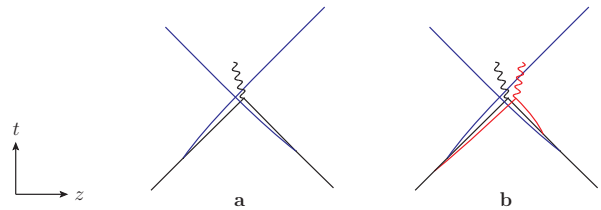

Figure 3: Spacetime structure of the pinch surfaces for sDY (left) and dDY (right). Figure taken from [7].

sum over possible final-state cuts. For this argument to work it is essential that the observable be insensitive to the position of the cut in the 'final state' spectator-spectator system.

3 Glauber gluon cancellation at all orders

In order to demonstrate the cancellation of Glauber exchanges in dDY production to all orders in QCD perturbation theory, we made use of the same techniques as were used in [3, 4] to show the all-order cancellation in sDY – in particular, we used the light-front ordered version of QCD perturbation theory (LCPT). We do not discuss the details of this proof here, referring the interested reader to [10]. The general idea is the same as the one-loop proof discussed above, however. Also in the all-order LCPT picture, one sees that from the point of view of the Glauber gluons, single and double scattering look rather similar, and that the troublesome 'final state' poles obstructing the deformation out of the Glauber region cancel after the sum over cuts. The argument is based on unitarity, and it can be cast into a form in which it is essentially the same for sDY and dDY.

One can get some insight into why the Glauber cancellation proceeds for dDY as it does for sDY by looking at the PSSs for the two processes in spacetime, given in figure 11 of [7] and reproduced here as figure 3. In the diagrams are drawn the collinear lines (black and red lines) as well as the hard vertices producing the colour-singlet particles. One observes that the hard vertices occur at the same point in spacetime for dDY, and that the locations of the collinear lines and hard vertices are the same for sDY and dDY. Thus, from the perspective of soft long-range gluons the two processes look essentially the same, and the Glauber cancellation that works for sDY should also work for dDY, as we indeed found.

References

[1] Geoffrey T. Bodwin, "Factorization of the Drell-Yan Cross-Section in Perturbation Theory," *Phys. Rev.*, **D31**(1985), 2616, [Erratum: Phys. Rev.D34,3932(1986)].

[2] John C. Collins, Davison E. Soper, and George F. Sterman, "Factorization for Short Distance Hadron - Hadron Scattering," *Nucl. Phys.*, **B261**(1985), 104.

[3] John C. Collins, Davison E. Soper, and George F. Sterman, "Soft Gluons and Factorization," *Nucl. Phys.*, **B308**(1988), 833.

[4] John Collins, Foundations of perturbative QCD, Cambridge University Press, 2013.

[5] N. Paver and D. Treleani, "Multi-Quark Scattering and Large p_T Jet Production in Hadronic Collisions," *Nuovo Cim.*, **A70**(1982), 215.

[6] M. Mekhfi, "Multiparton Processes: An Application to Double Drell-Yan," *Phys. Rev.*, **D32**(1985), 2371.

[7] Markus Diehl, Daniel Ostermeier, and Andreas Schafer, "Elements of a theory for multiparton interactions in QCD," *JHEP*, **03**(2012), 089, 1111.0910.

[8] B. Blok, Yu. Dokshitser, L. Frankfurt, and M. Strikman, "pQCD physics of multiparton interactions," *Eur. Phys. J.*, **C72**(2012), 1963, 1106.5533.

[9] Aneesh V. Manohar and Wouter J. Waalewijn, "A QCD Analysis of Double Parton Scattering: Color Correlations, Interference Effects and Evolution," *Phys. Rev.*, **D85**(2012), 114009, 1202.3794.

[10] Markus Diehl, Jonathan R. Gaunt, Daniel Ostermeier, Peter Plößl, and Andreas Schäfer, "Cancellation of Glauber gluon exchange in the double Drell-Yan process," *JHEP*, **01**(2016), 076, 1510.08696.

[11] Christian W. Bauer, Sean Fleming, and Michael E. Luke, "Summing Sudakov logarithms in $B \to X_s\gamma$ in effective field theory," *Phys. Rev. D*, **63**(2000), 014006, hep-ph/0005275.

[12] Christian W. Bauer, Sean Fleming, Dan Pirjol, and Iain W. Stewart, "An Effective field theory for collinear and soft gluons: Heavy to light decays," *Phys. Rev. D*, **63**(2001), 114020, hep-ph/0011336.

[13] Christian W. Bauer and Iain W. Stewart, "Invariant operators in collinear effective theory," *Phys. Lett. B*, **516**(2001), 134, hep-ph/0107001.

[14] Christian W. Bauer, Dan Pirjol, and Iain W. Stewart, "Soft collinear factorization in effective field theory," *Phys. Rev. D*, **65**(2002), 054022, hep-ph/0109045.

[15] Christian W. Bauer, Sean Fleming, Dan Pirjol, Ira Z. Rothstein, and Iain W. Stewart, "Hard scattering factorization from effective field theory," *Phys. Rev. D*, **66**(2002), 014017, hep-ph/0202088.

[16] M. Beneke, A.P. Chapovsky, M. Diehl, and T. Feldmann, "Soft collinear effective theory and heavy to light currents beyond leading power," *Nucl. Phys.*, **B643**(2002), 431, hep-ph/0206152.

[17] Ira Z. Rothstein and Iain W. Stewart, "An Effective Field Theory for Forward Scattering and Factorization Violation," (2016), 1601.04695.

[18] S. Coleman and R. E. Norton, "Singularities in the physical region," *Nuovo Cim.*, **38**(1965), 438.

[19] Jonathan R. Gaunt, "Glauber Gluons and Multiple Parton Interactions," *JHEP*, **07**(2014), 110, 1405.2080.

Study of observables for the measurement of MPI using Z + jets process

R. Kumar[1,2], M. Bansal[3], S. Bansal[1], and J. B. Singh[1]

[1]Panjab University, Chandigarh, INDIA
[2]Akal University, Talwandi Sabo, INDIA
[3]D.A.V. College, Sector 10, Chandigarh, INDIA

1 Introduction

For the study of high-p_{T}/mass particle production from multiple-parton interactions (MPI) in hadron-hadron collisions, a number of measurements has been performed [1–9], using various processes, $e.g.$, Z/W + jets, photon + jets, and 4-jets at different collision energies. These measurements use correlation observables between the particles produced from the first and second parton-parton scatterings. These observables show little sensitivity to MPI which lead to large systematic uncertainties in the tuned model parameters [10]. In addition, inclusive MPI selection is required for the correct estimation of the model parameters [11–13] on theoretical grounds, but experimental selection criteria restricts existing measurements to the double parton scattering (DPS) only. This paper presents a study of MPI with simulated Z + jets events in proton-proton collisions at a centre-of-mass energy of 13 TeV. The events are simulated using POWHEG followed by hadronization and parton-showering using PYTHIA8.

2 Analysis details

Simulated events for Z + jets process, produced in proton-proton (pp) collisions at 13 TeV, are generated upto NLO accuracy with POWHEG [14, 15]. POWHEG uses the "Multi-scale improved NLO" (MiNLO) method [16] which describes well the jet productions associated with W/Z boson. These hard scattering events are hadronized and parton showered using PYTHIA8 [17]. The MPI are also simulated with the PYTHIA8 [18]. The ATLAS A14 tune [19] with NNPDF2.3LO set of parton distribution functions (PDF) is used. This set of MPI model parameters is obtained by fitting the underlying event data obtained at the LHC.

The events with exactly two muons having p_{T} larger than 20 GeV/c and absolute pseudo-rapidity (η) less than 2.5, are selected. The dimuon invariant mass is required to be in the range of 60–120 GeV/c^2. The charged particle jets, having minimum transverse momentum of 20 GeV/c and absolute pseudo-rapidity less than 2, are used to construct the observables for measurements

of the multiple-parton interactions. Jets are clustered using anti-k_T algorithm [20] with the radius parameter equal to 0.5. This kinematic selection criteria is motivated from the trigger and the background constraints at the LHC experiments

The hard MPI analyses, at Tevatron [3, 4] and LHC [6–8], use correlation observables between decay products of the first and second hard interactions, for MPI measurements. These observables are based on the assumption that MPI are independent of each other. MPI contribution is then extracted by a template fit method [6, 7]. A little sensitivity to MPI is observed for these observables. The definitions of these observables also restrict the MPI measurement to DPS only. The variables which support inclusive MPI selection and show significantly high sensitivity are investigated. The jet multiplicity observable is proposed for MPI studies, which lead to inclusive MPI selection unlike the correlation observables. A visible effect ($\sim$ 20%) is observed using jet multiplicity observable as shown in Fig. 1 (a). The sensitivity of jet multiplicity observable is of the same level as that of correlation observables due to large background from the single parton scatterings (SPS). The contribution from SPS can be reduced by applying an upper cut on the p_{T} of Z-boson ($p_{\mathrm{T}}^{\mathrm{Z}}$). A gain, in terms of MPI sensitivity by a factor 3–4, is achieved by applying an upper cut of 10 GeV/c on the $p_{\mathrm{T}}^{\mathrm{Z}}$ as depicted in Fig. 1 (b).

The jet multiplicity observables also show large sensitivity to the variation in MPI parameters as compared to the correlation observables. This large sensitivity to the MPI parameters will lead to more accurate estimation of the model parameters with reduced systematic uncertainties.

3 Summary

This paper presents the analysis of the Z + jets events to explore the new observables and phase-space region which can enhance the sensitivity to the MPI. The Z + jets events are generated with POWHEG, followed by the hadronization and showering with PYTHIA8. The distributions of jet multiplicity associated with Z-boson can be useful in inclusive study of MPI. The sensitivity to the presence of MPI increases significantly by requiring an upper cut on the p_{T} of Z-boson. It is observed that parameters of the MPI model, have increased sensitivity in the jet multiplicity distribution than the correlation observables. Hence jet multiplicity distribution associated with Z-boson can be used to perform the inclusive MPI measurements at the LHC and constraint MPI model parameters with better precision.

Acknowledgements

This work is financially supported by Department of Science and Technology (DST), New Delhi and University Grant Commission (UGC), New Delhi. The authors would like to thank authors of POWHEG and PYTHIA8. The authors are grateful to organizers of workshop, 'Multiple-parton interactions at the LHC'.

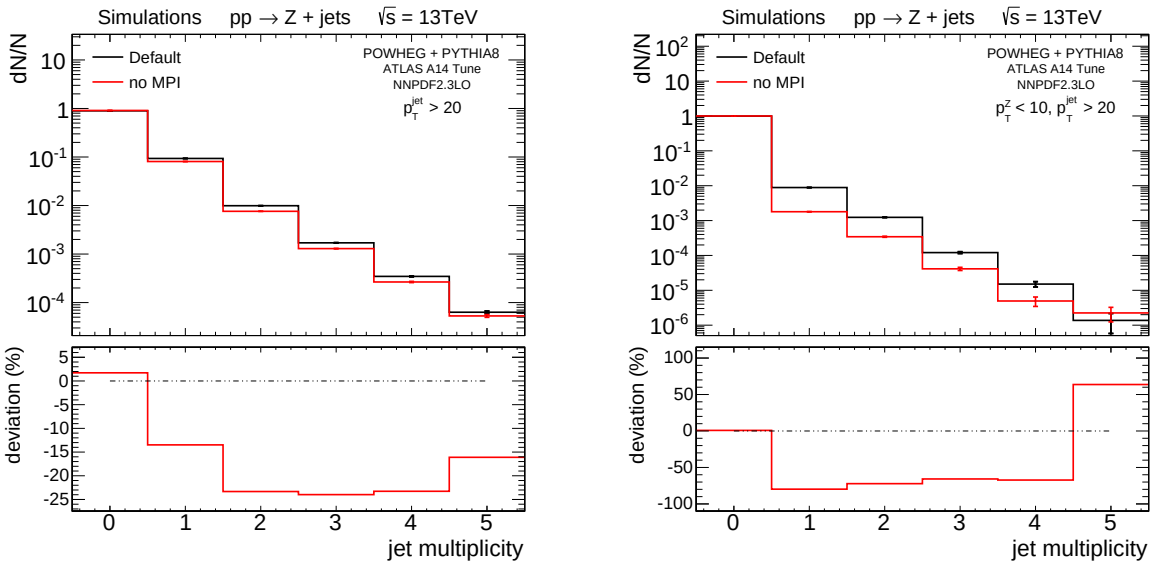

(a) (b)

Figure 1: Jet multiplicity distributions are compared for events with and without MPI. The events from Z + jets processes are generated using POWHEG, parton showered and hadronized with PYTHIA8. Jets with p_{T} larger than 20 GeV/c are considered. The distributions are shown (a) without any condition on $p_{\mathrm{T}}^{\mathrm{Z}}$ and (b) with $p_{\mathrm{T}}^{\mathrm{Z}}$ less than 10 GeV/c. The ratio plot in the bottom panel shows deviations of the distributions after switching off MPI.

References

[1] J. Alitti *et al.* (UA2), "A study of multi-jet events at the CERN $\bar{\mathrm{p}}\mathrm{p}$ collider and a search for double parton scattering," *Phys. Lett. B*, **268**(1991), 145.

[2] T. Akesson *et al.* (AFS), "Double parton scattering in pp collisions at $\sqrt{s}$ = 63 GeV," *Z. Phys. C*, **34**(1987), 163.

[3] V. M. Abazov *et al.* (D0), "Double parton interactions in photon + 3 jet events $\mathrm{p}\bar{\mathrm{p}}$ collisions at $\sqrt{s}$ = 1.96 TeV," *Phys. Rev. D*, **81**(2010), 052012, hep-ex/0912.5104.

[4] F. Abe *et al.* (CDF), "Double parton scattering in $\mathrm{p}\bar{\mathrm{p}}$ collisions at $\sqrt{s}$ = 1.8 TeV," *Phys. Rev. D*, **56**(1997), 3811.

[5] F. Abe *et al.* (CDF), "Study of four jet events and evidence for double parton interactions in $\mathrm{p}\bar{\mathrm{p}}$ collisions at $\sqrt{s}$ = 1.8 TeV," *Phys. Rev. D*, **47**(1993), 4857.

[6] Chatrchyan *et al.* (CMS), "Study of double parton scattering using W + 2-jet events in proton-proton collisions at $\sqrt{s}$ = 7 TeV," *JHEP*, **03**(2014), 032, 1312.5729.

[7] Georges Aad *et al.* (ATLAS), "Measurement of hard double-parton interactions in $W(\rightarrow l\nu)$+ 2 jet events at $\sqrt{s}$=7 TeV with the ATLAS detector," *New J. Phys.*, **15**(2013), 033038, 1301.6872.

[8] Chatrchyan *et al.* (CMS), "Study of double parton scattering in photon + 3 jets final state in proton-proton collisions at 7TeV," *CMS-PAS-FSQ-12-017*, (2015).

[9] Chatrchyan *et al.* (CMS), "Double Parton Scattering cross section limit from same-sign W bosons pair production in di-muon final state at LHC," *CMS-PAS-FSQ-13-001*, (2015).

[10] V. Khachatryan *et al.* (CMS), "Event generator tunes obtained from underlying event and multiparton scattering measurements," *Eur. Phys. J.*, **C76**(2016) (3), 155, 1512.00815.

[11] D. Treleani, "Double parton scattering, diffraction and effective cross section," *Phys. Rev. D*, **76**(2007), 076006, 0708.2603.

[12] Manuel Bähr, Miroslav Myska, Michael H. Seymour, and Andrzej Siodmok, "Extracting $\sigma_{\rm eff}$ from the CDF γ + 3 jets measurement," *JHEP*, **03**(2013), 129, 1302.4325.

[13] Michael H. Seymour and Andrzej Siodmok, "Extracting $\sigma_{\rm eff}$ from the LHCb double-charm measurement," (2013), 1308.6749.

[14] S. Frixione, Paolo Nason, and Carlo Oleari, "Matching NLO QCD computations with parton shower simulations: the POWHEG method," *JHEP*, **11**(2007), 070, 0709.2092.

[15] John M. Campbell, R. K. Ellis, Paolo Nason, and Giulia Zanderighi, "W and Z bosons in association with two jets using the POWHEG method," *JHEP*, **08**(2013), 005, 1303.5447.

[16] Keith Hamilton, Paolo Nason, and Giulia Zanderighi, "MINLO: Multi-Scale Improved NLO," *JHEP*, **10**(2012), 155, 1206.3572.

[17] T. Sjöstrand, S. Mrenna, and P. Z. Skands, "A Brief Introduction to PYTHIA 8.1," *Comput. Phys. Commun.*, **178**(2008), 852, 0710.3820.

[18] Richard Corke, "Multiple Interactions in Pythia 8," (2009), 0901.2852.

[19] Georges Aad *et al.* (ATLAS), "Summary of ATLAS Pythia 8 tunes," *ATL-PHYS-PUB-2012-003*, (2012).

[20] Matteo Cacciari, Gavin P. Salam, and Gregory Soyez, "The Anti-k(t) jet clustering algorithm," *JHEP*, **04**(2008), 063, 0802.1189.

A Brief Comment on Multi-Gluon Amplitudes and Double Parton Interactions

Daniele Treleani[1] and Giorgio Calucci[1]

[1]University of Trieste and INFN

Abstract

A typical contribution to a color ordered multi-gluon amplitude, which can split into two weakly correlated two-body gluon scattering amplitudes and may thus contribute to a Double Parton Interaction, is briefly discussed. We find that the color ordered amplitude is not enhanced in the typical configuration generated by a DPI, where the transverse momenta of final state gluons are compensated pairwise, while a dominant contribution to the multi-gluon amplitude is due to terms proportional to the fusion amplitude of two initial state gluons. Which corresponds to an amplitude effectively describing a two rather than a three-body partonic interaction.

The Double Parton Interaction cross section can be expressed as a contribution to the forward elastic scattering amplitude characterized by two independent loops (cfr. Fig.1), where the initial momenta of the partonic interactions are integrated independently in the amplitude and in its complex conjugate, is such a way that the process is not diagonal as a function of the initial parton's momenta [1]. To evaluate the loop integral, it is convenient to distinguish two qualitatively different terms in the vertex Φ, representing the hadron structure (cfr. Fig.2). Namely the short distance contribution, ϕ, and the long distance contribution, ψ. In this way the interaction amplitude splits into 4 different terms. As shown in Fig.3, the first 3 terms contribute to DPIs, since the vertex ψ introduces a non perturbative dimensional factor in the amplitude, while the 4th term, where only ϕ vertices are present, contributes as a loop correction to the $2 \to 4$ parton scattering amplitude [2] [3].

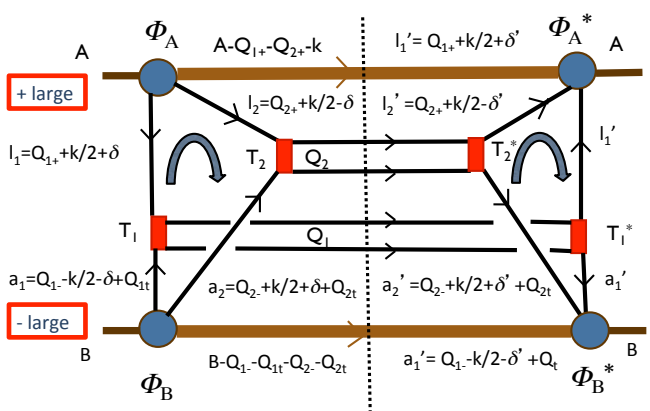

Figure 1: Double parton scattering contribution to the forward elastic amplitude

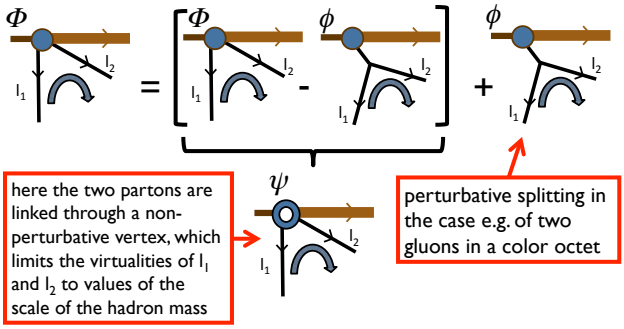

Figure 2: Non perturbative and perturbative contributions to the double parton vertex

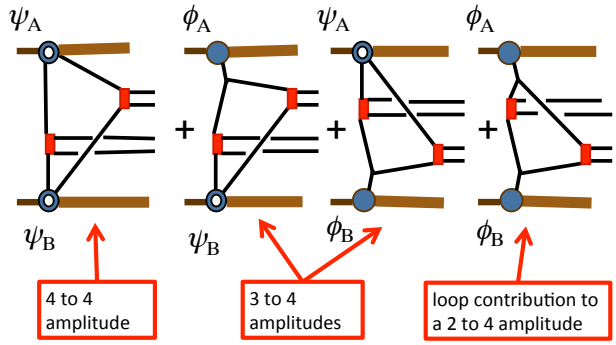

Figure 3: Different $4 \to 4$, $3 \to 4$ and $2 \to 4$ contributions to the interaction amplitude

The non perturbative dimension, characterizing the vertices ψ_A and ψ_B, limits the virtualities of the partons in the the loop to values of the order of the hadronic mass. As a consequence, the upper part of the loop in the interaction amplitude is characterized by large light cone '$+$' components, while the lower part of the loop is characterized by large light cone '$-$' components, in such a way that the loop integrations on the light cone '$+$' and '$-$' integration variables can be done independently.

In the case of the $4 \to 4$ scattering process, the feature is illustrated in Eq.(1) where the integrations on the loop variables δ_- and δ_+ define the functions Ψ_A and Ψ_B, which allow introducing the Double Parton Distribution Functions and thus expressing the DPI cross section in the familiar factorized form.

$$\int \frac{\psi_A}{l_1^2 l_2^2} T_1 T_2 \frac{\psi_B}{a_1^2 a_2^2} d\delta_- d\delta_+ \approx \left(\int d\delta_- \frac{\psi_A}{l_1^2 l_2^2} \right) \times \Big\{ T_1 T_2 \Big\} \times \left(\int d\delta_+ \frac{\psi_B}{a_1^2 a_2^2} \right) \equiv \Psi_A \times \Big\{ T_1 T_2 \Big\} \times \Psi_B \qquad (1)$$

The case of the $3 \to 4$ contributions is more elaborate. A partonic process contributing to the DPI amplitude is schematically shown in Fig.4. When looking at Feynman diagrams, one finds that, in the case of all gluons, the number of diagrams to be considered for the 7-gluon amplitude is huge: 2485 at tree level. A standard approach to the problem is therefore impractical. In the zero mass case, tree level amplitudes are nevertheless successfully worked out with the Spinor-Helicity formalism and, in the all-gluon case, tree level amplitudes have been worked out explicitly for any number of external gluons [4].

In the spinor-helicity formalism, the tree level amplitude of n gluons with colors $c_1, c_2 \ldots c_n$, momenta $p_1, p_2 \ldots p_n$ and helicities $\epsilon_1, \epsilon_2 \ldots \epsilon_n$, is expressed as

$$\mathcal{M}_n = \sum_{perms'} \mathrm{Tr}(T^{c_1} T^{c_2} \ldots T^{c_n}) A(p_1, \epsilon_1; p_2, \epsilon_2; \ldots; p_n, \epsilon_n) \qquad (2)$$

where the sum, $perms'$, is over all $non-cyclic$ permutations of 1,2,...,n and the T's are the SU(3) generators. The partial amplitudes $A(1, 2, ..., n)$ are called color ordered amplitudes and satisfy

various important properties. In particular each $A(1,2,...,n)$ is a gauge invariant quantity and each different terms is incoherent in $\mathcal{M}_n$ to leading order in the number of colors [5].

The partial amplitudes are expressed in terms of the spinor products:

$$\langle ij\rangle = \sqrt{s_{ij}}\, e^{i\varphi}, \qquad [ij] = \sqrt{s_{ij}}\, e^{-i\varphi} \tag{3}$$

where $s_{ij} = (p_i + p_j)^2$ and φ is a phase factor that, in many cases, is not relevant for the final result. All contributions to the 7-gluon amplitudes of interest can be obtained from 4 different color ordered amplitudes [6]. Each one is expressed by various terms, characterized by singularities in different combinations of the external momenta, where the convention is to define all external momenta in the amplitude as outgoing. The simplest color ordered amplitude is

$$\begin{aligned} &A(1^-2^-3^-4^+5^+6^+7^+) \\ &\quad = A(1^-2^-3^-4^+5^+6^+7^+)|_a + A(1^-2^-3^-4^+5^+6^+7^+)|_b + A(1^-2^-3^-4^+5^+6^+7^+)|_c \end{aligned} \tag{4}$$

As apparent in Fig.4, to contribute to a DPI, a multi-parton amplitude has to be characterized by at least two multi-particle singularities. In the actual case the condition is satisfied by $A|_c$:

$$A(1^-2^-3^-4^+5^+6^+7^+)|_c = -\frac{\langle 3|(4+5)(6+7)|1\rangle^3}{P_{345}^2 P_{671}^2 \langle 34\rangle\langle 45\rangle\langle 6|7+1|2]\langle 67\rangle\langle 71\rangle\langle 5|4+3|2]} \tag{5}$$

Analogously to the $4 \to 4$ case, to study the effect of the loop integration on the term $A|_c$, one can integrate on the loop integration variables δ_+ and δ_- (cfr. Fig.4) by keeping into account of the dependence on δ_- only in the upper part of the loop and of the dependence on δ_+ only in the lower part of the loop. The integration on δ_+ thus defines the function Ψ_B and fixes the values of the fractional momentum components of P_{345} and of P_{671} with respect to p_2, actually z and $1-z$, while the integration on δ_- is estimated with the singularities of $1/(P_{345}^2 P_{671}^2)$ in $A|_c$:

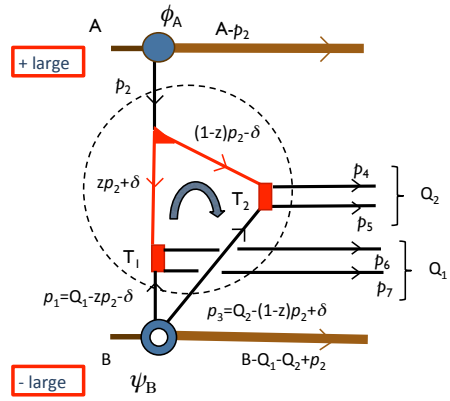

Figure 4: $3 \to 4$ contributions to the DPI interaction amplitude

$$P_{345} \equiv -p_3 + p_4 + p_5 \equiv zp_2 + \delta, \;\; P_{671} \equiv p_6 + p_7 - p_1 \equiv (1-z)p_2 - \delta$$

$$\int d\delta_- \frac{1}{P_{345}^2 P_{671}^2} = \int \frac{d\delta_-}{\big((zp_2+\delta)^2 + i\epsilon\big)\big((1-z)p_2 - \delta)^2 + i\epsilon\big)} = \frac{2\pi i}{\delta_t^2\, p_{2+}} \tag{6}$$

The final expression of the amplitude is obtained after integrating on the transverse components δ_t. Notice that when $\delta_t = 0$ the two intermediate gluons, with momenta P_{345} and P_{671}, are on mass shell and the process factorizes into the product of a splitting amplitude and of two on shell scattering amplitudes, in such a way that the final state has the characteristic signature of a DPI, namely the transverse momenta compensated pairwise.

A main point is thus the behavior of the integrand in the limit of small δ_t. At small δ_t one has:

$$\int A|_c d\delta_- \simeq \frac{\left(z\langle 32\rangle\langle\delta 1\rangle + (1-z)\langle 3\delta\rangle\langle 21\rangle\right)^3 [\delta 2]}{\langle 34\rangle\langle 45\rangle\langle 67\rangle\langle 71\rangle\langle\delta 6\rangle\langle\delta 5\rangle} \times \frac{2\pi i}{\delta_t^2 p_{2+}} \to \frac{\text{const.}}{\delta_t} \quad \text{for} \quad \delta_t \to 0 \tag{7}$$

The integration of $A|_c$ on $d^2\delta_t$ thus washes out the singularity at $\delta_t = 0$, which implies that the amplitude is *not enhanced* in the configuration where the transverse momenta of the two pairs of large p_t partons are compensated pairwise. The contribution of $A|_c$ is thus of the same order of magnitude of the other two contributions $A|_a$ and $A|_b$ to the same gauge invariant color ordered amplitude A.

One can show that this property does not hold only for the particular case discussed here. It holds also for all other contributions to the tree level 7-gluon amplitude, characterized by multi-particle singularities.

At tree level, in each color ordered amplitude, one thus finds terms, which can be factorized into a splitting amplitude and two almost on shell $2 \to 2$ scattering amplitudes. However these contributions to the color ordered amplitude are *not enhanced*, because of the loop integration on the initial momenta, and have to be added coherently with all other contributions (which are of similar magnitude) to the same, gauge invariant, color ordered amplitude. One will then conclude that the $3 \to 4$ terms cannot contribute in a relevant amount to cross sections, characterized by final state configurations where transverse momenta are compensated pairwise.

A further remark is that the complete $3 \to 4$ scattering amplitude results from the sum of all color ordered contributions. In the actual case of interest one has two gluons in the initial state, which are originated by the same hadron and which thus have a rather small relative transverse momentum. The color ordered terms, where the almost parallel initial state gluons are cyclically-adjacent in the amplitude, are singular in the invariant obtained by the sum of the two almost parallel momenta [7] and therefore give a leading contribution to the amplitude. A main contribution to the 7-gluon amplitude, in the kinematics considered here, is therefore factorized into a fusion amplitude and a 6-gluon scattering amplitude, the latter with only two gluons in the initial state.

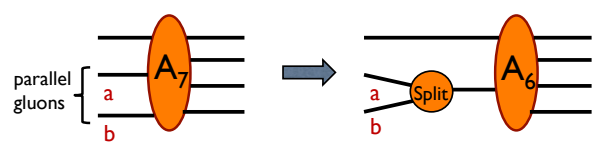

Figure 5: 7-gluon amplitude with two parallel gluons in the initial state

While initiated by three partons, a main contribution to the cross section is thus effectively given by a $2 \to 4$, rather than by a $3 \to 4$ parton process.

References

[1] N. Paver and D. Treleani, "Multi - Quark Scattering and Large p_T Jet Production in Hadronic Collisions," *Nuovo Cim.*, **A70**(1982), 215.

[2] B. Blok, Yu. Dokshitser, L. Frankfurt, and M. Strikman, "pQCD physics of multiparton interactions," *Eur. Phys. J.*, **C72**(2012), 1963, 1106.5533.

[3] Markus Diehl, Daniel Ostermeier, and Andreas Schafer, "Elements of a theory for multiparton interactions in QCD," *JHEP*, **03**(2012), 089, 1111.0910.

[4] Ruth Britto, Bo Feng, Radu Roiban, Marcus Spradlin, and Anastasia Volovich, "All split helicity tree-level gluon amplitudes," *Phys. Rev.*, **D71**(2005), 105017, hep-th/0503198.

[5] Michelangelo L. Mangano and Stephen J. Parke, "Multiparton amplitudes in gauge theories," *Phys. Rept.*, **200**(1991), 301, hep-th/0509223.

[6] Ruth Britto, Freddy Cachazo, and Bo Feng, "New recursion relations for tree amplitudes of gluons," *Nucl. Phys.*, **B715**(2005), 499, hep-th/0412308.

[7] Lance J. Dixon, "A brief introduction to modern amplitude methods," in "Proceedings, 2012 European School of High-Energy Physics (ESHEP 2012): La Pommeraye, Anjou, France, June 06-19, 2012," 31–67, 2014, 1310.5353, URL http://inspirehep.net/record/1261436/files/arXiv:1310.5353.pdf.

Effects of double-parton scattering in four-jet production at the LHC

Rafał Maciuła[1] and Antoni Szczurek[1,2]

[1]Institute of Nuclear Physics, Polish Academy of Sciences, Radzikowskiego 152, PL-31-342 Kraków, Poland
[2]University of Rzeszów, PL-35-959 Rzeszów, Poland

1 Introduction

Four-jet production was traditionally discussed in the context of double parton scattering. However, in most of the past as well as current analyses the DPS contribution to four-jet production is relatively small and single parton scattering (SPS) mechanism dominate (see e.g. Ref. [1] and references therein). A more evident observation of DPS in four-jet production would clearly provide a new impulse for the MPI community.

In our recent studies we have shown how big can be the contribution of DPS for two jets widely separated in rapidity [2]. Understanding of this contribution is important in the context of searching for BFKL effects or in general QCD higher-order effects.

Here we wish to extend our recent collinear-approach-based studies of DPS effects in four-jet sample [1], by application of the k_t-factorization approach in which higher-order effects are effectively included and calculation of different correlation observables become more accurate. An updated discussion of further maximalization of the DPS contribution by selecting relevant kinematical cuts is presented.

2 Theoretical formalism

Each step of DPS is obtained here in the k_t-factorization approach. According to this framework, the SPS cross section for dijet production can be written as:

$$\frac{d\sigma^{SPS}(pp \to jjX)}{dy_1 dy_2 d^2p_{1,t} d^2p_{2,t}} = \frac{1}{16\pi^2 (x_1 x_2 S)^2} \int \frac{d^2k_{1t}}{\pi} \frac{d^2k_{2t}}{\pi} \overline{|\mathcal{M}_{RR\to jj}|^2} \times \delta^2\left(\vec{k}_{1t} + \vec{k}_{2t} - \vec{p}_{1t} - \vec{p}_{2t}\right) \mathcal{F}(x_1, k_{1t}^2, \mu^2) \mathcal{F}(x_2, k_{2t}^2, \mu^2). \quad (1)$$

Here the four-momenta of the initial-state gluons or quarks are parameterized as a sum of longitudinal and transverse components $k_{1,2} = x_{1,2}P_{1,2} + k_{t1,2}$, $k_{t1,2} = (0, \vec{k}_{t1,2}, 0)$, $k_{1,2}^2 = -\vec{k}_{t1,2}^2$, $P_{1,2}$

are the four-momenta of the protons, $2P_1P_2 = S$, $\overline{|\mathcal{M}_{RR\to jj}|^2}$ are the partonic cross sections with Reggeized gluons or quarks (R) in the initial state. Fully gauge invariant treatment of the initial-state off-shell gluons or quarks can be achieved in k_t-factorization approach only when they are considered as Reggeized gluons or Reggeons. The squared amplitudes of the partonic subprocess are taken from Ref. [3] where the useful analytical formulae are presented. The unintegrated parton distributions functions (UPDFs) are taken in the form proposed some time ago by Kimber-Martin-Ryskin (KMR) [4].

The multi-dimensional differential cross section for DPS mechanism can be written as:

$$\frac{d\sigma^{DPS}(pp \to \text{4jets } X)}{dy_1 dy_2 d^2p_{1,t} d^2p_{2,t} dy_3 dy_4 d^2p_{3,t} d^2p_{4,t}} = \sum_{i_1,j_1,k_1,l_1;i_2,j_2,k_2,l_2} \frac{\mathcal{C}}{\sigma_{eff}} \times \frac{d\sigma(i_1 j_1 \to k_1 l_1)}{dy_1 dy_2 d^2p_{1,t} d^2p_{2,t}} \frac{d\sigma(i_2 j_2 \to k_2 l_2)}{dy_3 dy_4 d^2p_{3,t} d^2p_{4,t}} , \tag{2}$$

where $\mathcal{C} = \left\{ \begin{array}{ll} \frac{1}{2} & \text{if } i_1 j_1 = i_2 j_2 \wedge k_1 l_1 = k_2 l_2 \\ 1 & \text{if } i_1 j_1 \neq i_2 j_2 \vee k_1 l_1 \neq k_2 l_2 \end{array} \right\}$ and partons $j, k, l, m = g, u, d, s, \bar{u}, \bar{d}, \bar{s}$. The combinatorial factors include identity of the two subprocesses. In the calculations presented here we have taken σ_{eff} = 15 mb.

The SPS production mechanisms of four-jet production is calculated within the LO event generator ALPGEN [5] where only light quarks/antiquarks are included. Weighted events from the generator are used to construct distributions presented in the next section. In order to effectively include higher-order effects an extra phenomenological K-factor is used. It was found that the NLO contributions to four-jet production are important and the global K-factor for the integrated cross section is only about 0.5.

3 Numerical results

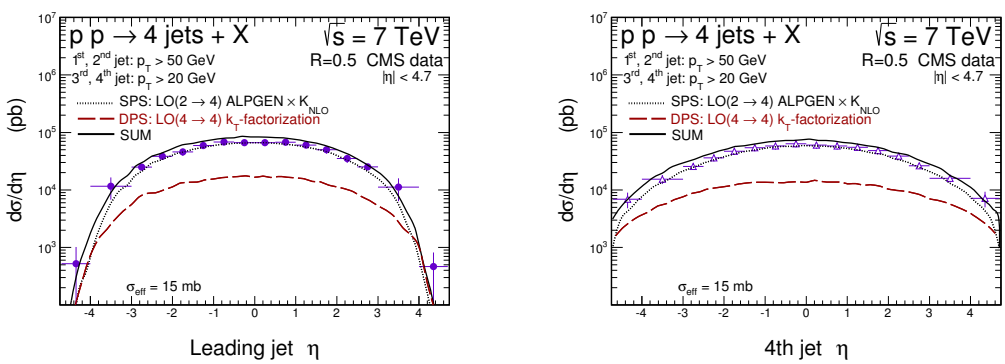

Figure 1: Pseudorapidity distributions for the leading (left panel) and fourth (right panel) jet together with the CMS data. Details are shown on the plot.

In Fig. 1 we show the calculated SPS and DPS pseudorapidity distributions of the leading and fourth jet together with the CMS data [6]. We observe that the DPS contribution increases when

going to large pseudorapidities. Clear improvements are achieved at large pseudorapidities ($|\eta| > 3$) when the DPS contribution is added to the SPS contribution. The presented CMS data were not optimized for searching for DPS effects and now we wish to explore how to improve the situation. i.e. to enhance sample of the DPS events.

In Fig. 2 we show some correlation distributions which may be useful to increase relative DPS contribution in four-jet case. In the left panel we present the distribution in rapidity distance between the most remote jets and in the right panel the azimuthal angle distribution between them. In order to enhance the DPS cross section the lower cut on p_t of all four jets is taken ($p_t > 20$ GeV). Lowering the lower cut on jet transverse momentum to 20 GeV for all four jets gives already about 70% of DPS. Imposing in addition that the distance between the most remote jets is bigger than $\Delta Y > 7$ enhances the DPS contribution to about 80%. Thus imposing such cuts would help to extract fairly precisely the σ_{eff} parameter.

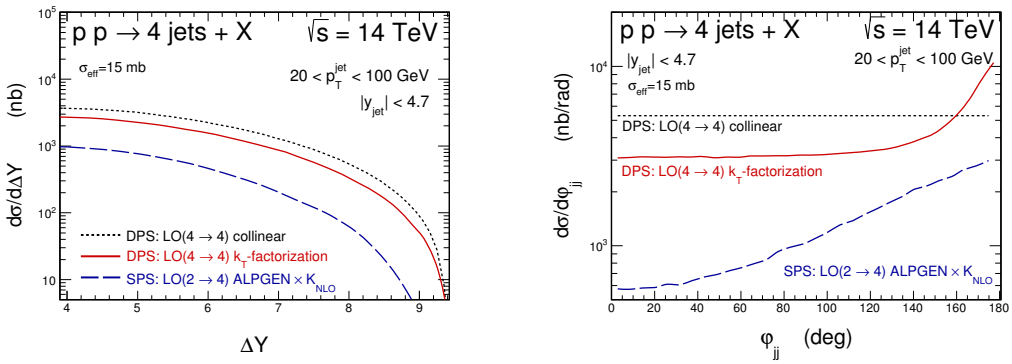

Figure 2: Distribution in rapidity distance (left) and azimuthal angle (right) of the most remote jets from the four-jet sample.

Acknowledgements

This study was partially supported by the Polish National Science Centre grant DEC-2014/15/B/ST2/02528.

References

[1] Rafal Maciula and Antoni Szczurek, "Searching for and exploring double-parton scattering effects in four-jet production at the LHC," *Phys. Lett.*, **B749**(2015), 57, 1503.08022.

[2] Rafal Maciula and Antoni Szczurek, "Double-parton scattering contribution to production of jet pairs with large rapidity separation at the LHC," *Phys. Rev.*, **D90**(2014) (1), 014022, 1403.2595.

[3] M. A. Nefedov, V. A. Saleev, and A. V Shipilova, "Dijet azimuthal decorrelations at the LHC in the parton Reggeization approach," *Phys. Rev.*, **D87**(2013) (9), 094030, 1304.3549.

[4] M. A. Kimber, Alan D. Martin, and M. G. Ryskin, "Unintegrated parton distributions," *Phys. Rev.*, **D63**(2001), 114027, hep-ph/0101348.

[5] Michelangelo L. Mangano, Mauro Moretti, Fulvio Piccinini, Roberto Pittau, and Antonio D. Polosa, "ALPGEN, a generator for hard multiparton processes in hadronic collisions," *JHEP*, **07**(2003), 001, hep-ph/0206293.

[6] Serguei Chatrchyan *et al.* (CMS), "Measurement of four-jet production in proton-proton collisions at $\sqrt{s} = 7$TeV," *Phys. Rev.*, **D89**(2014) (9), 092010, 1312.6440.

Single and double parton production of $c\bar{c}c\bar{c}$ - new ideas

Antoni Szczurek[1,2] and Rafał Maciuła[1]

[1]Institute of Nuclear Physics, Polish Academy of Sciences, Radzikowskiego 152, PL-31-342 Kraków, Poland
[2]University of Rzeszów, PL-35-959 Rzeszów, Poland

1 Introduction

Some time ago we predicted that at large energies the production of double charm should be dominated by the double-parton scattering (DPS) mechanism [1]. The leading-order double $c\bar{c}$ production was extended next to the k_t-factorization approach [2, 3]. A good description of the LHCb experimental data [4] was achieved for both the total cross section as well as the dimeson correlation observables. In these calculations the standard scale-independent Peterson fragmentation function [5] was used. The single-parton scattering (SPS) $gg \to c\bar{c}c\bar{c}$ contribution was discussed carefully in both collinear [3] and k_t-factorization [6] approaches.

Studies of inclusive D meson production at the LHC based on scale-independent FFs have been done in the k_t-factorization [7]. In turn, in Ref. [8] the calculation was done according to the GM-VFNS NLO collinear scheme together with the several scale-dependent fragmentation functions [9, 10]. A similar calculation were done recently also in the k_t-factorization approach with parton Reggeization hypothesis [11].

Very recently [12] we have investigated how important is the gluon fragmentation mechanism for the double D-meson production, i.e. double fragmentation of each of the gluons in the gluon dijets in SPS production and double fragmentation of each of the gluons in the gluon jet in DPS production mechanism. Here the gluon and digluon production is considered in the k_t-factorization approach. via subprocesses $RR \to g$ and $RR \to gg$, where R is the Reggeized gluon. In this analysis we used scale-dependent fragmentation functions from [13].

2 A short sketch of theoretical formalism

In the traditional scenario the $gg \to c\bar{c}$ is the dominant production mechanism. In the scenario proposed in [11] also $g \to D$ is included. When going to $c\bar{c}c\bar{c}$ the situation becomes even more complicated as discussed in our recent paper [12]. Naturally a new single-parton scattering mechanism (called here SPS $gg \to DD$) appears (top-right panel in Fig.1). Since here the two produced gluons are correlated, the mechanism naturally leads to an azimuthal correlation between the DD

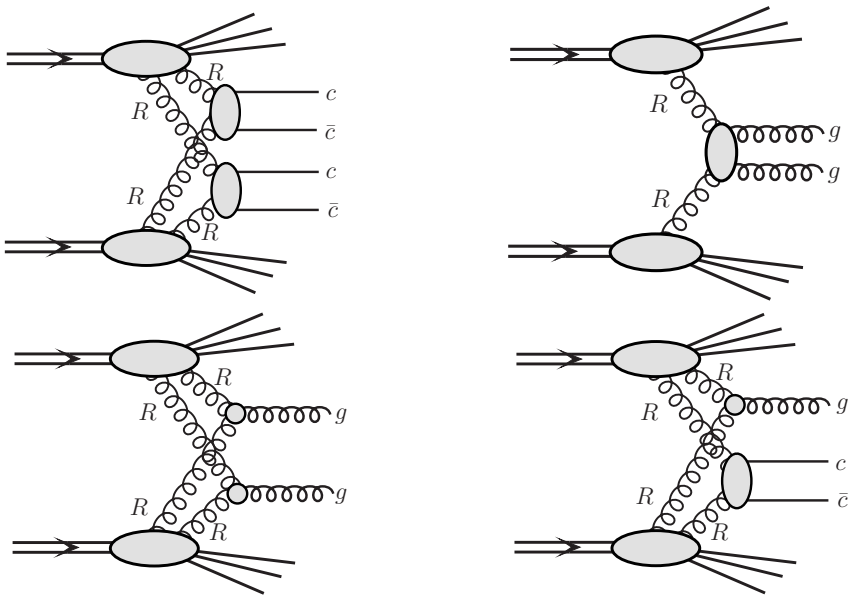

Figure 1: A diagrammatic illustration of the mechanisms considered in Ref. [12]. The $c \to D$, $\bar{c} \to \bar{D}$ and $g \to D, \bar{D}$ is not shown explicitly, but is included in the calculation.

(or $\bar{D}\bar{D}$) mesons. Such a correlation was actually observed in the LHCb data [4] and could not be explained by the SPS $2 \to 4$ perturbative $gg \to c\bar{c}c\bar{c}$ contribution (see e.g. Ref. [6]).

In addition to the SPS double gluon fragmentation there are three classes of DPS contributions. In addition to the coventional DPS $cc \to DD$ (top-left panel in Fig.1) considered in Refs. [2, 3, 6] there is a double $g \to D$ (or double $g \to \bar{D}$) fragmentation mechanism, called here DPS $gg \to DD$ (bottom-left panel in Fig.1) as well as the mixed DPS $gc \to DD$ contribution (bottom-right panel in Fig.1).

Details of our calculation can be found in Ref. [12].

3 Preliminary results

Now we wish to show some preliminary results.

In Fig. 2 we compare results of our calculation with experimental distribution in transverse momentum of one of the meson from the D^0D^0 (or $\bar{D}^0\bar{D}^0$) pair. We show results for the traditional scenario when the standard Peterson FF is used for the $c \to D^0$ (or $\bar{c} \to \bar{D}^0$) fragmentation (left panel) as well as the result for the new scenario when more mechanisms are included and when FFs with DGLAP evolution for $c \to D^0$ (or $\bar{c} \to \bar{D}^0$) and $g \to D^0$ (or $g \to \bar{D}^0$) are used. In this calculation $\mu^2 = m_{t,c}^2$ is used as a scale for the fragmentation function. The different new mechanisms shown in Fig. 1 give contributions of similar size. We can obtain agreement in the second case provided the σ_{eff} parameter is increased from conventional 15 mb to 30 mb. Even then we overestimate the LHCb data for $3 < p_T < 5$ GeV. The larger value in the second scenario

is surprising but not excluded as discussed in Ref. [12].

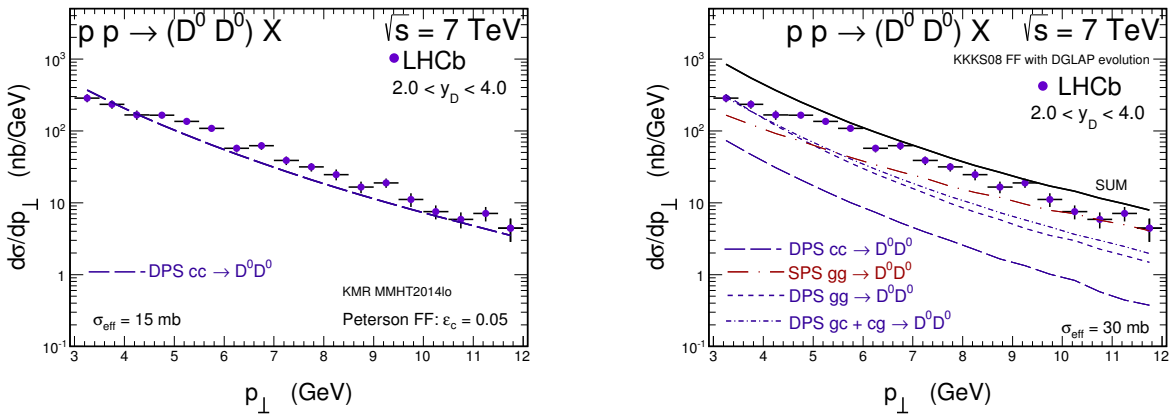

Figure 2: D^0 meson transverse momentum distribution within the LHCb acceptance region. The left panel is the first scenario and for Peterson $c \to D$ fragmentation function while the right panel is the new scenario and for the fragmentation function that undergo DGLAP evolution equation.

In addition in Fig. 3 we show dimeson invariant mass distribution $M_{D^0D^0}$. In the first scenario we get a good agreement only for small invariant masses while in the new scenario we get a good agreement only for large invariant masses. The large invariant masses are strongly correlated with large transverse momenta, so the situation here is quite similar as in Fig. 2.

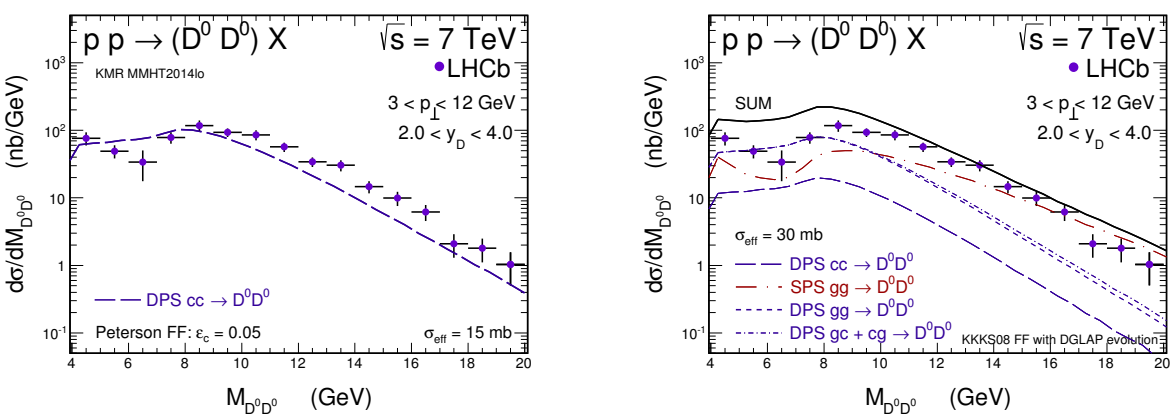

Figure 3: $M_{D^0D^0}$ dimeson invariant mass distribution within the LHCb acceptance region. The left panel is the conventional scenario and the right panel is the new scenario.

In Ref. [12] we discuss more distributions.

4 Conclusions

We have found that several new mechanisms appear if one allows $g \to D, \bar{D}$ fragmentation with scale dependent fragmentation functions.

We have included the mechanism in double charm production. When added together the new mechanisms give similar result as the traditional scenario with one subprocess ($cc \to DD$) and fixed (scale-independent) fragmentation function. However, some correlation observables, such as dimeson invariant mass or azimuthal correlations between D mesons, are slightly better described.

In our calculation within the new scenario a larger value of σ_{eff} is needed to describe the LHCb data than found in the literature for other DPS processes.

The presence of the new single-parton scattering mechanism (non DPS type) may mean that the extraction of σ_{eff} directly from the LHCb experimental data [4] may be incorrect.

Acknowledgements

This study was partially supported by the Polish National Science Centre grant DEC-2014/15/B/ST2/02528.

References

[1] Marta Luszczak, Rafal Maciula, and Antoni Szczurek, "Production of two $c\bar{c}$ pairs in double-parton scattering," *Phys. Rev.*, **D85**(2012), 094034, 1111.3255.

[2] Rafal Maciula and Antoni Szczurek, "Production of $c\bar{c}c\bar{c}$ in double-parton scattering within k_t-factorization approach – meson-meson correlations," *Phys. Rev.*, **D87**(2013) (7), 074039, 1301.4469.

[3] Andreas van Hameren, Rafal Maciula, and Antoni Szczurek, "Single-parton scattering versus double-parton scattering in the production of two $c\bar{c}$ pairs and charmed meson correlations at the LHC," *Phys. Rev.*, **D89**(2014) (9), 094019, 1402.6972.

[4] R. Aaij *et al.* (LHCb collaboration), "Observation of double charm production involving open charm in pp collisions at $\sqrt{s}$=7 TeV," *JHEP*, **1206**(2012), 141, 1205.0975.

[5] C. Peterson, D. Schlatter, I. Schmitt, and Peter M. Zerwas, "Scaling Violations in Inclusive e+ e- Annihilation Spectra," *Phys. Rev.*, **D27**(1983), 105.

[6] Andreas van Hameren, Rafa Maciua, and Antoni Szczurek, "Production of two charm quark-antiquark pairs in single-parton scattering within the k_t-factorization approach," *Phys. Lett.*, **B748**(2015), 167, 1504.06490.

[7] Rafal Maciula and Antoni Szczurek, "Open charm production at the LHC - k_t-factorization approach," *Phys. Rev.*, **D87**(2013) (9), 094022, 1301.3033.

[8] B. A. Kniehl, G. Kramer, I. Schienbein, and H. Spiesberger, "Inclusive Charmed-Meson Production at the CERN LHC," *Eur. Phys. J.*, **C72**(2012), 2082, 1202.0439.

[9] Bernd A. Kniehl and Gustav Kramer, "D0, D+, D+(s), and Lambda+(c) fragmentation functions from CERN LEP1," *Phys. Rev.*, **D71**(2005), 094013, hep-ph/0504058.

[10] Bernd A. Kniehl and Gustav Kramer, "Charmed-hadron fragmentation functions from CERN LEP1 revisited," *Phys. Rev.*, **D74**(2006), 037502, hep-ph/0607306.

[11] Anton V. Karpishkov, Maxim A. Nefedov, Vladimir A. Saleev, and Alexandera V. Shipilova, "Open charm production in the parton Reggeization approach: Tevatron and the LHC," *Phys. Rev.*, **D91**(2015) (5), 054009, 1410.7139.

[12] Rafal Maciula, Vladimir A. Saleev, Alexandra V. Shipilova, and Antoni Szczurek, "New mechanisms for double charmed meson production at the LHCb," (2016), 1601.06981.

[13] T. Kneesch, B. A. Kniehl, G. Kramer, and I. Schienbein, "Charmed-meson fragmentation functions with finite-mass corrections," *Nucl. Phys.*, **B799**(2008), 34, 0712.0481.

Momentum conservation factor in DPS

S.P. Baranov[1] and A.V. Lipatov, M.A. Malyshev, A.M. Snigirev, N.P. Zotov[2]

[1]P.N. Lebedev Institute of Physics, Lenin Avenue 53, 119991 Moscow, Russia,
[2]Skobeltsyn Institute of Nuclear Physics, Lomonosov Moscow State University,
119991 Moscow, Russia

1 Abstract

The violation of DPS factorization ansatz due to the evident restriction on the total parton momentum is discussed. Numerically the corrections from the limited partonic phase space amount to a factor 2 in the total rates at the LHCb conditions with ZD or WD associated production taken as examples.

2 Introduction

The existence of multi-parton interactions (MPI) in hadron-hadron collisions [1–4] at high energies is a natural consequence of the fast increase of the parton flux at small parton longitudinal momentum fractions and the requirement of unitarization of the cross sections in perturbative QCD. The great splash of investigation activity around MPI in last years [1–4] has been stimulated by the experimental evidence for double parton scattering (DPS) in the processes producing two independently identified hard particles in the same collision. Such processes have been observed in proton-proton and proton-antiproton collisions by a number of collaborations for the final states containing four jets, $\gamma + 3$ jets, $W + 2$ jets, double J/ψ and others.

In our recent publication [5] we have considered associated production of charged gauge bosons $W^{\pm}$ and charged charmed mesons $D^{(*)\pm}$ at the LHC and came to the conclusion that same-sign $W^{\pm}$ $D^{(*)\pm}$ events could serve as an indicator of DPS. Our investigation was only restricted to central region, i.e. to CMS [6] and ATLAS [7] kinematic conditions, since these were the only collaborations who provided the data (though not on same-sign WD configurations). LHCb Collaboration is also going to measure the production cross sections for all of the four WD charge combinations. It is very tempting to foreshow the experimental measurement with theoretical prediction. At the LHCb conditions the probed longitudinal momentum fractions are not far from the phase space boundary where the evident restriction on the total parton momentum may spoil the factorization hypothesis commonly used in DPS. The possible influence of the momentum conservation factor on the total rates at the LHCb conditions with ZD or WD associated production taken as examples is main purpose of this talk.

3 Formalism and results

As far as the single parton scattering (SPS) are concerned, the calculations were done [5] in the k_t-factorization technique. The evaluation of DPS contributions was done in accordance with the formula

$$\sigma_{\rm DPS}^{\rm WD} = \frac{\sigma_{\rm SPS}^{W}\sigma_{\rm SPS}^{D}}{\sigma_{\rm eff}}, \tag{1}$$

where $\sigma_{\rm eff}$ is a normalization constant that encodes all "DPS unknowns" into a single phenomenological parameter (for details see the reviews [1–4] and references therein). This simple formula is usually derived under the two following simplifying approximations: (i) the double parton distribution functions can be decomposed into longitudinal and transverse components, and (ii) the longitudinal component $D_p^{ij}(x_1, x_2; Q_1^2, Q_2^2)$ reduces to the diagonal product of two independent single parton distribution functions:

$$D_p^{ij}(x_1, x_2; Q_1^2, Q_2^2) = D_p^i(x_1; Q_1^2) D_p^j(x_2; Q_2^2) \tag{2}$$

(here x_1 and x_2 are the longitudinal momentum fractions of two parton of type i and j undergoing the hard subprocesses at scale Q_1 and Q_2). The latter approximation is acceptable in collider experiments where only small x_1 and x_2 values are probed. However, this cannot be said of the LHCb conditions, especially with respect to as heavy systems as gauge bosons. At the LHCb conditions, the probed longitudinal momentum fractions x_1 and x_2 are not far from the phase space boundary where the evident restriction on the total parton momentum $x_1 + x_2 \leq 1$ violates the DPS factorization ansatz commonly used.

Setting the boundary condition in the form of theta-function $\Theta(1 - x_1 - x_2)$ would result in a step-like discontinuity at the edge of the phase space. This does not seem physically consistent for double parton distribution functions. In more accurate approach [8–15]

$$D_p^{ij}(x_1, x_2; Q_1^2, Q_2^2) = D_p^i(x_1; Q_1^2) D_p^j(x_2; Q_2^2) \times (1 - x_1 - x_2)^n. \tag{3}$$

The factor $(1 - x_1 - x_2)^n$ smoothly imposes the kinematical constraints and $n > 0$ is a parameter to be fixed phenomenologically. One chooses n to be 2 often. This choice of phase space factor can be partly justified [8, 10] in the framework of perturbative QCD and gives the double parton distribution functions which satisfy the momentum sum rules [9] reasonably well. We use $n = 3$ also to get feeling of possible effects related to the kinematical constraints, The case without the kinematical constraints is just $n = 0$. A numerical value of $\sigma_{\rm eff} \simeq 15$ mb has earlier been obtained empirically from fits to $p\bar{p}$ and pp data.

Having considered the production of $Z^0D, W^{\pm}D$ states at the LHCb conditions we found [16]: As a general rule for the production of electroweak bosons in the DPS channel, the simple DPS factorization formula needs to be corrected for the limited partonic phase space. Numerically, these corrections amount to a factor of 2 in the total rates and, when taken into account, lead to better agreement with the available data [on Z^0D production [17]] than it seemed before.

Acknowledgements

A.M.S. wishes to express the gratitude to the organizers of 7th International Workshop on MPI at the LHC for the warm welcome and hospitality.

References

[1] P. Bartalini *et al.*, arXiv:1111.0469 [hep-ph].

[2] H. Abramowicz *et al.*, arXiv:1306.5413 [hep-ph].

[3] S. Bansal *et al.*, arXiv:1410.6664 [hep-ph].

[4] R. Astalos *et al.*, arXiv:1506.05829 [hep-ph].

[5] S.P. Baranov, A.V. Lipatov, M.A. Malyshev, A.M. Snigirev, and N.P. Zotov, Phys. Lett. B **746**, 100 (2015).

[6] S. Chatrchyan *et al.* (CMS Collaboration), J. High Energy Phys. **1402**, 013 (2014).

[7] G. Aad *et al.* (ATLAS Collaboration), J. High Energy Phys. **1405**, 068 (2014).

[8] V.L. Korotkikh and A.M. Snigirev, Phys. Lett. B **594**, 171 (2004).

[9] J.R. Gaunt and W.J. Stirling, J. High Energy Phys. **1003**, 005 (2010).

[10] A.M. Snigirev, Phys. Rev. D **83**, 034028 (2011).

[11] H.-M. Chang, A.V. Manohar, and W.J. Waalewijn, Phys. Rev. D **87**, 034009 (2013).

[12] M. Rinaldi, S. Scopetta, and V. Vento, Phys. Rev. D **87**, 114021 (2013).

[13] K. Golec-Biernat and E. Lewandowska, Phys. Rev. D **90**, 014032 (2014).

[14] F.A. Ceccopieri, Phys. Lett. B **734**, 79 (2014).

[15] A.M. Snigirev, N.A. Snigireva, and G.M. Zinovjev, Phys. Rev. D **90**, 014015 (2014).

[16] S.P. Baranov, A.V. Lipatov, M.A. Malyshev, A.M. Snigirev, and N.P. Zotov, in preparation.

[17] R. Aaij *et al.* (LHCb Collaboration), J. High Energy Phys. **1401**, 091 (2014).

The effective cross section of double parton scattering in a Light-Front quark model

Matteo Rinaldi[1]

[1]Dipartimento di Fisica e Geologia, Università degli studi di Perugia and INFN section of Perugia

This contribution deals with double parton scattering, whose cross section, studied through the so called "effective cross section", σ_{eff}, depends on non-perturbative quantities, the so called double parton distribution functions (dPDFs), describing the joint probability of finding two partons at a given transverse distance with given longitudinal momentum fractions. dPDFs are related to the three-dimensional (3D) nucleon structure, as discussed in Ref. [1]. However, since there are no data available for dPDFs, they must be estimated through non perturbative methods, such as using model calculations, see Refs. [2–5]. In particular, in Ref. [5], dPDFs have been calculated by means of the Light-Front (LF) approach, which allows one to achieve a Poincaré covariant treatment, an essential feature to reproduce the dPDFs sum rules. Thanks to this procedure we have a correct starting point for a precise perturbative QCD (pQCD) evolution. In this scenario, dPDFs are estimated at a low energy scale, $Q_0 \sim \Lambda_{\rm QCD}$, as extensively done for the PDFs, and then the results must be evolved using pQCD in order to match data taken at an energy scale $Q > Q_0$. dPDF evolution is described in, e.g., Refs. [4, 6–8]. We stress that in our approach, there is only evolution on $x_{1,2}$, the one on $k_\perp$ being still an open challenge and, since we are interested in the valence region, only the homogenous part of the evolution equations has been taken into account in our calculations. Thanks to this scheme, our model calculations can be relevant for the analysis of high-energy data. In Ref. [9], we have evaluated σ_{eff} in the dynamical framework of Ref. [5], deriving a suitable expression of σ_{eff}, in terms of PDFs and dPDFs. In particular, we started from the phenomenological definition of σ_{eff} and then, following the strategy described in details in Ref. [9], one finds:

$$\sigma_{eff}(x_1, x_1', x_2, x_2') = \frac{\sum_{i,k,j,l} F_i(x_1) F_k(x_1') F_j(x_2) F_l(x_2') C_{ik} C_{jl}}{\sum_{i,j,k,l} C_{ik} C_{jl} \int D_{ij}(x_1, x_2; \mathbf{k}_\perp) D_{kl}(x_1', x_2'; -\mathbf{k}_\perp) \frac{d\mathbf{k}_\perp}{(2\pi)^2}} \,, \tag{1}$$

where $F^p_{i(k)}$ is the standard single PDF, $i = \{q, \bar{q}, g\}$, C_{ij} are color factors which stay in the ratio $C_{gg} : C_{qg} : C_{qq} = 1 : (4/9) : (4/9)^2$ and $D_{ij}(x_1, x_2; \mathbf{k}_\perp)$, is the so called "double generalized

parton distribution" ($_2GPD$, [10, 11]). This quantity, depending on $\mathbf{k}_\perp$, the transverse momentum imbalance of the partons 1 and 2, is the the Fourier transform of the dPDFs $D_{ij}(x_1, x_2; \mathbf{r}_\perp)$, depending on $\mathbf{r}_\perp$, the transverse distance in coordinate space. This is the non-perturbative input describing soft Physics. In Eq. (1), neglecting parton correlations, a factorized form of dPDFs, in terms of standard PDFs, e.g., $D_{ij}(x_1, x_2; \mathbf{k}_\perp) \propto F_i(x_1)F_j(x_2)T(\mathbf{k}_\perp)$, can be used. In this scenario, a constant value of σ_{eff} w.r.t. to x_i is obtained, see e.g. Refs. [10, 11]). This condition is often guessed for the extraction of σ_{eff} from data. For discussions on the uncorrelated ansatz see, e.g., Refs. [6,7]. Anyhow, in the valence region we are interested here, this assumption is not supported by model calculations [2, 3, 5]. However, in the present experimental scenario, σ_{eff}, measured by different experiments [12–17], with different final states and values of the center-of-mass energy, is consistent with a constant value. Nevertheless, the large experimental errorbars could hide the fundamental x_i-dependence, an important feature strictly related to the 3D nucleon structure [1]. Usually, information on the 3D structure of nucleons, associated to the transverse position of partons, is investigated through Generalized Parton Distributions (GPDs) in impact parameter space. However they are one-body distribution while, dPDFs are two-body densities, sensitive to correlations, which encode information on the relative transverse distance of partons, a complementary information w.r.t. the one described in GPDs. This issue motivates the present study. For the calculation of σ_{eff}, the quark model, adopted to estimate PDFs and dPDFs, is the one used in Ref. [5], being capable to reproduce the light baryon spectrum. Moreover, we focus our analysis on the the kinematics of the old AFS data [12], being the ones including the valence region, i.e. $x_1 \simeq x_1', x_2 \simeq x_2'$ and $0.2 \leq x_{1,2} \leq 0.3$ and the energy scale turns out to be $Q^2 \simeq 250$ GeV^2. In Fig. 1, σ_{eff} is shown at the scale of the model, $\mu_0^2 \simeq 0.1$ GeV^2, and after non-singlet evolution to Q^2. A strong $x_{1,2}$ dependence has been found in this kinematical range in both the scenarios. As one can see in Ref. [9], the average value of σ_{eff}, $\bar{\sigma}_{eff} \sim 10.9$ mb, is in good agreement with the experimental data [12–14]. Preliminary results of the evaluation of σ_{eff}, in the valence region, including also gluons and sea quarks, perturbatively generated, are qualitatively in agreement with the the ones shown in Fig. 1 In all these calculations, a strong x-dependence has been found in the valence region, due to the presence of correlations before and after pQCD evolution. One should notice that the three old experimental extractions of σ_{eff} [12–14], which include the valence region, lie in the obtained range of values of σ_{eff} shown in Fig. 1. and Fig. 2. We conclude remarking that we have found a suitable expression of σ_{eff} for microscopic calculations. σ_{eff} has been estimated within a relativistic Poincaré covariant quark model and our investigation predicts an x_i dependence of σ_{eff}, whose values are consistent with data including the valence region. The measurement of σ_{eff}, in restricted x_i ranges, would lead to a first signature of double parton correlations in the proton, a novel and interesting aspect of the 3D structure of the nucleon.

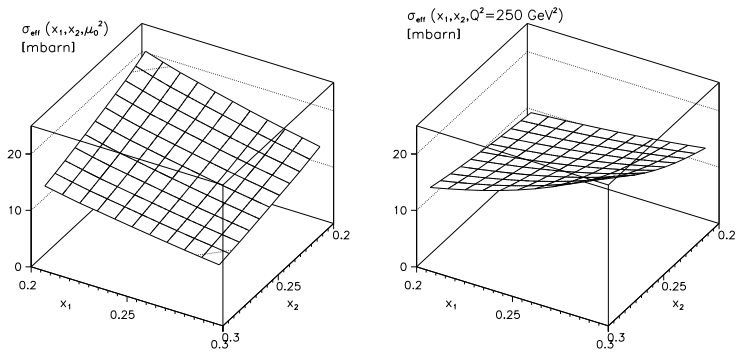

Figure 1: $\sigma_{eff}(x_1, x_2, Q^2)$ for the values of x_1, x_2 measured in Ref. [14] Left panel: hadronic scale; right panel: Q^2 = 250 GeV^2.

References

[1] G. Calucci and D. Treleani, "Proton structure in transverse space and the effective cross-section," *Phys. Rev.*, **D60**(1999), 054023.

[2] H.M. Chang, A.V. Manohar, and W.J. Waalewijn, "Double Parton Correlations in the Bag Model," *Phys. Rev.*, **D87**(2013), 034009.

[3] M. Rinaldi, S. Scopetta, and V. Vento, "Double parton correlations in constituent quark models," *Phys. Rev.*, **D87**(2013), 114021.

[4] W. Broniowski and E. Ruiz Arriola, "Valence double parton distributions of the nucleon in a simple model," *Few Body Syst.*, **55**(2014), 381, 1310.8419.

[5] M. Rinaldi, S. Scopetta, M. Traini, and V. Vento, "Double parton correlations and constituent quark models: a Light Front approach to the valence sector," *JHEP*, **1412**(2014), 028.

[6] J.R. Gaunt and W.J. Stirling, "Double Parton Distributions Incorporating Perturbative QCD Evolution and Momentum and Quark Number Sum Rules," *JHEP*, **1003**(2010), 005.

[7] M. Diehl, D. Ostermeier, and A. Schafer, "Elements of a theory for multiparton interactions in QCD," *JHEP*, **1203**(2012), 089.

[8] V.P. Shelest, A.M. Snigirev, and G.M. Zinovev, "The Multiparton Distribution Equations In Qcd," *Phys. Lett.*, **B113**(1982), 325.

[9] M. Rinaldi, S. Scopetta, M. Traini, and V. Vento, "Double parton scattering: a study of the effective cross section within a Light-Front quark model," *Phys. Lett.*, **B752**(2016), 40.

[10] B. Blok, Y. Dokshitzer, L. Frankfurt, and M. Strikman, "pQCD physics of multiparton interactions," *Eur. Phys. J.*, **C72**(2012), 1963.

[11] B. Blok, Y. Dokshitzer, L. Frankfurt, and M. Strikman, "Perturbative QCD correlations in multi-parton collisions," *Eur. Phys. J.*, **C74**(2014), 2926.

[12] T. Akesson *et al.* (Axial Field Spectrometer collaboration), "Double parton scattering in pp collisions at $\sqrt{s} = 63$ GeV," *Z. Phys.*, **C34**(1987), 163.

[13] J. Alitti *et al.* (UA2 collaboration), "A Study of multi - jet events at the CERN anti-p p collider and a search for double parton scattering," *Phys. Lett.*, **B268**(1991), 45.

[14] F. Abe *et al.* (CDF collaboration), "Double parton scattering in $\bar{p}p$ collisions at $\sqrt{s} = 1.8$TeV," *Phys.Rev.*, **D56**(1997), 3811.

[15] V.M. Abazov *et al.* (D0 collaboration), "Double parton interactions in $\gamma+$ 3 jet events in $p\bar{p}$ collisions $\sqrt{s} = 1.96$ TeV," *Phys.Rev.*, **D81**(2010), 052012, 0912.5104.

[16] Georges Aad *et al.* (ATLAS Collaboration), "Measurement of hard double-parton interactions in W+ 2 jet events at sqrt(s)=7 TeV with the ATLAS detector," *New J.Phys.*, **15**(2013), 033038, 1301.6872.

[17] S. Chatrchyan *et al.*, "Study of double parton scattering using W + 2-jet events in proton-proton collisions at $\sqrt{s}$ = 7 TeV," *JHEP*, **1403**(2014), 032.

Double parton scattering in the ultraviolet: addressing the double counting problem

Markus Diehl[1] and Jonathan R. Gaunt[2]

[1]Deutsches Elektronen-Synchroton DESY, 22603 Hamburg, Germany
[2]Nikhef Theory Group and VU University Amsterdam, De Boelelaan 1081, 1081 HV Amsterdam, The Netherlands

1 Ultraviolet behaviour of double parton scattering

The familiar factorisation formula for double parton scattering (DPS) reads

$$\frac{d\sigma_{\text{DPS}}}{dx_1\,d\bar{x}_1\,dx_2\,d\bar{x}_2} = \frac{1}{C}\,\hat{\sigma}_1\hat{\sigma}_2 \int d^2\boldsymbol{y}\; F(x_1,x_2,\boldsymbol{y})\,F(\bar{x}_1,\bar{x}_2,\boldsymbol{y})\,, \tag{1}$$

where C is a combinatorial factor, $\hat{\sigma}_{1,2}$ is the cross section for the first or second hard-scattering subprocess, and $F(x_1,x_2,\boldsymbol{y})$ is a double parton distribution (DPD). $\boldsymbol{y}$ denotes the transverse distance between the two partons. A field theoretical definition of $F(x_1,x_2,\boldsymbol{y})$ is naturally given by the matrix element between proton states of two twist-two operators at relative transverse distance $\boldsymbol{y}$. As explained in [1], the leading behaviour of DPDs at small $\boldsymbol{y}$ is controlled by the splitting of one parton into two, shown in figure 1a. The corresponding expression reads

$$F(x_1,x_2,\boldsymbol{y}) = \frac{1}{\boldsymbol{y}^2}\,\frac{\alpha_s}{2\pi^2}\,\frac{f(x_1+x_2)}{x_1+x_2}\,T\!\left(\frac{x_1}{x_1+x_2}\right) \qquad \text{for small } \boldsymbol{y}\,. \tag{2}$$

For simplicity we dropped labels for the different parton species and polarisations, as we already did in (1).

Inserting the short-distance limit (2) in the cross-section formula (1) reveals an immediate problem: the integration over $\boldsymbol{y}$ diverges strongly in the ultraviolet. In fact, the approximations that lead to (1) are not valid when $\boldsymbol{y}$ becomes too small (compared with the inverse of the large momentum scale Q of the hard scattering). This unphysical ultraviolet divergence signals another problem, namely one of double counting: the graph in figure 1b shows a contribution to double parton scattering, with perturbative splitting in each DPD. Drawn as in figure 1c, the same graph gives however a contribution to single parton scattering (SPS) at higher loop order. For multi-jet production this problem was already pointed out in [2].

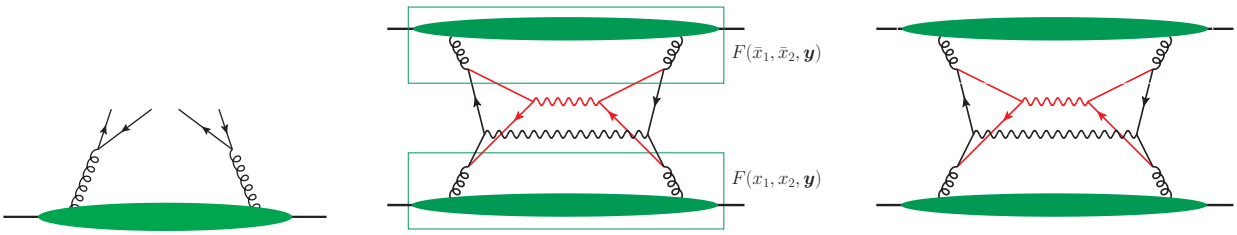

Figure 1: (a) Perturbative splitting contribution to a DPD. (b) Contribution of double perturbative splitting to DPS, also called "1 vs 1" graph. (c) Single hard scattering contribution.

2 A consistent scheme

The following scheme provides a consistent treatment of single and double scattering contributions to a given process, and it removes the ultraviolet divergence in the naive double scattering formula just discussed. We regulate the DPS cross section (1) by inserting a function under the integral over DPDs,

$$\int d^2\boldsymbol{y} \, \big[\Phi(\nu y)\big]^2 \, F(x_1, x_2, \boldsymbol{y}) \, F(\bar{x}_1, \bar{x}_2, \boldsymbol{y}) \,, \tag{3}$$

which is chosen such that $\Phi(u) \to 0$ for $u \to 0$ and $\Phi(u) \to 1$ for $u \gg 1$. (We take the square of Φ in order to have a closer connection to the case discussed in section 5.) This removes contributions with distances $y = |\boldsymbol{y}|$ below $1/\nu$ from what is *defined* to be double parton scattering. An appropriate choice for this cutoff scale is $\nu \sim Q$. Double and single parton scattering are then combined as

$$\sigma_{\text{DPS}} - \sigma_{\text{sub}} + \sigma_{\text{SPS}} \,, \tag{4}$$

where σ_{DPS} is the regulated DPS cross section and σ_{SPS} the SPS cross section computed in the usual way (given by figure 1c and its crossed variants in our example). The subtraction term σ_{sub} is given by the DPS cross section with both DPDs replaced by the splitting expression (2), computed at fixed order in perturbation theory and used at all $\boldsymbol{y}$. Note that at any order in α_s, the computation of σ_{sub} is technically much simpler than the one of σ_{SPS}.

Let us see how this construction solves the double counting problem. We work differentially in $\boldsymbol{y}$, which is Fourier conjugate to a specific transverse momentum variable as specified in [1] and can thus be given an unambiguous meaning, not only in the DPS cross section but also in the box graph of figure 1c and the associated term σ_{SPS}. For $y \lesssim 1/Q$ one has $\sigma_{\text{DPS}} \approx \sigma_{\text{sub}}$ because the perturbative approximation (2) of the DPD works well in that region. The dependence on the cutoff function $\Phi(\nu y)$ then cancels between σ_{DPS} and σ_{sub}, and one is left with $\sigma \approx \sigma_{\text{SPS}}$. For $y \gg 1/Q$ one has $\sigma_{\text{sub}} \approx \sigma_{\text{SPS}}$, because in that region the box graph can be approximated just as is done in the DPS formula. One is thus left with $\sigma \approx \sigma_{\text{DPS}}$ at large y, and the cutoff function $\Phi(y\nu) \approx 1$ does not have any effect there. The construction just explained is a special case of

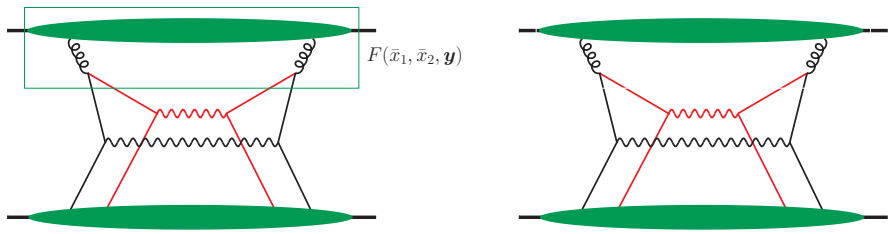

Figure 2: (a) Contribution of single perturbative splitting to DPS, also called "1 vs 2" graph. (b) Graph with a twist-two distribution for one proton and a twist-four distribution for the other.

the general subtraction formalism discussed in chapter 10 of [3], and it works order by order in perturbation theory.

3 Splitting and intrinsic contributions to DPDs

At small $\boldsymbol{y}$ a DPD – defined as a hadronic matrix element as already mentioned – contains not only the perturbative splitting contribution described by (2) but also an "intrinsic" part in which the two partons do not originate from one and the same "parent" parton. We emphasise that our scheme does not need to distinguish these "splitting" and "intrinsic" contributions when setting up the factorisation formula for the cross section. In fact, we do not know how such a separation could be realised in a field theoretic definition valid at all $\boldsymbol{y}$. It is only when writing down a parameterisation of $F(x_1, x_2, \boldsymbol{y})$ that has the small-y limit predicted by QCD that we separate the DPD into splitting and intrinsic pieces.

If we consider the DPS cross section formula at small y and take the splitting contribution for only one of the two protons, then we obtain the "1 vs 2" contribution depicted in figure 2a, which has been discussed in detail in [4, 5], [6, 7] and [8]. The corresponding integral in the cross section goes like $d^2\boldsymbol{y}/\boldsymbol{y}^2$ and thus still diverges at small y if treated naively. In our regulated DPS integral (3), it gives a finite contribution with a logarithmic dependence on the cutoff scale ν.

Just as the 1 vs 1 contribution of figure 1b corresponds to the SPS graph 1c, the 1 vs 2 contribution of figure 2a corresponds to a contribution with a twist-two distribution (i.e. a usual parton density) for one proton and a twist-four distribution for the other proton, shown in figure 2b. The complete cross section is then obtained as

$$\sigma = \sigma_{\text{DPS}} - \sigma_{\text{sub (1vs1)}} + \sigma_{\text{SPS}} - \sigma_{\text{sub (1vs2)}} + \sigma_{\text{tw2} \times \text{tw4}} \,. \tag{5}$$

The DPS term contains the full DPDs and thus generates 1 vs 1, 1 vs 2 and the usual 2 vs 2 contributions. The terms $\sigma_{\text{sub (1vs1)}}$ and σ_{SPS} were discussed in the previous section. The term $\sigma_{\text{tw2} \times \text{tw4}}$ corresponds to figure 2b, and the associated subtraction term $\sigma_{\text{sub (1vs2)}}$ is obtained from the DPS formula by replacing one DPD with its perturbative splitting approximation (2) and the other DPD with a twist-four distribution.

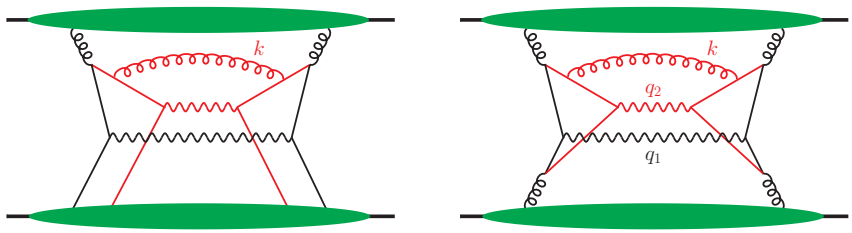

(a) (b)

Figure 3: Graphs with additional gluon emission that give rise to DGLAP logarithms in strongly ordered kinematics, as explained in the text.

Since very little is known about parton distributions of twist four, including $\sigma_{\text{tw2} \times \text{tw4}} - \sigma_{\text{sub (1vs2)}}$ in the cross section is a challenge for phenomenology. One can however show that with the choice $\nu \sim Q$ this combination is subleading in logarithms $\log(Q/\Lambda)$ compared to the 1 vs 2 part of σ_{DPS} and can hence be dropped at leading logarithmic accuracy.

4 DGLAP logarithms

As discussed in [1], the DPDs $F(x_1, x_2, \boldsymbol{y})$ are subject to homogeneous DGLAP evolution, with one DGLAP kernel for the parton with momentum fraction x_1 and another for the parton with momentum fraction x_2. One can show that the evolved distributions in the DPS cross section correctly resum large DGLAP logarithms in higher-order graphs. An example is the 1 vs 2 graph in figure 3a, which builds up a logarithm $\log^2(Q/\Lambda)$ in the region $\Lambda \ll |\boldsymbol{k}| \ll Q$, compared with the single $\log(Q/\Lambda)$ of the graph without gluon emission. Similarly, the higher-order SPS graph in figure 3b builds up a logarithm $\log(Q_2/Q_1)$ in the region $Q_1 \ll |\boldsymbol{k}| \ll Q_2$ if the scales Q_1 and Q_2 of the two hard scatters are strongly ordered among themselves. This type of logarithm is readily included in the cross section by taking separate renormalisation scales $\mu_{1,2} \sim Q_{1,2}$ for the two partons in the DPDs.

5 Extension to measured transverse momenta

So far we have discussed DPS and SPS in collinear factorisation, where the net transverse momentum $\boldsymbol{q}_1$ and $\boldsymbol{q}_2$ of the particles produced by each hard scatter is integrated over. As shown in [1], DPS can also be formulated for small measured $\boldsymbol{q}_1$ and $\boldsymbol{q}_2$ by generalising the corresponding formalism for SPS (which is e.g. documented in chapter 13 of [3]). Our scheme is readily extended to this case. The DPS cross section then involves a regularised integral

$$\int d^2\boldsymbol{y}\, d^2\boldsymbol{z}_1\, d^2\boldsymbol{z}_2\; e^{-i\boldsymbol{q}_1\boldsymbol{z}_1 - i\boldsymbol{q}_2\boldsymbol{z}_2}\, \Phi(\nu y_+)\, \Phi(\nu y_-)\, F(x_1, x_2, \boldsymbol{z}_1, \boldsymbol{z}_2, \boldsymbol{y})\, F(\bar{x}_1, \bar{x}_2, \boldsymbol{z}_1, \boldsymbol{z}_2, \boldsymbol{y})\,, \tag{6}$$

where $F(x_1, x_2, \boldsymbol{z}_1, \boldsymbol{z}_2, \boldsymbol{y})$ is a transverse-momentum dependent DPD transformed to impact parameter space. The perturbative splitting mechanism renders these distributions singular at the

points $y_\pm = \left|\boldsymbol{y} \pm \frac{1}{2}(\boldsymbol{z}_1 - \boldsymbol{z}_2)\right|$, as seen in section 5.2 of [1], and the function Φ regulates the logarithmic divergences that appear in the naive DPS formula.

References

[1] Markus Diehl, Daniel Ostermeier, and Andreas Schäfer, "Elements of a theory for multiparton interactions in QCD," *JHEP*, **03**(2012), 089, 1111.0910.

[2] Matteo Cacciari, Gavin P. Salam, and Sebastian Sapeta, "On the characterisation of the underlying event," *JHEP*, **04**(2010), 065, 0912.4926.

[3] John Collins, Foundations of perturbative QCD, Cambridge University Press, 2013, URL http://www.cambridge.org/de/knowledge/isbn/item5756723.

[4] B. Blok, Yu. Dokshitser, L. Frankfurt, and M. Strikman, "pQCD physics of multiparton interactions," *Eur. Phys. J.*, **C72**(2012), 1963, 1106.5533.

[5] B. Blok, Yu. Dokshitzer, L. Frankfurt, and M. Strikman, "Perturbative QCD correlations in multi-parton collisions," *Eur. Phys. J.*, **C74**(2014), 2926, 1306.3763.

[6] M. G. Ryskin and A. M. Snigirev, "A Fresh look at double parton scattering," *Phys. Rev.*, **D83**(2011), 114047, 1103.3495.

[7] M. G. Ryskin and A. M. Snigirev, "Double parton scattering in double logarithm approximation of perturbative QCD," *Phys. Rev.*, **D86**(2012), 014018, 1203.2330.

[8] Jonathan R. Gaunt, "Single Perturbative Splitting Diagrams in Double Parton Scattering," *JHEP*, **01**(2013), 042, 1207.0480.

Studies of double parton scattering with the ATLAS detector

Orel Gueta
on behalf of the ATLAS collaboration

Tel Aviv University

Interactions with more than one pair of incident partons in the same hadronic collision have been discussed on theoretical grounds since the introduction of the parton model to the description of particle production in collisions with hadronic initial states [1–3]. The simplest case of multi-parton interactions, referred to as double parton scattering (DPS), has been the focus of many phenomenological studies and experimental measurements [4]. For a process in which a final state A + B is being produced, the simplified formalism of [5,6] yields

$$\sigma_{\mathrm{A+B}}^{\mathrm{DPS}} = \frac{1}{1+\delta_{\mathrm{AB}}}\frac{\sigma_{\mathrm{A}}\sigma_{\mathrm{B}}}{\sigma_{\mathrm{eff}}}\,, \tag{1}$$

where σ_{A} (σ_{B}) is the cross-section for the final state A (B). The quantity δ_{AB} is the Kronecker delta used to construct a symmetry factor such that for identical final states with identical phase space, the DPS cross-section is divided by two. The σ_{eff} is a purely phenomenological parameter determining the overall size of DPS cross-sections. At values typical for hadronic cross-sections, it has been measured to range between 10 and 20 mb. Described here are four studies of ATLAS [7] in various final states [8–11].

The production of W bosons in association with two jets in pp collisions at a center-of-mass energy of $\sqrt{s} = 7$ TeV has been analyzed for the presence of DPS using data corresponding to an integrated luminosity of 36 pb^{-1} [8]. The fraction of events arising from DPS, f_{DPS}, has been measured through the normalized p_{T} balance between the two jets, $\Delta_{\mathrm{jets}}^{\mathrm{n}}$,

$$\Delta_{\mathrm{jets}}^{\mathrm{n}} = \frac{|\vec{p}_{\mathrm{T}}^{\,J_1} + \vec{p}_{\mathrm{T}}^{\,J_2}|}{|\vec{p}_{\mathrm{T}}^{\,J_1}| + |\vec{p}_{\mathrm{T}}^{\,J_2}|}\,, \tag{2}$$

which shows good differentiating power between the production of the $W + 2$ jets final state in a single parton scattering (SPS) and in a DPS. A fit was performed to the normalized, detector-level, background-corrected data distribution of $\Delta_{\mathrm{jets}}^{\mathrm{n}}$ using two normalized templates, denoted by A and B. The result of the fit of the form $(1-f_{\mathrm{DPS}})\cdot\mathrm{A}+f_{\mathrm{DPS}}\cdot\mathrm{B}$ is shown in Figure 1. Template A represents the expected contribution to the distribution of $\Delta_{\mathrm{jets}}^{\mathrm{n}}$ from SPS events and was selected from events generated with the ALPGEN Monte Carlo generator, interfaced with HERWIG and JIMMY

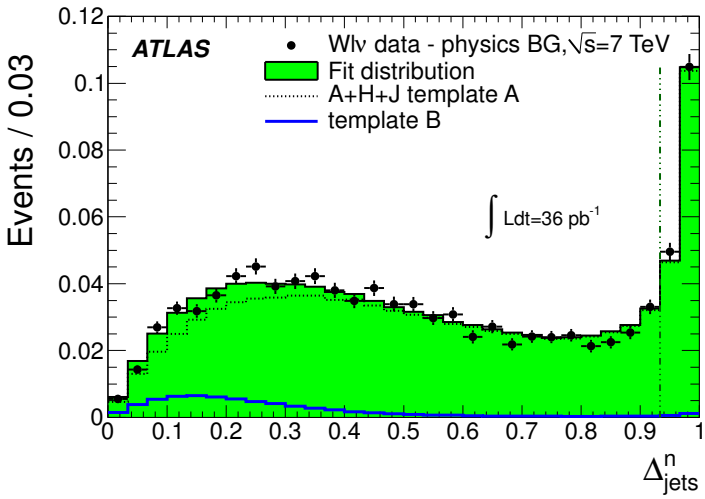

Figure 1: Distribution of $\Delta^{\mathrm{n}}_{\mathrm{jets}}$ from background-subtracted data (dots) compared to the result from the best fit for f_{DPS} [8]. The result of the fit is shown as the green histogram. The bins to the right of the vertical dash-dotted line were excluded from the fit. Data and the overall fit have been normalized to unity, Template A (dashed line) to $1 - f_{\mathrm{DPS}}$ and Template B (blue solid line) to f_{DPS}.

(AHJ). Template B represents the expected contribution from DPS events and was estimated from dijet events in data.
For jets with transverse momentum $p_{\mathrm{T}} \geq 20$ GeV and rapidity $|y| \leq 2.8$, a central value of

$$f_{\mathrm{DPS}} = 0.08 \pm 0.01\ (\mathrm{stat.}) \pm 0.02\ (\mathrm{sys.}) \tag{3}$$

was obtained. The result for f_{DPS} was used to extract σ_{eff},

$$\sigma_{\mathrm{eff}}(7\ \mathrm{TeV}) = 15 \pm 3\ (\mathrm{stat.})\ ^{+5}_{-3}\ (\mathrm{sys.})\ \mathrm{mb}. \tag{4}$$

The $W + J/\psi$ cross-section, corrected for the detector acceptance and the branching ratio of $J/\psi \to \mu^+\mu^-$, was measured relative to the inclusive W boson cross-section ($R^{\mathrm{incl}}_{J/\psi}$) using the 2011 ATLAS dataset of 4.5 fb^{-1} at $\sqrt{s} = 7$ TeV [9]. The value of σ_{eff} measured in the $W + 2$ jets final state, together with the prompt J/ψ cross-section from the ATLAS measurement [12], were then used to estimate the DPS contribution to the $W + J/\psi$ final state, $f_{\mathrm{DPS}} = 0.38^{+0.22}_{-0.20}\ (\mathrm{tot.})$. The distribution of $R^{\mathrm{incl}}_{J/\psi}$ as a function of the p_{T} of the J/ψ is shown in Figure 2(a) together with the estimated DPS contribution.

The first measurement of associated $Z + J/\psi$ production was performed in ATLAS using 20.3 fb^{-1} of data at $\sqrt{s} = 8$ TeV [10]. In DPS producing the $Z + J/\psi$ final state, the azimuthal angle between the Z boson and the J/ψ ($\Delta\phi(Z, J/\psi)$) is expected to be uniform, while in SPS producing the same final state the angle is expected to be $\sim \pi$ at leading-order. Assuming that all of the events with $\Delta\phi(Z, J/\psi) < \pi/5$ originate from DPS, a limit on the maximum DPS contribution to the observed $Z + J/\psi$ signal was obtained (see Figure 2(b)). The upper limit on f_{DPS} was found to be $f_{\mathrm{DPS}} < 0.29$ at 68% confidence level, corresponding to the lower limit on σ_{eff},

$$\sigma_{\mathrm{eff}}(8\ \mathrm{TeV}) > 5\ \mathrm{mb}. \tag{5}$$

For the purpose of measuring σ_{eff} in the four-jet final state [11], the 2010 ATLAS dataset, corresponding to 37 pb^{-1} at $\sqrt{s} = 7$ TeV, was used to select three samples of events, two dijet samples

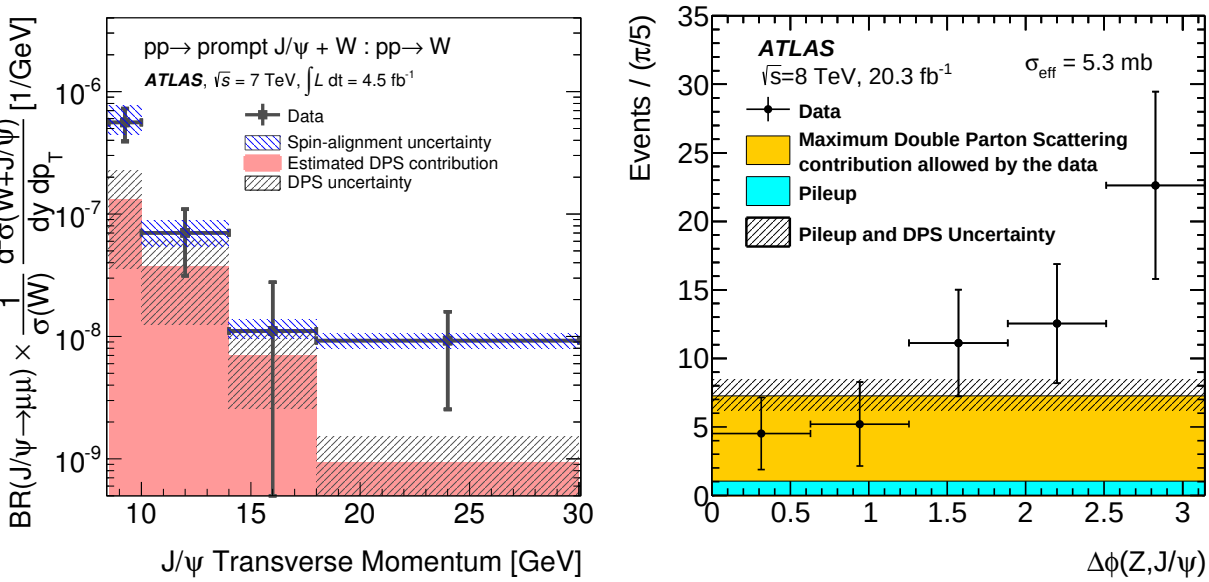

(a) (b)

Figure 2: (a) The cross-section ratio $\mathrm{d}R^{\mathrm{incl}}_{J/\psi}/\mathrm{d}p_{\mathrm{T}}$ as a function of the J/ψ transverse momentum [9]. The shaded uncertainty corresponds to the variations due to the various spin-alignment scenarios. The estimated contribution from DPS is overlaid with its uncertainty shown by a shaded region. (b) Distribution of the azimuthal angle between the Z boson and the J/ψ meson for prompt J/ψ production, overlaid with the pileup contribution [10]. The maximum DPS contribution allowed by the data is shown as the yellow band. The hashed region shows the DPS and pileup uncertainties added in quadrature.

and one four-jet sample. The former have at least two jets in the final state and the latter has at least four. Jets are required to have $p_{\mathrm{T}} \geq 20$ GeV and $|\eta| \leq 4.4$. In each event, jets are sorted in decreasing order of their transverse momenta. Denoting p^i_{T} the transverse momentum of the $i^{\,\mathrm{th}}$ jet in an event, the jet with the highest-p_{T}, p^1_{T}, is referred to as the leading jet. The leading jet in four-jet events is required to have $p^1_{\mathrm{T}} \geq 42.5$ GeV to comply with the requirements of the available jet triggers.

Based on Monte Carlo studies, DPS contributes in two ways. In one contribution, the secondary scatter produces two of the four leading jets in the event; such events are classified as complete-DPS (cDPS). In the second contribution of DPS to four-jet production, three of the four leading jets are produced in the hardest scatter, and one jet is produced in the secondary scatter; such events are classified as semi-DPS (sDPS). The contribution of DPS to the four-jet final state was estimated using the expected topology of the jets in SPS, cDPS and sDPS events. The SPS and sDPS samples were extracted from a multi-jet sample generated with AHJ and the cDPS sample was constructed by overlaying dijet events from data. The kinematic relations between pairs of jets were then used as input in the training of an artificial neural network (NN). The fraction of

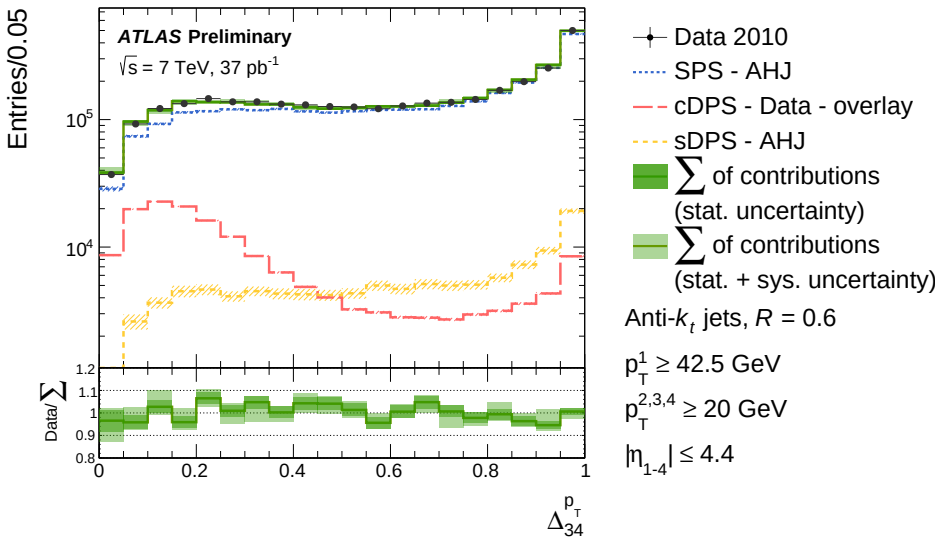

Figure 3: Comparison between the distribution of the variable $\Delta_{34}^{p_{\mathrm{T}}}$, defined in Eq.(7), in four-jet events in data and the sum of the SPS, cDPS and sDPS contributions, as indicated in the legend [11]. The sum of the contributions is normalized to the cross-section measured in data and the various contributions are normalized to their respective fractions obtained from the fit. In the sum of contributions distribution, statistical uncertainties are shown as the dark shaded area and the light shaded area represents the sum in quadrature of the statistical and systematic uncertainties. The ratio of data to the sum distribution is shown in the bottom panels.

DPS events was estimated with a template fit to the NN output distribution in data,

$$f_{\mathrm{DPS}} = 0.084\,^{+0.009}_{-0.012}\,(\mathrm{stat.})\,^{+0.054}_{-0.036}\,(\mathrm{syst.})\,. \tag{6}$$

The distribution of the variable

$$\Delta_{34}^{p_{\mathrm{T}}} = \frac{|\vec{p}_{\mathrm{T}}^{\,3} + \vec{p}_{\mathrm{T}}^{\,4}|}{p_{\mathrm{T}}^{3} + p_{\mathrm{T}}^{4}}\,, \tag{7}$$

in data is compared to a combination of the distributions in the three samples, SPS, cDPS and sDPS in Figure 3. The latter three distributions are normalized to their respective fraction in the data as obtained by the fit. A good description of the data is achieved. The fraction in Eq.(6) was used to extract σ_{eff}, yielding

$$\sigma_{\mathrm{eff}}(7\ \mathrm{TeV}) = 16.1\,^{+2.0}_{-1.5}\,(\mathrm{stat.})\,^{+6.1}_{-6.8}\,(\mathrm{syst.})\ \mathrm{mb}\,. \tag{8}$$

This value is consistent within the quoted uncertainties with previous measurements, performed in ATLAS and in other experiments [8, 10, 11, 13–20], some of which are summarized in Figure 4. Within the large uncertainties, the measurements are consistent with no $\sqrt{s}$ dependence of σ_{eff}.

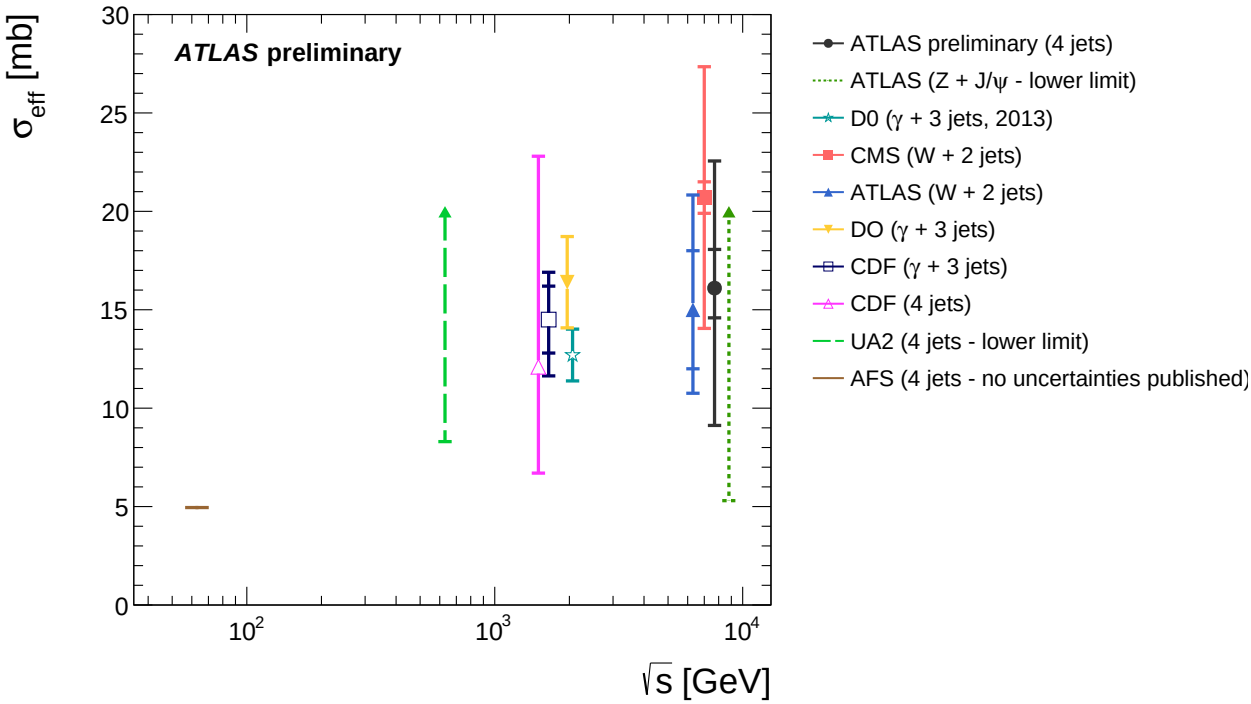

Figure 4: The effective overlap area between the interacting hadrons, σ_{eff}, as a function of the center-of-mass energy, $\sqrt{s}$, for different processes and in different experiments [8, 10, 11, 13–20]. The inner error bars (where visible) correspond to the statistical uncertainties and the outer error bars represent the sum in quadrature of the statistical and systematic uncertainties. Dashed arrows indicate lower limits and the horizontal line represents the AFS measurement published without uncertainties. For clarity, measurements at identical center-of-mass energies are slightly offset in $\sqrt{s}$. Figure taken from Ref. [11].

References

[1] P. V. Landshoff and J. C. Polkinghorne, "Calorimeter triggers for hard collisions," *Phys. Rev. D*, **18**(1978), 3344.

[2] F. Takagi, "Multiple Production of Quark Jets off Nuclei," *Phys. Rev. Lett.*, **43**(1979), 1296.

[3] C. Goebel, D. M. Scott, and F. Halzen, "Double Drell-Yan annihilations in hadron collisions: Novel tests of the constituent picture," *Phys. Rev. D*, **22**(1980), 2789.

[4] R. Astalos *et al.*, "Proceedings of the Sixth International Workshop on Multiple Partonic Interactions at the Large Hadron Collider," (2015), arXiv:1506.05829.

[5] B. Humpert and R. Odorico, "Multiparton scattering and QCD radiation as sources of four jet events," *Phys. Lett. B*, **154**(1985), 211.

[6] L. Ametller, N. Paver, and D. Treleani, "Possible signature of multiple parton interactions in collider four jet events," *Phys. Lett. B*, **169**(1986), 289.

[7] ATLAS Collaboration, "The ATLAS Experiment at the CERN Large Hadron Collider," *JINST*, **3**(2008), S08003.

[8] ATLAS Collaboration, "Measurement of hard double-parton interactions in $W(\rightarrow l\nu)$+ 2 jet events at $\sqrt{s}$=7 TeV with the ATLAS detector," *New J. Phys*, **15**(2013), 033038.

[9] ATLAS Collaboration, "Measurement of the production cross section of prompt J/ψ mesons in association with a $W^{\pm}$ boson in pp collisions at $\sqrt{s} = 7$ TeV with the ATLAS detector," *JHEP*, **04**(2014), 172.

[10] ATLAS Collaboration, "Observation and measurements of the production of prompt and non-prompt J/ψ mesons in association with a Z boson in pp collisions at $\sqrt{s}$ = 8 TeV with the ATLAS detector," *Eur. Phys. J. C*, **75**(2015), 229.

[11] ATLAS Collaboration, "Study of hard double parton scattering in four-jet events in pp collisions at $\sqrt{s} = 7$ TeV with the ATLAS experiment at the LHC," Technical Report ATLAS-CONF-2015-058, http://cds.cern.ch/record/2108894.

[12] ATLAS Collaboration, "Measurement of the differential cross-sections of inclusive, prompt and non-prompt J/ψ production in proton-proton collisions at $\sqrt{s} = 7$ TeV," *Nucl. Phys. B*, **850**(2011), 387.

[13] AFS Collaboration, T. Akesson *et al.*, "Double Parton Scattering in pp Collisions at $\sqrt{s} = 63$ GeV," *Z. Phys. C*, **34**(1987), 163.

[14] UA2 Collaboration, J. Alitti *et al.*, "A study of multi-jet events at the CERN pp collider and a search for double parton scattering," *Phys. Lett. B*, **268**(1991), 145.

[15] CDF Collaboration, F. Abe *et al.*, "Study of four-jet events and evidence for double parton interactions in $p\bar{p}$ collisions at $\sqrt{s} = 1.8$ TeV," *Phys. Rev. D*, **47**(1993), 4857.

[16] CDF Collaboration, F. Abe *et al.*, "Measurement of double parton scattering in $\bar{p}p$ collisions at $\sqrt{s} = 1.8$ TeV," *Phys. Rev. Lett.*, **79**(1997), 584.

[17] CDF Collaboration, F. Abe *et al.*, "Double parton scattering in $\overline{p}p$ collisions at $\sqrt{s} = 1.8$TeV," *Phys. Rev. D*, **56**(1997), 3811.

[18] D0 Collaboration, V.M. Abazov *et al.*, "Double parton interactions in photon+3 jet events in p p-bar collisions $\sqrt{s}$ = 1.96 TeV," *Phys. Rev. D*, **81**(2010), 052012.

[19] D0 Collaboration, V.M. Abazov *et al.*, "Double parton interactions in photon + 3 jet and photon + b/c jet + 2 jet events in $p\bar{p}$ collisions at $\sqrt{s} = 1.96$ TeV," *Phys. Rev. D*, **89**(2014), 072006.

[20] CMS Collaboration, "Study of double parton scattering using W + 2-jet events in proton-proton collisions at $\sqrt{s}$ = 7 TeV," *JHEP*, **1403**(2014), 032.

Double parton scattering in same sign W pairs

Diego Ciangottini[1]

[1]INFN, Perugia, IT

The internal partonic structure of the hadron is an open issue that has a huge impact especially in experiments at hadron colliders as LHC. In fact the increasing center of mass energy, reached at colliders, makes the description of final states more complicated as the time goes by. In first place that is due to the increasing energy of the parton with a same x, that in collision with larger s enhances the probability of the production of an hard parton. Therefore a good understanding of parton interactions is essential in performing precise physics measurements.

The evidence for Multi Parton Interactions (MPI) came from high p_T events observed in hadron collisions at the ISR at CERN [1] and later at the Fermilab Tevatron collider [2,3]. The introduction of MPI models (extending the perturbative description in a soft regime) in Monte Carlo tools, improved the description of those observations. Only a phenomenological approach can be used, due to the fact that its dynamics are not well understood since they are governed by soft and semi-hard interactions. In almost all cases, MPI are implemented by assuming a Poissonian distribution of elementary partonic interactions, with an average number depending on the impact parameter of the hadronic collision. The cross section is characterized by a stronger dependence on the incoming parton flux (as compared with the single pair case). Therefore MPI becomes increasingly important at higher centre-of-mass energies [4, 5] of the colliding hadrons, where partons with smaller and smaller fractional momenta play an active role.

All the actual Monte Carlos used for event simulation at CMS have to include MPI in order to make their predictions compatible with some observables of inelastic events such as the final state multiplicities, energy densities and many others.

In order to characterize MPI one can try to access a more controlled scenario by directly observing MPI processes; the simplest case is in the Double Parton Scattering (DPS), where two among all the parton-parton interactions can be described perturbatively (Double hard Parton Scattering). The talk is focused in the characterization of the MPI through same sign W boson pairs final state, as a first attempt to observe DPS in a model independent scenario.

This analysis studied DPS events with two same sign muons and two respectively associated neutrinos in the final state at 8 TeV [6]. In case of DPS the two W bosons are produced in first approximation independent of each other, and they are expected to be randomly distributed in the azimuthal plane and with less transverse momentum (p_T) as compared to SPS production. Hence, the muons produced from DPS are less boosted as compared to the leptons produced from SPS and there would not be any correlation between the two muons in the azimuthal plane.

The final state leptons can be studied using several observables. The scalar sum p_T of two muons and their p_T can be used for the discrimination purpose. For the same reason the azimuthal separations between the muon direction and MET have been studied as well. The invariant transverse mass of a muon and MET and the invariant transverse mass on two muon system are studied since they are sensitive to energy imbalance in the two W boson system.

After applying a standard selection for same sign W final states, background contributions are normalized for the considered integrated luminosity, and simulation-based events are used to evaluate the standard model background of WZ, Wγ, ZZ and single parton scattering WW processes. The predicted contribution on the total yield for those processes, after event selection, is less than 30%; the dominant part of background is due to events in which one (or two) muons coming from heavy-flavour decays are misidentified as coming from a *prompt* decay of W or Z boson. We will refer to misidentified muon will as *fake*, while *prompt* muons are those directly coming from W or Z boson decays. The method used to evaluate backgrounds with fake muons is data-oriented and consists in taking a fake muon enriched control sample and then extrapolating that to the background of the signal sample. Both control samples and extrapolation factors are derived directly from data.

After several control and validation studies, a Multi-Variate Analysis (MVA) using a Boosted Decision Tree (BDT) [7] has been performed in order to improve sensitivity to DPS events with respect to a single observable study. BDT's have been successfully used in High Energy Physics analyses, $e.g.$, by the MiniBooNE experiment [8], in which the selection is done on a majority vote on the result of several decision trees, which are all derived from the same training sample by supplying different event weights during the training. For BDT selection, an event is successively subjected to the whole set of decision trees and depending on how often it is classified as signal, a "likelihood" estimator is constructed for the event being signal or background. The idea is to use the BDT estimator to get a response shape with the highest possible DPS sensitivity; therefore many sensitive kinematic observables have been put into the BDT training process.

BDT response is studied on top of the same-sign offline base selection and results are shown the following (Figure 1).

In order to evaluate a limit on the DPS yield, we computed the expected and observed upper limits on the ratio of measured DPS yield with respect to the yield expected from simulation (at 95% C.L). We used the CL_s method which is based on the modified frequentist approach [9, 10]. Table 1 shows the results for expected and measured limits on DPS yields.

Then a further study is performed in order to investigate the results: "limit vs σ_{WW}^{DPS}" plots (fig. 2), shows on x-axis different MC assumptions on σ_{WW}^{DPS}, then for each of these hypothesis the limit on DPS yield ratio is calculated (both expected and observed). In this way it is visible how sensitivity changes for different σ_{eff} scenario.

Although no direct measurements of DPS yield are allowed with current statistics, an exclusion limit on DPS signal strength can be set. The limit estimation excludes at 95% CLs a signal strength $r > 1.897$ (28 DPS events), with an expected exclusion of $r > 2.01$ (30 DPS events), which means an upper limit on $\sigma_{WW}^{DPS} < 1.12\ pb$ at 95% of confidence level. Considering the two scattering to be independent and no correlation between interacting partons, one can put in relation the limit on σ_{WW}^{DPS} with the σ_{eff} using the factorization formula. Considering the cross section for

the production of a W boson that decays leptonically $\sigma_{W\to l\nu} = 37509pb$ and the corresponding branching ratio $BR_{W\to l\nu} = 0.326$, the limit on the σ_{eff} can be written as:

$$\sigma_{eff} > \frac{(\sigma_{W\to l\nu})^2}{2\cdot(BR^2_{W\to l\nu})\cdot\sigma^{DPS}_{WW}} = 5.91mb.$$

A scenario with 10 times more luminosity of the presented analysis has been preliminarily investigated and, considering additional final states from W leptonic decays, would allow a direct measurement of σ_{eff} with the incoming LHC Run-II.

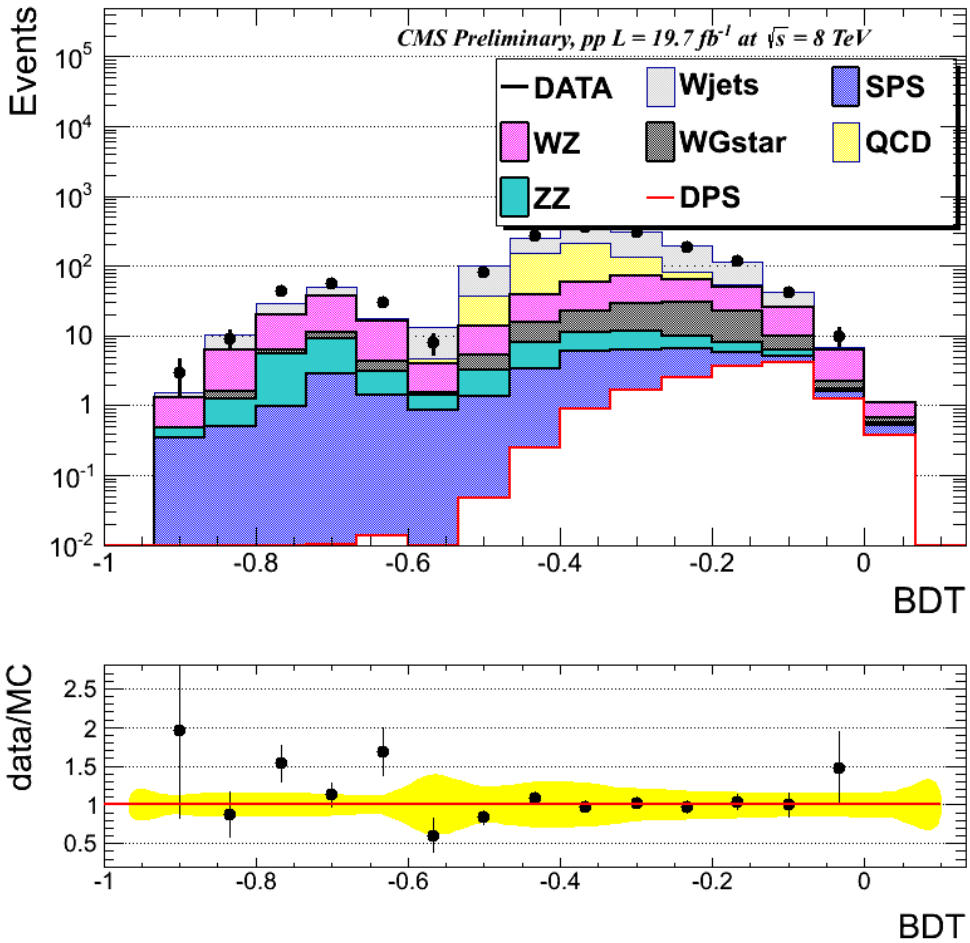

Figure 1: BDT response for events passing offline base selection. Yellow bands are systematics uncertainties, error bars on point are statistical uncertainties.

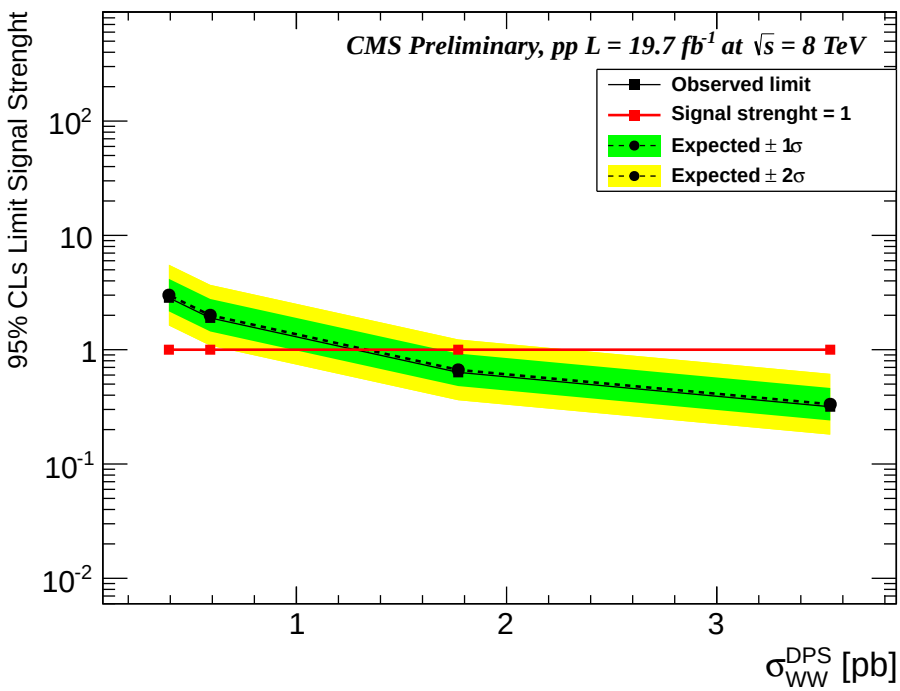

Figure 2: DPS yield limit vs σ_{WW}^{DPS} plot for BDT response

Table 1: 95% CLs Limit on DPS signal strength

	95% CLs
BDT	
Expected	$r < 2.001$
Expected $\pm 1\sigma$	[1.443,2.778]
Expected $\pm 2\sigma$	[1.085,3.691]
Observed	$r < 1.897$

References

[1] T. Akesson et. al., "Double parton scattering in p p collisions at pS = 63 GeV," *Z. Phys. C34 (1987) 163.*, (1987).

[2] F. Abe et. al., "Measurement of double parton scattering in anti-p p collisions at ps = 1.8 TeV," *Phys. Rev. Lett. 79 (1997) 58458*, (1997).

[3] M. Abazov et. al., "Double parton interactions in photon+3 jet events in p-p collisions ps=1.96 TeV,," *Phys. Rev. D81 (2010) 052012, [arXiv:0912.5104]*, (2010).

[4] Torbjorn Sjöstrand and Maria Van Zijl, "Multiple parton-parton interactions in an impact parameter picture," *Phys. Lett. B*, **188**(1987), 149, URL http://www.sciencedirect.com/science/article/pii/0370269387907222.

[5] L. Frankfurt, M. Strikman, and C. Weiss, "Transverse nucleon structure and diagnostics of hard parton-parton processes at LHC," *Phys. Rev. D*, **83**(2011), 054012, 1009.2559, URL http://link.aps.org/doi/10.1103/PhysRevD.83.054012.

[6] The CMS Collaboration, "Double Parton Scattering cross section limit from same-sign W bosons pair production in di-muon final state at LHC," *CMS-PAS-FSQ-13-001*, (2015).

[7] Yann Coadou, "Boosted Decision Trees and Applications," *EPJ Web Conf.*, **55**(2013), 02004.

[8] Hai-Jun Yang, Byron P. Roe, and Ji Zhu, "Studies of boosted decision trees for MiniBooNE particle identification," *Nucl.Instrum.Meth.*, **A555**(2005), 370, physics/0508045.

[9] Thomas Junk, "Confidence level computation for combining searches with small statistics," *Nucl.Instrum.Meth.*, **A434**(1999), 435, hep-ex/9902006.

[10] "Procedure for the LHC Higgs boson search combination in summer 2011," (2011).

Dynamical approach to MPI in four jet, W+dijet and Z+dijet production within the PYTHIA event generator

B.Blok[1] and P. Gunnellini[2]

[1]Physics Department, Technion, Haifa 32000 Israel
[2]Deutsches Elektronen-Synchrotron (DESY), Notkestrase 85, 22607 Hamburg, Germany

It is widely realized now that hard *Multiple Parton Interactions* (MPI) play an important role in the description of inelastic proton-proton (pp) collisions at high center-of-mass energies. Starting from the eighties [1,2] until the last decays the detailed theoretical, experimental and Monte Carlo (MC) studies were performed (see e.g. [3–12] (and references therein) for the latest work on the subject).

Recently, a new approach based on perturbative Quantum Chromodynamics (pQCD) has been developed [6–9] for describing the MPI.Its main ingredients are:

- the MPI cross sections are expressed through new objects, namely double Generalized Parton distributions (GPD_2);
- besides the conventional mean field parton model approach to MPI, represented by the so-called $2 \otimes 2$ mechanism (see Fig. 1 left), an additional $1 \otimes 2$ mechanism (Fig. 1 right) is included. In this mechanism, which can be described in pQCD, the parton from one of the nucleons splits at some hard scale and creates two hard partons that may participate in MPI. This mechanism leads to a significant transverse-scale dependence of MPI cross sections;
- the contribution of the $2 \otimes 2$ mechanism to GPD_2 is calculated in a mean field approximation with model-independent parameters.

Recently, the first step towards implementation of this approach in MC generators was done in [13, 14]. We use the standard simulation of the MPI implemented in PYTHIA [17], but with values of σ_{eff} calculated by using the QCD-based approach of [6–9], i.e. including $1 \otimes 2$ processes.

We use a single gaussian to model the matter distribution function of the protons in PYTHIA [15–17]. With these settings, the value of $\sigma_{eff}^{(0)}$ would however be constant and independent on the scale. In order to implement the x and the scale dependence of σ_{eff} in collisions where a hard MPI occur, according to [6–9], the Pythia-8 generated events are reweighted according to:

$$\sigma_{eff} = \frac{\sigma_{eff}^{(0)}}{1+R}, \tag{1}$$

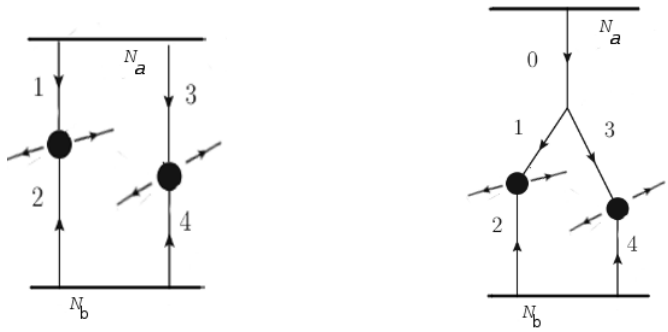

Figure 1: Sketch of the two considered MPI mechanisms: $2 \otimes 2$ (left) and $1 \otimes 2$ (right) mechanism.

where $\sigma_{eff}^{(0)}$ is the effective cross section in the mean field approach calculated in a model independent way from GPD_1, parameterized from HERA data [6, 18, 19], and R corresponds to the correction due to $1 \otimes 2$ mechanism [7–9]. This approach gives a unified description of experimental data at both hard (DPS) and morderate (UE) scales, with good accuracy and no new fit parameters, specific for MPI, except Q_0^2 whose value is expected to lie in the range 0.5-2 GeV^2, and that describes the separation between hard and soft scales. The transverse scale dependent function R is calculated numerically by solving the nonlinear evolution equation [8, 9].

The new tune, that includes reweighting according to Eq. (1) is called in the graphs below "UE tune dynamic $\sigma_{\rm eff}$ ", and the number is a Q_0 value.

For underlying event we use the following observables:$N_{\rm charge}$ and $\sum p_\perp$ density.

For DPS we use the following observables for 4 jet final states:

$$\Delta S = \arccos\left(\frac{\vec{p}_T(pair_1)\cdot\vec{p}_T(pair_2)}{|\vec{p}_T(pair_1)|\times|\vec{p}_T(pair_2)|}\right), \tag{2}$$

$$\Delta^{rel}p_T = \frac{|\vec{p}_T^{\,jet_1}+\vec{p}_T^{\,jet_2}|}{|\vec{p}_T^{\,jet_1}|+|\vec{p}_T^{\,jet_2}|}, \tag{3}$$

while for W+dijet, and Z+dijet we have:

$$\Delta{\rm S} = \arccos\left(\frac{\vec{p}_T({\rm boson})\cdot\vec{p}_T({\rm jet}_{1,2})}{|\vec{p}_T({\rm boson})|\times|\vec{p}_T({\rm jet}_{1,2})|}\right), \tag{4}$$

$$\Delta^{\rm rel}p_{\rm T} = \frac{|\vec{p}_T^{\,{\rm jet}_1}+\vec{p}_T^{\,{\rm jet}_2}|}{|\vec{p}_T^{\,{\rm jet}_1}|+|\vec{p}_T^{\,{\rm jet}_2}|}, \tag{5}$$

where boson may be the W or Z boson, $\rm jet_{1,2}$ is the jet pair and $\rm jet_1$ ($\rm jet_2$) is the leading (subleading) jet.

Our results are depicted in Figs. 2-4 for 4 jet case, and 5,6 for W and Z+dijet production.

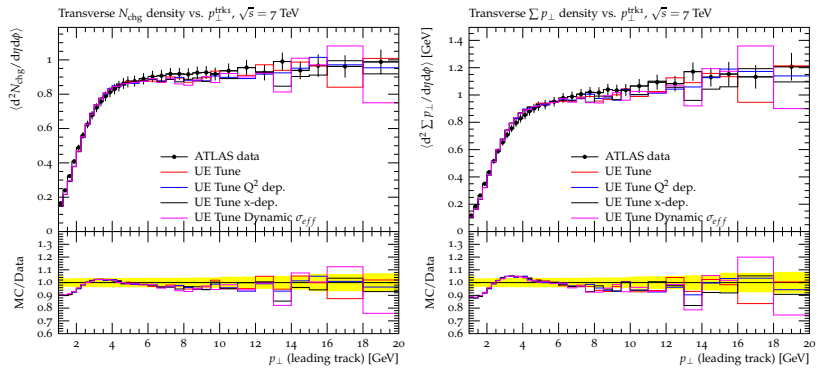

Figure 2: Charged particle density (left) and $\sum p_t$ density (right) as a function of the leading charged particle in the transverse regions, measured by the ATLAS experiment at 7 TeV. The data are compared to various predictions: the UE tune with constant σ_{eff} value (red curve), the UE tune with σ_{eff} x dependence applied (blue curve), the UE tune with σ_{eff} scale dependence with Q_0^2=1.0 GeV^2 applied (black curve) and the UE tune with both σ_{eff} x and scale dependence with Q_0^2=1.0 GeV^2 applied (pink curve). The lower panel shows the ratio between the various prediction and the experimental points.

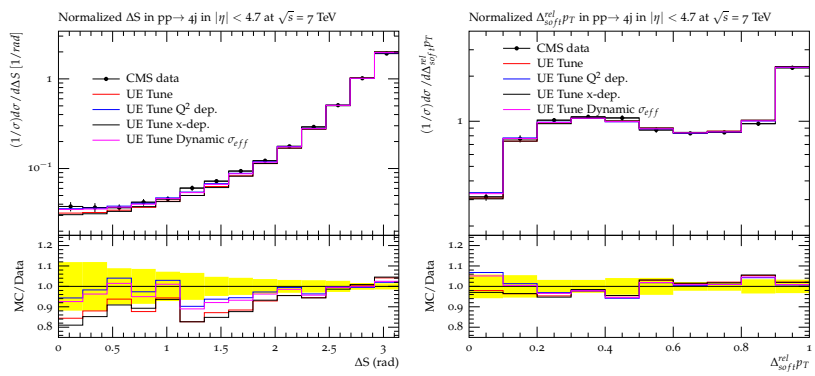

Figure 3: Normalized cross section distributions as a function of the correlation observables ΔS (left) and $\Delta^{rel}_{soft}p_T$ (right) measured in a four-jet scenario by the CMS experiment at 7 TeV. The data are compared to various predictions: the new UE tune (red curve), the new UE tune with the x dependence applied (blue curve), the new UE tune with only the scale dependence with Q_0^2=1.0 GeV^2 applied (black curve) and the new UE tune with both x and scale dependence with Q_0^2=1.0 GeV^2 applied (pink curve). The lower panel shows the ratio between the various prediction and the experimental points.

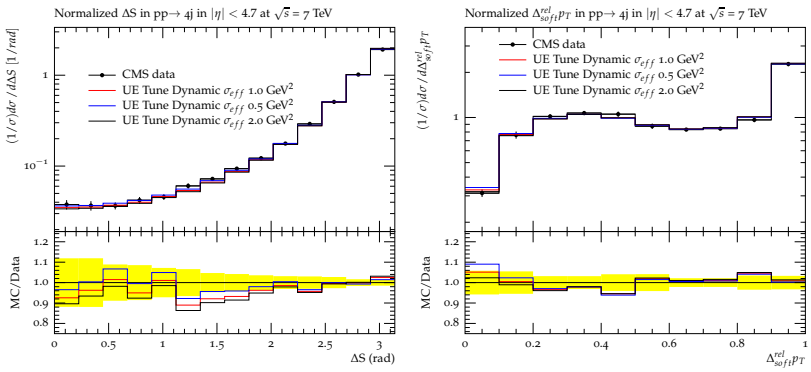

Figure 4: Normalized cross section distributions as a function of the correlation observables ΔS (left) and $\Delta^{rel}_{soft}p_T$ (right) measured in a four-jet scenario by the CMS experiment at 7 TeV . The data are compared to various predictions obtained with the new UE tune where both x and scale dependence have been applied with Q^2_0 equal to 1.0 (red curve), 0.5 (blue curve) and 2.0 (black curve) GeV^2. The lower panel shows the ratio between the various prediction and the experimental points.

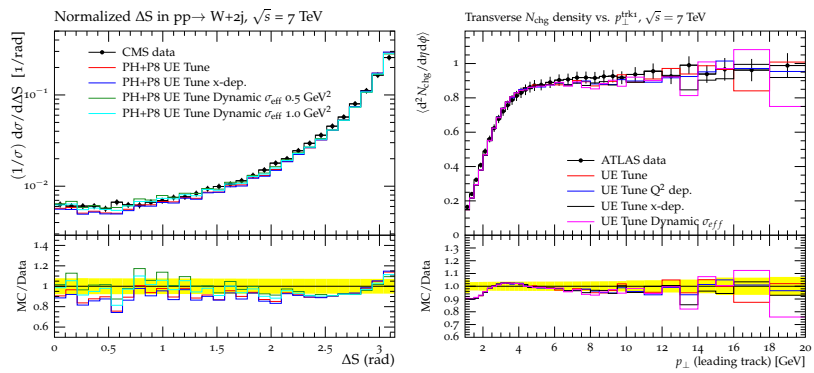

Figure 5: CMS data at 7 TeV for the normalized distributions of the correlation observables ΔS (*left*) and $\Delta^{\mathrm{rel}}p_{\mathrm{T}}$ (*right*) in the W+dijet channel, compared to predictions of POWHEG interfaced to PYTHIA 8 UE Tune with different σ_{eff} dependence applied: no reweighting applied (red line), x-dependent σ_{eff} values (blue line), x- and scale-dependent σ_{eff} values with $Q^2_0 = 0.5$ GeV^2 (green line) and x- and scale-dependent σ_{eff} values with $Q^2_0 = 1$ GeV^2 (pink line). Also shown are the ratios of these tunes to the data.

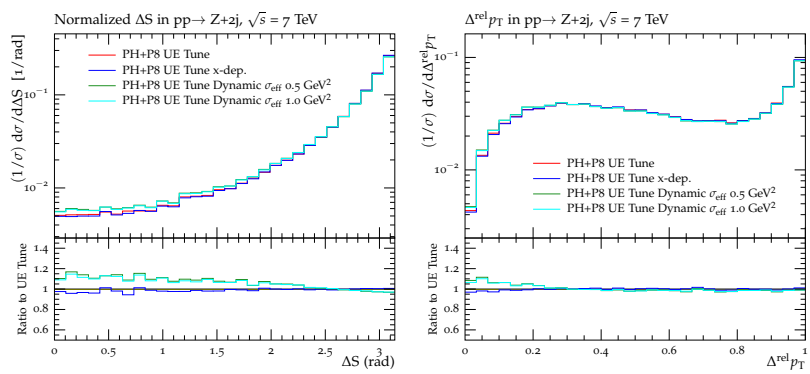

Figure 6: Predictions at 7 TeV for the normalized distributions of the correlation observables ΔS (*left*) and $\Delta^{\text{rel}}p_{\text{T}}$ (*right*) in the Z+dijet channel, of simulations performed with POWHEG interfaced to PYTHIA 8 UE Tune with different σ_{eff} dependence applied: no σ_{eff} reweighting applied (red line), x-dependent σ_{eff} values (blue line), x- and scale-dependent σ_{eff} values with $Q_0^2 = 0.5$ GeV^2 (green line) and x- and scale-dependent σ_{eff} values with $Q_0^2 = 1$ GeV^2 (pink line). Also shown are the ratios of each curve to the predictions of the UE Tune.

The Atlas and CMS data is given in [20–22].

We achieve for the first time a unified description of MPI at moderate and hard transverse momenta within a consistent framework, in good agreement with experimental data measured at 7 TeV both for 4 jet and Wjj and Zjj final states. The corresponding code implementing the new MPI approach is publicly available at http://desy.de/∼gunnep/SigmaEffectiveDependence/.

Acknowledgements

The authors thank Yu. Dokshitzer,H. Jung and M. Strikman for usefull discussions at various stages of this project.

References

[1] N. Paver and D. Treleani, Nuovo Cim. A **70** (1982) 215.

[2] M. Mekhfi, Phys. Rev. D**32**, 2371 (1985).

[3] M. Diehl, D. Ostermeier and A. Schafer, JHEP **1203** (2012) 089 [arXiv:1111.0910 [hep-ph]].

[4] J.R. Gaunt and W.J. Stirling, JHEP **1003**, 005 (2010) [arXiv:0910.4347 [hep-ph]];
J.R. Gaunt, C.H. Kom, A. Kulesza and W.J. Stirling, Eur. Phys. J. C **69**, 53 (2010) [arXiv:1003.3953 [hep-ph]].

[5] J.R. Gaunt and W.J. Stirling, JHEP **1106**, 048 (2011) [arXiv:1103.1888 [hep-ph]].

[6] B. Blok, Yu. Dokshitzer, L. Frankfurt and M. Strikman, Phys. Rev. D **83**, 071501 (2011) [arXiv:1009.2714 [hep-ph]].

[7] B. Blok, Yu. Dokshitser, L. Frankfurt and M. Strikman, Eur. Phys. J. C **72**, 1963 (2012) [arXiv:1106.5533 [hep-ph]].

[8] B. Blok, Yu. Dokshitser, L. Frankfurt and M. Strikman, arXiv:1206.5594v1 [hep-ph] (unpublished).

[9] B. Blok, Y. Dokshitzer, L. Frankfurt and M. Strikman, Eur. Phys. J. C **74** (2014) 2926 [arXiv:1306.3763 [hep-ph]].

[10] J. R. Gaunt, R. Maciula and A. Szczurek, arXiv:1407.5821 [hep-ph].

[11] M. Diehl, J. R. Gaunt, D. Ostermeier, P. Pll and A. Schfer, JHEP **1601** (2016) 076 doi:10.1007/JHEP01(2016)076 [arXiv:1510.08696 [hep-ph]].

[12] R. Astalos *et al.*, "Proceedings of the Sixth International Workshop on Multiple Partonic Interactions at the Large Hadron Collider," arXiv:1506.05829 [hep-ph].

[13] B. Blok and P. Gunnellini, Eur. Phys. J. C **75** (2015) no.6, 282 [arXiv:1503.08246 [hep-ph]].

[14] B. Blok and P. Gunnellini, arXiv:1510.07436 [hep-ph].

[15] T. Sjostrand, S. Mrenna and P. Z. Skands, Comput. Phys. Commun. **178** (2008) 852 [arXiv:0710.3820 [hep-ph]].

[16] R. Corke and T. Sjostrand, JHEP **1105** (2011) 009 [arXiv:1101.5953 [hep-ph]].

[17] R. Corke and T. Sjostrand,Corke:2011yy JHEP **1103** (2011) 032 [arXiv:1011.1759 [hep-ph]].

[18] L. Frankfurt, M. Strikman and C. Weiss, Phys. Rev. D **69**, 114010 (2004) [arXiv:hep-ph/0311231]; Ann. Rev. Nucl. Part. Sci. **55**, 403 (2005) [arXiv:hep-ph/0507286].

[19] L. Frankfurt, M. Strikman and C. Weiss, Phys. Rev. D **83** (2011) 054012 [arXiv:1009.2559 [hep-ph]].

[20] S. Chatrchyan *et al.* [CMS Collaboration], Phys. Rev. D **89** (2014) 9, 092010 [arXiv:1312.6440 [hep-ex]].

[21] G. Aad *et al.* [ATLAS Collaboration], Phys. Rev. D **83** (2011) 112001 [arXiv:1012.0791 [hep-ex]].

[22] S. Chatrchyan *et al.* [CMS Collaboration], JHEP **1403** (2014) 032 [arXiv:1312.5729 [hep-ex]].

Chapter 4

Working Group
MPI & small x & diffraction

Convenors:

Francesco Hautmann (Theory),
Oldrich Kepka (ATLAS)

Multiparton Interactions, Small-x and Diffraction Session: Introduction

F Hautmann and O Kepka

The central role of small-x physics in the study of multiple parton interactions in hadronic collisions emerges from the following two observations.

i) The contribution of multiple parton interactions (MPI) becomes more important with increasing parton densities. The parton densities rise steeply in the region of small longitudinal momentum fractions x, where they become dominated by gluon and sea quark distributions.

ii) MPI affect primarily highly differential cross sections and the detailed distribution of multiparticle final states produced by parton evolution. Theoretical predictions for MPI observables are thus sensitive to the theory of final states associated with small longitudinal fractions x.

One of the main consequences of these observations concerns the treatment of QCD factorization and evolution in the context of processes with MPI [1, 2]. While collinear factorization and evolution are expected to accurately describe inclusive cross sections, high-energy observables which are sensitive to the exclusive components of final states require generalizations of QCD methods to non-collinear factorization/evolution. This implies the use of transverse momentum dependent (TMD) parton distributions [3, 4]. TMD factorization theorems in QCD exist both for the low-q_T region [5–7] and high-energy region [8–10].

A substantial part of the Small-x and Diffraction section at the Multi-parton Interaction Workshop MPI@LHC 2015 is thus devoted to the theory and phenomenology of QCD factorization beyond the collinear approximation. On the theory side, this includes the calculational program [11] of scattering amplitudes with off-shell partons in the high-energy limit; the development of improved factorization formulas [12] which interpolate between the low-q_T and low-x regions; the coordinate-space approach [13] to investigate gluon transverse-momentum dependent distributions both at small x and at large x. On the phenomenology side, double scattering contributions to small-x processes at the LHC are investigated [14] using TMD pdf fits to DIS experimental data [15, 16]; the effects of diffraction and soft color rescattering [17] are implemented in Monte Carlo event generators LEPTO [18] and CASCADE [19]. A new model for including diffraction in PYTHIA [20–22] is now also available.

Connections between the main theme of the workshop, multi-parton interactions, and soft QCD dynamics are further explored in the Small-x and Diffraction section with the discussion of soft hadronic cross sections [23] and measurements by ATLAS [24] and LHCf [25].

One of the most basic open questions on multi-parton interactions remains the role of parton correlations and how one can gain insight into this. It is appropriate to address this question

in terms of parton showers, as the detailed structure of final states is central to measurements of MPI effects. Color dipole cascades in the Lund DIPSY model [26, 27] may be used to analyze final-state effects of color coherence from small-distance correlations due to strings overlapping in transverse coordinate space [28], and to model high-energy collisions of nuclei [29]. Initial-state effects from color coherence at small x [30, 31] are predicted to influence angular correlations, multiplicity distributions and energy flow observables associated with multi-jet production at the LHC. Taking into account the parton correlations implied by all of these dynamical effects may well influence, ultimately, the amount of MPI needed to describe experimental data at colliders.

An example of the interplay between multi-parton interactions and higher-order coherence effects from soft multi-gluon radiation was discussed in [32, 33] in the case of the energy flow associated with jets produced at high rapidity in pp collisions at the LHC. New calculations for multi-jet observables have been presented at MPI@LHC 2015 in the BFKL [34] and color glass condensate [35] approaches, as well as experimental measurements of multi-jet cross sections by CMS [36–38] probing the physics of jet correlations, strong coupling, parton distributions, and the potential influence of multi-parton interactions.

References

[1] M. Diehl, J. R. Gaunt, D.l Ostermeier, P. Ploessl, and A. Schaefer, *JHEP*, **01**(2016), 076.

[2] B. Blok, Y. Dokshitzer, L. Frankfurt, and M. Strikman, *Eur. Phys. J.*, **C74**(2014), 2926.

[3] R. Angeles-Martinez *et al.*, *Acta Phys. Polon.*, **B46**(2015), 2501.

[4] F. Hautmann, *Acta Phys.Polon.*, **B40**(2009), 2139.

[5] J. C. Collins, D. E. Soper, and G. F. Sterman, *Nucl.Phys.*, **B250**(1985), 199.

[6] J. C. Collins, D. E. Soper, and G. F. Sterman, *Nucl.Phys.*, **B223**(1983), 381.

[7] J. C. Collins, *Foundations of perturbative QCD*, (CUP, 2011).

[8] S. Catani, M. Ciafaloni, and F. Hautmann, *Phys.Lett.*, **B242**(1990), 97.

[9] S. Catani, M. Ciafaloni, and F. Hautmann, *Nucl. Phys.*, **B366**(1991), 135.

[10] S. Catani and F. Hautmann, *Nucl.Phys.*, **B427**(1994), 475.

[11] A. van Hameren, *Acta Phys. Polon.*, **B46**(2015), 2105.

[12] E. Petreska, 2015, 1511.09403.

[13] I. O. Cherednikov, *J. Phys. Conf. Ser.*, **678**(2016), 012049.

[14] B. Ducloue, L. Szymanowski, and S. Wallon, *Phys. Rev.*, **D92**(2015), 076002.

[15] F. Hautmann, *et al.*, *Eur. Phys. J.*, **C74**(2014), 3220.

[16] F. Hautmann and H. Jung, *Nucl. Phys.*, **B883**(2014), 1.

[17] G. Ingelman, R. Pasechnik, and D. Werder, (2015), 1511.06317.

[18] G. Ingelman, A. Edin, and J. Rathsman, *Comput. Phys. Commun.*, **101**(1997), 108.

[19] H. Jung *et al.*, *Eur. Phys. J.*, **C70**(2010), 1237.

[20] C. O. Rasmussen and T. Sjostrand, *JHEP*, **02**(2016), 142.

[21] C. O. Rasmussen, *Acta Phys. Polon. Supp.*, **8**(2015), 849.

[22] C. O. Rasmussen, 2015, 1512.05872.

[23] R. Fiore, L. Jenkovszky, and R. Schicker, *Eur. Phys. J.*, **C76**(2016), 38.

[24] G. Aad *et al.* (ATLAS), *Nucl. Phys.*, **B889**(2014), 486.

[25] O. Adriani *et al.* (LHCf), *Phys. Lett.*, **B750**(2015), 360.

[26] C. Flensburg, G. Gustafson, and L. Lonnblad, *JHEP*, **08**(2011), 103.

[27] C. Flensburg, G. Gustafson, L. Lonnblad, and A. Ster, *JHEP*, **06**(2011), 066.

[28] C. Bierlich, G. Gustafson, L. Lonnblad, and A. Tarasov, *JHEP*, **03**(2015), 148.

[29] G. Gustafson, L. Lonnblad, A. Ster, and T. Csorgo, *JHEP*, **10**(2015), 022.

[30] M. Deak, F. Hautmann, H. Jung, and K. Kutak, *JHEP*, **09**(2009), 121.

[31] S. Dooling, F. Hautmann, and H. Jung, *Phys. Lett.*, **B736**(2014), 293.

[32] F. Hautmann, 221–226, 2012, 1205.5411.

[33] M. Deak, F. Hautmann, H. Jung, and K. Kutak, *Eur. Phys. J.*, **C72**(2012), 1982.

[34] G. Chachamis, 2015, 1512.04430.

[35] J. Jalilian-Marian, *EPJ Web Conf.*, **112**(2016), 02007.

[36] V. Khachatryan *et al.* (CMS), (2016), 1601.06713.

[37] V. Khachatryan *et al.* (CMS), *Eur. Phys. J.*, **C75**(2015), 288.

[38] V. Khachatryan *et al.* (CMS), *Eur. Phys. J.*, **C75**(2015), 186.

Multi(3)-particle production in DIS at small x

Jamal Jalilian-Marian[1]

[1]Natural Sciences Department, Baruch College, 17 Lexington Ave, New York NY 10010
and CUNY Graduate Center, 365 Fifth Ave., New York NY 10016

1 Introduction

Multi-particle production and the (azimuthal or polar) angular correlations between the produced particles in Deeply Inelastic Scattering (DIS) of electrons (positrons) on protons and nuclei carry a wealth of information about the rich dynamics of QCD. In particular azimuthal angular correlations between hadrons produced in the kinematic region where small x partons in the target are probed can shed light on the largely unexplored region of QCD kinematic phase space where novel and exciting phenomena such as gluon saturation are expected to occur. Here we report on the progress made toward calculating three-parton differential cross section in DIS at small x using the Color Glass Condensate formalism.

The Color Glass Condensate formalism [1, 2] describes the dynamics of gluon saturation expected to occur at small x (equivalently at high energy or large rapidity). It encodes two effects which are not included in the collinear factorization approach to collisions; first it includes multiple-scatterings and second, it re-sums quantum corrections which are enhanced by large logs of x rather than Q^2. It has been applied to many processes where at least one hadron is present in the initial sate of a high energy collision [3, 4]. Here we [5] consider production of three partons in DIS at small x due to two reasons; first a DIS process is much "cleaner" than a proton-nucleus collision both theoretically and experimentally. Second, in a three-parton production process one has two azimuthal angles that one can control. This will give an additional handle on probing saturation of gluons in the target. Furthermore this calculation will serve as the contribution of real diagrams to the Next to Leading Order corrections to di-hadron correlations after one of the three final state partons is integrated out.

2 Three-parton production in DIS at small x

We consider the process where a virtual photon splits in a quark anti-quark pair which (either quark or anti-quark) then radiates a gluon, i.e. $\gamma^\star \to q\,\bar{q}\,g$. The diagrams where the gluon is radiated from a quark are shown in figure 1. One also needs to include the diagrams where the gluon is radiated from the anti-quark (bottom line). These can be obtained by a simple re-labeling

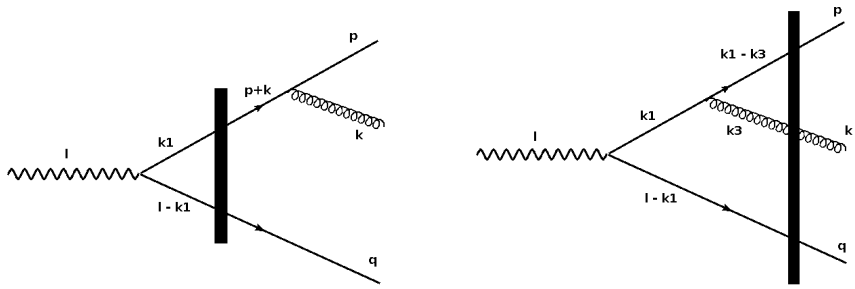

Figure 1: Leading Order 3-parton production diagrams corresponding to $\mathcal{A}_1$ (left) and $\mathcal{A}_2$ (right). The solid thick line represents interactions with the target (shock wave). The diagrams where the anti-quark radiates the gluon ($\mathcal{A}_3$ and $\mathcal{A}_4$) are not shown.

of momenta. The essential ingredients are the quark (anti-quark) and gluon propagators in a background field defined as

$$\begin{aligned} S_F(p,q) &\equiv S_F^0(2\pi)^4\delta^4(p-q) + S_F^0\tau_F(p,q)S_F^0(q) \\ G_{\mu\nu}^{ab}(p,q) &\equiv G_{\mu\nu}^{0\,ab}(p)\,\delta^{ab}\,(2\pi)^4\delta^4(p-q) + G^0{}_{\mu\lambda}(p)\tau_g^{ab}(p,q)G^{0,\lambda}{}_{\nu}(q) \end{aligned} \tag{1}$$

where $S_F^0, G^{0,ab}_{\mu\nu}$ are the free fermion and gluon propagators,

$$S_F^0(p) = \frac{i(\not{p}+m)}{p^2-m^2+i\epsilon} \qquad G^{0,ab}_{\mu\nu}(k) = \frac{id_{\mu\nu}(k)}{k^2+i\epsilon}\,\delta^{ab} \tag{2}$$

with the projector

$$d_{\mu\nu}(k) \equiv \left[-g_{\mu\nu} + \frac{k_\mu n_\nu + k_\nu n_\mu}{n\cdot k}\right] \tag{3}$$

and τ_F, τ_g contain the all-order scattering from the target color field, defined via

$$\begin{aligned} \tau_F(p,q) &\equiv (2\pi)\delta(p^- - q^-)\gamma^- \int d^2x_t e^{i(p_t-q_t)\cdot x_t}\left\{\theta(p^-)\left[V(x_t)-1\right] - \theta(-p^-)\left[V^\dagger(x_t)-1\right]\right\} \\ \tau_g(p,q) &\equiv -(2\pi)\delta(p^- - q^-)2p^- \int d^2x_t e^{i(p_t-q_t)\cdot x_t}\left\{\theta(p^-)\left[U(x_t)-1\right] - \theta(-p^-)\left[U^\dagger(x_t)-1\right]\right\} \end{aligned}$$

where V, U are Wilson lines in the fundamental and adjoint representation of $SU(N_c)$,

$$\begin{aligned} V(x_t) &\equiv \hat{P}exp\left\{ig\int dx^- A_a^+(x^-,x_t)\,t_a\right\} \\ U(x_t) &\equiv \hat{P}exp\left\{ig\int dx^- A_a^+(x^-,x_t)\,T_a\right\} \end{aligned}$$

and t_a and T_a are the corresponding generators. $\epsilon_\nu(l), \epsilon_\mu(k)$ are the polarization vectors of the incoming virtual photon and the outgoing gluon respectively. Transverse momentum of the virtual photon is set equal to zero so that $l^+ = -Q^2/2l^-$ without any loss of generality.

The Leading Order (LO) amplitude can be written as

$$\mathcal{A}^a = \mathcal{A}^a_1 + \mathcal{A}^a_2 + \mathcal{A}^a_3 + \mathcal{A}^a_4 \tag{4}$$

with

$$\begin{aligned}
\mathcal{A}^a_1 &= (ie)(ig)\bar{u}(p)\,\gamma^\mu\,t^a\,S_F(p+k,k_1)\gamma^\nu\,S_F(l-k_1,q)\left[S^0_F(q)\right]^{-1}\,v(q)\,\epsilon^\star_\nu(l)\,\epsilon_\mu(k)\,\frac{d^4k_1}{(2\pi)^4}\\
\mathcal{A}^a_2 &= (ie)(ig)\bar{u}(p)\,\left[S^0_F(p)\right]^{-1}\,S_F(p,k_1-k_3)\gamma^\lambda\,t^c\,S^0_F(k_1)\gamma^\nu\,S_F(l-k_1,q)\,\left[S^0_F(q)\right]^{-1}\,v(q)\\
&\quad \left[G^{\,\delta}_{\lambda}\right]^{ca}(k_3,k)\left[G^{0\mu}_{\delta}(k)\right]^{-1}\,\epsilon^\star_\nu(l)\,\epsilon_\mu(k)\,\frac{d^4k_1}{(2\pi)^4}\frac{d^4k_3}{(2\pi)^4}\\
\mathcal{A}^a_3 &= (ie)(ig)\bar{u}(p)\,\left[S^0_F(p)\right]^{-1}\,S_F(p,k_1)\,\gamma^\nu S_F(l-k_1,q+k)\,\gamma^\mu\,t^a\,v(q)\,\epsilon^\star_\nu(l)\,\epsilon_\mu(k)\,\frac{d^4k_1}{(2\pi)^4}\\
\mathcal{A}^a_4 &= (ie)(ig)\bar{u}(p)\,\left[S^0_F(p)\right]^{-1}\,S_F(p,k_1)\,\gamma^\nu\,S^0_F(l-k_1)\gamma^\lambda\,t^c\,S_F(l-k_1-k_3,q)\,\left[S^0_F(q)\right]^{-1}\\
&\quad \left[G^{\,\delta}_{\lambda}\right]^{ca}(k_3,k)\left[G^{0\mu}_{\delta}(k)\right]^{-1}\,\epsilon^\star_\nu(l)\,\epsilon_\mu(k)\,\frac{d^4k_1}{(2\pi)^4}\frac{d^4k_3}{(2\pi)^4}
\end{aligned} \tag{5}$$

The momentum integrations in terms A_1, A_3 can be done analytically but not in A_2, A_4 which need to be evaluated numerically. We then need to square the amplitude and to evaluate the Dirac traces which is done using FORM. The resulting expression involves trace of products of multiple Wilson lines [6] whose evolution equations are known. The resulting expressions will then allow us to investigate transverse momentum and azimuthal angular dependence of the three-produced partons (hadrons or jets).

Acknowledgements

This is based on work done in collaboration with A. Ayala, M. Hentschinski and M. E. Tejeda-Yeomans. J.J-M. acknowledges support by the DOE Office of Nuclear Physics through Grant No. DE-FG02-09ER41620 and from The City University of New York through the PSC-CUNY Research Award Program, grant 67732-0045.

References

[1] E. Iancu and R. Venugopalan, In *Hwa, R.C. (ed.) et al.: Quark gluon plasma* 249-3363; H. Weigert, Prog. Part. Nucl. Phys. **55**, 461 (2005); J. Jalilian-Marian, Y. V. Kovchegov, Prog. Part. Nucl. Phys. **56**, 104-231 (2006); F. Gelis, E. Iancu, J. Jalilian-Marian, R. Venugopalan, Ann. Rev. Nucl. Part. Sci. **60**, 463-489 (2010). [arXiv:1002.0333 [hep-ph]]; J. Jalilian-Marian, Y. V. Kovchegov, Prog. Part. Nucl. Phys. **56**, 104-231 (2006); J. L. Albacete and C. Marquet, Prog. Part. Nucl. Phys. **76**, 1 (2014).

[2] A. Ayala, J. Jalilian-Marian, L. D. McLerran and R. Venugopalan, Phys. Rev. D **52**, 2935 (1995), Phys. Rev. D **53**, 458 (1996); J. Jalilian-Marian, A. Kovner, L. D. McLerran and H. Weigert,

Phys. Rev. D **55**, 5414 (1997); J. Jalilian-Marian, A. Kovner, A. Leonidov and H. Weigert, Nucl. Phys. B **504**, 415 (1997), Phys. Rev. D **59**, 014014 (1999), Phys. Rev. D **59**, 014015 (1999), Phys. Rev. D **59**, 034007 (1999), A. Kovner, J. G. Milhano and H. Weigert, Phys. Rev. D **62**, 114005 (2000); A. Kovner and J. G. Milhano, Phys. Rev. D **61**, 014012 (2000); E. Iancu, A. Leonidov and L. D. McLerran, Nucl. Phys. A **692**, 583 (2001), Phys. Lett. B **510**, 133 (2001); E. Ferreiro, E. Iancu, A. Leonidov and L. McLerran, Nucl. Phys. A **703**, 489 (2002); H. Weigert, Nucl. Phys. **A703**, 823-860 (2002); J. -P. Blaizot, E. Iancu, H. Weigert, Nucl. Phys. **A713**, 441-469 (2003).

[3] A. Dumitru and J. Jalilian-Marian, Phys. Rev. Lett. **89**, 022301 (2002); J. Jalilian-Marian, Y. Nara and R. Venugopalan, Phys. Lett. B **577**, 54 (2003); J. Jalilian-Marian, J. Phys. G **30**, S751 (2004), Nucl. Phys. A **748**, 664 (2005), Phys. Rev. C **70**, 027902 (2004), Nucl. Phys. A **739**, 319 (2004); A. Dumitru, A. Hayashigaki and J. Jalilian-Marian, Nucl. Phys. A **765**, 464 (2006), Nucl. Phys. A **770**, 57 (2006); F. Gelis and J. Jalilian-Marian, Phys. Rev. D **76**, 074015 (2007); D. Boer, A. Utermann and E. Wessels, Phys. Rev. D **77**, 054014 (2008); E. R. Cazaroto, V. P. Gonçalves, F. S. Navarra, Nucl. Phys. A **872**, 196 (2011); J. Jalilian-Marian and A. H. Rezaeian, Phys. Rev. D **85**, 014017 (2012), Phys. Rev. D **86**, 034016 (2012); A. H. Rezaeian, Phys. Rev. D **86**, 094016 (2012); J. L. Albacete, A. Dumitru, H. Fujii and Y. Nara, Nucl. Phys. A **897**, 1 (2013); T. Altinoluk and A. Kovner, Phys. Rev. D **83**, 105004 (2011); G. A. Chirilli, B. -W. Xiao and F. Yuan, Phys. Rev. Lett. **108**, 122301 (2012), Phys. Rev. D **86**, 054005 (2012); Z. -B. Kang, I. Vitev and H. Xing, arXiv:1403.5221 [hep-ph].

[4] C. Marquet, Nucl. Phys. A **796**, 41 (2007); J. Jalilian-Marian and Y. V. Kovchegov, Phys. Rev. D **70**, 114017 (2004) [Erratum-ibid. D **71**, 079901 (2005)]; A. Kovner and M. Lublinsky, JHEP **0611**, 083 (2006), Phys. Rev. D **84**, 094011 (2011), Phys. Rev. D **83**, 034017 (2011); J. Jalilian-Marian, Eur. Phys. J. C **61**, 789 (2009), Nucl. Phys. A **770**, 210 (2006); J. L. Albacete and C. Marquet, Phys. Rev. Lett. **105**, 162301 (2010); F. Dominguez, C. Marquet, B. -W. Xiao and F. Yuan, Phys. Rev. D **83**, 105005 (2011); A. Stasto, B. -W. Xiao and F. Yuan, Phys. Lett. B **716**, 430 (2012); F. Dominguez, C. Marquet, A. M. Stasto and B. -W. Xiao, Phys. Rev. D **87**, no. 3, 034007 (2013); T. Lappi and H. Mantysaari, Nucl. Phys. A **908**, 51 (2013); E. Iancu and D. N. Triantafyllopoulos, JHEP **1311**, 067 (2013).

[5] A. Ayala, M. Hentschinski, J. Jalilian-Marian and M. E. Tejeda-Yeomans, work in progress.

[6] A. Dumitru and J. Jalilian-Marian, Phys. Rev. D **82**, 074023 (2010), Phys. Rev. D **81**, 094015 (2010); A. Dumitru, J. Jalilian-Marian, T. Lappi, B. Schenke and R. Venugopalan, Phys. Lett. B **706**, 219 (2011); E. Iancu and D. N. Triantafyllopoulos, JHEP **1111**, 105 (2011); F. Dominguez, A. H. Mueller, S. Munier and B. -W. Xiao, Phys. Lett. B **705**, 106 (2011); J. Jalilian-Marian, Phys. Rev. D **85**, 014037 (2012); A. Ayala, E. R. Cazaroto, L. A. Hernndez, J. Jalilian-Marian and M. E. Tejeda-Yeomans, Phys. Rev. D **90**, no. 7, 074037 (2014); S. Jeon and R. Venugopalan, Phys. Rev. D **71**, 125003 (2005); A. Dumitru, J. Jalilian-Marian, E. Petreska, Phys. Rev. **D84**, 014018 (2011); A. Dumitru and E. Petreska, Nucl. Phys. A **879**, 59 (2012); J. Jalilian-Marian, S. Jeon and R. Venugopalan, Phys. Rev. D **63**, 036004 (2001).

Application and calculation of amplitudes with off-shell partons

A. van Hameren[1]

[1]Institute of Nuclear Physics, Polisch Academy of Sciences

1 $c\bar{c}\,c\bar{c}$-production in k_T-factorization

It was shown in [1,2] that

$$pp \to c\bar{c}\,c\bar{c}\,X \tag{1}$$

is a golden reaction to study double-parton scattering (DPS) processes at hadron colliders. The theoretical prediction of a large cross section for the production of two mesons, both containing c or $\bar{c}$ quarks, was confirmed by the LHCb collaboration [3]. The single-parton scattering (SPS) contribution to the process was calculated in [4] in a high-energy approximation, neglecting certain contributions, and in [5] at complete tree-level within collinear factorization. In both papers it was found that the SPS contribution is much smaller than the DPS contribution.

The DPS contribution was calculated in the k_T-factorization approach [6,7]. One of the advantages over collinear factorization is that it allows for a momentum imbalance in $2 \to 2$ processes, giving a more realistic description of the process without the need of a parton shower. It requires so-called unintegrated gluon distribution functions (UGDFs), and the Kimber-Martin-Ryskin (KMR) model of UGDFs [8] is believed to include dominant higher-order corrections.

Another ingredient are matrix elements with off-shell initial-state partons. For $g^*g^* \to c\bar{c}$, the asterisk indicating off-shellness, these were already calculated in [6,7]. In order to have both the DPS and the SPS contribution to Eq.(1) in a uniform approach, and in order to investigate the possibility that the SPS contribution may be enhanced, the SPS contribution was calculated within k_T-factorization in [9]. The main challenge was the calculation of the matrix element with the off-shell partons, now for a $2 \to 4$ process. This was done with the help of A Very Handy LIBrary [10], which numerically evaluates helicity amplitudes, defined for off-shell partons following [11,12]. The latter papers provide a formulation that leads to manifestly gauge invariant amplitudes with off-shell partons. The calculation in [9] showes that k_T-factorization indeed leads to an enhancement of the SPS contribution, but nowhere close to the size of the DPS contribution.

2 Recursive calculation of off-shell amplitudes

The formulation of [11, 12] also allows for the application of efficient recursive techniques [13, 14], already widely applied in the calculation of tree-level amplitudes for on-shell partons. This *Dyson-Schwinger* recursion is mainly useful for numerical applications. In [15, 16] it was shown that the formulation of [11, 12] also allows for the application of the recursion devised by Britto, Cachazo, Feng, and Witten (BCFW) [17], leading to compact analytical expressions for the amplitudes. Whereas the Dyson-Schwinger recursion was implemented in AVHLIB, compact expressions for off-shell amplitudes obtained via BCFW recursion were implemented in AMP4HEF for numerical evaluation. Both libraries can be retrieved from

`http://bitbucket.org/hameren`

AMP4HEF computes the value of helicity amplitudes as well as matrix elements summed over helicities and colors for the processes $g^*g^* \to 4g$, $g^*q \to q + 2g$, $gq^* \to q + 2g$, and all processes with fewer on-shell gluons, all processes with fewer off-shell partons, and all processes with anti-quarks instead of quarks. More processes are planned to be added. It is practical in use, and can be used both in Fortran and C++ programs.

AVHLIB computes amplitudes and matrix elements for any process with the Standard Model, for essentially any number of final-state particles, and for any off-shell initial-state partons. It includes a complete Monte Carlo framework in Fortran with efficient phase space integration for the calculation of arbitrary observables. Due to its flexibility and completeness, it is less practical in use if one would only be interested in the matrix elements.

References

[1] Marta Łuszczak, Rafał Maciuła, and Antoni Szczurek, "Production of two $c\bar{c}$ pairs in double-parton scattering," *Phys. Rev.*, **D85**(2012), 094034, 1111.3255.

[2] Rafał Maciuła and Antoni Szczurek, "Production of $c\bar{c}c\bar{c}$ in double-parton scattering within k_t-factorization approach – meson-meson correlations," *Phys. Rev.*, **D87**(2013) (7), 074039, 1301.4469.

[3] R Aaij *et al.* (LHCb), "Observation of double charm production involving open charm in pp collisions at $\sqrt{s}$ = 7 TeV," *JHEP*, **06**(2012), 141, [Addendum: JHEP03,108(2014)], 1205.0975.

[4] Wolfgang Schafer and Antoni Szczurek, "Production of two $c\bar{c}$ pairs in gluon-gluon scattering in high energy proton-proton collisions," *Phys. Rev.*, **D85**(2012), 094029, 1203.4129.

[5] Andreas van Hameren, Rafał Maciuła, and Antoni Szczurek, "Single-parton scattering versus double-parton scattering in the production of two $c\bar{c}$ pairs and charmed meson correlations at the LHC," *Phys. Rev.*, **D89**(2014) (9), 094019, 1402.6972.

[6] S. Catani, M. Ciafaloni, and F. Hautmann, "High-energy factorization and small x heavy flavor production," *Nucl. Phys.*, **B366**(1991), 135.

[7] John C. Collins and R. Keith Ellis, "Heavy quark production in very high-energy hadron collisions," *Nucl.Phys.*, **B360**(1991), 3.

[8] M. A. Kimber, Alan D. Martin, and M. G. Ryskin, "Unintegrated parton distributions," *Phys. Rev.*, **D63**(2001), 114027, hep-ph/0101348.

[9] Andreas van Hameren, Rafał Maciuła, and Antoni Szczurek, "Production of two charm quark-antiquark pairs in single-parton scattering within the k_t-factorization approach," *Phys. Lett.*, **B748**(2015), 167, 1504.06490.

[10] M. Bury and A. van Hameren, "Numerical evaluation of multi-gluon amplitudes for High Energy Factorization," *Comput. Phys. Commun.*, **196**(2015), 592, 1503.08612.

[11] A. van Hameren, P. Kotko, and K. Kutak, "Helicity amplitudes for high-energy scattering," *JHEP*, **01**(2013), 078, 1211.0961.

[12] A. van Hameren, K. Kutak, and T. Salwa, "Scattering amplitudes with off-shell quarks," *Phys. Lett.*, **B727**(2013), 226, 1308.2861.

[13] Frits A. Berends and W. T. Giele, "Recursive Calculations for Processes with n Gluons," *Nucl. Phys.*, **B306**(1988), 759.

[14] F. Caravaglios, Michelangelo L. Mangano, M. Moretti, and R. Pittau, "A New approach to multijet calculations in hadron collisions," *Nucl. Phys.*, **B539**(1999), 215, hep-ph/9807570.

[15] A. van Hameren, "BCFW recursion for off-shell gluons," *JHEP*, **07**(2014), 138, 1404.7818.

[16] Andreas van Hameren and Mirko Serino, "BCFW recursion for TMD parton scattering," *JHEP*, **07**(2015), 010, 1504.00315.

[17] Ruth Britto, Freddy Cachazo, Bo Feng, and Edward Witten, "Direct proof of tree-level recursion relation in Yang-Mills theory," *Phys. Rev. Lett.*, **94**(2005), 181602, hep-th/0501052.

Colour Dipole Cascades

Gösta Gustafson[1]

[1]Dept. of Astronomy and Theoretical Physics, Lund University, Lund Sweden

1 The role of pertubation theory and unitarity constraints

HERA has shown that the parton density at small x grows rapidly $\sim 1/x^{1.3}$, as predicted by the perturbative BFKL pomeron. For pp collisions this implies a very large probability for gluon-gluon subcollisions, which implies that unitarity constraints are very important. These constraints lead to saturation of the gluon density, and suppression of partons with $k_\perp < Q_s^2$, which may explain why models based on multiple perturbative partonic subcollisions (like PYTHIA [1, 2]) are very successful at high energies. One can then ask: if perturbative physics dominates, is it then possible to calculate the result from basic principles, without input pdf's?

Unitarity constraints and saturation is most easily described in impact parameter space. Rescattering is represented by a convolution in $\mathbf{k}_\perp$-space, which simplifies to a product in $\mathbf{b}$-space. The small size of $\mathrm{Re}\, A_{el}^{pp}$ indicates that pp interaction is driven by absorption. If the absorption probability in Born approx. equals $2F(b)$, the optical theorem and the eikonal approximation gives the result: $d\sigma_{el}/d^2b = T^2 = (1-e^{-F})^2$, $d\sigma_{tot}/d^2b = 2T = 2(1-e^{-F})$.

2 Dipole cascade evolution

Mueller's dipole cascade model [3, 4] is a formulation of LL BFKL evolution in impact parameter space. A colour charge is always screened by an accompanying anticharge, forming a dipole. The dipole emits bremsstrahlung gluons coherently, which splits the dipole in two dipoles. The new dipoles splits repeatedly, developing into a cascade. When two cascades collide, s-channel unitarity is restored in the eikonal approximation.

The *Lund cascade model, DIPSY* [5–7], is a generalization of Mueller's model. Thus it is based on BFKL evolution, but includes a set of important corrections:

1) Important non-leading effects in BFKL evolution. (The most essential are related to energy conservation and running α_s.)

2) Saturation from pomeron loops in the evolution. (This is not included by Mueller or in the BK equation.)

3) Confinement, which also implies t-channel unitarity.

4) The DIPSY MC gives also fluctuations and correlations.

5) It can be applied to collisions between electrons, protons, and nuclei.

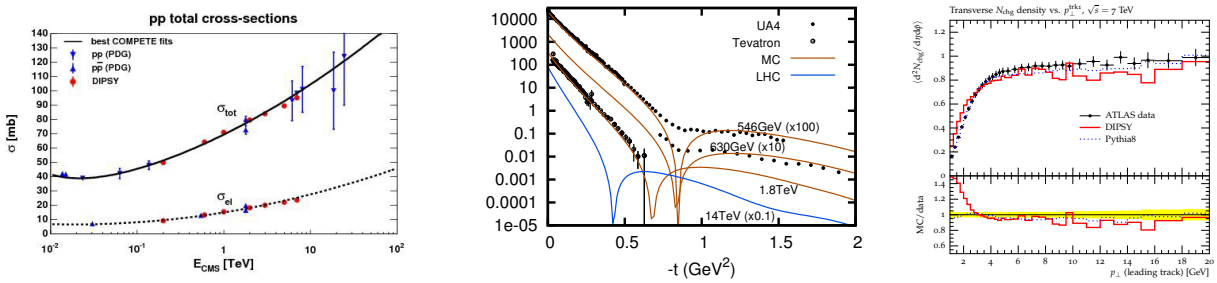

Figure 1: Left: σ_{tot} and σ_{el} vs $\sqrt{s}$. Middle: $d\sigma_{el}/dt$. Right: N_{ch} vs $p_\perp^{lead}$ at 7 TeV. Data from ATLAS.

Some DIPSY results

Cross sections: As examples fig. 1 shows results from DIPSY for the total and elastic pp cross sections. *Note that these results are obtained without input pdf's tuned to experimental data.* The increased cross sections and shrinking forward peak follow directly from the perturbative evolution. As an example for final state properties, N_{ch} vs $p_\perp^{lead}$ is also shown in fig. 1.

Correlations: The BFKL evolution is a stochastic process, and the DIPSY MC can also describe correlations and fluctuations. Results for two-parton correlations are given in ref. [8]. The result depends on both x and Q^2, and a spike (or a hotspot) is developed at larger Q^2 for small transverse separations, corresponding to large momentum imbalance Δ.

Fluctuations and Diffractive excitation

A projectile with a substructure may be diffractively excited to a different mass eigenstate. This can be described in the Good–Walker formalism as the result of fluctuations. Assume that the projectile and the target are linear combinations of diffractive eigenstates, Φ_n, with definite eigenvalues T_n. The elastic amplitude is then given by $\langle\Psi_{in}|T|\Psi_{in}\rangle$, where the average is taken over both projectile and target states. The differential total and elastic cross sections are then given by

$$d\sigma_{tot}/d^2b = 2\langle T\rangle, \quad d\sigma_{el}/d^2b = \langle T\rangle^2.$$

The total diffractive cross section, including elastic scattering, is given by $\langle\, T^2\,\rangle$. Diffractive excitation is obtained subtracting the elastic, and thus given by the fluctuations $\langle\, T^2\,\rangle - \langle T\rangle^2$. For the single and double excitations it is necessary to separate the averages over projectile and target states, below denoted by subscripts p and t respectively. Thus single excitation of the projectile and of the target is given by:

$$d\sigma_{SD,p}/d^2b = \langle\, \langle T\rangle_t^2\,\rangle_p - \langle T\rangle_{p,t}^2, \quad d\sigma_{SD,t}/d^2b = \langle\, \langle T\rangle_p^2\,\rangle_t - \langle T\rangle_{p,t}^2.$$

It is also shown in ref. [9] that the stochastic nature of the BFKL evolution implies that this Good–Walker formalism actually agrees with the more commonly used triple-pomeron analysis.

Fig. 2 shows a comparison between DIPSY and CDF results for single diffraction vs max M_X^2 [10]. It is also possible to calculate diffractive final states. Some results are here also shown in fig. 2 [11]. Note in particular that the MC is here only tuned to $\sigma_{\rm tot}$ and $\sigma_{\rm el}$, with no new parameter.

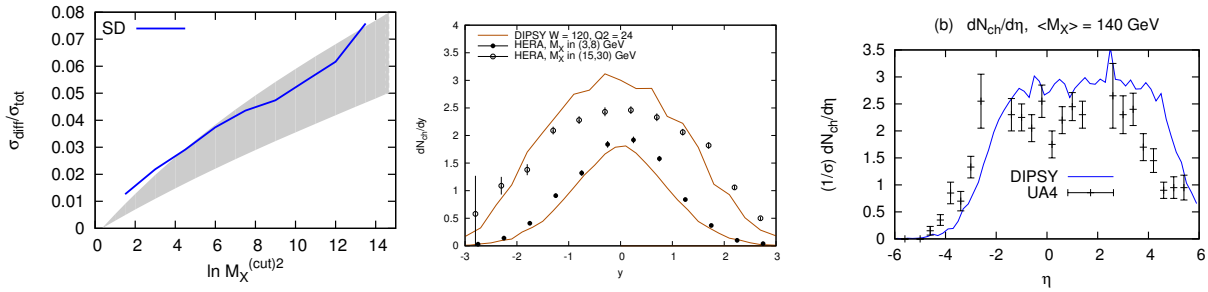

Figure 2: Left: $\int dM_X^2\, d\sigma_{SD}/dM_X^2$ for $M_X < M_X^{(cut)}$. The shaded area is an estimate of CDF results. Middle: $dn_{ch}/d\eta$ in 2 M_X-bins for DIS at $W = 120$ GeV, $Q^2 = 24$ GeV^2. Data from H1. Right: $dn_{ch}/d\eta$ in $p\bar{p}$ collisions at 546 GeV and $\langle M_X \rangle$= 140 GeV. Data from UA4.

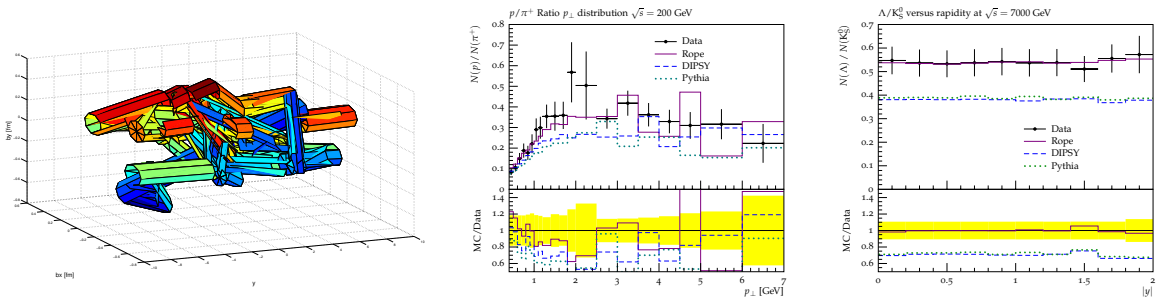

Figure 3: Left: Overlapping strings in $(\mathbf{r}_\perp, y)$-space in pp at 7 TeV. For clarity the radius in the figure is set to 0.1 fm. Middle: p/π ratio at 200 GeV. Right: Λ/K ratio at 7 TeV. Data from STAR and CMS.

3 Final state saturation, Ropes

It has been an old problem that the s/u ratio is higher in pp than in e^+e^- collisions. Also at LHC one observes higher fractions of strange particles and baryons. It was early proposed by Biro, Nielsen, and Knoll [12] that many strings close in transverse space may form "ropes". These authors studied collisions with nuclei, but at high energies there will be many overlapping strings also in pp collisions. This is illustrated in fig. 3, which shows the extension of strings in $(\mathbf{r}_\perp, y)$-space in a pp event at 7 TeV. The string diameter is expected to be of the order of 1 fm, but for a more clear picture, the string radius in fig. 3 is set to 0.1 fm. This shows that there is a very high degree of overlap between the strings.

If overlapping strings interact coherently as a rope, the colour charge at the end of such a rope is obtained from a random walk in colour space. Lattice calculations show that the tension in the rope is then given by the second Casimir operator. In ref. [13] we assume that the rope breaks

by repeated production of $q\bar{q}$ pairs. This implies that the "effective string tension" is determined by the *difference* in rope tension before and after the pair production. The result is a reduction in the number of produced quarks, and a higher rate of strange particles and baryons. Fig. 3 shows some results for p/π and Λ/K ratios.

4 Collisions with nuclei

The DIPSY model is directly generalizable to collisions with nuclei. It here gives a full partonic picture, a dense gluon soup. The model accounts for saturation in the cascades, correlations and fluctuations in the partonic states, and finite size effects. Understanding the initial states is essential for the interpretation of collective final state effects, and models for initial states in AA collisions can be tested in pA or γ^*A. While the nucleus is rather transparent in γ^*A, it is more absorptive in pA. Thus the pA cross section scales approximately with the interaction area $\propto (A^{1/3}+1)^2$ [14]. It is also seen that the colour interference between different nucleons in the nucleus is a small effect in the almost black pA total cross section, but an order 10% effect in γ^*Au, which is more transparent.

Interpreting results for pA collisions, it is interesting to estimate the number of interacting "wounded" nucleons. Gribov showed early that diffractive excitation of the nucleons is important in such an analysis, and it is important to separate the absorptive, non-diffractive, from the inelastic cross section. Diffractive excitation is here most easily treated in the Good–Walker formalism. In many analyses the problem with diffraction is neglected. To our knowledge, also those who include it take only excitation of the projectile into account. A study of the fluctuations causing the excitations, including also effects of excitation of target nucleons, is in progress.

References

[1] Torbjorn Sjostrand and Maria van Zijl, *Phys. Lett.*, **B188**(1987), 149.

[2] Torbjorn Sjostrand, *et al.*, *Comput. Phys. Commun.*, **191**(2015), 159, 1410.3012.

[3] Alfred H. Mueller, *Nucl. Phys.*, **B415**(1994), 373.

[4] Alfred H. Mueller and Bimal Patel, *Nucl. Phys.*, **B425**(1994), 471, hep-ph/9403256.

[5] Emil Avsar, Gosta Gustafson, and Leif Lonnblad, *JHEP*, **07**(2005), 062, hep-ph/0503181.

[6] Emil Avsar, Gosta Gustafson, and Leif Lonnblad, *JHEP*, **01**(2007), 012, hep-ph/0610157.

[7] Christoffer Flensburg, Gosta Gustafson, and Leif Lonnblad, *JHEP*, **08**(2011), 103, 1103.4321.

[8] Ch. Flensburg, G. Gustafson, L. Lonnblad, and A. Ster, *JHEP*, **06**(2011), 066, 1103.4320.

[9] Gosta Gustafson, *Phys. Lett.*, **B718**(2013), 1054, 1206.1733.

[10] Christoffer Flensburg and Gosta Gustafson, *JHEP*, **10**(2010), 014, 1004.5502.

[11] Christoffer Flensburg, Gosta Gustafson, and Leif Lonnblad, *JHEP*, **12**(2012), 115, 1210.2407.

[12] T. S. Biro, Holger Bech Nielsen, and Joern Knoll, *Nucl. Phys.*, **B245**(1984), 449.

[13] Ch. Bierlich, G. Gustafson, L. Lonnblad, and A. Tarasov, *JHEP*, **03**(2015), 148, 1412.6259.

[14] G. Gustafson, L. Lonnblad, A. Ster, and T. Csorgo, *JHEP*, **10**(2015), 022, 1506.09095.

Dynamic colour rescattering for diffractive DIS

Dominik Werder[1], Gunnar Ingelman[1], and Roman Pasechnik[2]

[1]Department of Physics and Astronomy, Uppsala University, Box 516, 75120 Uppsala, Sweden
[2]Department of Astronomy and Theoretical Physics, Lund University, 22362 Lund, Sweden

1 Introduction

Diffractive deep inelastic scattering (DDIS) has been previously described via Pomeron exchange in Regge theory [1, 2]. An alternative approach is to model the diffractive process by an effective colour screened interaction via the exchange of soft gluons. The underlying hard process is hereby assumed to be the same as in the corresponding non-diffractive process. Because of the assumed low scale of the additional soft gluon exchanges, the kinematics of the underlying hard process is not affected. However, the exchange of colour charge modifies the colour topology and can lead to forward final state protons and large rapidity gaps.

The original soft colour interaction model (SCI) [3] assumes random colour exchanges between the final state partons, determined by a fixed probability which is a free parameter of the model.

In the case of DDIS a more theoretically motivated basis for soft colour exchanges has been obtained [4, 5] using perturbative methods. It is based on the hard process at a small spacetime scale occurring in the gluon background field of the proton, with which the outgoing partons of the hard process may interact further. For these additional gluon exchanges, an amplitude was derived in the eikonal approximation to all orders in perturbation theory with a dependence on the event kinematics. This dynamic model for colour screening was recently implemented in a Monte Carlo study and we present the results [6] in this contribution.

2 Dynamic colour screening model

We consider the impact parameter representation in the proton rest frame, as in the colour dipole picture of the process, where the γ^* fluctuates into a $q\bar{q}$. After the hard subprocess, the $q\bar{q}$ interacts softly with the proton background field. In the forward limit where the total transverse momentum exchange $\boldsymbol{\delta}_\perp$ from the soft exchanges is small, the DDIS amplitude can be written in the high energy limit as

$$M_{\text{diff}}(\mathbf{k}_\perp, \boldsymbol{\delta}_\perp) \propto \int d^2r d^2b \, M_g(x_P; \mathbf{r}, \mathbf{b}) \, \mathcal{A}_{\text{DCS}}(\mathbf{r}, \mathbf{b}) \, e^{i\mathbf{r}\mathbf{k}_\perp} e^{i\mathbf{b}\boldsymbol{\delta}_\perp} \, ,$$

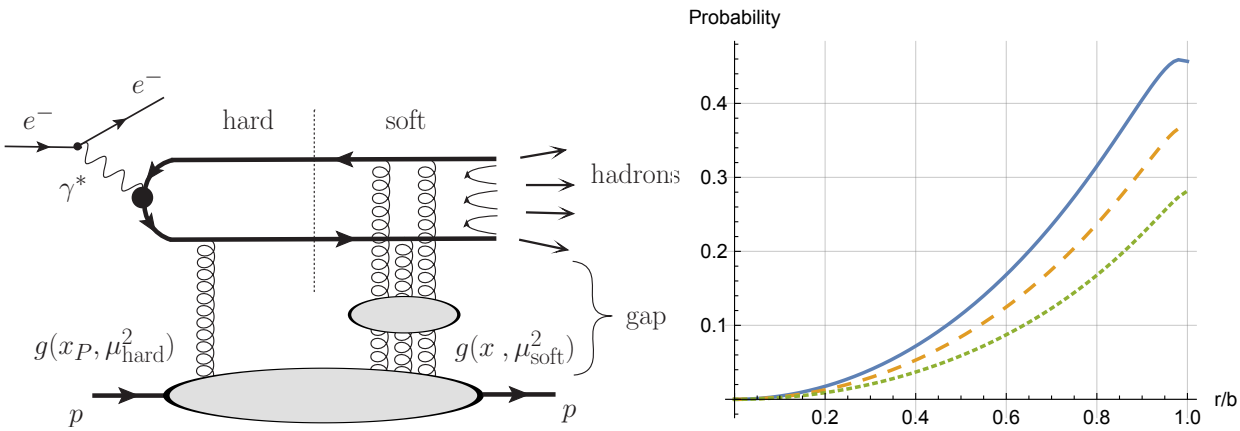

Figure 1: The DDIS process with the matrix element of the hard subprocess $\gamma^* g^* \to q\bar{q}$ with additional soft interactions of the $q\bar{q}$ dipole with the proton colour field. Right: The screening probability $P(r/b)$ for different values of $\alpha_s^{\rm eff} \in \{0.7, 0.6, 0.5\}$ (upper to lower curve).

where $\mathbf{k}_\perp$ is the relative quark transverse momentum in the $q\bar{q}$ dipole in the lowest order subprocess $g^* + \gamma^* \to q\bar{q}$. The dynamic colour screening (DCS) amplitude $\mathcal{A}_{\rm DCS}$ can be written as

$$\mathcal{A}_{\rm DCS}(\mathbf{r}, \mathbf{b}) = 1 - \exp\left(iC_F \alpha_s^{\rm eff}(\mu^2_{\rm soft})\ \ln \frac{|\mathbf{b} - \mathbf{r}|}{|\mathbf{b}|}\right) . \tag{1}$$

Here, C_F is the colour factor for the single gluon exchange amplitude and $\alpha_s^{\rm eff}$ is the effective coupling constant at the soft hadronic scale $\mu_{\rm soft}$.

In our study we obtain a probability for the colour screened process from the soft amplitude $\mathcal{A}_{\rm DCS}$ by writing

$$\frac{|M_{\rm diff}(\mathbf{r}, \mathbf{b})|^2}{|M_{\rm incl}(\mathbf{r}, \mathbf{b})|^2} = |\mathcal{A}_{\rm DCS}(\mathbf{r}, \mathbf{b})|^2 \equiv P(\mathbf{r}, \mathbf{b}) . \tag{2}$$

With $\mathbf{r} \cdot \mathbf{b} \equiv rb\cos\varphi$ and under the requirement that $r/b < 1$, we average over the unobserved angle to obtain the probability in terms of r/b as

$$P(r/b) = \int \frac{d\varphi}{2\pi} |\mathcal{A}_{\rm DCS}|^2 \ . \tag{3}$$

The resulting probability is shown in figure 1 for different choices of $\alpha_s^{\rm eff}$. We note the key properties of the levelling off at large r/b resembling the saturation feature of the dipole scattering amplitude, and the vanishing of the probability for small dipoles $r/b \ll 1$ which is compatible with the colour transparency property.

For the application in our Monte Carlo based study, we associate the transverse size r with the smallest $k_\perp$ difference within the partonic X-system, $r \simeq 1/k_{\perp \rm min}$. Similarily, we associate the impact parameter b with the soft transverse momentum $b \simeq 1/q_\perp$, which is a free parameter. To

avoid a possible divergent behaviour in the Monte Carlo based treatment, we introduce a regulator $k_{\perp 0}$ in the ratio $r/b = q_\perp/\sqrt{k^2_{\perp\min} + k^2_{\perp 0}}$ which constitutes the second free parameter of the model.

Since experimental data covers a wide kinematic range where it is possible to have $M_X^2 \gg Q^2$, we expect CCFM evolution [7, 8, 9] to be better suited to our process because of the resummation of potential large logarithms $\ln M_X^2/Q^2 \simeq -\ln\beta$, with $\beta = x/x_P$.

3 Results and Conclusions

Our main result in figure 2 shows an agreement with HERA data, where the diffractive observable $\sigma^D(Q^2, \beta, x_P)$ is defined in terms of a forward small-mass system with proton quantum numbers. From the fit to data we obtain the parameters $k_{\perp 0} = 0.72\,\text{GeV}$ and $q_\perp = 0.58\,\text{GeV}$. We conclude that the dynamic colour screening model with its two physically motivated parameters can give a good fit to data over a wide region of the kinematic range. However, the model is below data at large x_P, small Q^2 and small β. One reason for the remaining discrepancy could be the fact that not the full phase space is included, for example because of the lack of gluon emission from the quark propagator. This could potentially be improved by a NLO matrix element or by the addition of quarks to the CCFM parton evolution.

Acknowledgements: DW would like to thank the organizers of the MPI@LHC 2015 for the interesting workshop and the generous support.

References

[1] Jeffrey R. Forshaw and D. A. Ross, "Quantum chromodynamics and the pomeron," *Cambridge Lect. Notes Phys.*, **9**(1997), 1.

[2] G. Ingelman and P. E. Schlein, *Phys. Lett.*, **B152**(1985), 256.

[3] G. Ingelman A. Edin and J. Rathsman, *Phys.Lett. B*, **366**(1996), 371.

[4] S. J. Brodsky, R. Enberg, P. Hoyer, and G. Ingelman, *Phys. Rev.*, **D71**(2005), 074020.

[5] R. Pasechnik, R. Enberg, and G. Ingelman, *Phys. Rev.*, **D82**(2010), 054036, 1005.3399.

[6] Gunnar Ingelman, Roman Pasechnik, and Dominik Werder, (2015), 1511.06317.

[7] S. Catani, F. Fiorani, and G. Marchesini, *Nucl. Phys.*, **B336**(1990), 18.

[8] S. Catani, M. Ciafaloni, and F. Hautmann, *Nucl. Phys.*, **B366**(1991), 135.

[9] Giuseppe Marchesini, *Nucl. Phys.*, **B445**(1995), 49, hep-ph/9412327.

[10] F. D. Aaron *et al.* (H1), *Eur. Phys. J.*, **C72**(2012), 2074, 1203.4495.

[11] H. Jung and G. P. Salam, *Eur. Phys. J.*, **C19**(2001), 351.

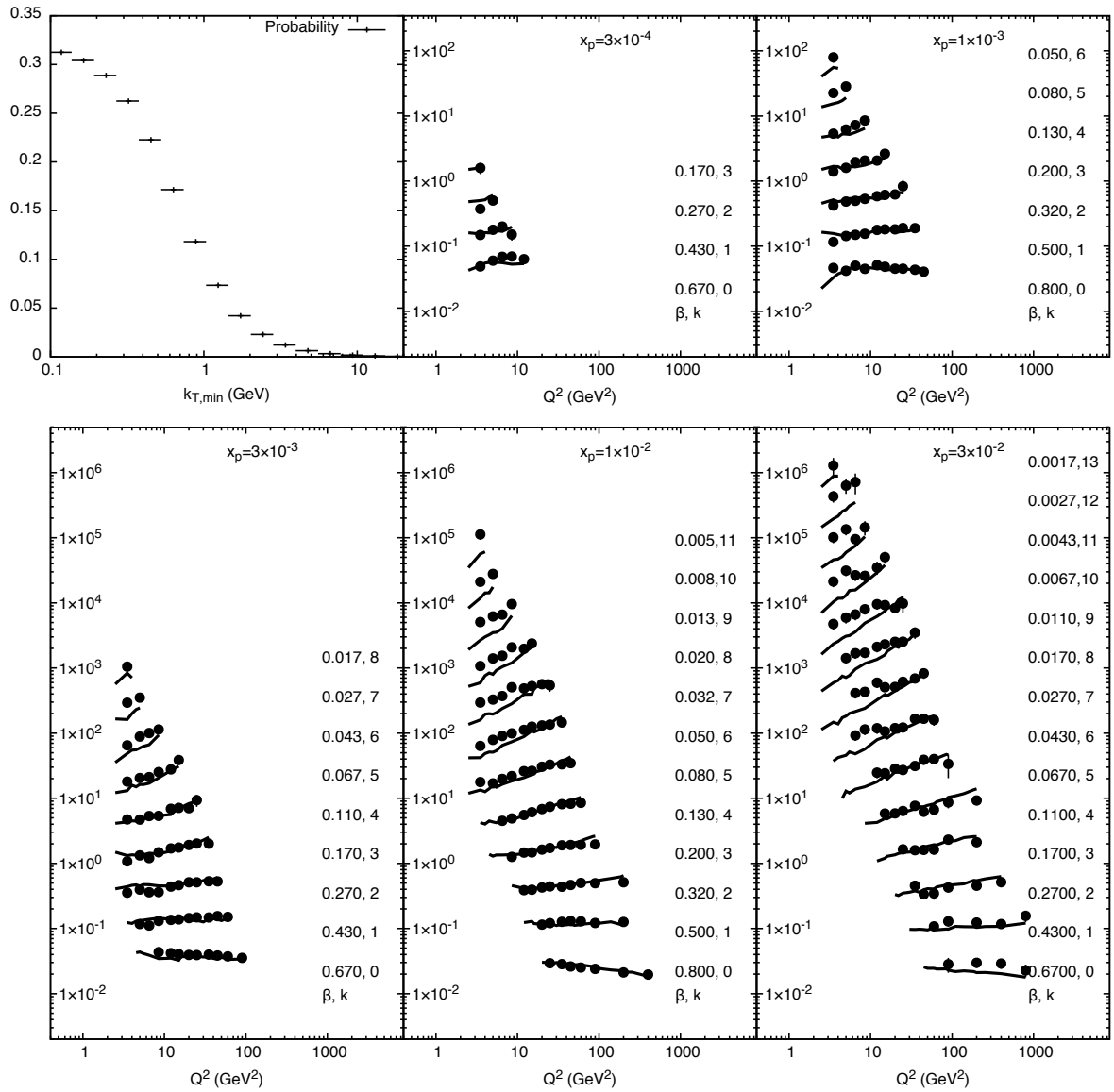

Figure 2: The reduced diffractive cross section $\sigma^D(Q^2, \beta, x_P)$ in comparison with the H1 data [10]. The model prediction uses dynamic colour screening with the parameters $k_{\perp 0} = 0.72\,\text{GeV}$ and $q_\perp = 0.58\,\text{GeV}$ and the CASCADE [11] event generator with CCFM evolution. $P(k_{\perp\min})$ for the fitted parameters is shown in the upper-left corner. Diffractive events in the model are defined as having a remnant system Y with proton quantum numbers and invariant mass $M_Y < 1.6\,\text{GeV}$. Rows for different values of β are offset by a factor 3^k as indicated on the figure.

Improved TMD factorization for forward dijet production in pA collisions

Elena Petreska[1,2]

[1]Centre de Physique Théorique, École Polytechnique, CNRS, Université Paris-Saclay, F-91128 Palaiseau, France ,
[2]Departamento de Física de Partículas and IGFAE, Universidade de Santiago de Compostela, 15782 Santiago de Compostela, Spain

We study the production of forward dijets in proton-nucleus high-energy collisions. When both of the jets are produced in the forward rapidity direction, the collision probes the large-x parton distributions in the projectile and the small-x gluons in the target. We derive a factorization formula for this process valid for an arbitrary value of the momentum imbalance k_t of the jets [1][1]:

$$\frac{d\sigma^{pA\to \text{dijets}+X}}{d^2P_t d^2k_t dy_1 dy_2} = \frac{\alpha_s^2}{(x_1x_2s)^2}\sum_{a,c,d} x_1 f_{a/p}(x_1,\mu^2)\sum_{i=1}^{2} K^{(i)}_{ag^*\to cd}(k_t)\Phi^{(i)}_{ag\to cd}(k_t)\,\frac{1}{1+\delta_{cd}}\,. \qquad (1)$$

The proton's large-x_1 partons are described with parton distributions functions of collinear factorization $f_{a/p}(x_1,\mu^2)$, while the target is represented with a total of six, two per channel, transverse momentum dependent (TMD) gluon distributions $\Phi^{(i)}_{ag\to cd}(k_t)$. The dependence on the transverse momentum k_t of the small-x_2 gluon is also explicitly present in the hard factors $K^{(i)}_{ag^*\to cd}(k_t)$ for the partonic subprocesses [2]. The factorization formula, Eq.(1), is therefore applicable for the whole range of k_t values between the saturation scale Q_s and the hard typical momentum of the jets P_t.

The new formula interpolates between the regions of validity of two factorization formulas for dijet production applicable for only certain limits of k_t values. The first framework is the high-energy factorization (HEF) [2–4] valid for large k_t on the order of the momentum of the jets, $Q_s \ll k_t \sim P_t$. The HEF formula has k_t dependent matrix elements, but only one gluon distribution for the target. It can be derived from the color glass condensate (CGC) cross section in the dilute target approximation [1]. The CGC formalism [5] captures the multi-gluon scatterings of the projectile parton with the saturated field of the target from first principles, but the CGC cross section for dijet production can not be written in a factorized form in the most general case. We

[1]The rapidities of the outgoing particles are y_1 and y_2, and s is the center of mass energy squared.
[2]The expressions for the hard factors can be found in Ref. [1].

show that by restricting the interactions to two gluon exchanges (dilute target limit) the CGC cross section involves only the HEF gluon distribution for the target, and complete equivalence with the HEF formula is achieved.

The second formalism is the TMD factorization [6,7] with on-shell hard factors and eight TMD gluon distributions for the target. It is valid for small k_t values, $k_t \sim Q_s \ll P_t$. The TMD distributions are the result of the resummation of collinear gluons from the target that couple to the hard part. We improve the TMD formula that was derived in Ref. [7] by including all finite-N_c corrections, reducing the number of independent distributions to two per channel, and restoring the k_t dependence in the hard part. The resulting formula, Eq. (1), encompasses both formalisms, the HEF and TMD factorization.

The TMD gluon distributions $\Phi^{(i)}_{ag\to cd}(k_t)$ are specific for this process and are determined by the color structure of the hard partonic scattering. For large-N_c they can be written as a convolution of only two fundamental distributions, the *dipole distribution*, and the *Weizsäcker-Williams gluon distribution*. We calculate the gluon densities in the large-N_c limit in the Golec-Biernat-Wusthoff model [8]:

$$
\begin{aligned}
\Phi^{(1)}_{qg\to qg}(x_2,k_t) &= \frac{N_c S_\perp}{2\pi^3\alpha_s}\frac{S_\perp}{Q_s^2(x_2)}k_t^2\exp\left[-\frac{k_t^2}{Q_s^2(x_2)}\right],\\
\Phi^{(2)}_{qg\to qg}(x_2,k_t) &= \frac{N_c S_\perp}{2\pi^3\alpha_s}\exp\left[-\frac{k_t^2}{Q_s^2(x_2)}\right]\int_1^\infty\frac{dt}{t(t+2)}\exp\left[\frac{2k_t^2}{(t+2)Q_s^2(x_2)}\right],\\
\Phi^{(1)}_{gg\to q\bar{q}}(x_2,k_t) &= \frac{N_c S_\perp}{16\pi^3\alpha_s}\exp\left[-\frac{k_t^2}{2Q_s^2(x_2)}\right]\left(2+\frac{k_t^2}{Q_s^2(x_2)}\right),\\
\Phi^{(2)}_{gg\to q\bar{q}}(x_2,k_t) &= -\frac{N_c^3 S_\perp}{16\pi^3\alpha_s}\exp\left[-\frac{k_t^2}{2Q_s^2(x_2)}\right]\left(2-\frac{k_t^2}{Q_s^2(x_2)}\right),\\
\Phi^{(1)}_{gg\to gg}(x_2,k_t) &= \frac{N_c S_\perp}{8\pi^3\alpha_s}\exp\left[-\frac{k_t^2}{2Q_s^2(x_2)}\right]\left(\frac{1}{2}+\frac{k_t^2}{4Q_s^2(x_2)}+\int_1^\infty\frac{dt}{t(t+1)}\exp\left[\frac{k_t^2}{2(t+1)Q_s^2(x_2)}\right]\right),\\
\Phi^{(2)}_{gg\to gg}(x_2,k_t) &= \frac{N_c S_\perp}{4\pi^3\alpha_s}\exp\left[-\frac{k_t^2}{2Q_s^2(x_2)}\right]\left(\frac{1}{2}-\frac{k_t^2}{4Q_s^2(x_2)}+\int_1^\infty\frac{dt}{t(t+1)}\exp\left[\frac{k_t^2}{2(t+1)Q_s^2(x_2)}\right]\right)
\end{aligned}
\tag{2}
$$

We also obtain their high-k_t behavior in the McLerran-Venugopalan model [9]. To leading order all the distributions scale as Q_s^2/k_t^2.

The factorization formula in Eq. (1) can be used for phenomenological studies of dijet azimuthal correlations in dilute-dense collisions, with both, analytical input for the TMD gluons, Eq. (2), or numerical calculations that implement small-x evolution. The results will be presented in a forthcoming publication.

Acknowledgements

I thank my collaborators Piotr Kotko, Krzysztof Kutak, Cyrille Marquet, Sebastian Sapeta and Andreas van Hameren, with whom this work was completed. I also thank the European Research Council grant HotLHC ERC-2011-StG-279579, Ministerio de Ciencia e Innovación of Spain under

project FPA2014-58293-C2-1-P and Xunta de Galicia (Consellería de Educación) within the Strategic Unit AGRUP2015/11.

References

[1] P. Kotko, *et al.*, "Improved TMD factorization for forward dijet production in dilute-dense hadronic collisions," *JHEP*, **09**(2015), 106, 1503.03421.

[2] S. Catani, M. Ciafaloni, and F. Hautmann, "High-energy factorization and small x heavy flavor production," *Nucl. Phys.*, **B366**(1991), 135.

[3] M. Deak, F. Hautmann, H. Jung, and K. Kutak, "Forward Jet Production at the Large Hadron Collider," *JHEP*, **09**(2009), 121, 0908.0538.

[4] Krzysztof Kutak and Sebastian Sapeta, "Gluon saturation in dijet production in p-Pb collisions at Large Hadron Collider," *Phys. Rev.*, **D86**(2012), 094043, 1205.5035.

[5] Francois Gelis, Edmond Iancu, Jamal Jalilian-Marian, and Raju Venugopalan, "The Color Glass Condensate," *Ann. Rev. Nucl. Part. Sci.*, **60**(2010), 463, 1002.0333.

[6] C. J. Bomhof, P. J. Mulders, and F. Pijlman, "The Construction of gauge-links in arbitrary hard processes," *Eur. Phys. J.*, **C47**(2006), 147, hep-ph/0601171.

[7] Fabio Dominguez, Cyrille Marquet, Bo-Wen Xiao, and Feng Yuan, "Universality of Unintegrated Gluon Distributions at small x," *Phys. Rev.*, **D83**(2011), 105005, 1101.0715.

[8] Krzysztof J. Golec-Biernat and M. Wusthoff, "Saturation effects in deep inelastic scattering at low Q**2 and its implications on diffraction," *Phys. Rev.*, **D59**(1998), 014017, hep-ph/9807513.

[9] Larry D. McLerran and Raju Venugopalan, "Computing quark and gluon distribution functions for very large nuclei," *Phys. Rev.*, **D49**(1994), 2233, hep-ph/9309289.

Inclusive three jet production at the LHC as a new BFKL probe

F. Caporale[1], G. Chachamis[1], B. Murdaca[2], and A. Sabio Vera[1]

[1]Instituto de Física Teórica UAM/CSIC, Nicolás Cabrera 15 & Universidad Autónoma de Madrid, E-28049 Madrid, Spain.
[2]Istituto Nazionale di Fisica Nucleare, Gruppo Collegato di Cosenza, I-87036 Arcavacata di Rende, Cosenza, Italy

1 Introduction

The Balitsky-Fadin-Kuraev-Lipatov (BFKL) formalism [1–3] is one of the most important resummation programmes in high energy QCD. A typical BFKL observable at the LHC is the azimuthal angle (ϕ) decorrelation of two tagged forward/backward jets widely separated in rapidity, Y, in the so-called Mueller-Navelet jets setup [4]. This multiple emission appears as a fast decrease of $\langle \cos(n\,\phi)\rangle$ as a function of Y [5–8]. However, these differential distributions suffer from a large influence of collinear regions in phase space, so it was proposed to remove the $n=0$ dependence by studying the ratios $\mathcal{C}_{m,n} = \langle \cos(m\,\phi)\rangle / \langle \cos(n\,\phi)\rangle$ [9–11]. In recent studies [12,13], a BFKL analysis at NLL is able to fit the large Y tail of the Mueller-Navelet $\mathcal{C}_{m,n}$ ratios.

In Ref. [14], we proposed new observables related to final states with two tagged forward jets separated by a large rapidity span, along with a third tagged jet produced in the central region of rapidity, allowing for inclusive radiation in the remaining areas of the detectors.

The two tagged forward jets A and B have transverse momentum $\vec{k}_{A,B}$, azimuthal angle $\theta_{A,B}$ and rapidity $Y_{A,B}$. The central jet is characterized by $\vec{k}_J$, θ_J and y_J and the differential cross section on these variables can be written in the form

$$\frac{d^3\sigma^{3-\text{jet}}}{d^2\vec{k}_J dy_J} = \frac{\bar{\alpha}_s}{\pi k_J^2}\int d^2\vec{p}_A \int d^2\vec{p}_B\,\delta^{(2)}\left(\vec{p}_A+\vec{k}_J-\vec{p}_B\right)\varphi\left(\vec{k}_A,\vec{p}_A,Y_A-y_J\right)\varphi\left(\vec{p}_B,\vec{k}_B,y_J-Y_B\right) \quad (1)$$

where we assume that $Y_A > y_J > Y_B$ and k_J lies above the experimental resolution scale. φ are BFKL gluon Green functions normalized to $\varphi(\vec{p},\vec{q},0) = \delta^{(2)}(\vec{p}-\vec{q})$ and $\bar{\alpha}_s = \alpha_s N_c/\pi$. Now, new distributions can be defined using the projections on the two relative azimuthal angles formed by

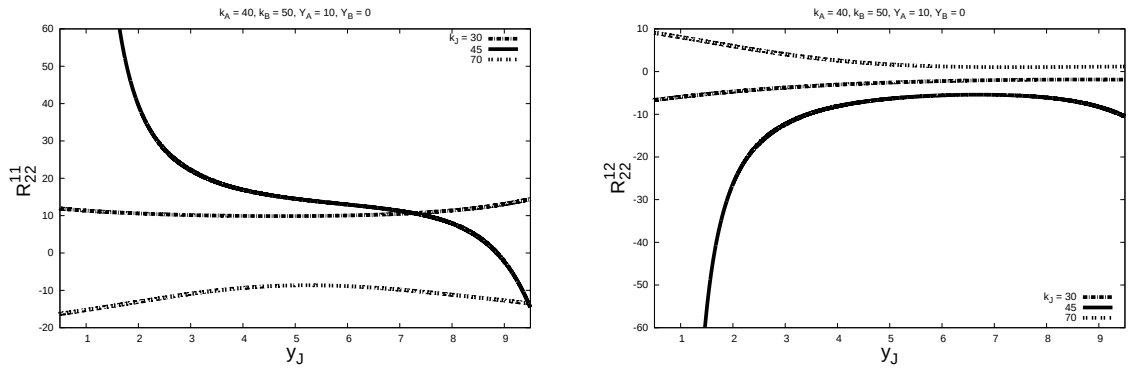

Figure 1: The ratios $\mathcal{R}^{1,1}_{2,2}$ and $\mathcal{R}^{1,2}_{2,2}$ as a function of the rapidity of the central jet y_J.

each of the forward jets with the central jet, $\theta_A - \theta_J - \pi$ and $\theta_J - \theta_B - \pi$:

$$\int_0^{2\pi} d\theta_A \int_0^{2\pi} d\theta_B \int_0^{2\pi} d\theta_J \cos\left(M\left(\theta_A - \theta_J - \pi\right)\right) \cos\left(N\left(\theta_J - \theta_B - \pi\right)\right) \frac{d^3\sigma^{3-\text{jet}}}{d^2\vec{k}_J dy_J}$$
$$= \bar{\alpha}_s \sum_{L=0}^{N} \binom{N}{L} \left(k_J^2\right)^{(L-1/2)} \int_0^{\infty} dp^2 \ \left(p^2\right)^{(N-L/2)} \int_0^{2\pi} d\theta \frac{(-1)^{M+N} \cos\left(M\theta\right) \cos\left((N-L)\theta\right)}{\sqrt{\left(p^2 + k_J^2 + 2\sqrt{p^2 k_J^2}\cos\theta\right)^N}}$$
$$\times \ \phi_M\left(p_A^2, p^2, Y_A - y_J\right) \phi_N\left(p^2 + k_J^2 + 2\sqrt{p^2 k_J^2}\cos\theta, p_B^2, y_J - Y_B\right), \tag{2}$$

with ϕ_n defined in Ref. [14]. The experimentally relevant observable is the mean value in the selected events of the two cosines, *i.e.*

$$\left\langle \cos\left(M\left(\theta_A - \theta_J - \pi\right)\right) \cos\left(N\left(\theta_J - \theta_B - \pi\right)\right)\right\rangle \tag{3}$$
$$= \frac{\int_0^{2\pi} d\theta_A d\theta_B d\theta_J \cos\left(M\left(\theta_A - \theta_J - \pi\right)\right) \cos\left(N\left(\theta_J - \theta_B - \pi\right)\right) \frac{d^3\sigma^{3-\text{jet}}}{d^2\vec{k}_J dy_J}}{\int_0^{2\pi} d\theta_A d\theta_B d\theta_J \frac{d^3\sigma^{3-\text{jet}}}{d^2\vec{k}_J dy_J}}.$$

In order to have optimal perturbative convergence and eliminate collinear contamination, we can remove the contributions from zero conformal spin by defining the ratios:

$$\mathcal{R}^{M,N}_{P,Q} = \frac{\left\langle \cos\left(M\left(\theta_A - \theta_J - \pi\right)\right) \cos\left(N\left(\theta_J - \theta_B - \pi\right)\right)\right\rangle}{\left\langle \cos\left(P\left(\theta_A - \theta_J - \pi\right)\right) \cos\left(Q\left(\theta_J - \theta_B - \pi\right)\right)\right\rangle}, \ \text{with} \ M,\, N,\, P,\, Q = 1,\, 2. \tag{4}$$

2 Results and Outlook

Now, different momenta configurations can be investigated. Here, in Fig. 1, two ratios $\mathcal{R}^{M,N}_{P,Q}$ with $M, N = 1, 2$ are shown while the momenta of the forward jets are fixed to $k_A = 40$ GeV and

$k_B = 50$ GeV and their rapidities also fixed to $Y_A = 10$ and $Y_B = 0$. The central jet transverse momentum takes three values, $k_J = 30, 45, 70$ GeV and the rapidity of the central jet y_J is varied in between the forward/backward jet rapidities.

It will be very interesting to see the predictions from fixed order analyses as well as from the BFKL inspired Monte Carlo `BFKLex` [15–21] for these and other similar observables [22] where the projection on azimuthal angles is used. This type of observables will be crucial to define the region of phenomenological applicability of the BFKL resummation.

Acknowledgements

G.C. acknowledges support from the MICINN, Spain, under contract FPA2013-44773-P. A.S.V. acknowledges support from Spanish Government (MICINN (FPA2010-17747,FPA2012-32828)) and, together with F.C and B.M., to the Spanish MINECO Centro de Excelencia Severo Ochoa Programme (SEV-2012-0249). The work of B.M. was supported in part by the grant RFBR-13-02-90907 and by the European Commission, European Social Fund and Calabria Region, that disclaim any liability for the use that can be done of the information provided here.

References

[1] E. A. Kuraev, L. N. Lipatov, and Victor S. Fadin, "Multi - Reggeon Processes in the Yang-Mills Theory," *Sov. Phys. JETP*, **44**(1976), 443, [Zh. Eksp. Teor. Fiz.71,840(1976)].

[2] E. A. Kuraev, L. N. Lipatov, and Victor S. Fadin, "The Pomeranchuk Singularity in Nonabelian Gauge Theories," *Sov. Phys. JETP*, **45**(1977), 199, [Zh. Eksp. Teor. Fiz.72,377(1977)].

[3] I. I. Balitsky and L. N. Lipatov, "The Pomeranchuk Singularity in Quantum Chromodynamics," *Sov. J. Nucl. Phys.*, **28**(1978), 822, [Yad. Fiz.28,1597(1978)].

[4] Alfred H. Mueller and H. Navelet, "An Inclusive Minijet Cross-Section and the Bare Pomeron in QCD," *Nucl. Phys.*, **B282**(1987), 727.

[5] Vittorio Del Duca and Carl R. Schmidt, "Dijet production at large rapidity intervals," *Phys. Rev.*, **D49**(1994), 4510, `hep-ph/9311290`.

[6] W. James Stirling, "Production of jet pairs at large relative rapidity in hadron hadron collisions as a probe of the perturbative pomeron," *Nucl. Phys.*, **B423**(1994), 56, `hep-ph/9401266`.

[7] Lynne H. Orr and W. James Stirling, "Dijet production at hadron hadron colliders in the BFKL approach," *Phys. Rev.*, **D56**(1997), 5875, `hep-ph/9706529`.

[8] J. Kwiecinski, Alan D. Martin, L. Motyka, and J. Outhwaite, "Azimuthal decorrelation of forward and backward jets at the Tevatron," *Phys. Lett.*, **B514**(2001), 355, `hep-ph/0105039`.

[9] Agustin Sabio Vera, "The Effect of NLO conformal spins in azimuthal angle decorrelation of jet pairs," *Nucl. Phys.*, **B746**(2006), 1, hep-ph/0602250.

[10] Agustin Sabio Vera and Florian Schwennsen, "The Azimuthal decorrelation of jets widely separated in rapidity as a test of the BFKL kernel," *Nucl. Phys.*, **B776**(2007), 170, hep-ph/0702158.

[11] M. Angioni, G. Chachamis, J. D. Madrigal, and A. Sabio Vera, "Dijet Production at Large Rapidity Separation in N=4 SYM," *Phys. Rev. Lett.*, **107**(2011), 191601, 1106.6172.

[12] B. Ducloue, L. Szymanowski, and S. Wallon, "Evidence for high-energy resummation effects in Mueller-Navelet jets at the LHC," *Phys. Rev. Lett.*, **112**(2014), 082003, 1309.3229.

[13] Francesco Caporale, Dmitry Yu. Ivanov, Beatrice Murdaca, and Alessandro Papa, "Mueller-Navelet jets in next-to-leading order BFKL: theory versus experiment," *Eur. Phys. J.*, **C74**(2014) (10), 3084, [Erratum: Eur. Phys. J.C75,no.11,535(2015)], 1407.8431.

[14] F. Caporale, G. Chachamis, B. Murdaca, and A. Sabio Vera, "BFKL predictions for inclusive three jet production at the LHC," *Phys. Rev. Lett.*, **116**(2016) (1), 012001, 1508.07711.

[15] G. Chachamis, M. Deak, A. Sabio Vera, and P. Stephens, "A Comparative study of small x Monte Carlos with and without QCD coherence effects," *Nucl. Phys.*, **B849**(2011), 28, 1102.1890.

[16] G. Chachamis and A. Sabio Vera, "The Colour Octet Representation of the Non-Forward BFKL Green Function," *Phys. Lett.*, **B709**(2012), 301, 1112.4162.

[17] G. Chachamis and A. Sabio Vera, "The NLO N =4 SUSY BFKL Green function in the adjoint representation," *Phys. Lett.*, **B717**(2012), 458, 1206.3140.

[18] G. Chachamis, A. Sabio Vera, and C. Salas, "Bootstrap and momentum transfer dependence in small x evolution equations," *Phys. Rev.*, **D87**(2013) (1), 016007, 1211.6332.

[19] F. Caporale, G. Chachamis, J. D. Madrigal, B. Murdaca, and A Sabio Vera, "A study of the diffusion pattern in N = 4 SYM at high energies," *Phys. Lett.*, **B724**(2013), 127, 1305.1474.

[20] G. Chachamis and A. Sabio Vera, "A Monte Carlo study of double logarithms in the small x region," (2015), 1511.03548.

[21] G. Chachamis and A. Sabio Vera, "The high-energy radiation pattern from BFKLex with double-log collinear contributions," (2015), 1512.03603.

[22] F. Caporale, Francesco Giovanni Celiberto, G. Chachamis, and A. Sabio Vera, "Multi-Regge kinematics and azimuthal angle observables for inclusive four-jet production," (2015), 1512.03364.

Relating hadronic total cross sections to low-x nuclear structure functions

László Jenkovszky[1]

[1]Bogolyubov Institute for Theoretical Physics, National Academy of Sciences of Ukraine, Kiev, 03680 Ukraine

In the additive quark model, the hadron-hadron total cross section can be written as a product of the cross sections of the constituents, σ_{qq} [1,2], *e.g.*

$$\sigma(s)^t_{pp} = \sigma_{qq}[n_V + n_S(s)]^2, \tag{1}$$

where n_V is the number of valence quarks and $n_S(s)$ is that of sea quarks, their number increasing with energy.

It was suggested in Refs. [1, 2] that the increasing number of sea quarks is related to the Bjorken scaling-violating contribution to the deep inelastic lepton-hadron structure function (DIS SF), namely to the momentum fraction of the relevant quarks given by the integral over the DIS structure function $F_2(x, Q^2)$. In Ref. [1] a simple model for the DIS structure function, known at those times, was used, resulting in the following expression for the total cross section, compatible with the data

$$\sigma(s)^t_{pp} = \sigma_{qq} n_V^2 (1 + 0.0.16 \ln(s/Q_0^2), \tag{2}$$

where σ_{qq} is a free parameter, Q_0^2 was fitted to the DIS data, and $n_V = 3$.

In Ref. [2] the DIS SF was related to hadronic cross sections by means of finite-energy sum rules in Q^2.

In Ref. [3] following ansatz for the small-x singlet part (labelled by the upper index $S, 0$) of the proton structure function, interpolating between the soft (VMD, Pomeron) and hard (GLAP evolution) regimes was proposed:

$$F_2^{(S,0)}(x, Q^2) = A \left(\frac{Q^2}{Q^2 + a} \right)^{1+\tilde{\Delta}(Q^2)} e^{\Delta(x,Q^2)}, \tag{3.1}$$

with the "effective power"

$$\widetilde{\Delta}(Q^2) = \epsilon + \gamma_1 \ell n \left(1 + \gamma_2 \ell n \left[1 + \frac{Q^2}{Q_0^2} \right] \right), \tag{3.2}$$

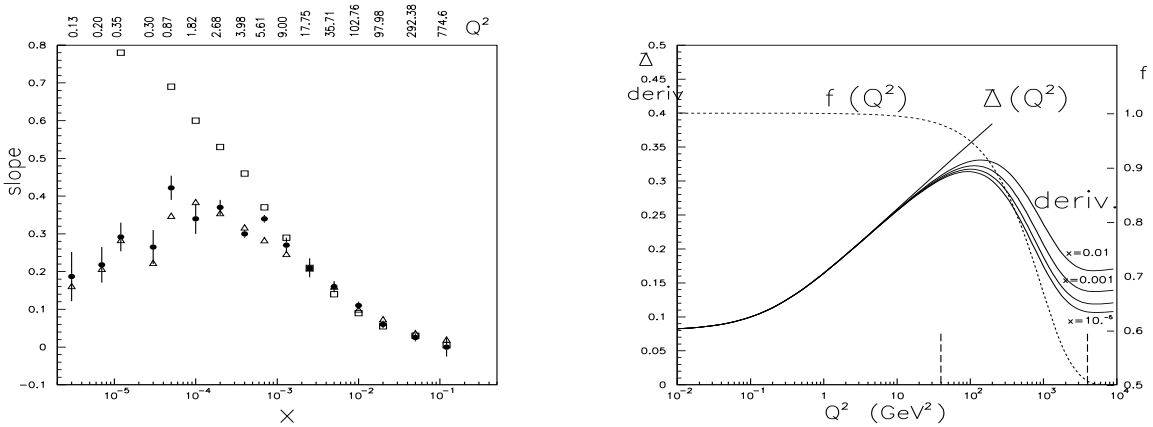

Figure 1: Slope of the structure function $F_2(x, Q^2)$.

and

$$\Delta(x, Q^2) = \left(\widetilde{\Delta}(Q^2)\ell n\frac{x_0}{x}\right)^{f(Q^2)}, \tag{3.3}$$

where

$$f(Q^2) = \frac{1}{2}\left(1 + e^{-Q^2/Q_1^2}\right). \tag{3.4}$$

At small and moderate values of Q^2, the exponent $\widetilde{\Delta}(Q^2)$ (3.2) may be interpreted as a Q^2-dependent "effective Pomeron intercept", as shown in Fig. 1.

The function $f(Q^2)$ has been introduced in order to provide for the transition from the Regge behaviour, where $f(Q^2) = 1$, to the asymptotic solution of the GLAP evolution equation, where $f(Q^2) = 1/2$.

In Ref. [3] the above singlet SF was appended by a non-singlet part, important at large values of x. The parameters were fitted to the DIS data in a wide range of x and Q^2. The values of the fitted parameters are: $A = 0.1623,\ \ a = 0.2916$ GeV^2, $\ \gamma_2 = 0.01936,\ \ Q_0^2 = 0.1887$ GeV^2, $\ Q_1^2 = 916.1$ GeV^2; $\ x_0 = 1,\ \ \epsilon = 0.08,\ \ \gamma_1 + 2.4$ were fixed (by QCD-related arguments). The resulting fits and more details can be found in Ref. [3].

The proton-proton total cross section is cast by integrating Eqs. (3) between $x = 0$ and $x = 1$. At high energies, only the singlet part of the SF, Eqs. (3) (the "Pomeron") is relevant. Integration can be performed numerically. The result is in reasonable agreement with the data on pp total cross sections, including those from the LHC.

Acknowledgement

Warm hospitality and support during the Conference is gratefully acknowledged.

References

[1] L.L. Jenkovszky and B.V. Struminsky: *Violation of scale invariance in deep-inelastic lepton-hadron scattering and rise of hadronic cross-sections*, ITP-77-37E Preprint, Kiev, 1977.

[2] L.L. Jenkovszky and B.V. Struminsky: Yadernaya Fizika (English translation: Sov. J. Nucl. Phys.), **38**(1983), 1568.

[3] P. Desgrolard, Laszlo L. Jenkovszky, F. Paccanoni, *Interpolating between soft and hard dynamics in deep inelastic scattering*. LYCEN-9808, Eur. Phys. J. C7 (1999) 263-270; hep-ph/9803286.

Results of the LHCf experiment so far and future prospects

K.Kasahara on behalf of the LHCf collaboration

RISE, Waseda University, Japan

1 Introduction

The LHCf is one of the LHC experiments; it is a small experiment both in the detector size and the number of participants, and its purpose is quite different from the others.

Existence of ultra high energy (UHE) cosmic-rays ($10^{15} \sim 10^{20}$ eV), especially those at the highest energies, poses a fundamental (astro-)physical questions: where their birth place is, how they are accelerated and propagated to the Earth. To get (clues to) the answer, we need to know the energy, species, arrival direction etc of the cosmic rays.

Direct detection of UHE cosmic-rays is impossible and they are observed via air showers they produce. To get a reliable guess of the primary cosmic-ray energy etc, we need good hadronic interaction models which are used in Monte Carlo (MC) simulation of air shower development; observed characteristics of air showers are always compared with corresponding MC to derive the incident energy etc.

However, the energy scale of the playground is so high and, before LHC, we had almost no means to measure the relevancy of the models. Now, the LHC energy reaches $\sqrt{s} = 13$ TeV of which equivalent laboratory energy is almost 10^{17} eV.

Our purpose is to afford stuff for selecting good models or for tuning the models by measuring, at LHC, high energy neutral particles emitted in the very forward region which is important for air shower development (but measurement is usually not easy)[1].

2 LHCf Detectors

Two detectors (called Arm1 and Arm2) are placed at the both sides of the beam Interaction Point (IP) of ATLAS. For further details, see [1].

3 Results

We compare our experimental results with several interaction models used in the cosmic-ray field (Sibyll 2.1 [2], QGSJET II-03/04 [3], EPOS 1.99/EPOS-LHC3700 [4], DPMJET3.04 [5]), and PYTHIA8.145/8.815 [6] used in high energy physics.

3.1 π^0 spectrum

Figure 1 shows P_z spectrum of π^0 at $\sqrt{s} = 7$ TeV pp collisions in 3 different important P_T regions. We see that

[1] In terms of Feynman X_F, we may say $0.05 < X_F < 0.5$ region is important though LHCf sensitivity becomes less and less for smaller X_F and smaller $\sqrt{s}$ due to geometrical constraint.

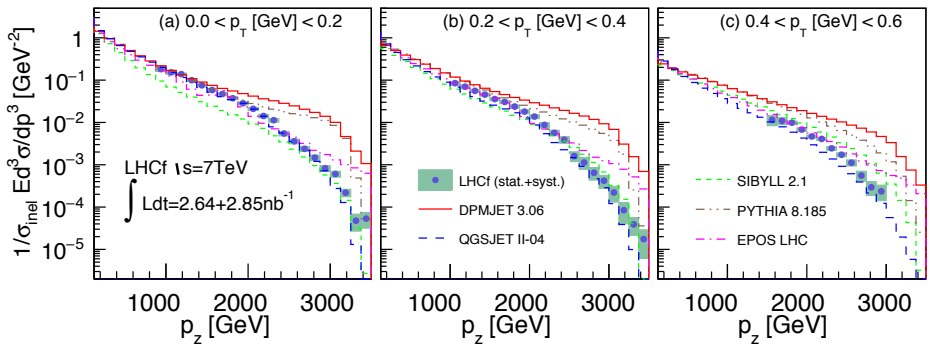

Figure 1: P_z spectrum of π^0 at 7 TeV.

- DPMJET3 and PYTHIA show similar tendency, i.e, in the high P_z region, the spectrum is too hard as compared with the data.
- QGSJET and EPOS show more or less consistent results with the data.
- SIBYLL is very good in $0.2 < P_T < 0.4$ GeV/c, but in other P_T regions (also in $P_T > 0.6$ GeV/c not shown here), deviation from the data is obvious. This is due to that P_T distribution is too hard in SIBYLL.
- The photon energy spectrum (not shown here) shows naturally quite similar tendency.
- We have π^0 data for pPb at 5.02 TeV. In this case, it is found that the UPC (ultra-peripheral collision) effect is strong. After correcting the UPC effect, we see model vs data tendecy is similar to the 7 TeV pp case but due to the nucleus effect, hardness of DPMJET3 spectrum is decreased.

3.2 Neutron energy spectrum

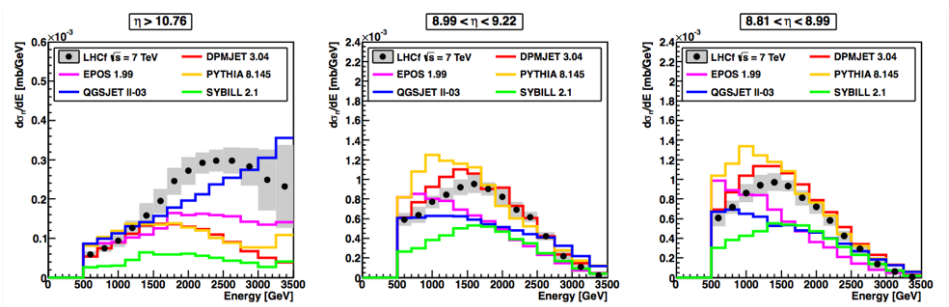

Figure 2: Unfolded neutron energy spectrum at 7 TeV.

Neutral hadrons (mostly neutrons) are also observed but the energy resolution of our detector to hadrons is $\sim$ 40 % so we applied a multidimensional-spectra unfolding method [7] to get Fig.2. It is interesting to note that in the very forward region (pseudo rapidity $\eta > 10.76$), only QGSJET gives a comparable yield to the data, while at larger angles ($\eta < 9.22$), DPMJET3 is quite good. This feature will give an important hint for tuning interaction models. However, it would be premature to discuss how this feature affects the air shower development, since the leading proton (which we cannot measure) + leading neutron is important for the air shower development.

4 Future Prospects

4.1 Common trigger with ATLAS

In 5.02 TeV pPb run, we did a trial common trigger with ATLAS. One example of its effectiveness is shown in Fig.3; the angular distribution of very forward neutron is dominated by the UPC effect [8]. This type of events would not trigger the ATLAS central detector. Indeed, if we require that ATLAS observes at least one charged particle, most of very forward neutrons are dramatically eliminated.

This indicates that if we use signals from ATLAS in 13 TeV pp runs (for this, we did the common trigger), we will be able to extract single and/or double diffraction events and analyze such events. In fact, a MC study with PYTHIA shows that, we can select 35∼40% of the diffraction events with ~ 1 % contamination of non-diffractive ones. These indicate possibility of testing a theory that small mass diffraction has a key to UHE air showers [9].

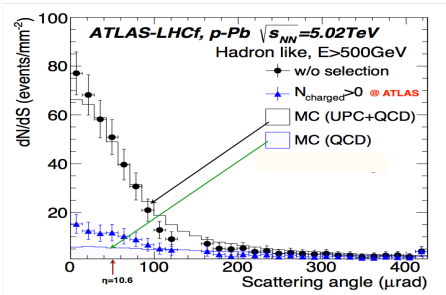

Figure 3: Angular distribution of neutrons. Black dots: data. Blue: data with $N_{ch} \geq 1$ in ATLAS. Histograms are MC simulations for QCD+UPC and QCD only.

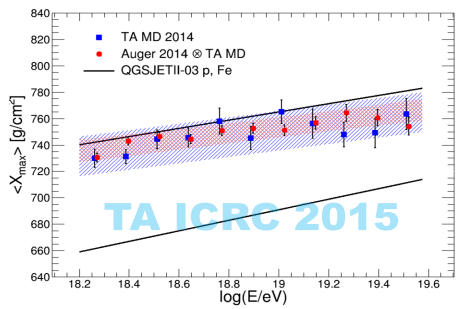

Figure 4: $< X_{\max} >$ as a function of primary energy: Folded TA and Auger data (see text).

4.2 Scaling Feature

The π^0 energy spectra at 2.76 TeV and 7 TeV are compared in terms of the Feynman X_F variables. At $X_F > 0.6$ ($P_T < 0.4$ GeV/c), the data shows scaling feature within $15 \sim 20$ %. To see the scaling feature (or its break) in a wider incident energy and X_F region, an experiment at RHIC of BNL (where a larger phase space can be covered for $\sqrt{s}$ =0.51 TeV with the current LHCf detectors) is planned [10]. Together with LHC 13 TeV data, we will be able to get more reliable expectation for $> 10^{17}$ eV.

5 Summary and Remarks

• Models having been used in the cosmic-ray field are not perfect but not off the wall.
• QGSJET II and EPOS (especially LHC tunned ones) are fairly good.
• Figure 4 shows the average maximum development depth of UHE air showers as a function of primary energy [11]. The observational data is compiled by a working group formed by the TA and Auger group. The data is compared with prediction by the proton and Fe incident case using QGSJET II-03. The TA group says the composition is light, but almost pure proton case cannot be excluded with this statistics and errors.

If we add other predictions (relative to QGSJET II-03) for the proton primary at 10^{19} eV, EPOS 1.99 would sit at $+27$, EPOS-LHC $+24$ and QGSJET II-04 $+5$ g/cm^2, respectively. Then, if the EPOS prediction is good, it would be rather difficult to conceive dominance of very light composition such as p and He. Recently, the TA group announced a possible discovery of a hot spot [12] (localized origin of UHECR's)

which favors proton dominance in a simple scenario. In view of this, we may say that further refined model test is needed, suggesting importance of 13 TeV data as well as those from other detectors such as Castor [13] observing charged particles at larger angles ($-6.6 < \eta < -5.2$) than LHCf.
• Uncertainty of pion interaction is one problem at UHE. We may use one pion exchange process in analogy to γ+ p $\rightarrow$ n + X; i.e, p+p$\rightarrow$ n + X where p goes n + π^+ and π^+ interacts with p to produce X. LHCf Arm1 may detect a leading n and ATLAS and LHCf Arm2 detect π^+p interaction. This may give a clue to the pion interaction at very high energies [14]

Acknowledgment

Thanks are due to the CERN staff for successful operation of LHCf. We are supported by Grant-in-Aids for Scientific Research by MEXT of Japan (26247037, 23740183, 23244050, 23340076), and by INFN in Italy.

References

[1] O.Adriani et al, *J. Mod. Phys.*, **A28**(2013).

[2] E.-J.Ahn R.Engel T.K.Gaisser P.Lipari and T.Stanev, *Phys. Rev.*, **D 80**(2009).

[3] S.Ostapchenko, *Nucl. Phys. B, Proc. Suppl.*, **151**(2006), 143.

[4] K.Werner F.-M. Liu and T.Perog, *Phys. Rev. C*, **74**(2006).

[5] F.W.Bopp J.Ranft R.Engel and S.Roesler, *Phys. Rev. C*, **77**(2008).

[6] T.Sjöstand S.Mrenna and P.Skands, *Comput. Phys. Comm.*, **178**(2008), 852.

[7] Agostini, *Nucl.Instrum.Meth.*, **A362**(1995), 487.

[8] *ATLS-PHYS-PUB-2015-038*, (2015).

[9] S.Ostapchenko, *Talk at HESZ2015; http://indico.cern.ch/event/407524/contribution/12/attachments/1153402/1656761/ostapchenko-hszd2.pdf*.

[10] T.Sako, *Talk at HESZ2015; http://indico.cern.ch/event/407524/contribution/32/attachments/1144651/1656758/HESZ-RHICf-sako.pdf*.

[11] C.Jui, *Talk at ICRC 2015; https://indico.cern.ch/event/344485/session/86/contribution/1375*.

[12] R.U.Abbasi et al; TA collaboration, *Astrophys, J. Lett.*, **790:L21**(2014).

[13] C.Baus, *http://lhcfs1.stelab.nagoya-u.ac.jp/PukiWiki/?plugin=attach&refer=Seminar&openfile=CBaus20140129_CASTOR.pdf*.

[14] R.Engle and T.Pierog, *Private communication.*, (2015).

Double scattering contribution to small-x processes: Mueller-Navelet jets at the LHC

B. Ducloué[1,2], L. Szymanowski[3], and S. Wallon[4,5]

[1]Department of Physics, University of Jyväskylä, P.O. Box 35, 40014 University of Jyväskylä, Finland
[2]Helsinki Institute of Physics, P.O. Box 64, 00014 University of Helsinki, Finland
[3]National Centre for Nuclear Research (NCBJ), Warsaw, Poland
[4]Laboratoire de Physique Théorique, UMR 8627, CNRS, Univ. Paris Sud, Université Paris-Saclay, 91405 Orsay, France
[5]UPMC Univ. Paris 06, Faculté de Physique, 4 place Jussieu, 75252 Paris Cedex 05, France

The study of the production of two jets separated by a large interval of rapidity at hadron colliders was proposed by Mueller and Navelet [1] to test QCD in the high energy limit, described by the Balitsky-Fadin-Kuraev-Lipatov (BFKL) approach [2–5]. The standard mechanism for this process is based on single parton scattering (SPS) illustrated in the left panel of Fig. 1 and involves usual parton distribution functions (PDF) of incident partons inside the scattered protons. The classical observable in this process is the azimuthal correlation of the produced jets: in the approach based on collinear factorization of QCD at leading order the two jets would be emitted back-to-back whereas in the BFKL case, with multiple emissions between the two jets described by the BFKL Green's function G, one should expect a stronger decorrelation in the azimuthal angle between the two jets. The azimuthal correlations of Mueller- Navelet jets were measured for the first time at the LHC by the CMS collaboration. In our recent studies we have shown in [6] that the measured data on decorrelation coefficients can be well described by a complete next-to-leading logarithmic (NLL) BFKL calculation [7,8] supplemented by the use of the Brodsky-Lepage-Mackenzie procedure adapted to BFKL dynamics to fix the renormalization scale (for details we refer the reader to [6]). These results are not severely affected by energy-momentum non-conservation [9].
However, at high energies and low transverse momenta probed at the LHC, parton densities can become large enough that contributions where two partons from the same incoming hadron take part in the interaction could become important. In the case of Mueller-Navelet jets production such a mechanism is illustrated in the middle panel of Fig. 1. Thus it is natural to ask about the potential impact of such double parton scattering (DPS) contributions on the good agreement of our earlier results based on single parton scattering (SPS) with experimental data. This was the subject of our recent study [10].

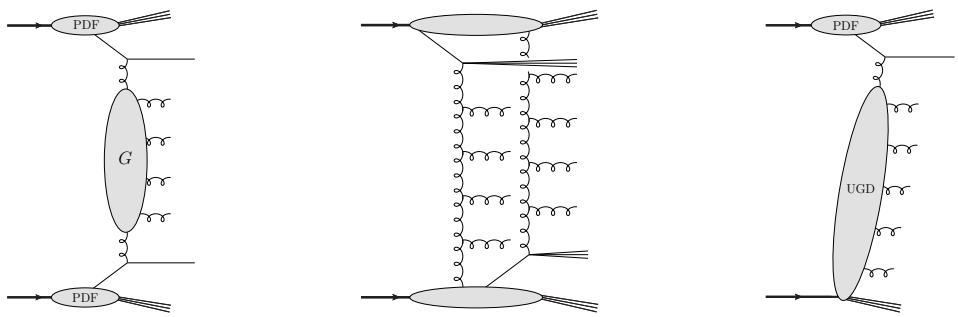

Figure 1: Left: The SPS contribution to Mueller-Navelet jets production at LL accuracy; Middle: The DPS contribution; Right: Inclusive forward jet production.

The main assumption of the analysis in [10] concerns the independence of the production of each jet. This is the basis of the so-called "pocket formula" for the cross section in the DPS mechanism

$$\sigma_{\rm DPS} = \frac{\sigma_{\rm fwd}\sigma_{\rm bwd}}{\sigma_{\rm eff}}\,, \tag{1}$$

where $\sigma_{\rm fwd(bwd)}$ is the inclusive cross section for one jet in the forward (backward) direction as shown in the right panel of Fig. 1 and $\sigma_{\rm eff}$ is a phenomenological quantity related to the density of the proton in the transverse plane. According to measurements at the Tevatron and the LHC, $\sigma_{\rm eff}$ should be of the order of 15 mb but there is some discrepancy between these measurements. To account for this uncertainty we vary $\sigma_{\rm eff}$ between 10 and 20 mb in our calculation.
A more refined approach to compute the DPS contribution shown in the middle panel of Fig. 1 would require to introduce some kind of "hybrid" double parton distribution, related to the probability for a proton to emit both a collinear parton and a gluon with some transverse momentum. Since almost nothing is known about such distributions we are forced to use the simplistic factorized model (1).
The cross section for one forward jet production, $\sigma_{\rm fwd}$, shown in the right panel of Fig. 1 requires the knowledge of the unintegrated gluon density (UGD). Contrary to usual collinear parton distributions (PDF), the unintegrated gluon distributions are not very well known. To estimate the uncertainty of our calculation due to this fact, we will use several sets found in the literature to see the impact of this choice on our final results. For each set we fix the normalization by a comparison with CMS data on inclusive forward jet production (for more details see [10]).
Our analysis about the importance of DPS in Mueller-Navelet jets production is performed for four choices of kinematical cuts on $\sqrt{s}$ and the transverse momenta of the jets relevant for present and forthcoming experiments at the LHC:

- $\sqrt{s} = 7$ TeV, $|\mathbf{k}_{J,1}| = |\mathbf{k}_{J,2}| = 35$ GeV,
- $\sqrt{s} = 14$ TeV, $|\mathbf{k}_{J,1}| = |\mathbf{k}_{J,2}| = 35$ GeV,
- $\sqrt{s} = 14$ TeV, $|\mathbf{k}_{J,1}| = |\mathbf{k}_{J,2}| = 20$ GeV,
- $\sqrt{s} = 14$ TeV, $|\mathbf{k}_{J,1}| = |\mathbf{k}_{J,2}| = 10$ GeV.

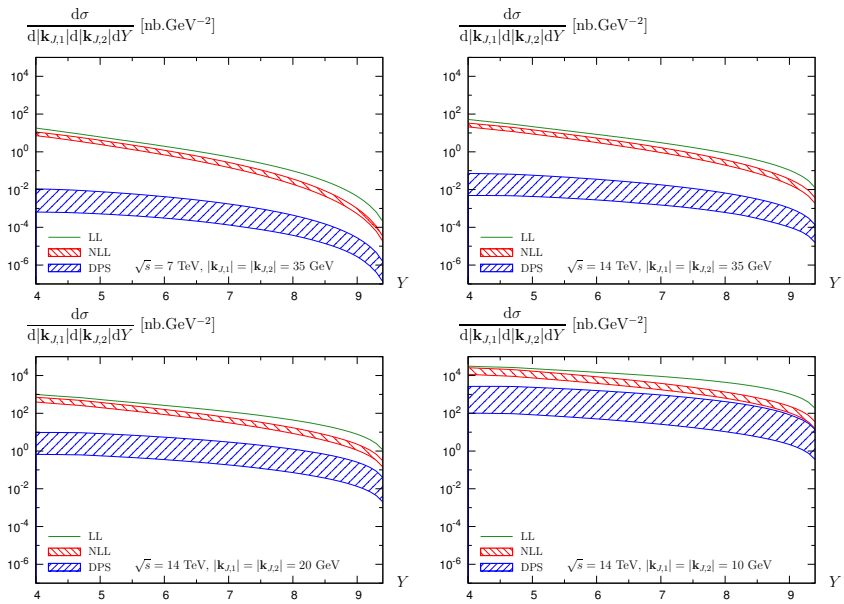

Figure 2: Comparison of the differential cross section obtained at LL (green) and NLL (red) accuracy in the BFKL approach and the DPS cross section (blue) for the four kinematical cuts described in the text.

The resulting predictions for the differential cross section and the decorrelation coefficient $\langle \cos \varphi \rangle$ are shown on Figs. 2 and 3 respectively. One can see that in most cases the DPS cross section is much smaller than the SPS one and thus the impact of this contribution on the azimuthal correlation is rather small. However, if one considers the set of parameters giving the largest DPS contribution, for low transverse momenta and large rapidity separations the effect of DPS can become larger than the uncertainty on the NLL BFKL calculation. Therefore in this region a more careful analysis or experimental data would be required to conclude.

Acknowledgements

This work is supported by French grant ANR PARTONS No. ANR-12-MONU-0008-01. B. D. is supported by the Academy of Finland, project 273464. L. S. was partially supported by grant of National Science Center, Poland, No. 2015/17/B/ST2/01838. This work was done using computing resources from CSC – IT Center for Science in Espoo, Finland.

References

[1] Alfred H. Mueller and H. Navelet, "An Inclusive Minijet Cross-Section and the Bare Pomeron in QCD," *Nucl. Phys.*, **B282**(1987), 727.

[2] Victor S. Fadin, E.A. Kuraev, and L.N. Lipatov, "On the Pomeranchuk Singularity in Asymptotically Free Theories," *Phys. Lett.*, **B60**(1975), 50.

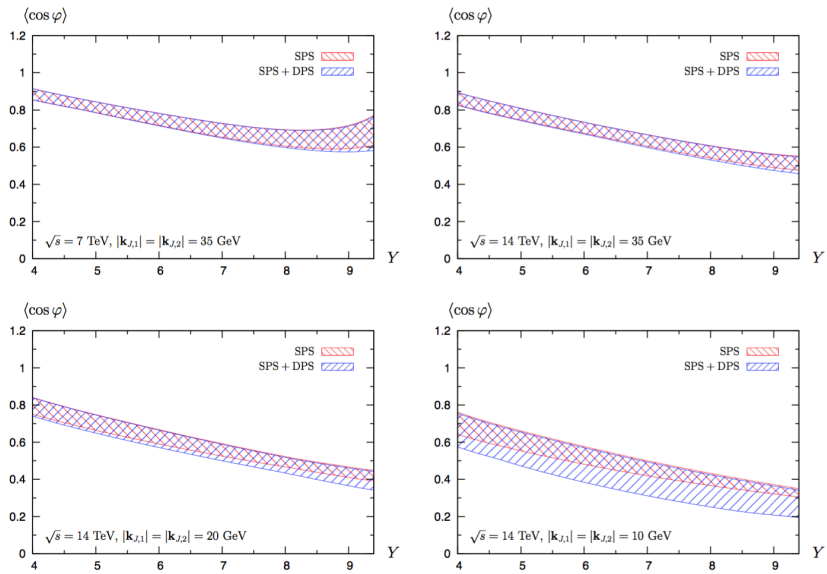

Figure 3: $\langle \cos \varphi \rangle$ as a function of Y without (red) and with (blue) the DPS contribution for the four kinematical cuts described in the text.

[3] E. A. Kuraev, L. N. Lipatov, and Victor S. Fadin, "Multi - Reggeon Processes in the Yang-Mills Theory," *Sov. Phys. JETP*, **44**(1976), 443.

[4] E.A. Kuraev, L.N. Lipatov, and Victor S. Fadin, "The Pomeranchuk Singularity in Nonabelian Gauge Theories," *Sov. Phys. JETP*, **45**(1977), 199.

[5] I.I. Balitsky and L.N. Lipatov, "The Pomeranchuk Singularity in Quantum Chromodynamics," *Sov. J. Nucl. Phys.*, **28**(1978), 822.

[6] B. Ducloué, L. Szymanowski, and S. Wallon, "Evidence for high-energy resummation effects in Mueller-Navelet jets at the LHC," *Phys. Rev. Lett.*, **112**(2014), 082003, 1309.3229.

[7] D. Colferai, F. Schwennsen, L. Szymanowski, and S. Wallon, "Mueller Navelet jets at LHC - complete NLL BFKL calculation," *JHEP*, **1012**(2010), 026, 1002.1365.

[8] B. Ducloué, L. Szymanowski, and S. Wallon, "Confronting Mueller-Navelet jets in NLL BFKL with LHC experiments at 7 TeV," *JHEP*, **1305**(2013), 096, 1302.7012.

[9] B. Ducloué, L. Szymanowski, and S. Wallon, "Violation of energy-momentum conservation in Mueller-Navelet jets production," *Phys. Lett.*, **B738**(2014), 311, 1407.6593.

[10] B. Ducloué, L. Szymanowski, and S. Wallon, "Evaluating the double parton scattering contribution to Mueller-Navelet jets production at the LHC," *Phys. Rev.*, **D92**(2015) (7), 076002, 1507.04735.

Multi-jet measurements at CMS

Grigory Safronov[1,*]

[1]Institute for Theoretical and Experimental Physics
[*]*On behalf of the CMS Collaboration*

1 Introduction

Hadronic jets carry information about partons produced in pp-interaction. Hard parton scattering is described within the perturbative QCD (pQCD) framework. Fixed order analytic predictions for jet production observables are available in the next-to-leading-order (NLO) or next-to-next-to-leading order (NNLO) pQCD. For observables sensitive to higher order parton radiation resummation of full perturbative series enhanced by large logarithms of energy scale ratios such as performed by DGLAP [1–4] or BFKL [5–7] frameworks is important. Measurements of hadronic jets production allows to test perturbative QCD calculation methods and gives direct access to basic QCD components like the parton density functions or the strong coupling constant.

In this review selected CMS analyses performing extraction of PDF or α_s as well as measurements sensitive to higher-order pQCD radiation are discussed.

2 Inclusive jet and 3-jet production cross-section measurements

The inclusive jet production cross-section is directly sensitive to the proton PDFs and α_s. CMS has measured the inclusive jet production cross-section for 7, 8 and 2.76 TeV pp-collisions energies [8–11]. Measurement performed differentially in p_T and η allows to extract PDF for the wide range of Q and x values. CMS has performed extraction of PDFs and α_s from 7 TeV inclusive jet cross-section in the work [12]. For the extraction of PDFs inclusive jet data was combined with HERA DIS data. Comparison with the HERA-only PDF shows shift in central value and clear improvement in the uncertainty of the PDFs (Fig. 12-17 of the reference [12]).

The cross section of 3-jet production is proportional to α_s^3 at the LO of pQCD. Therefore it should be particularly sensitive to α_s variations. The measurement of the inclusive double differential 3-jet production and extraction of the α_s was performed in the work [13]. The dataset corresponding to 5 fb^{-1} of 7 TeV proton-proton collisions was used. The cross-section was measured differentially in the mass of the 3-jet system, m_3. Measurement was performed for the range of 3-jet system masses of $445 < m_3 < 3270$ (GeV). Data is in agreement with NLO pQCD predictions within the experimental and theoretical uncertaintites. For the extraction of α_s the CT10 NLO PDF set was used which includes variations in α_s. The running $\alpha_s(Q)$ was determined for the set of m_3

ranges corresponding to range in Q: $0.4 < Q < 1.4$ (TeV). The obtained result summarised in Fig. 7 of the reference [13] is in agreement with previous mesurements and extends the Q range to 1.4 TeV. The value of $\alpha_s(M_Z)$ was determined from the combined fit of the data in the range $m_3 > 664$ GeV. The obtained value of $\alpha_s(M_Z) = 0.1171 \pm 0.0013(\text{exp}) \pm 0.0024(\text{PDF}) \pm 0.0008(\text{NP}) ^{+0.0069}_{-0.0040}(\text{scale})$ is in agreement with the world-average.

3 Dijet azimuthal decorrelation measurements

The leading order pQCD contribution to the dijet production is $2 \to 2$ process. Outgoing jets in $2 \to 2$ process are back-to-back in the xy plane and azimuthal angle between them is $\Delta\phi = \pi$. In real life an additional higher-order hard parton radiation leads to decrease of azimuthal angle between jets. Therefore measurement of azimuthal angle between jets is sensitive to hard parton radiation and may allow to test various models of parton showers or analytic pQCD resummation methods.

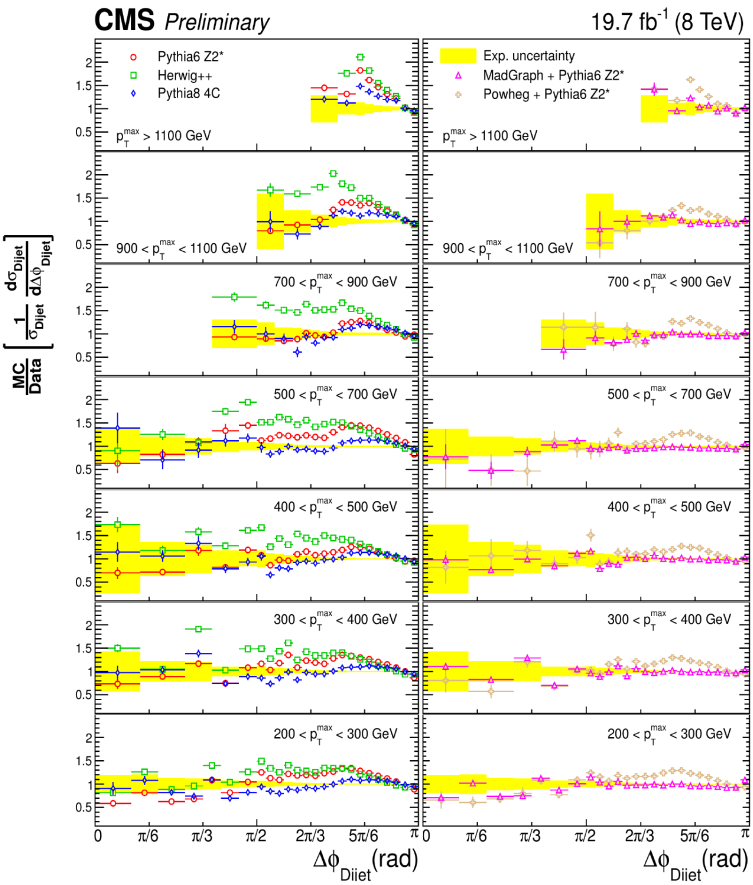

Figure 1: Normalised cross-section for dijet production differential in $\Delta\phi$ for the set of bins in p_T of the leading jet. Good description of the data is given by MADGRAPH+PYTHIAMC

CMS has measured azimuthal angle distributions between jets using the full dataset of 8 TeV pp-collisions of 19.7 fb^{-1} [14]. Events in which two leading jets have $y < 2.5$ and the leading jet have $p_T > 200$ GeV were selected. The normalised dijet cross-section differential in $\Delta\phi_{dijet}$ was measured. Results of the measurement were compared to predictions of analytic calculations in NLO pQCD, predictions from Monte-Carlo generators and fixed-order calculations matched to different parton shower simulations. Monte Carlo generators PYTHIA6 [15], PYTHIA8 [16] and HERWIG++ [17] use LO matrix elements complemented by parton shower simulations to account for higher-order radiaion. The MADGRAPH MC generator [18] uses LO matrix elements with up to 4 outgoing partons which can be matched to partons showers produced by PYTHIA or HERWIG++ programs. The POWHEG framework [19–21] provide the full NLO matrix elements which can also be matched to PYTHIAor HERWIG++ parton showers. Normalised cross-section for different bins in the p_T of the leading jet, $p_{T,\mathrm{MAX}}$, is presented at Fig. 1. Among the MC generators PYTHIA8 shows the smallest deviations from the measurement. The best description of the measurement is given by the MADGRAPH matched to PYTHIA6 for parton showering, hadronisation and multi-parton interactions.

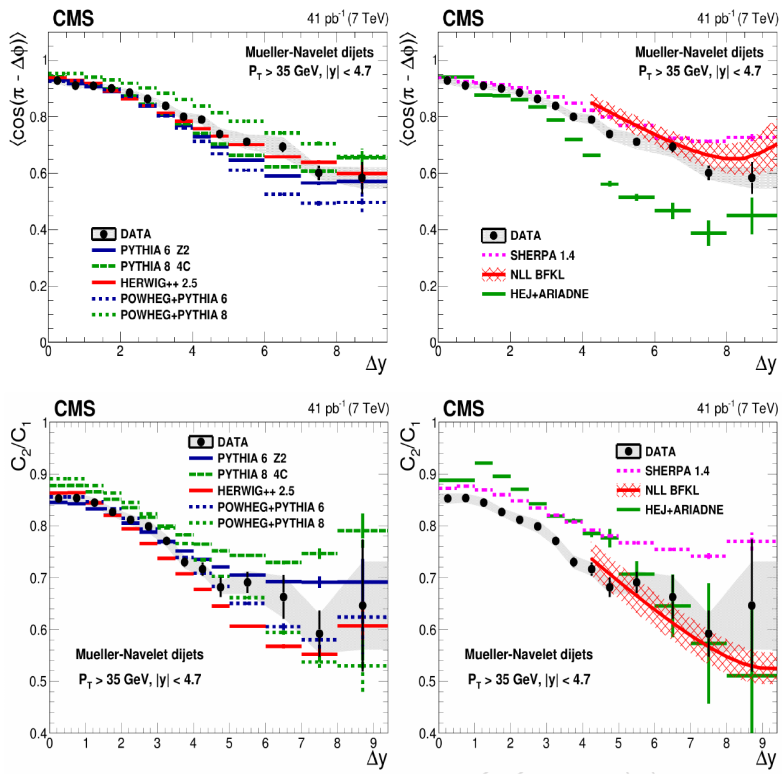

Figure 2: Average cosines (top) and cosine ratios (bottom) as a function of the rapidity separation between jets. Best desription of the data is given by the NLL BFKL calculation.

The production of jets with similarly low transverse momentum and large rapidity separation was proposed in the work [22] as a process probing dynamics beyond the description of DGLAP

approach. Indeed such final state has increased phase space for hard parton radiation ordered in rapidity and with random walk in p_T described in the BFKL framework. The important BFKL prediction is the strong growth of inclusive dijet cross-section with increasing rapidity interval between jets, $\sigma \sim e^{A\Delta y}, A > 1$. Therefore measurement of azimuthal decorrelation between low-p_T jets as a function of rapidity separation may reveal features not described by the DGLAP-based PS models or analytic calculations. In the work [23] CMS has measured azimuthal decorrelations of jets using the low-pileup 7 TeV dataset. Decorrelations were measured as normalised cross-sections differential in $\Delta\phi$ for three bins of pseudorapidity for $\Delta y < 9.4$ and average cosines of azimuthal angle between jets $C_i = cos(n * (\pi - \Delta\phi)$ as a function of Δy (Fig. 2, top). In addition ratios of average cosines C_2/C_1 (Fig. 2, bottom) and C_3/C_2 were measured as a function of Δy according to suggestion from [24] where it was derived that cosine ratios are particularly sensitive to contributions from BFKL dynamics. Results corrected for the detector effects were compared to the predictions of Monte-Carlo generators PYTHIA6, PYTHIA8, HERWIG++, POWHEG complemented by parton showers and non-perturbative effects simulated with PYTHIA8 or HERWIG++ and to other theory predictions described below. The SHERPA Monte Carlo [25] which incorporates tree-level matrix elements with up to 4 outgoing partons and its own models of partons shower, hadronisation and multi-parton interactions. The HEJ Monte-Carlo generator [26] uses BFKL formalism for the description of wide-angle gluon emission, the measurement was compared to the predictions HEJ matched to ARIADNE program [27, 28] for the simulation of non-perturbative processes. Analytic calculations in the next-to-leading log (NLL) BFKL framework have become available recently [29, 30]. The presented measurement was compared to results from [29]. The results of theory comparison of presented measurement may be summarised as follows. The general - purpose MC PYTHIA8, PYTHIA6 and HERWIG++ show significant spread of predictions around the data for different observables, none of MC describes well the full set of measured observables. The improvement of MC with higher order matrix elements as performed in predictions of POWHEG and SHERPA matched to parton shower does not improve the agreement with the data. The HEJ MC incorporating elements of BFKL approach matched to ARIADNE program overestimates the hard parton radiation. The NLL BFKL prediction obtained in [29] describes all measured observables withing the experimental and theoretical obsrvables therefore giving the best overall description of the data.

4 Conclusion

The double differential inclusive jet production cross-section measured with full 7TeV dataset has been used for the PDF extraction in combination with HERA DIS data. The significant reduction of PDF uncertaintites has been observed. Results on the α_s extraction from the 3-jet data are in agreement with previous mesurements and extend the range of Q to 1.4 TeV.

The dijet azimuthal decorrelation for the leading in p_T dijet system was measured on the full 8 TeV dataset of 19.4 fb^{-1}. The best description of the data is given by the Monte-Carlo generator MADGRAPH matched to PYTHIA6 for parton showering, hadronisation and multi-parton interactions. The azimuthal decorrelation of jets widely seprated in rapidity was measured using the low-pielup 7 TeV dataset. Monte-Carlo generator predictions showed significant spread around

the data points. The best overall description is given by the NLL BFKL analytic calculation predictions.

Acknowledgements

The author of these proceedings is supported by RFBR (Russia) grant number 14-02-31388.

References

[1] V.N. Gribov and L.N. Lipatov, "Deep inelastic e p scattering in perturbation theory," *Sov. J. Nucl. Phys.*, **15**(1972), 438.

[2] L.N. Lipatov, "The parton model and perturbation theory," *Sov. J. Nucl. Phys.*, **20**(1975), 94.

[3] G. Altarelli and G. Parisi, "Asymptotic Freedom in Parton Language," *Nucl. Phys. B*, **126**(1977), 298.

[4] Y.L. Dokshitzer, "Calculation of the Structure Functions for Deep Inelastic Scattering and e+ e- Annihilation by Perturbation Theory in Quantum Chromodynamics," *Sov. Phys. JETP*, **46**(1977), 641.

[5] E.A. Kuraev and L.N. Lipatov and V.S. Fadin, "Multi - Reggeon Processes in the Yang-Mills Theory," *Sov. Phys. JETP*, **44**(1976), 443.

[6] E.A. Kuraev and L.N. Lipatov and V.S. Fadin, "The Pomeranchuk Singularity in Nonabelian Gauge Theories," *Sov. Phys. JETP*, **45**(1977), 199.

[7] I.I. Balitsky and L.N. Lipatov, "The Pomeranchuk Singularity in Quantum Chromodynamics," *Sov. J. Nucl. Phys.*, **28**(1978), 822.

[8] CMS Collaboration (CMS), "Measurements of differential jet cross sections in proton-proton collisions at $\sqrt{s} = 7$ TeV with the CMS detector," *Phys. Rev.*, **D87**(2013) (11), 112002, [Erratum: Phys. Rev.D87,no.11,119902(2013)], arXiv:1212.6660.

[9] CMS Collaboration (CMS), "Measurement of the double-differential inclusive jet cross section at sqrt(s) = 8 TeV with the CMS detector," **CMS-PAS-SMP-12-012**(2013).

[10] CMS Collaboration (CMS), "Measurement of jet cross sections at low transverse momentum in proton-proton collisions at 8 TeV," **CMS-PAS-FSQ-12-031**(2013).

[11] CMS Collaboration (CMS), "Measurement of the inclusive jet cross section in pp collisions at sqrt(s) 2.76 TeV," **CMS-PAS-SMP-14-017**(2015).

[12] CMS Collaboration (CMS), "Constraints on parton distribution functions and extraction of the strong coupling constant from the inclusive jet cross section in pp collisions at $\sqrt{s} = 7$ TeV," *Eur. Phys. J.*, **C75**(2015) (6), 288, arXiv:1410.6765.

[13] CMS Collaboration (CMS), "Measurement of the inclusive 3-jet production differential cross section in proton-proton collisions at 7 TeV and determination of the strong coupling constant in the TeV range," *Eur. Phys. J.*, **C75**(2015) (5), 186, arXiv:1412.1633.

[14] CMS Collaboration (CMS), "Measurement of dijet azimuthal decorrelations in pp collisions at sqrt(s) = 8 TeV," **CMS-PAS-SMP-14-015**(2015).

[15] Torbjorn Sjostrand, Stephen Mrenna, and Peter Z. Skands, "PYTHIA 6.4 Physics and Manual," *JHEP*, **05**(2006), 026, arXiv:hep-ph/0603175.

[16] Torbjorn Sjostrand, Stephen Mrenna, and Peter Z. Skands, "A Brief Introduction to PYTHIA 8.1," *Comput. Phys. Commun.*, **178**(2008), 852, arXiv:0710.3820.

[17] M. Bahr *et al.*, "Herwig++ Physics and Manual," *Eur. Phys. J.*, **C58**(2008), 639, arXiv:0803.0883.

[18] Johan Alwall, Michel Herquet, Fabio Maltoni, Olivier Mattelaer, and Tim Stelzer, "MadGraph 5 : Going Beyond," *JHEP*, **06**(2011), 128, arXiv:1106.0522.

[19] Paolo Nason, "A New method for combining NLO QCD with shower Monte Carlo algorithms," *JHEP*, **11**(2004), 040, arXiv:hep-ph/0409146.

[20] Stefano Frixione, Paolo Nason, and Carlo Oleari, "Matching NLO QCD computations with Parton Shower simulations: the POWHEG method," *JHEP*, **11**(2007), 070, arXiv:0709.2092.

[21] Simone Alioli, Paolo Nason, Carlo Oleari, and Emanuele Re, "A general framework for implementing NLO calculations in shower Monte Carlo programs: the POWHEG BOX," *JHEP*, **06**(2010), 043, arXiv:1002.2581.

[22] A.H. Mueller and H. Navelet, "An Inclusive Minijet Cross-Section and the Bare Pomeron in QCD," *Nucl. Phys. B*, **282**(1987), 727.

[23] CMS Collaboration (CMS), "Azimuthal decorrelation of jets widely separated in rapidity in pp collisions at sqrt(s) = 7 TeV," **CERN-PH-EP-2015-309**(2016), arXiv:1601.06713.

[24] A. Sabio Vera and F. Schwennsen, "The Azimuthal decorrelation of jets widely separated in rapidity as a test of the BFKL kernel," *Nucl. Phys. B*, **776**(2007), 170, arXiv:hep-ph/0702158.

[25] T. Gleisberg, *et al.*, "Event generation with SHERPA 1.1," *JHEP*, **0902**(2009), 007, arXiv:0811.4622.

[26] J. R. Andersen and J. M. Smillie, "Multiple Jets at the LHC with High Energy Jets," *JHEP*, **06**(2011), 010, arXiv:1101.5394.

[27] L. Lönnblad, "Ariadne version 4: A program for simulation of QCD cascades implementing the colour dipole model," *Comput. Phys. Commun.*, **71**(1992), 15.

[28] J. Andersen, L Lonnblad, and J. Smillie, "A Parton Shower for High Energy Jets," *JHEP*, **7**(2011), 110, arXiv:1104.1316.

[29] B. Ducloue, L. Szymanowski, and S. Wallon, "Evidence for high-energy resummation effects in Mueller-Navelet jets at the LHC," (2013), arXiv:1309.3229.

[30] F. Caporale, D.Y. .Ivanov, B. Murdaca, and A. Papa, "Mueller-Navelet small-cone jets at LHC in next-to-leading BFKL," *Nucl. Phys. B*, **877**(2013), 73, arXiv:1211.7225.

Gauge-invariant gluon TMD at the LHC: Higgs production

I.O. Cherednikov[1] and M. Pieters[1]

[1]EDF, Departement Fysica, Universiteit Antwerpen, Belgium

Factorization theorems are pivotal for the QCD description of the structure of the nucleon visible in high-energy hadronic processes. During recent years a particular framework, namely the transverse-momentum dependent (TMD) approach to the factorization beyond the collinear approximation [1], attracts more and more attention, as it allows us to describe non-perturbatively intrinsic collinear and transverse momenta and polarizations of the quarks and gluons in terms of the TMD parton distribution functions (TMD pdfs). This approach is important for the calculation of the differential cross-section in such semi-inclusive processes as the Drell-Yan process and the semi-inclusive deep inelastic scattering [2, 3].

At the LHC, the TMD pdfs are suitable for the low-$\mathbf{q}_T$ heavy particle production and for the high-energy (small-x) factorization [4]. To be more precise, let us consider the Higgs boson production through the gluon-gluon fusion. Because the Higgs boson does not directly couple to gluons, one can form a Higgs boson through the triangular quark loops. The appropriate effective Lagrangian is given by [5–7]

$$L_{\text{eff}} = -\frac{1}{4} g_\phi \Phi \, \mathcal{F}^{\mu\nu} \mathcal{F}_{\mu\nu}, \tag{1}$$

where g_ϕ stands for the effective coupling, Φ is the scalar boson field, and $\mathcal{F}^{\mu\nu}$ is the gluon field strength. The main contribution to the effective theory comes from the top quark loop as the masses of the other quarks are negligible compared to the mass of the top quark. For a recent discussion of the NNLO corrections within the effective theory, see, e.g., Ref. [8].

The Higgs production via the gluon-gluon fusion naturally introduces the gluon TMD pdfs (gTMDs), given that the gluons dominate at high energies in colliders such as the LHC. In general, depending on the region of the Bjorken-x under consideration, one can make use of the following approaches to define the gTMD[1]:

- In the small-x regime, the $\ln x$ provides a natural rapidity cutoff and the gTMD can be written as [13]

[1]Each of these functions contains the Wilson lines with light-like segments, which calls for an appropriate regularization of the rapidity/light-cone singularities [1, 9–12]. Hence an extra regulator shows up in each case.

$$\mathbf{G}^{ij}_{\mathrm{small-x}}(x,\mathbf{k}_\perp;\ln x;h)\sim\int dz^-d^2z_\perp \mathrm{e}^{ik_\perp z_\perp}\,\langle h|\,D^i\mathcal{W}_{\gamma_{\mathrm{LC}}}(z)\,\mathcal{W}^\dagger{}_{\gamma_{\mathrm{LC}}}(z)D^j\mathcal{W}_{\gamma_{\mathrm{LC}}}(0)\,\mathcal{W}^\dagger{}_{\gamma_{\mathrm{LC}}}(0)\,|h\rangle, \tag{2}$$

where $z=(0^+,z^-,\mathbf{z}_\perp)$ and D^i is a sort of the covariant derivative with boundary conditions.

- At moderate or large Bjorken-x, the $\ln x$ cannot be a rapidity cutoff anymore, so an extra regulator η must be introduced to make the "primordial" gTMD definition valid [14,15]

$$\mathbf{G}^{ij}_{\mathrm{large-x}}(x,\mathbf{k}_\perp;\eta;h)\sim\int dz^-d^2z_\perp \mathrm{e}^{-ixP^+z^-+ik_\perp z_\perp}\left\langle h|\,\mathcal{F}^{il}(z)\mathcal{W}_{\gamma_{\mathrm{LC}}}(z,0)\,\mathcal{F}^{lj}(0)\,|h\right\rangle. \tag{3}$$

- Another way to get rid of the rapidity divergences is to shift the Wilson lines from the light cone. To this end one adopts a new regulator, $\zeta=(2v\cdot P)/v^2$, where v stands for a non-light-like vector [16,17]

$$\mathbf{G}^{ij}_{\mathrm{off-LC}}(x,\mathbf{k}_\perp,\zeta;h)\sim\int dz^-d^2z_\perp \mathrm{e}^{-ixP^+z^-+ik_\perp z_\perp}\langle h|\,\mathcal{F}^{il}(z)\mathcal{W}_{\gamma_\zeta}(z,0)\,\mathcal{F}^{lj}(0)\,|h\rangle. \tag{4}$$

- More detailed analysis of the singularities entails a more sophisticated approach to the TMD pdf definition with a system of the Wilson lines and the soft factors [1].

Whatever the definition of the gTMD is adopted, an omnipresent object is the *generating matrix element* defined in the coordinate space:

$$\mathbf{G}^{\mu\nu|\mu'\nu'}_{\mathrm{gen.}}(z;h)=\langle h|\,\mathcal{F}^{\mu\nu}(z)\mathcal{W}_\gamma(z,0)\,\mathcal{F}^{\mu'\nu'}(0)\,|h\rangle, \tag{5}$$

where $\mathcal{W}_\gamma$ is a generic Wilson line (gauge link) evaluated along an arbitrary path γ. Speaking formally, the presence of the gauge links not only ensures the gauge invariance of the gTMDs, but is also a result of the resummation of soft gluons [18].

The 'standard' way to derive an operator definition of a TMD pdf starts from the identification of an appropriate factorisation scheme in a convenient gauge (in the small- or large-x regime). Thus one comes to an evidently gauge-dependent pdf. Then, through the soft gluon resummation one obtains a gauge-invariant pdf with Wilson lines, whose path-dependence is prescribed by the hard part of the factorized cross-section. The latter affects the structure of the gauge links via the relevant colour flows. An alternative approach we discuss here starts from the most general operator structure related to a given pdf. Such a generic gauge-invariant and heavily path-dependent object undergoes evolution in the coordinate space to fit a specific factorisation scheme (in the small- or large-x regime). Therefore, one gets a gauge-invariant pdf with the Wilson lines, whose path-dependence is prescribed by the factorisation.

More specifically, making use of non-Abelian Stokes' theorem (see Ref. [19] and Refs. therein)

$$\mathcal{P}_\gamma\exp\left[\oint_\gamma d\zeta_\rho\mathcal{A}^\rho(\zeta)\right]=\mathcal{P}_\gamma\mathcal{P}_\sigma\exp\left[\int_\sigma d\sigma_{\rho\rho'}(\zeta)\mathcal{F}^{\rho\rho'}(\zeta)\right], \tag{6}$$

where $\mathcal{P}_\sigma$ denotes the area-ordering, we see that the generating matrix element (5) can be re-written as

$$\tilde{\mathbf{G}}^{\mu\nu|\mu'\nu'}_{\text{gen.}}(z;h) = \frac{\delta}{\delta\sigma_{\mu\nu}(z)}\frac{\delta}{\delta\sigma_{\mu'\nu'}(0)}\langle h|\mathcal{W}_{\gamma^{[z,0]}}\,|h\rangle = \frac{\delta}{\delta\sigma_{\mu\nu}(z)}\frac{\delta}{\delta\sigma_{\mu'\nu'}(0)}\sum_X \langle h|\mathcal{W'}_{\gamma^{[z]}}|X\rangle\langle X|\mathcal{W'}_{\gamma^{[0]}}\,|h\rangle, \tag{7}$$

where the underlying (arbitrary) path $\gamma^{[z,0]}$ must contain the points z and 0. The key feature of this approach is that one first calculates the generating matrix element $\langle h|\mathcal{W}_{\gamma^{[z,0]}}\,|h\rangle$, choosing its underlying integration path to fit a specific factorization framework.

Let us demonstrate how this approach works in practice by considering the Abelian gauge theory, where the Wilson loops exponentiate

$$\langle h|\mathcal{W}_\gamma|h\rangle = \langle h|\mathcal{P}_\gamma \exp\left[\oint_\gamma d\zeta_\rho \mathcal{A}^\rho(\zeta)\right]|h\rangle = \exp\left[-\frac{g^2}{2}\oint_\gamma d\zeta_\rho \oint_\gamma d\zeta'_{\rho'}\, D^{\rho\rho'}(\zeta-\zeta')\right]. \tag{8}$$

The hadronic correlator $D^{\rho\rho'}(\zeta-\zeta') = \langle h|\mathcal{P}_\gamma\, A^\rho(\zeta)A^{\rho'}(\zeta')|h\rangle$ can be parameterized as

$$D_{\rho\rho'}(z) = g_{\rho\rho'}\, D_1(z,P) + \partial_\rho\partial_{\rho'}\, D_2(z,P) + \{P_\rho\partial_{\rho'}\}\, D_3(z,P) + P_\rho P_{\rho'}\, D_4(z,P). \tag{9}$$

Hence the area derivative can be calculated straightforwardly

$$\frac{\delta}{\delta\sigma_{\mu\nu}(z)}\langle h|\mathcal{W}_\gamma|h\rangle = -\frac{g^2}{2}\left[\partial_\mu\oint_\gamma d\zeta'_{\rho'}\, D_{\nu\rho'}(z-\zeta') - \partial_\nu\oint_\gamma d\zeta'_{\rho'}\, D_{\mu\rho'}(z-\zeta')\right]\langle h|\mathcal{W}_\gamma|h\rangle, \tag{10}$$

and expressed in terms of the invariant functions $D_{1,2,3,4}$. Therefore, the generating matrix element in the coordinate space can be evaluated completely in terms of the arbitrary Wilson loops and thereafter adjusted to fit a particular factorization scheme, Eqs. (2, 3, 4).

References

[1] J.C. Collins, "Foundations of Perturbative QCD", Cambridge University Press, 2011.

[2] J.C. Collins, D.E. Soper, and G.F. Sterman, "Transverse Momentum Distribution in Drell-Yan Pair and W and Z Boson Production," *Nucl. Phys.*, **B250**(1985), 199.

[3] P. M. Nadolsky, D. R. Stump, and C. P. Yuan, "Semiinclusive hadron production at HERA: The Effect of QCD gluon resummation," *Phys. Rev.*, **D61**(2000), 014003, [Erratum: Phys. Rev.D64,059903(2001)], `hep-ph/9906280`.

[4] R. Angeles-Martinez *et al.*, "Transverse Momentum Dependent (TMD) parton distribution functions: status and prospects," *Acta Phys. Polon.*, **B46**(2015) (12), 2501.

[5] S. Dawson, "Radiative corrections to Higgs boson production," *Nucl. Phys.*, **B359**(1991), 283.

[6] A. Djouadi, M. Spira, and P. M. Zerwas, "Production of Higgs bosons in proton colliders: QCD corrections," *Phys. Lett.*, **B264**(1991), 440.

[7] X.-d. Ji, J.-P. Ma, and F. Yuan, "Transverse-momentum-dependent gluon distributions and semi-inclusive processes at hadron colliders," *JHEP*, **07**(2005), 020, hep-ph/0503015.

[8] Ch. Anastasiou and K. Melnikov, "Higgs boson production at hadron colliders in NNLO QCD," *Nucl. Phys.*, **B646**(2002), 220, hep-ph/0207004.

[9] I. O. Cherednikov and N. G. Stefanis, "Renormalization, Wilson lines, and transverse-momentum dependent parton distribution functions," *Phys. Rev.*, **D77**(2008), 094001, 0710.1955.

[10] I. O. Cherednikov and N. G. Stefanis, "Wilson lines and transverse-momentum dependent parton distribution functions: A Renormalization-group analysis," *Nucl. Phys.*, **B802**(2008), 146, 0802.2821.

[11] I. O. Cherednikov and N. G. Stefanis, "Renormalization-group properties of transverse-momentum dependent parton distribution functions in the light-cone gauge with the Mandelstam-Leibbrandt prescription," *Phys. Rev.*, **D80**(2009), 054008, 0904.2727.

[12] I. Balitsky and A. Tarasov, "Rapidity evolution of gluon TMD from low to moderate x," *JHEP*, **10**(2015), 017, 1505.02151.

[13] F. Dominguez, C. Marquet, B.-W. Xiao, and Feng Yuan, "Universality of Unintegrated Gluon Distributions at small x," *Phys. Rev.*, **D83**(2011), 105005, 1101.0715.

[14] J. C. Collins and D. E. Soper, "Parton Distribution and Decay Functions," *Nucl. Phys.*, **B194**(1982), 445.

[15] P. J. Mulders and J. Rodrigues, "Transverse momentum dependence in gluon distribution and fragmentation functions," *Phys. Rev.*, **D63**(2001), 094021, hep-ph/0009343.

[16] X.-d. Ji, J.-P. Ma, and F. Yuan, "QCD factorization for semi-inclusive deep-inelastic scattering at low transverse momentum," *Phys. Rev.*, **D71**(2005), 034005, hep-ph/0404183.

[17] P. Sun, B.-W. Xiao, and F. Yuan, "Gluon Distribution Functions and Higgs Boson Production at Moderate Transverse Momentum," *Phys. Rev.*, **D84**(2011), 094005, 1109.1354.

[18] I. O. Cherednikov, T. Mertens, and F. F. Van der Veken, "Wilson Lines in Quantum Field Theory", De Gruyter, Berlin, 2014.

[19] Yu. Makeenko, "Methods of Contemporary Gauge Theory", Cambridge University Press, 2005.

MPI and UE corrections to jet measurements and influence on PDF determination and $\alpha_{\rm s}$

Salim Cerci (for the CMS collaboration)[1]

[1]Adiyaman University, Faculty of Arts and Sciences, Department of Physics, 02040 Adiyaman, Turkey.

1 Introduction

Events with jets which are collimated sprays of hadrons and signatures of quarks and gluons in the detector can be described by Quantum Chromodynamics (QCD) in terms of parton-parton scattering. The hard part of QCD considers perturbative QCD (pQCD), parton density functions (PDFs), initial and final state radiation (ISR, FSR) and parton shower (PS) modeling whereas the soft part of QCD deals with fragmentation, multiple parton interactions (MPI) and underlying event (UE). The inclusive jet cross section in pp collision is a fundamental quantity which can be measured and predicted within the framework of pQCD. Because of that, jet measurements can be used to determine the strong coupling constant $\alpha_{\rm s}$ and to constrain the PDFs. For a comparison of the jet production processes obtained in hadron-hadron collisions with the next-to-leading order (NLO) parton level theory calculations non-perturbative (NP) corrections have to be applied to account for MPI, UE and PS effects [1].

2 Results

NP correction factors are obtained by using Shower Monte Carlo (SMC) event generators. In order to take into account the NP effects coming from MPI and hadronization, the NP corrections factors are applied to next-to-leading order (NLO) theory calculations. A new approach treating NP corrections in the context of NLO-matched PS event generators is also introduced in Ref. [2]. NP correction factors can play important role for quantifying the relation between the perturbative hard processes and the softer interactions of particles involved in hadronization and PS. The leading order correction factors C_{LO}^{NP} are obtained by using leading-order Monte Carlo (LO-MC) generators HERWIG [3,4] and PYTHIA [5]. In this study, C_{LO}^{NP} is calculated as in Refs. [1,6,7]:

$$C_{LO}^{NP} = \frac{d^2\sigma}{dp_T dy}(\mathrm{LO}+\mathrm{PS}+\mathrm{MPI}+\mathrm{HAD})/\frac{d^2\sigma}{dp_T dy}(\mathrm{LO}+\mathrm{PS}) \quad (1)$$

where in the numerator PS, MPI and hadronization effects and in the denominator only PS effects were included in addition to the LO hard process. The NP correction for LO is evaluated by

averaging those provided by PYTHIA 6 (version 4.26), using tune Z2*, and HERWIG++ (version 2.4.2), using tune UE. This is the most obvious way to evaluate NP corrections when only the LO+PS event generators are available. However, once C_{LO}^{NP} corrections are applied on results at NLO parton-level, a potential inconsistency arises because the real correction of the first parton emission is treated differently in the NLO calculation and the PS. To avoid this, an alternative method [2], based on NLO Monte Carlo (NLO-MC) generators, can be used. This method makes possible to study separately correction factors to the fixed-order calculation due to PS effects. The NLO NP corrections are derived using POWHEG [8, 9], interfaced with PYTHIA 6 (version 4.26) for PS, MPI and hadronization. In this case averaging the results for two different tunes of PYTHIA 6, Z2* and P11 are taken. The correction factor between PS and the hadronic final state is defined [2, 10] as

$$C_{NLO}^{NP} = \frac{d^2\sigma}{dp_T dy}(\mathrm{NLO+PS+MPI+HAD})/\frac{d^2\sigma}{dp_T dy}(\mathrm{NLO+PS}) \tag{2}$$

$$C_{NLO}^{PS} = \frac{d^2\sigma}{dp_T dy}(\mathrm{NLO+PS})/\frac{d^2\sigma}{dp_T dy}(\mathrm{NLO}) \tag{3}$$

where the denominator in Eq. 3 is evaluated by switching off PS+MPI+HAD in the MC simulation. The difference between the correction factors in Eqs. 1 and 2 calculation is due to the matching of multiple parton interactions to the NLO calculation. The transverse momentum p_T scale of MPI is smaller than the p_T scale of the hard process, which is defined by the average p_T of the hard partons in the process. Thus the hard scale in LO and NLO is different, leading to a non-negligible numerical difference in the NP correction factor. In particular, this difference can be seen clearly in the forward rapidity $3.2 < |y| < 4.7$ region and at low p_T as shown in Fig. 1. The correction factor C_{NLO}^{PS} in Eq. 3, is evaluated with the NLO-MC simulation.

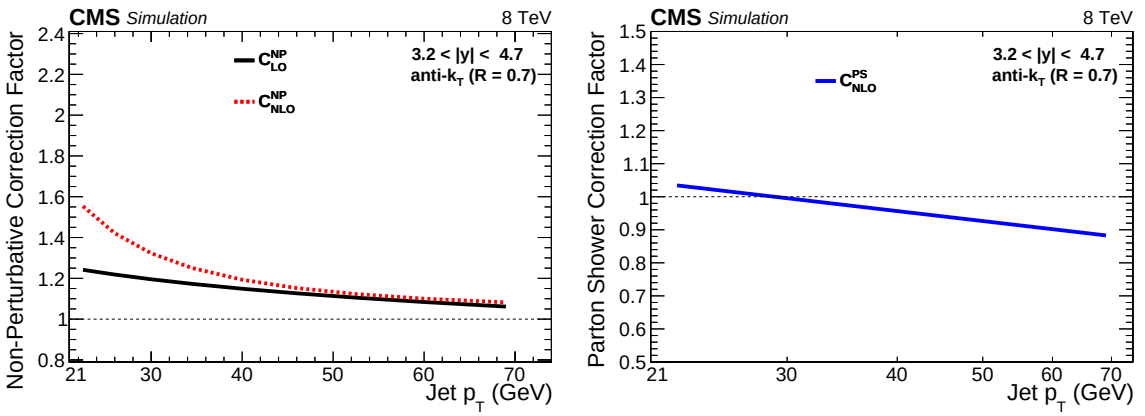

Figure 1: NP correction factor (left) and PS correction factor (right) shown for the forward rapidity $3.2 < |y| < 4.7$ as a function of jet p_T as determined in [1].

In this study, the three correction factors evaluated with Eq. 1, 2 and 3, are applied to NLO predictions (CT10 [11]). NP and PS corrections, depend on p_T and y, are obtained for central ($|y| < 3$)

and forward ($3.2 < |y| < 4.7$) regions of CMS [1]. Since the PS effect is largest at large y, only results from the forward region are presented in here. The obtained theoretical results are compared to inclusive jets measurement performed in forward region at $\sqrt{s} = 8$ [1]. Figure 2 (top left) shows the comparison of the experimental data with the theoretical jet distribution obtained by applying only the correction factor C_{LO}^{NP} to NLO prediction. The average of LO and NLO correction factors, $\frac{C_{LO}^{NP}+C_{NLO}^{NP}}{2}$, is applied to NLO prediction and the comparison with the experimental data is shown in Fig. 2 (top right). A further comparison of data to the NLO prediction, in which the correction factor $C_{NLO}^{PS} + (\frac{C_{LO}^{NP}+C_{NLO}^{NP}}{2})$ is applied, is shown in Fig. 2 (bottom). By looking at all the comparisons shown in Fig. 2, the NP corrections change the shape of jet distributions as well as affect significantly the comparison of theory predictions with the experimental data. The PS corrections contribute as well.

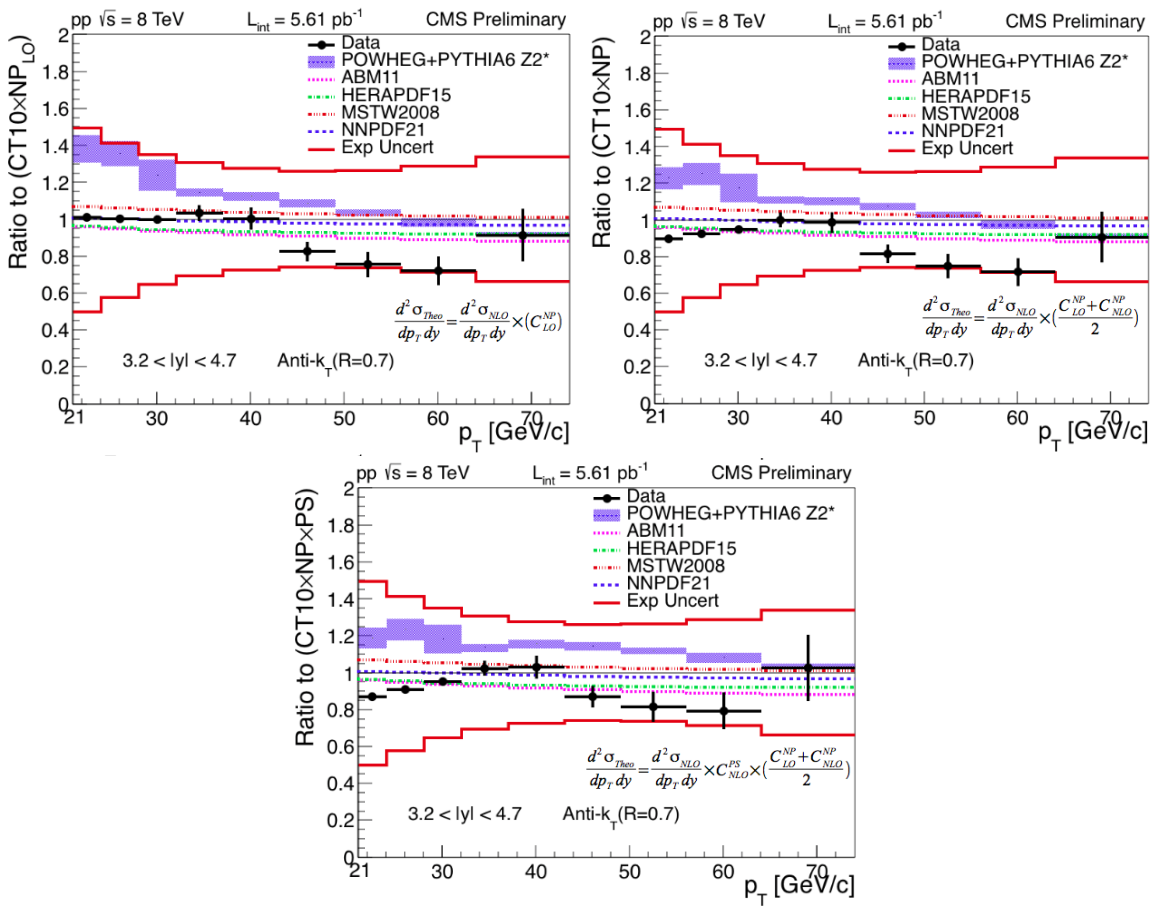

Figure 2: Ratio of inclusive jet cross sections to the theoretical prediction using the central value of the CT10 PDF set which are applied NP and PS correction for forward rapidity ([1])

It can be also concluded that NP corrections have influence on the determinations of parton distributions. Perturbative QCD, supplemented by a small NP correction, is able to describe well

the data over a wide range of p_T and y and over many orders of magnitude in cross section. A cross check including PS corrections is performed with CT10 NLO PDF set, and good agreement is observed with each other within the estimated uncertainty limits [1].

Acknowledgements

The author is grateful to ICTP for providing the partial financial support.

References

[1] CMS Collaboration, "Measurement of the double-differential inclusive jet cross section at sqrt(s) = 8 TeV," (2015) (CMS-PAS-SMP-14-001).

[2] S. Dooling, P. Gunnellini, F. Hautmann, and H. Jung, "Longitudinal momentum shifts, showering, and nonperturbative corrections in matched next-to-leading-order shower event generators," *Phys. Rev.*, **D87**(2013) (9), 094009, [arXiV:hep-ph/1212.6164].

[3] G. Corcella, *et al.*, "HERWIG 6: an event generator for hadron emission reactions with interfering gluons (including supersymmetric processes)," *JHEP*, **2001**(2001) (01), 010.

[4] G. Corcella, *et al.*, "HERWIG 6.5 release note," (2002), [arXiV:hep-ph/0210213].

[5] T. Sjöstrand, S. Mrenna, and P. Skands, "PYTHIA 6.4 physics and manual," *JHEP*, **05**(2006), 026, [arXiV:hep-ph/0603175].

[6] G. Aad *et al.* (ATLAS), "Measurement of inclusive jet and dijet production in pp collisions at $\sqrt{s} = 7$ TeV using the ATLAS detector," *Phys. Rev.*, **D86**(2012), 014022, [arXiV:hep-ex/1112.6297].

[7] S. Chatrchyan *et al.* (CMS), "Measurement of the Inclusive Jet Cross Section in pp Collisions at $\sqrt{s} = 7$ TeV," *Phys. Rev. Lett.*, **107**(2011), 132001, [arXiV:hep-ex/1106.0208].

[8] P. Nason, "A new method for combining NLO QCD with shower Monte Carlo algorithms," *JHEP*, **2004**(2004) (11), 040.

[9] S. Alioli, K. Hamilton, P. Nason, C. Oleari, and E. Re, "Jet pair production in POWHEG," *JHEP*, **04**(2011), 081, [arXiv:hep-ph/1012.3380].

[10] V. Khachatryan *et al.* (CMS), "Constraints on parton distribution functions and extraction of the strong coupling constant from the inclusive jet cross section in pp collisions at $\sqrt{s} = 7$ TeV," *Eur. Phys. J.*, **C75**(2015) (6), 288, [arXiV:hep-ex/1410.6765].

[11] H. L. Lai, *et al.*, "New parton distributions for collider physics," *Phys. Rev. D*, **82**(2010), 074024.

Chapter 5

Working Group
High multiplicities and interactions with nuclei

Convenors:

Paolo Bartalini (ALICE)
Boris Blok (Theory)

Introduction: High Multiplicities and Interactions with Nuclei

P.Bartalini[1] and B.Blok[2]

[1]Institute of Particle Physics, Central China Normal University, Wuhan 430079, China
[2]Physics Department, Technion, Haifa 32000, Israel

This recently introduced working group reflects the growing interest in the study of high multiplicity final states in pp and pA interactions. A deep investigation of these final states performed in the LHC RUN I allows to regard them as the contribution of several rather soft MPI [1,2].

The LHC RUN I highlights in this research field include the unexpected observation of "ridge" structures (long-range, near-side angular correlations) for high multiplicity final states in pp and pA interactions [3,4]. In heavy ion collisions the azimuthal modulation of the produced particles is typically considered the manifestation of a transport effect in dense matter (medium), however, what is giving rise to such effects in smaller systems?

In the context of this edition of the MPI@LHC workshop, all the LHC collaborations present updates on the phenomenology of long-range angular correlations, including the first RUN II results on pp at $\sqrt{s} = 13$ TeV from ATLAS and CMS [5,6] (presented by A. Moraes and A. Buckley, respectively) that indicate some nice $\sqrt{s}$ scaling properties of the correlation strength, found to basically depend just on the charged multiplicity N_{ch}.

In P. Tribedy's contribution (summarised in these proceedings), the ridge correlations are studied in the Color Glass Condensate (CGC) framework. It is argued that ridge correlations in pp collisions at $\sqrt{s} = 7$ and 13 TeV are in agreement with the expectations from the CGC effective theory of high energy QCD, which in particular can predict the scaling property of the correlation strength.

As stressed in the ALICE contribution presented by M. Floris, the collective flow, as measured in heavy ion collisions, is expected to follow a well defined mass dependence (heavier particles are modified in a more pronounced way by the collective expansion). In [7] ALICE shows that this is also the case for pA and that hydro predictions are in agreement with the observed phenomenology. Of course other explanations exist: the main competitor to hydro is CGC, though it offers no "natural" explanation for the mass dependence.

The LHCb ridge results [8] presented by Álvaro Dosil constitute the first measurement of a long-range correlation on the near side in pA collisions in the forward region and extend the previous observations in the central region.

C. Oppedisano (see her contribution in these proceedings) reports on the ALICE study of Multiple Parton Interactions patterns in pA collisions, focusing on the detailed topological investigation of the mini-jet structure, which is examined over a wide centrality range. Mini-jets shapes are basically found to be independent with respect to the overall multiplicity of the event (N_{ch}) while the mini-jet rate turns out to be proportional to N_{ch}, corroborating the evidence of a rather modest contribution of leading jet production to the high multiplicity final states. As important spin-off of this study one gets an improved criterion for centrality determination in pA interactions that tends to favour the adoption of very forward estimators.

M. Strikman's contribution (summarised in these proceedings) does focus on the study of color fluctuations in the proton. It is argued that the proton (photon) - nucleus collisions at LHC energies can be used to probe fluctuations of the strength of pp and pA interactions. The dependence of hard pA collisions on centrality observed at LHC and at RHIC for large x_p is explained as a consequence of the small cross section of proton configurations with $x_p \geq 0.3$. It is also suggested that strong fluctuations in the interaction strength are responsible for a factor of ~ 2 suppression of the $\gamma A \to \rho A$ cross section as compared to predictions of the vector dominance model. Also in this case it is reported an important application to the centrality determination in pA at the LHC [9].

Z. Conesa del Valle reports on the ALICE measurements of heavy flavour yields at different charged particle multiplicities in pp and pA collisions [10]. In a naïve picture, N_{ch} and all the event yields should be roughly proportional to the number of MPI, however the observed deviations to this rule may point to flow-like effects: see the contribution of K. Werner in the Monte Carlo section of these proceedings.

Hints of flow-like patterns in small systems have also been reported in studies focusing on identified particle yields [11]. As stressed in the presentation of E. Fragiacomo, the hardening of the p_T spectra and mass-ordering in pA collisions provide a first hint on the presence of collective behavior, whose observation is well consolidated in heavy ion collisions. B. A. Hess (see his contribution to these proceedings) presents the ALICE measurement of the identified hadron production as a function of event multiplicity in pp collisions at $\sqrt{s} = 7$ TeV. The yield normalised to pion production rises faster with multiplicity for baryons with higher strangeness content, while it turns out to be constant for protons. Therefore this still unexplained feature doesn't seem to be baryon-related, but rather strangeness-related.

As already reported in the previous edition of this workshop, alternative explanations to these flow-like phenomena may be provided by MPI models with color reconnections (CR). That's why it is particularly important to dedicate some resources to the tuning of the MPI models with CR in estreme conditions (high multiplicity final states). Of course hydro, CGC and other models should also be tested against the observables sensitive to CR. Both the presentations of Guy Paić and Antonio Ortiz focus on such aspect (see the relative contributions to these proceedings).

In A. Bylinkin's presentation (summarised in these proceedings) the author studies the transverse momentum spectrum of charged particles in pp collisions on the basis of the two component model, which combines the power-like and the exponential terms in p_T.

In B. Blok's presentation (summarised in these proceedings) the pseudorapidity distribution of final hadrons on the basis of Double logarithmic Approximation and Local Parton Hadron duality

is calculated and compared with HERA data. The calculation is done in the pQCD framework.

O. Zenin's contribution (summarised in these proceedings) reports the ATLAS study focusing on the multiplicity dependence of Bose Einstein Correlation (BEC) parameters characterising the correlation strength and the source size. These observables are investigated for charged particle multiplicities of up to 240 and a saturation effect in the multiplicity dependence of the correlation source size parameter is observed.

The panorama of the presentations in our section is completed by S.Heppelmann (see his contribution to the proceedings) reporting on the transverse proton polarisation dependence of forward neutral pion production in p-Au collisions in STAR.

The LHC beams of RUN II should soon switch to the pA mode, achieving a factor 10 increase in the integrated luminosity with respect to the figures obtained in RUN I. This should allow to focus on additional challenges as the study of the Double Parton Scattering (DPS) in pA collisions where - due to anti-shadowing effects - the signal/background ratios are expected to be strongly enhanced with respect to the corresponding pp processes.

References

[1] Serguei Chatrchyan *et al.* (CMS), "Jet and underlying event properties as a function of charged-particle multiplicity in proton?proton collisions at $\sqrt{s}$ = 7 TeV," *Eur. Phys. J.*, **C73**(2013) (12), 2674, 1310.4554.

[2] Betty Abelev *et al.* (ALICE), "Transverse sphericity of primary charged particles in minimum bias proton-proton collisions at $\sqrt{s} = 0.9$, 2.76 and 7 TeV," *Eur. Phys. J.*, **C72**(2012), 2124, 1205.3963.

[3] Vardan Khachatryan *et al.* (CMS), "Observation of Long-Range Near-Side Angular Correlations in Proton-Proton Collisions at the LHC," *JHEP*, **09**(2010), 091, 1009.4122.

[4] Serguei Chatrchyan *et al.* (CMS), "Observation of long-range near-side angular correlations in proton-lead collisions at the LHC," *Phys. Lett.*, **B718**(2013), 795, 1210.5482.

[5] Vardan Khachatryan *et al.* (CMS), "Measurement of long-range near-side two-particle angular correlations in pp collisions at $\sqrt{s}$ = 13 TeV," (2015), 1510.03068.

[6] Georges Aad *et al.* (ATLAS), "Observation of long-range elliptic anisotropies in $\sqrt{s}$ =13 and 2.76 TeV *pp* collisions with the ATLAS detector," (2015), 1509.04776.

[7] Betty Abelev *et al.* (ALICE), "Long-range angular correlations on the near and away side in *p*-Pb collisions at $\sqrt{s_{NN}} = 5.02$ TeV," *Phys. Lett.*, **B719**(2013), 29, 1212.2001.

[8] Roel Aaij *et al.* (LHCb), "Measurements of long-range near-side angular correlations in $\sqrt{s_{\rm NN}} = 5$TeV proton-lead collisions in the forward region," (2015), 1512.00439.

[9] Georges Aad *et al.* (ATLAS), "Measurement of the centrality dependence of the charged-particle pseudorapidity distribution in proton–lead collisions at $\sqrt{s_{\rm NN}} = 5.02$ TeV with the ATLAS detector," (2015), 1508.00848.

[10] Jaroslav Adam *et al.* (ALICE), "Measurement of charm and beauty production at central rapidity versus charged-particle multiplicity in proton-proton collisions at $\sqrt{s} = 7$ TeV," *JHEP*, **09**(2015), 148, 1505.00664.

[11] Betty Bezverkhny Abelev *et al.* (ALICE), "Multiplicity Dependence of Pion, Kaon, Proton and Lambda Production in p-Pb Collisions at $\sqrt{s_{NN}}$ = 5.02 TeV," *Phys. Lett.*, **B728**(2014), 25, 1307.6796.

Measurement of identified hadron production as a function of event multiplicity in pp collisions at $\sqrt{s} = 7\,\text{TeV}$ with ALICE

Benjamin Andreas Hess (for the ALICE Collaboration)[1]

[1]Physikalisches Institut, University of Tübingen, Germany

1 Introduction

The two-particle correlations in high-multiplicity proton-proton (pp) and proton-lead (p-Pb) collisions were observed to exhibit flow-like patterns similar to those in lead-lead (Pb-Pb) collisions [1]. Also, similar features in p-Pb and Pb-Pb collisions for particle ratios such as $\Lambda/K^0_{\rm S}$ were recently discovered [2]. In order to understand the origin of these effects, it is important to complement the existing measurements with corresponding ones in pp collisions.

2 Analysis technique

The ALICE detector [3, 4] at the LHC is used in this analysis to study the production of charged light flavour, strange and multi-strange hadrons (π, K, p, Λ, Ξ, Ω) in the mid-rapidity region $|y| < 0.5$. The Inner Tracking System (ITS) and the Time Projection Chamber (TPC) are used for primary and secondary vertex determination and tracking. Pions, kaons and protons are identified with a technique that combines the information on the specific energy loss $\mathrm{d}E/\mathrm{d}x$ in the ITS and the TPC with the Time-Of-Flight (TOF) measurement. The relativistic rise of the $\mathrm{d}E/\mathrm{d}x$ inside the TPC allows for a statistical particle identification to momenta of up to $20\,\text{GeV}/c$ and beyond [5]. Short-lived particles as $K^0_{\rm S}$, Λ, Ξ and Ω are detected via their (weak) decay topologies. Their yields are extracted using a bin-counting technique (see [6] for a detailed description).

The analysis was performed on data from low-pile-up pp collisions at $\sqrt{s} = 7\,\text{TeV}$ recorded in 2010 with a minimum bias trigger. The dataset was restricted to events with at least one reconstructed charged track (segment) within $|\eta| < 1$. After tagging events with more than one primary vertex as pile-up and removing them, the dataset contains up to about 180 million events.

The multiplicity selection is performed via the sum of the signal amplitudes of the V0 plastic scintillator arrays at forward and backward rapidity (V0M). The events are classified by the percentiles of the V0 amplitude distribution. For each multiplicity class, the average pseudo-rapidity density of primary charged particles $\langle \mathrm{d}N_{\rm ch}/\mathrm{d}\eta \rangle_{|\eta|<0.5}$ is measured [7].

A Monte Carlo simulation with PYTHIA 6 Perugia 0 with particle transport through the ALICE geometry via GEANT3 was used to determine acceptance and efficiency.

3 Results

The transverse-momentum spectra (p_{T}) of charged pions and of $\Xi^- + \overline{\Xi}^+$ are shown in Fig. 1 for various V0M multiplicity classes. Both species show a similar evolution with multiplicity. The spectra become harder with increasing multiplicity and the ratio to the multiplicity-integrated spectrum ($0 - 100\%$) becomes approximately constant for $p_{\mathrm{T}} \gtrsim 4\,\mathrm{GeV}/c$. The same trends are also observed for all the other species considered in this analysis. The unaltered spectral shapes at high p_{T} could possibly indicate the presence of a scaling with the number of multi-parton interactions.

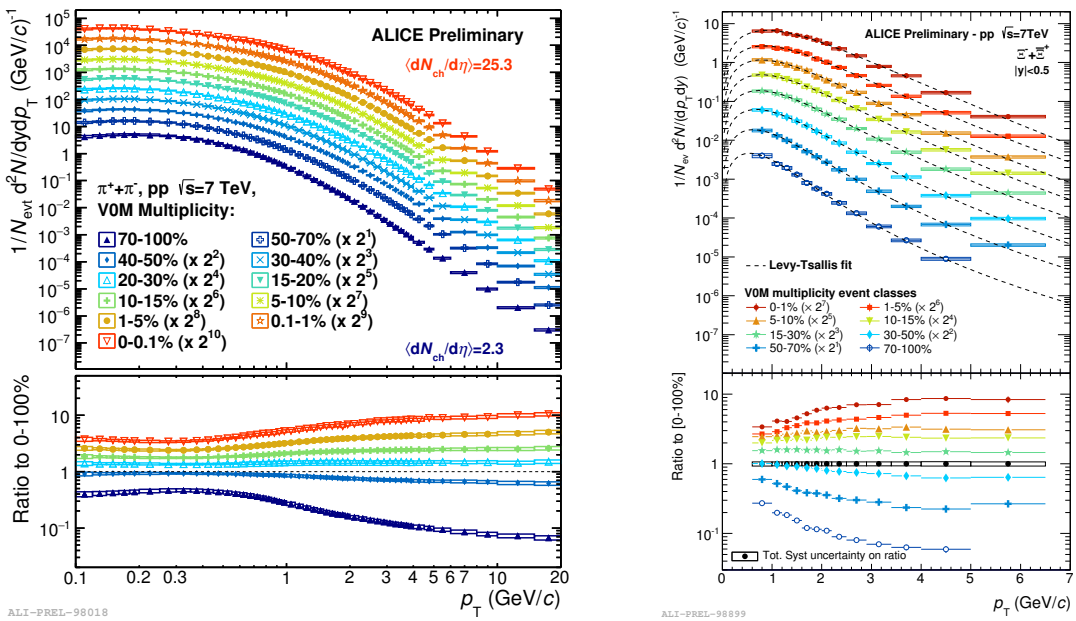

Figure 1: Charged pion yield (left) and $\Xi^- + \overline{\Xi}^+$ yield (right) as a function of p_{T} for various V0M multiplicity classes. The lower panel shows the ratios to the $0 - 100\%$ spectrum. The error bars (smaller than the marker size) represent the statistical uncertainties and the error boxes indicate the systematic uncertainties.

To compare different collision systems, the spectral ratio of Λ/K^0_{S} is shown in Fig. 2 for pp, p-Pb and Pb-Pb collisions. It exhibits a maximum around $p_{\mathrm{T}} \sim 2 - 3\,\mathrm{GeV}/c$ and changes with multiplicity in a qualitatively similar way for all three collision systems. The magnitude of the change is larger in Pb-Pb than in p-Pb and pp. However, it has to be noted that $\langle \mathrm{d}N_{\mathrm{ch}}/\mathrm{d}\eta \rangle_{|\eta|<0.5}$ for the most central V0M multiplicity class shown in the figure is two orders of magnitude larger in Pb-Pb than in p-Pb and pp. Indeed, an earlier study [2] of this ratio in p-Pb and Pb-Pb showed a quantitative agreement of the evolution as a function of $\langle \mathrm{d}N_{\mathrm{ch}}/\mathrm{d}\eta \rangle_{|\eta|<0.5}$ in both systems. This strikingly similar behaviour is observed for the spectral ratio of p/π as well. Also in that case, the ratio exhibits a maximum at intermediate p_{T}.

In order to obtain the p_{T}-integrated yields, the transverse-momentum spectra have been fitted with a Levy-Tsallis function, which is then used to extrapolate to the full p_{T} range. The p_{T}-integrated yield ratios of Ξ/π and Ω/π are shown in Fig. 3. The functional dependence on the multiplicity is the same in pp and p-Pb, as is also observed for the K/π and p/π ratios. The

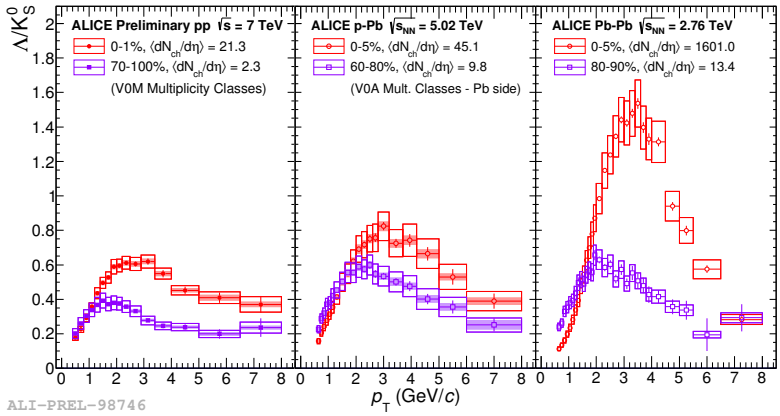

Figure 2: $(\Lambda + \overline{\Lambda})/K^0_{\rm S}$ ratio as a function of $p_{\rm T}$ in a high and a low V0M multiplicity class. The ratios for pp (left) are compared to p-Pb (middle) and Pb-Pb (right). The error bars represent the statistical uncertainties, the empty boxes indicate the total and the shaded boxes the uncorrelated (with respect to multiplicity) systematic uncertainties.

yield ratios in both systems approach those in Pb-Pb reaching the grand-canonical saturation limit calculated in two different implementations of the statistical model (THERMUS v3.0 [8] and the GSI-Heidelberg model [9]) in case of the Ξ, but stay slightly below for the Ω. The pp results are compared to predictions from three different versions of PYTHIA. None of the considered versions reproduces the rising trend with multiplicity. Switching on or off colour reconnection has only little impact and does not change this observation. The same holds true for $K^0_{\rm S}/\pi$ and Λ/π.

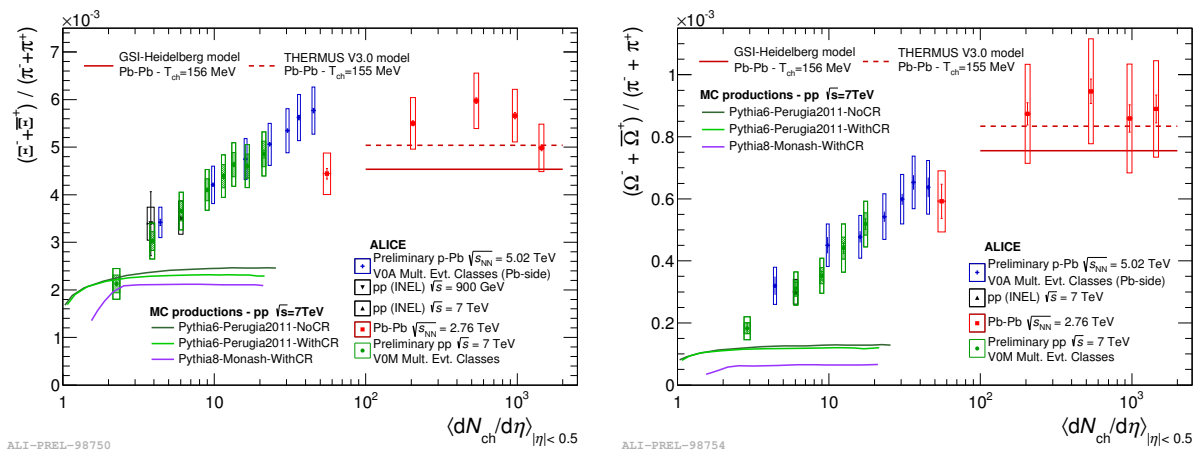

Figure 3: $(\Xi^- + \overline{\Xi}^+)/(\pi^- + \pi^+)$ (left) and $(\Omega^- + \overline{\Omega}^+)/(\pi^- + \pi^+)$ (right) ratios as a function of $\langle {\rm d}N_{\rm ch}/{\rm d}\eta \rangle_{|\eta|<0.5}$ in pp (green), p-Pb (blue) and Pb-Pb (red) collisions. The error bars represent the statistical uncertainties, the empty boxes indicate the total and the shaded boxes the uncorrelated (with respect to multiplicity) systematic uncertainties.

To quantify how fast the yield ratio to pions increases with multiplicity for various species, each ratio normalised to the pp inclusive value is shown in Fig. 4 for pp and p-Pb. As before, the multiplicity dependence is similar in both systems. The ratio is constant at unity for p/π, but rises with multiplicity for strange hadrons. The relative increase of the ratio with multiplicity is more pronounced for hadrons with higher strangeness content. These observations suggest that the yield increase is not baryon-related, but strangeness-related.

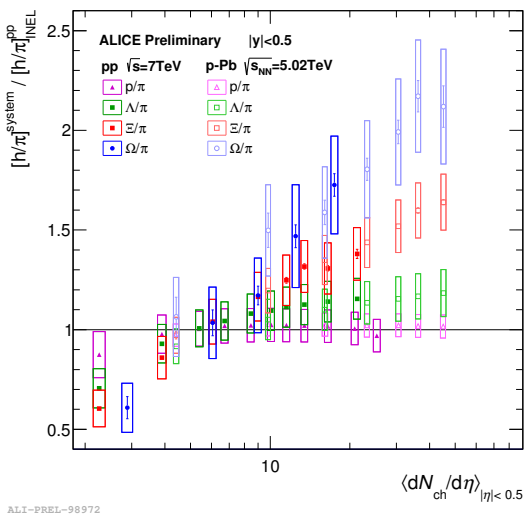

Figure 4: Particle ratios of protons and strange baryons to pions normalised to the corresponding ratio in pp in the $0-100\%$ multiplicity class. The ratios are shown as a function of $\langle \mathrm{d}N_{\mathrm{ch}}/\mathrm{d}\eta \rangle_{|\eta|<0.5}$ for pp (full symbols) and p-Pb (open symbols). The error bars represent the statistical uncertainties and the error boxes indicate the systematic uncertainties. Note that the latter are highly correlated among multiplicity bins.

4 Conclusions

First measurements of the identified hadron production as a function of event multiplicity in pp collisions at $\sqrt{s} = 7\,\mathrm{TeV}$ have been presented by the ALICE collaboration. The p_{T} spectra of π, K, p, Λ, Ξ and Ω all become harder with multiplicity and their shape is unaltered with respect to inclusive at high p_{T}. The p_{T}-differential baryon/meson ratios (p/π, Λ/K^0_{S}) exhibit a qualitatively similar evolution with multiplicity in pp, p-Pb and Pb-Pb collisions, when multiplicity classes corresponding to similar $\langle \mathrm{d}N_{\mathrm{ch}}/\mathrm{d}\eta \rangle_{|\eta|<0.5}$ values are compared. In all systems, the baryon production at mid-p_{T} is observed to be enhanced in high-multiplicity events. The p_{T}-integrated yield ratios to pions (h/π) show the same multiplicity dependence in pp and p-Pb, which indicates that the underlying mechanisms are similar in both systems. The ratios rise faster with multiplicity for baryons with higher strangeness content, while the ratio is constant for protons. This suggests that this feature is not baryon-related, but strangeness-related. The observed trends are not reproduced by commonly used PYTHIA tunes.

References

[1] V. Khachatryan *et al.* (CMS), *JHEP*, **09**(2010), 091.
[2] B. Abelev *et al.* (ALICE), *Phys. Lett.*, **B728**(2014), 25.
[3] K. Aamodt *et al.* (ALICE), *JINST*, **3**(2008), S08002.
[4] B. Abelev *et al.* (ALICE), *Int. J. Mod. Phys.*, **A29**(2014), 1430044.
[5] B. A. Hess, Ph.D. thesis, University of Tübingen, 2015, CERN-THESIS-2015-158.
[6] K. Aamodt *et al.* (ALICE), *Eur. Phys. J.*, **C71**(2011), 1594.
[7] B. Abelev *et al.* (ALICE), *Phys. Rev. Lett.*, **110**(2013) (3), 032301.
[8] J. Cleymans, I. Kraus, H. Oeschler, K. Redlich, and S. Wheaton, *Phys. Rev.*, **C74**(2006), 034903.
[9] A. Andronic, P. Braun-Munzinger, and J. Stachel, *Phys. Lett.*, **B673**(2009), 142, [Erratum: Phys. Lett.B678,516(2009)].

Measurements of Bose-Einstein correlations with the ATLAS detector

Oleg Zenin[1]

[1]State Research Center Institute for High Energy Physics (Protvino), NRC KI, Russia

On behalf of the ATLAS collaboration

Presented at 7th International Workshop on Multiple Partonic Interactions at the LHC, 23-27 November 2015, ICTP, Italy

Abstract

This report summarizes studies of Bose-Einstein Correlations (BEC) for pairs of like-sign charged particles measured in the kinematic range $p_T > 100$ MeV and $|\eta| < 2.5$ in pp collisions at $\sqrt{s} = 0.9$ and 7 TeV with the ATLAS detector at LHC. The integrated luminosities are approximately 7 μb^{-1}, 190 μb^{-1} and 12.4 nb^{-1} for 0.9 and 7 TeV minimum-bias and 7 TeV high-multiplicity data samples, respectively. The multiplicity dependence of BEC parameters characterizing the correlation strength and the correlation source size are investigated for charged-particle multiplicities of up to 240. A saturation effect in the multiplicity dependence of the correlation source size parameter is observed using the high-multiplicity 7 TeV data sample. The dependence of the BEC parameters on the average transverse momentum of the particle pair is also investigated. ATLAS results are compared to other experiments at the same and lower centre-of-mass energies, where possible.

1 Introduction

Particle correlations play an important role in the understanding of multiparticle production. Bose-Einstein correlations (BEC) between identical bosons are manifested as an enhancement in the production rate of identical bosons that are close together in the momentum space. Studying BEC in terms of a relative momentum difference between identical bosons, in dependence on the average particle momentum and the total multiplicity in the event, allows to probe geometry and, to some extent, dynamics of multihadron production.

In this report, studies of one-dimensional BEC effect in pp collisions at center-of-mass energies of 0.9 and 7 TeV, using the ATLAS detector [1] at the Large Hadron Collider (LHC), are presented. The analysis [2] extends previously published LHC studies [3–6] to total charged multiplicities up to 240.

2 Observables and their parameterization

Bose-Einstein correlations are measured in terms of a two-particle four-momentum density function $\rho(p_1, p_2)$ for identical bosons normalized to a two-particle reference function $\rho_0(p_1, p_2)$, ideally containing all correlations present in $\rho(p_1, p_2)$ excluding BEC,

$$C_2(p_1, p_2) = \frac{\rho(p_1, p_2)}{\rho_0(p_1, p_2)}\,. \tag{1}$$

As no particle identification is attempted in the present analysis, $\rho = \rho(++, --)$ and $\rho_0 = \rho(+-)$ are constructed, respectively, from pairs of like- and opposite-sign charged particles uniformly treated as pions. The purity of the like-sign sample is estimated from MC to be approximately 70%, where 69% and 1% are $\pi^{\pm}\pi^{\pm}$ and $K^{\pm}K^{\pm}$ pairs, respectively. Same-sign sample impurity effects are absorbed by the correlation strength parameter λ.

The C_2 function is parameterized in terms of the Lorentz-invariant four-momentum difference, $Q = \sqrt{-(p_1 - p_2)^2}$. A typical parameterization of $C_2(Q)$ is

$$C_2(Q) = \frac{\rho(Q)}{\rho_0(Q)} = C_0\left[1 + \Omega(\lambda, QR)\right](1 + \epsilon Q)\,, \tag{2}$$

where R is the effective radius of the production region, and λ is the correlation strength parameter characterizing relative contributions of coherent and non-coherent emissions of identical bosons. The BEC effect vanishes in case of a fully coherent emission, $\lambda = 0$, and reaches a maximum strength for fully chaotic emissions $\lambda = 1$ [7]. C_0 is the normalization constant adjusted so that $C_2(Q) \to 1$ at large Q and, finally, ϵ is the fitted parameter accounting for correlations not fully removed by normalization to the reference function ρ_0. The functional form of $\Omega(\lambda, QR)$ will be discussed later.

The effect of resonances in $\rho(+-)$ is cancelled by normalizing the measured C_2 function to the one obtained using Monte Carlo simulation without BEC effects but known to correctly describe resonances and their reflections. The double ratio $R_2(Q)$ is defined as

$$R_2(Q) = \frac{C_2(Q)}{C_2^{\mathrm{MC}}(Q)} = \frac{\rho(++, --)}{\rho(+-)} \Big/ \frac{\rho^{\mathrm{MC}}(++, --)}{\rho^{\mathrm{MC}}(+-)} \tag{3}$$

In what follows, R and λ parameters of the emission model will be extracted from the fits of $R_2(Q)$ parameterization to the data. Among various parameterizations of the $\Omega(\lambda, R)$ function in Eq. 2, each assuming a specific geometry of the hadron production region, the exponential parameterization of a static source with a radial Lorentzian density distribution [8] was found to better reproduce the observed two-particle spectrum at low Q:

$$\Omega = \lambda \cdot \exp(-RQ) \tag{4}$$

3 Data and MC samples

The analysis utilizes ATLAS pp datasets collected at $\sqrt{s} = 0.9$ and 7 TeV with the minimum-bias trigger [9, 10], as well as $\sqrt{s} = 7$ TeV dataset recorded with the high-multiplicity track trigger

(HMT). The HMT selects events with at least 124 charged tracks with $p_T > 400$ MeV originating from a single vertex, as reconstructed at the trigger level. The final event and track selection criteria reproduce the ones used in ATLAS minimum-bias multiplicity analysis [9]. All events are required to have at least one vertex reconstructed from more than two tracks with $p_T > 100$ MeV and consistent with the beam spot position. Tracks with $p_T > 100$ MeV and $|\eta| < 2.5$ originating from the vertex with the maximum $\sum p_T^2$ of tracks and satisfying the quality criteria [9], are selected for the analysis. Events triggered by the HMT are selected if they contain more than 120 such tracks.

The datasets collected with the minimum-bias trigger at $\sqrt{s} = 0.9$ and 7 TeV contain 3.6×10^5 events with a total of 4.5×10^6 selected tracks and 10^7 events with 2.1×10^8 tracks, respectively. This corresponds to integrated luminosities of approximately 7 μb^{-1} at 0.9 TeV and 190 μb^{-1} at 7 TeV. The high-multiplicity 7 TeV dataset contains 1.8×10^4 events with 2.7×10^6 selected tracks in total, corresponding to the integrated luminosity of approximately 12.4 nb^{-1}.

Monte Carlo samples of minimum-bias and high-multiplicity events were generated using PYTHIA 6.421 MC generator [11] with the ATLAS MC09 set of optimized parameters [12]. Single-, double- and non-diffractive processes contribute to the sample in proportions predicted by the PYTHIA model. As mentioned previously, the MC model does not include BEC effects. The generated events were passed through a full GEANT4 based detector simulation [13] and the reconstruction chain identical to the one applied to the data.

For the study of systematic effects, additional MC samples were produced with PHOJET 1.12.1.35 [14], PYTHIA with the Perugia0 tune [15], and, for the high-multiplicity analysis, the EPOS 1.99_v2965 [16] Monte Carlo generators.

The MC models correctly predict $C_2(Q)$ single-ratio functions at $Q > 0.5$ GeV, while BEC enhancement seen in the data at $Q < 0.5$ GeV is not reproduced in the MC, as expected.

4 Data correction procedure

The data correction procedure closely follows the one applied in the previous ATLAS minumum-bias measurements [9, 10]. Each track enters the observables with a weight accounting for track reconstruction inefficiency, for contribution of secondary particles, for migration of primary particles into and outside the kinematic range, and for contribution of fake tracks. Each like- and opposite-sign particle pair is assigned Gamow correction factor accounting for a charge-dependent shift in the relative momentum Q due to the final state Coulomb interaction (see, e.g., [17]). In addition, each event is assigned an overall multiplicative weight accounting for trigger and vertex reconstruction inefficiencies.

The multiplicity distributions are unfolded to the particle level using the Bayesian approach, as described in [9, 10]. The folding matrix giving a probability to select n_{sel} reconstructed tracks in an event with n_{ch} charged primary particles within the kinematic range was constructed using PYTHIA with ATLAS MC09 tune [12]. The unfolding procedure was validated by applying it to simulated MC events and comparing the results to the known particle level distributions.

5 Systematic uncertainties

The leading systematic uncertainty on the fitted parameters λ and R originates from the MC model dependence of the $R_2(Q)$ correlation function. The uncertainty due to Coulomb correction estimated by varying its size by $\pm 20\%$ is also sizeable but affects mostly the λ parameter. Other non-negligible uncertainty sources include the dependence on the fitted Q range and on the size of Q bins. Track related uncertainties are lower due to their cancellation in the double ratio. The effect of photon conversions into e^+e^- pairs, as well as the effect of treating all charged particles as pions were found to be negligible. The total systematic uncertainty on R and λ parameters amounts to approximately 10-15% (see Table 1 of Ref. [2]).

6 Results

In Fig. 1 $R_2(Q)$ distributions measured at 0.9 and 7 TeV are compared with the Gaussian [8] and the exponential (Eqs. 2,4) fitting functions. The Gaussian function does not provide a satisfactory description of the low Q region, thus in what follows only exponential fits are considered.

The multiplicity dependence of the fitted parameters λ and R is shown in Fig. 2. The λ parameter decreases with n_{ch} as $\sim e^{-\delta \cdot n_{ch}}$, with a larger slope for lower $\sqrt{s}$. The R parameter scales as $\sim n_{ch}^{1/3}$ up to $n_{ch} \simeq 55$ independently of the center-of-mass energy, as predicted in Refs. [18, 19]. At $n_{ch} \gtrsim 55$, the fitted R parameter saturates at $\sim 2r_p$, in a qualitative consistence with Pomeron-based models [20]. However, a decrease of R at higher multiplicities predicted in these models is not observed in the data. The saturation of R at high multiplicities is observed for the first time.

The dependence of λ and R parameters on the average transverse momentum of the particle pair, $k_T = \frac{1}{2}|\vec{p}_{T,1} + \vec{p}_{T,2}|$, is shown in Fig. 3. The fitted chaoticity parameter λ tends to exponentially decrease with k_T, almost independently of $\sqrt{s}$. The R parameter also decreases with k_T exponentially, with a $\sqrt{s}$ independent slope and the intercept increasing with $\sqrt{s}$, as confirmed by the measurements at center-of-mass energies ranging from 200 GeV to 7 TeV.

7 Conclusion

In summary, the two-particle Bose-Einstein correlations were studied in pp collisions at $\sqrt{s} = 0.9$ and 7 TeV using pairs of like-sign charged particles with $p_T > 100$ MeV and $|\eta| < 2.5$ in events with the total charged multiplicity up to $n_{ch} = 240$.

The BEC effect manifested as an enhancement in the double-ratio $R_2(Q)$ (Eq. 3) at $Q < 200$ MeV was quantified by fitting the measured double-ratio by the function $R_2(Q) = 1 + \lambda \exp(-RQ)$, where R is an effective radius of the hadron production region and λ is the degree of emission incoherence. The effective radius R increases as $\sim n_{ch}^{1/3}$ for $n_{ch} \lesssim 55$, without a significant dependence on $\sqrt{s}$, and remains approximately constant for $55 < n_{ch} < 240$. The saturation of R at high multiplicities was observed for the first time at $\sqrt{s} = 7$ TeV only. The incoherence parameter λ was found to decrease with n_{ch}, with a slope increasing as $\sqrt{s}$ decreases. As a function of the average transverse momentum of the pair k_T, R exponentially decreases towards higher k_T values for any n_{ch}, while λ decreases with k_T without a significant n_{ch} dependence.

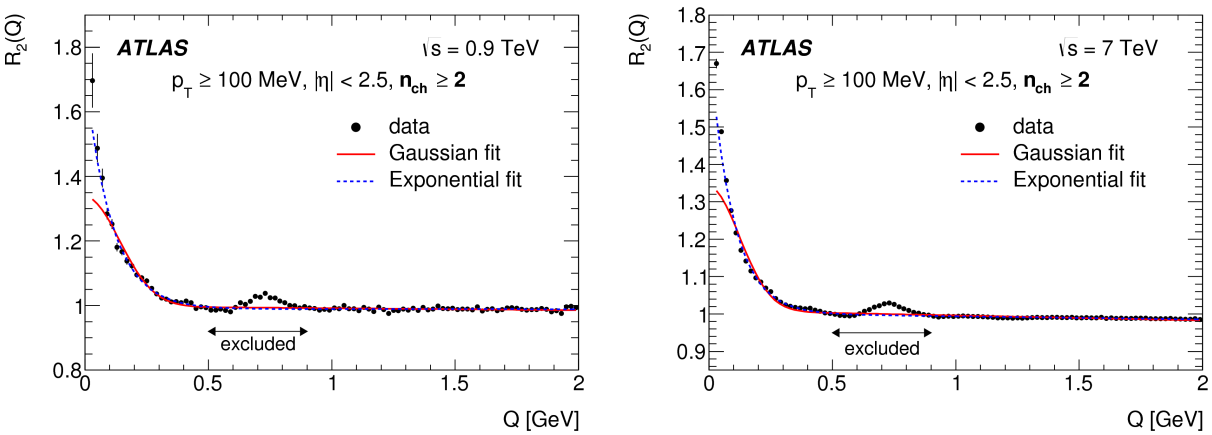

Figure 1: The two-particle double-ratio correlation function $R_2(Q)$ for charged particles in pp collisions at $\sqrt{s} = 0.9$ TeV (left) and 7 TeV (right). The lines show the Gaussian and exponential fits. The region affected by an overestimate of $\rho(770)$ production rate in the MC is excluded from the fits as indicated. The error bars represent the statistical uncertainties [2].

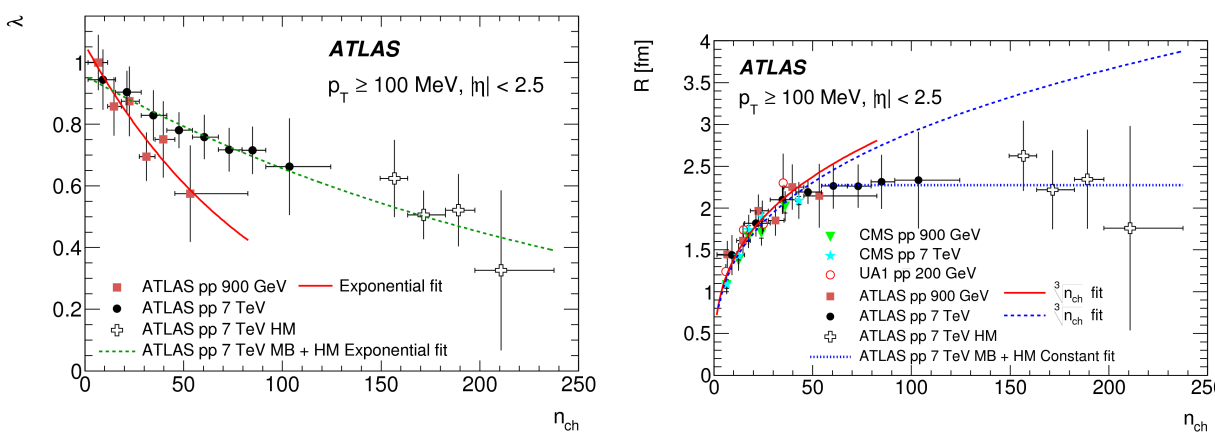

Figure 2: Multiplicity, n_{ch}, dependence of the parameters λ (left) and R (right) obtained from the exponential fit to $R_2(Q)$ at $\sqrt{s} = 0.9$ and 7 TeV, compared to the equivalent measurements of the CMS [3,4] and UA1 [21] experiments. The error bars represent the quadratic sum of the statistical and systematic uncertainties [2].

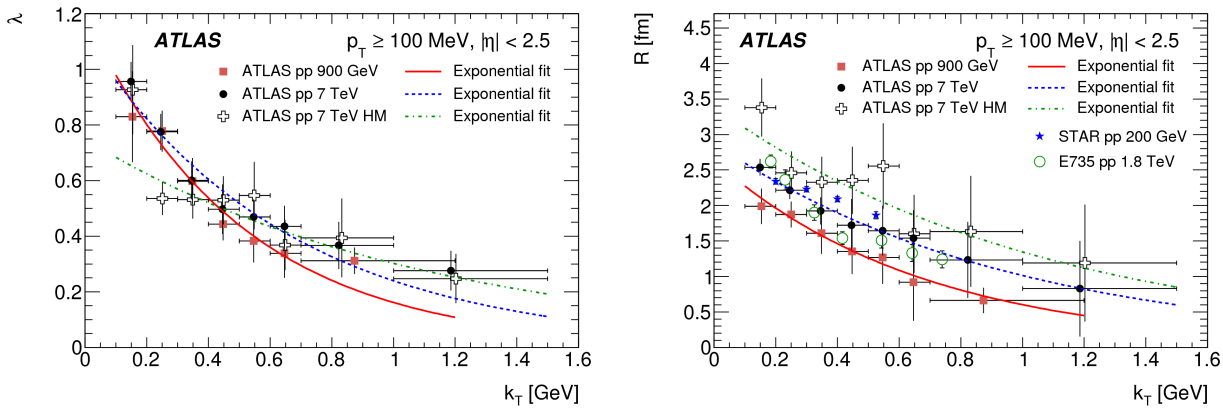

Figure 3: The k_T dependence of (a) λ and (b) R obtained from the exponential fit of $R_2(Q)$ at $\sqrt{s} = 0.9$ TeV, 7 TeV and 7 TeV high-multiplicity events. The average transverse momentum k_T of the particle pairs is defined as $k_T = |\vec{p}_{T,1} + \vec{p}_{T,2}|/2$. The solid, dashed and dash-dotted curves are results of the exponential fits at 0.9 TeV, 7 TeV and 7 TeV HMT, respectively. The results are compared to the corresponding measurements by the E735 experiment at the Tevatron [22], and by the STAR experiment at RHIC [23]. The error bars represent the quadratic sum of the statistical and systematic uncertainties [2].

The presented ATLAS measurement confirms the results obtained in other experiments at the same and lower energies, and extends them towards higher multiplicities and transverse momenta.

Acknowledgements

The full list of acknowledgements can be found in the original ATLAS paper [2]. The speaker is partially supported by Presidential Grant NSh-999.2014.2 (Russia) and Russian MES Grant RFMEFI61014X0005.

References

[1] ATLAS Collaboration, "The ATLAS Experiment at the CERN Large Hadron Collider," *JINST*, **3** (2008), S08003.

[2] ATLAS Collaboration, "Two-particle BoseEinstein correlations in pp collisions at $\sqrt{s} =$ 0.9 and 7 TeV measured with the ATLAS detector," *Eur. Phys. J.*, **C75** (2015) (10), 466, arXiv:1502.07947.

[3] CMS Collaboration, "First Measurement of Bose-Einstein Correlations in proton-proton Collisions at $\sqrt{s}$ =0.9 and 2.36 TeV at the LHC," *Phys. Rev. Lett.*, **105** (2010), 032001, arXiv:1005.3294.

[4] CMS Collaboration, "Measurement of Bose-Einstein Correlations in pp Collisions at $\sqrt{s} = 0.9$ and 7 TeV," *JHEP*, **05** (2011), 029, arXiv:1101.3518.

[5] K. Aamodt *et al.* (ALICE Collaboration), "Two-pion Bose-Einstein correlations in pp collisions at $\sqrt{s} = 900$ GeV," *Phys. Rev.*, **D82** (2010), 052001, arXiv:1007.0516.

[6] K. Aamodt *et al.* (ALICE Collaboration), "Femtoscopy of pp collisions at $\sqrt{s} = 0.9$ and 7 TeV at the LHC with two-pion Bose-Einstein correlations," *Phys. Rev.*, **D84** (2011), 112004, arXiv:1101.3665.

[7] M. Deutschmann *et al.* (Aachen-Berlin-Bonn-CERN-Cracow-London-Vienna-Warsaw Collaboration), "A Study of Second Order Interference for Pions Produced in Various Hadronic Interactions," *Nucl. Phys.*, **B204** (1982), 333.

[8] W. Kittel and E. A. De Wolf, Soft multihadron dynamics, ISBN-9789812562951, 2005.

[9] ATLAS Collaboration, "Charged-particle multiplicities in pp interactions at $\sqrt{s} = 900$ GeV measured with the ATLAS detector at the LHC," *Phys. Lett.*, **B688** (2010), 21, arXiv:1003.3124.

[10] ATLAS Collaboration, "Charged-particle multiplicities in pp interactions measured with the ATLAS detector at the LHC," *New J. Phys.*, **13** (2011), 053033, arXiv:1012.5104.

[11] Torbjorn Sjostrand, Stephen Mrenna, and Peter Z. Skands, "PYTHIA 6.4 Physics and Manual," *JHEP*, **05** (2006), 026, hep-ph/0603175.

[12] ATLAS Collaboration, "ATLAS Monte Carlo tunes for MC09," *ATL-PHYS-PUB-2010-002*, URL https://cds.cern.ch/record/1247375.

[13] ATLAS Collaboration, "The ATLAS Simulation Infrastructure," *Eur. Phys. J.*, **C70** (2010), 823, arXiv:1005.4568.

[14] R. Engel, "Photoproduction within the two component dual parton model. 1. Amplitudes and cross-sections," *Z. Phys.*, **C66** (1995), 203.

[15] Peter Z. Skands, "The Perugia Tunes," in "Proceedings, 1st International Workshop on Multiple Partonic Interactions at the LHC (MPI08)," 284–297, 2009, arXiv:0905.3418.

[16] K. Werner, Iu. Karpenko, T. Pierog, M. Bleicher, and K. Mikhailov, "Evidence for hydrodynamic evolution in proton-proton scattering at 900 GeV," *Phys. Rev.*, **C83** (2011), 044915, arXiv:1010.0400.

[17] Boris Tomasik and Urs Achim Wiedemann, "Central and noncentral HBT from AGS to RHIC," (2002), hep-ph/0210250.

[18] N. Suzuki and M. Biyajima, "Multiplicity dependence of identical particle correlations in the quantum optical approach," *Phys. Rev.*, **C60** (1999), 034903, hep-ph/9907348.

[19] Gideon Alexander and Edward Sarkisian, "The Many sources effect on the genuine multi - hadron correlations," *Nucl. Phys. Proc. Suppl.*, **92** (2001), 211, [,211(2000)], hep-ph/0008174.

[20] V. A. Schegelsky, A. D. Martin, M. G. Ryskin, and V. A. Khoze, "Pomeron universality from identical pion correlations at the LHC," *Phys. Lett.*, **B703** (2011), 288, arXiv:1101.5520.

[21] C. Albajar *et al.* (UA1 Collaboration), "Bose-Einstein Correlations in $\bar{p}p$ Interactions at $\sqrt{s}$ = 0.2 to 0.9 TeV," *Phys. Lett.*, **B226** (1989), 410, [Erratum: Phys. Lett.B229,439(1989)].

[22] T. Alexopoulos *et al.*, "A Study of source size in p anti-p collisions at s**(1/2) = 1.8-TeV using pion interferometry," *Phys. Rev.*, **D48** (1993), 1931.

[23] M. M. Aggarwal *et al.* (STAR Collaboration), "Pion femtoscopy in $p+p$ collisions at $\sqrt{s} = 200$ GeV," *Phys. Rev.*, **C83** (2011), 064905, arXiv:1004.0925.

Jet effects in high-multiplicity pp events

Antonio Ortiz[1], Gyula Bencédi[1,2], Héctor Bello[1,3], and Satyajit Jena[4]

[1]Instituto de Ciencias Nucleares, UNAM, 04510, México D. F., México
[2]Wigner Research Centre for Physics of the H.A.S., H-1121, Budapest, Hungary
[3]Facultad de Ciencias Físico Matemáticas, BUAP, 1152, Puebla, México
[4]University of Houston, Houston, TX 77204, USA

1 Introduction

The study of the high-multiplicity pp events has become important because we need to understand the origin of the fluid-like features which have been found in such small systems [1–4].

In this work we concentrate on the radial flow signatures, which not only hydrodynamical models can explain. Namely, the effect has been also found in PYTHIA [5] and it is attributed to multi-parton interactions (MPI) and color reconnection (CR) via boosted color strings [6]. For high-multiplicity events, the blast-wave parametrization, a hydro inspired model, has been found to fit very well the transverse momentum ($p_{\rm T}$) spectra of different particle species [7]. Although, the quality of the fits become worse for low-multiplicity events, we see that the parameter related to the average transverse expansion velocity ($\langle\beta_{\rm T}\rangle$) increases with increasing multiplicity. This effect is qualitatively similar to what has been seen at the LHC [8].

In PYTHIA, color reconnection was originally introduced in order to explain the rise of the average $p_{\rm T}$ with the event multiplicity. In short, the model allows the interaction among the partons which originate from MPI and initial-/final-state radiation. There are different implementations, e.g., the default MPI-based model of PYTHIA8.212 introduces a probability which is the largest for a low-$p_{\rm T}$ system to be reconnected with one of a harder $p_{\rm T}$ scale. And the interaction between two systems of high-$p_{\rm T}$ scales is not allowed. Such a soft-hard interaction also suggests that jets may play a role in the observed radial flow-like patterns as highlighted in [7,9].

In this work, the role of jets in high-multiplicity pp collisions is investigated using PYTHIA 8.212. The inclusive $p_{\rm T}$ spectra of identified particles are studied for events with and without jets, where the jets are reconstructed using the anti-$k_{\rm T}$ algorithm implemented in FastJet [10].

2 Results

Proton-proton collisions at $\sqrt{s} = 7$ TeV were simulated with PYTHIA8.212 using the tune Monash 2013 [11]. Events were classified according with their event multiplicity ($N_{\rm ch}$) and leading jet $p_{\rm T}$

($p_{\rm T}^{\rm jet}$). All the observables were calculated counting particles within $|\eta|<1$. For the jet finder only detectable particles (including charged and neutral particles) are considered within cone radius of 0.4, while for the $p_{\rm T}$ spectra and event multiplicity only charged particles are taken into account.

To investigate on the radial flow-like effects in jets we first study the proton-to-pion ratio in low-multiplicity events and as a function of $p_{\rm T}^{\rm jet}$ (see Fig. 1). It is worth noticing that events without jets[1] dominate for momenta below 2 GeV/c, while at larger momenta, jets start playing a more important role. In addition, a bump at intermediate $p_{\rm T}$ is observed in all the event classes. The $p_{\rm T}$, where the peak emerges, increases with increasing $p_{\rm T}^{\rm jet}$. This structure resembles one observed in the different colliding systems at the LHC [1, 12] and which sometimes is referred as a "flow peak" [6]. This effect is the same in events generated with and without color reconnection.

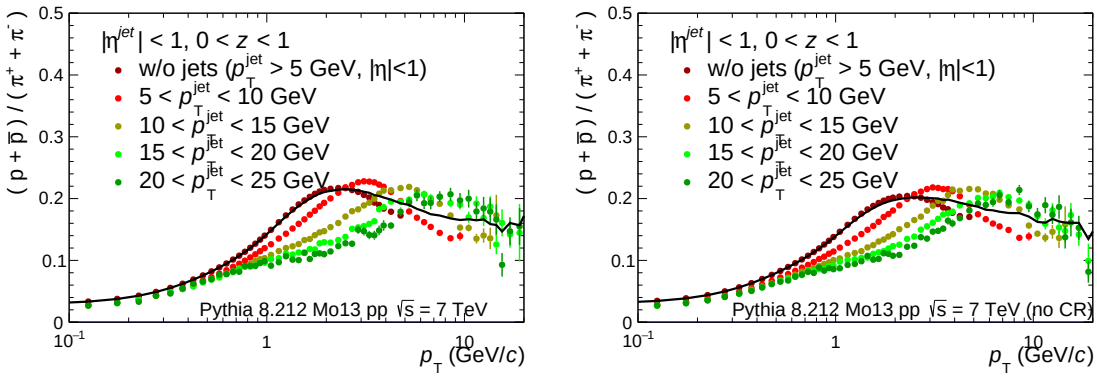

Figure 1: (Color online). Leading jet $p_{\rm T}$ dependence of the proton-to-pion ratio as a function of transverse momentum for low-multiplicity pp collisions at $\sqrt{s} = 7$ TeV. The results for the different $p_{\rm T}^{\rm jet}$ intervals (markers) are compared with the inclusive case (solid line). Events with (left) and without (right) color reconnection are shown.

The blast-wave analysis of the $p_{\rm T}$ spectra has been performed using the same particle species and $p_{\rm T}$ intervals described in [7]. Figure 2 shows that the hydro model can describe the PYTHIA $p_{\rm T}$ spectra when jets with momentum above 5 GeV/c are part of the event. Actually, a $\langle\beta_{\rm T}\rangle$ of $\approx$0.5 can be achieved when the jet $p_{\rm T}$ is larger than 20 GeV/c. Contrarily, the model does not describe the spectra in events without jets. This result is consistent with the spherocity analysis reported in [7], where it was argued that the fast parent parton being a boosted system can mimic radial flow too. The same analysis was also implemented for high-multiplicity events, in that case, thanks to color reconnection, the quality of the fit improves in events without jets, however a small $\langle\beta_{\rm T}\rangle$ ($\approx$0.37) is obtained and it increases up to $\approx$0.51 when a high-$p_{\rm T}$ jet is identified in the event. Actually, when a high-$p_{\rm T}$ jet was required, a very weak multiplicity dependence of $\langle\beta_{\rm T}\rangle$ is observed.

[1]Events without jets are those where the jet finder can not reconstruct one with $p_{\rm T}^{\rm jet}>5$ GeV/c.

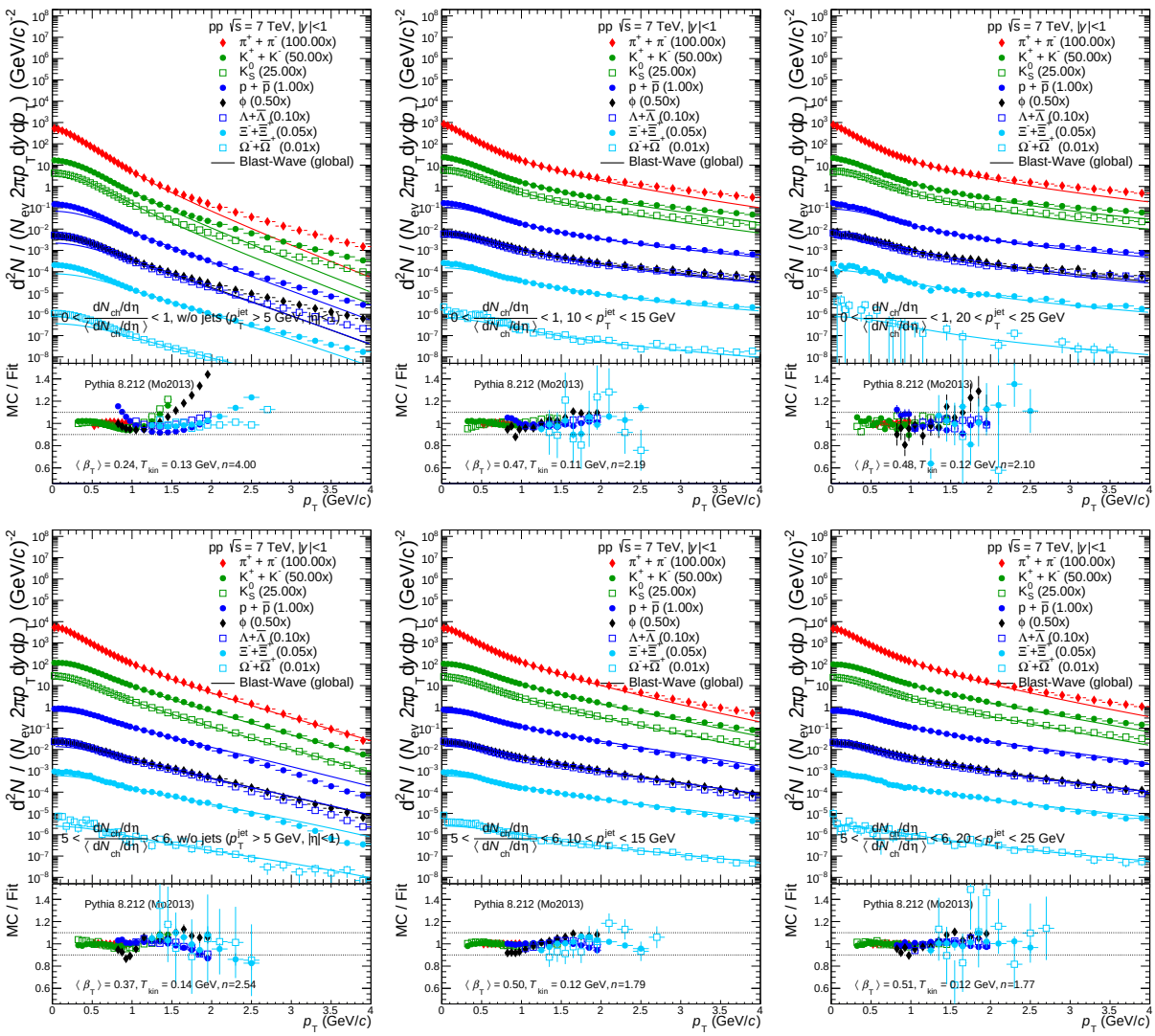

Figure 2: (Color online). Leading jet p_{T} dependence of the transverse momentum spectra for low (top) and high (bottom) multiplicity pp collisions at $\sqrt{s} = 7$ TeV. The blast-wave parametrization is shown with solid lines.

3 Summary

In summary, we have studied the role of jets in the radial flow-like features of PYTHIA. We have found that even in low-multiplicity events the blast-wave model is able to describe the p_{T} spectra of different particle species only when jets are part of the event. At high-multiplicity, $\langle\beta_{\mathrm{T}}\rangle$ can be very small in events without jets ($\approx$0.37). The interaction of jets with the soft component is therefore important to produce the observed effects in PYTHIA. This seems to be a promising tool which could be exploited by the experiments in order to understand better the LHC data.

Acknowledgements

The authors acknowledge the useful discussions with Guy Paić, Eleazar Cuautle, Peter Christiansen and Gergely Barnaföldi. Support for this work has been received from CONACYT under the grant No. 260440; from DGAPA-UNAM under PAPIIT grants IA102515, IN105113, IN107911 and IN108414; and OTKA under the grant NK106119. The EPLANET program supported the mobility from Mexico to Europe and vis.

References

[1] A. Ortiz (ALICE), "Overview of ALICE results," *Nuclear and Particle Physics Proceedings*, **267-269**(2015), 403, x Latin American Symposium of High Energy Physics.

[2] Jaroslav Adam *et al.* (ALICE), "Multiplicity dependence of charged pion, kaon, and (anti)proton production at large transverse momentum in p-Pb collisions at $\sqrt{s_{\mathrm{NN}}}$ = 5.02 TeV," (2016), 1601.03658.

[3] N. Armesto and E. Scomparin, "Heavy-ion collisions at the Large Hadron Collider: a review of the results from Run 1," (2015), 1511.02151.

[4] I. Bautista, A. Fernandez, and P. Ghosh, "Indication of change of phase in high-multiplicity proton-proton events at LHC in String Percolation Model," *Phys. Rev.*, **D92**(2015) (7), 071504.

[5] T. Sjöstrand, S. Ask, J. R. Christiansen, R. Corke, N. Desai, P. Ilten, S. Mrenna, S. Prestel, C. O. Rasmussen and P. Z. Skands, "An Introduction to PYTHIA 8.2," *Comput. Phys. Commun.*, **191**(2015), 159.

[6] A. Ortiz, P. Christiansen, E. Cuautle, I. Maldonado, Ivonne and G. Paić, "Color Reconnection and Flowlike Patterns in pp Collisions," *Phys. Rev. Lett.*, **111**(2013) (4), 042001.

[7] A. Ortiz, E. Cuautle and G. Paić, "Mid-rapidity charged hadron transverse spherocity in pp collisions simulated with Pythia," *Nucl. Phys.*, **A941**(2015), 78.

[8] B. Abelev et al. (ALICE), "Multiplicity Dependence of Pion, Kaon, Proton and Lambda Production in p-Pb Collisions at $\sqrt{s_{NN}}$ = 5.02 TeV," *Phys. Lett.*, **B728**(2014), 25.

[9] A. Ortiz, "Mean p_{T} scaling with m/n_q at the LHC: Absence of (hydro) flow in small systems?" *Nucl. Phys.*, **A943**(2015), 9.

[10] G. P. Salam M. Cacciari and G. Soyez, "FastJet User Manual," *Eur. Phys. J.*, **C72**(2012), 1896.

[11] S. Carrazza P. Skands and J. Rojo, "Tuning PYTHIA 8.1: the Monash 2013 Tune," *Eur. Phys. J.*, **C74**(2014) (8), 3024.

[12] J. Adam et al. (ALICE), "Centrality dependence of the nuclear modification factor of charged pions, kaons, and protons in Pb-Pb collisions at $\sqrt{s_{\mathrm{NN}}} = 2.76$ TeV," (2015), 1506.07287.

Color fluctuation phenomena in high energy hadron and photon nucleus collisions

Mark Strikman[1]

[1]Penn State University, Univeristy Park, PA 16802, USA

1 Introduction

An important feature of high energy QCD processes is the color coherence. It is a consequence of compositeness of the bound states and the Lorentz slowing down of interaction. Here we focus on the evidence for color fluctuation effects from pA collisions at the LHC and coherent photoproduction of ρ-mesons. We also outline briefly perspectives of future studies of this phenomenon in electron (photon) nucleus collisions.

An early manifestation of the coherence of high energy interaction was the observation that the contribution of planar diagrams of exchange by two ladders corresponds to the amplitudes decreasing with energy as $1/s$. The physical reason for this behavior is that a sufficiently energetic hadron being a composite particle can be considered as the superposition of configurations of constituents described by the wave function of a hadron. Due to the Lorentz slowing down of interaction such configurations are frozen during the coherent length/ time interval

$$l_{coh} = 2P_h/(m^2_{conf} - m^2_h), \tag{1}$$

when coherence length is much larger that the proton/nucleus size. Thus at high energies interaction of the projectile hadron with a target is given by the sum over the interactions of frozen configurations of constituents of the projectile. This is the origin of coherence phenomena specific for high energy processes.

Hence a projectile hadron scatters off the nucleus in different configurations of constituents, each of which is frozen during the passing through the nucleus. Thus the strength of its interactions with nucleons along its path should remain constant and it is legitimate to introduce probability distribution for the hadron to be in configuration with the interaction strength σ – $P_h(\sigma)$ For small σ it was expressed in QCD in terms of the wave function of projectile [1]. The sum rules $\int P_h(\sigma)d\sigma = 1$, $\int P_h(\sigma)\sigma d\sigma = \langle\sigma\rangle \equiv \sigma_{tot}$ follow from the probability conservation and from the definition of the configuration-averaged cross section. The variance of the distribution is given by

$$\left\langle\sigma^2\right\rangle / \left\langle\sigma\right\rangle^2 - 1 = \omega_\sigma \tag{2}$$

Eq. 2 follows directly from the optical theorem and the definition of $P_h(\sigma)$, and was first introduced in [2] by reinterpreting formulae of quasieikonal approximation in the spirit of the scattering eigenstate formalism. These and several other considerations constrain the shape of $P_h(\sigma)$ [1]. In our numerical studies we will use parametrization of $P_h(\sigma)$ for the proton suggested in [1]

$$P_N(\sigma_{tot}) = \frac{\rho}{\sigma_0}\left(\frac{\sigma_{tot}}{\sigma_{tot}+\sigma_0}\right)\exp\left\{-\frac{(\sigma_{tot}/\sigma_0-1)^2}{\Omega^2}\right\}. \quad (3)$$

2 Color fluctuation effects in pA collisions

Account for fluctuations of the strength of the interaction which we will refer to as color fluctuations (CF) leads to a broadening of the distribution over the number of wounded nucleons, ν. The distribution is expressed through $P_{in}(\sigma)$ - differential probability that projectile interacts with a particular inelastic cross section:

$$\sigma_\nu = \int d\sigma P_{in}(\sigma)\frac{A!}{(A-\nu)!\,\nu!}\int d^2\vec{b}\,x(b)^\nu\left[1-x(b)\right]^{A-\nu}, \quad (4)$$

where $x(b)=\sigma_{in}T(b)/A$ and the normalization is $\int d^2\vec{b}\,T(b)=A$. $P_{in}(\sigma)$ and $P_{tot}(\sigma)$ are trivially related under a natural assumption that σ_{el}/σ_{tot} is approximately the same for different configurations. The Glauber model expression [3] corresponds to the limit $P_{in}(\sigma)=\delta(\sigma_{in}-\sigma)$.

Eq.4 resembles formulae of the Gribov Reggeon calculus, where the factor of $x(b)^\nu$ corresponds to ν cut Pomeron exchanges and the factor of $[1-x(b)]^{A-\nu}$ — to $A-\nu$ uncut Pomeron exchanges while the integral over σ with weight $P_{in}(\sigma)$ describes the ν-Pomeron – projectile coupling. Eq. 4 is essentially probabilistic, reflecting the semiclassical picture of high energy inelastic interactions with nuclei. The Monte Carlo (MC) which includes accurately both geometry of the NN interactions and nuclear correlations was presented in [4]. The calculation confirms much broader distribution over ν in the CF approach. In the calculation we use parametrization Eq.3 with $\omega_\sigma=0.1$ which corresponds to our estimate of ω_σ at the LHC energies using Eq.2 and limited LHC data on diffraction. The predicted broader distribution over ν and $\omega_\sigma\sim 0.1$ is consistent with the analysis of ATLAS which studied dependence of the multiplicity at the central rapidities as a function of transverse energy, $\sum E_T$ at -4.9 $<\eta<$ - 3.2 in the nucleus-going direction in pA have collisions at $\sqrt{s}$ = 5.02 TeV [5].

It was argued that quarks with large x in the fast frame belong to configurations with large relative momenta in the rest frame and, thus, of a smaller size and it was suggested to test this expectation in the p -A scattering by measuring the x dependence of average ν for events where a hard process involve a large x parton [6]. The studies of the centrality dependence of the jet production in pA scattering were reported in [7, 8]. The pattern of deviation from the Glauber model is consistent with the above expectations. A quantitative analysis of the ATLAS data was reported in [9] focusing on production of jets in the kinematics where jet production involves scattering off a quark of the proton with large $x\sim 0.6$. It was demonstrated that $\langle\sigma(x\sim 0.6)\rangle/\sigma_{in}$ describes well the jet rate as a function of centrality. Further studies of this process at the LHC as well as analysis of a similar effect observed in $d-Au$ collisions at BNL are under way.

3 Color fluctuation effects in ultra peripheral processes

The coherent photoproduction of ρ mesons in the $\gamma A \to \rho A$ process is usually considered as due to transition of $\gamma \to \rho$ and consequent interaction of the ρ meson with a target A. Recently this process was studied at significantly larger energies in ultra peripheral collisions (UPC) of heavy ions at the LHC [10]. A comparison of the data with a "classical" vector dominance model (VDM) in which one assumes that $\sigma_{tot}(\rho N) = \sigma_{tot}(\pi N)$ and takes into account for elastic shadowing significantly overestimates cross section of the coherent ρ-meson production in $\gamma Pb \to \rho Pb$ at $W \sim 50GeV$. Our analysis [11]. has demonstrated that CFs in the case of transition of the photon to hadronic configurations which produce ρ-mesons are much larger than in the case of the proton interactions resulting in a large enhancement of the nuclear shadowing which explains the ALICE data.

The experimental studies of the jet production in pA scattering described in section 2 indicate that in the case when average configurations in nucleon are selected by the trigger, the distribution in ΣE_T gives an accurate information about *average* strength of interaction of nucleon with the nucleons. Conversely, one can extract from the distribution in ΣE_T at rapidities far enough from the projectile average strength of interaction for a particular trigger.

At the LHC it is feasible to study the ultraperipheral ion collisions at least up to $W_{\gamma N} \sim 0.5TeV$ [12]. This opens a way to exploring the high energy photon wave function in great detail along the lines we described in section 2 for pA scattering. In fact, CF effects should be larger in this case. Indeed for the component corresponding to the VDM contribution we expect $\omega_\sigma \sim 0.5 \div 0.6$ like for the pion. A large fraction of the non VDM contribution originates from aligned jet configurations (large mass, low transverse momentum $q\bar{q}$ configurations) which interact with a strength comparable to that of pion, cf discussion of the aligned jet model in [13] and likely to have similar CFs. There is also a contribution from small size $q\bar{q}$ dipoles. Distribution over ν for γA scattering can be calculated using Eq.4. The production of hadrons at large negative rapidities is expected to be very similar for proton and photon projectiles for the same ν. Hence by studying distribution in ΣE_T for different forward triggers it would be possible to determine both $\langle\sigma\rangle$ and variance of the distribution for selected configuration. A starting point would be to investigate the direct photon ($x_\gamma = 1$) dijet production. For $x_A \geq 0.01$ we expect $\nu \approx 1$. In this case the distribution over ΣE_T should be similar to that in γp scattering. For smaller x_A the leading twist shadowing sets in resulting in a broader distribution over ν, see discussion in sections 6.3, 6.4 of [14]. With a decrease of x_γ distribution over ΣE_T should become broader and approach for small x_γ distribution for generic γA collisions. Our first numerical estimates indicate that the distribution over ν should be very broad with a significant fraction of events with $\nu \geq 5$. Other interesting triggers are production of leading charm, strangeness, etc.

Acknowledgements

I thank collaborators in the studies summarized above: M. Alvioli, G.Baym, B. Cole, L. Frankfurt, V.Guzey, D. Perepelitsa, M.Zhalov for numerous discussions.

References

[1] B. Blaettel, G. Baym, L. L. Frankfurt, and M. Strikman, "How transparent are hadrons to pions?" *Phys. Rev. Lett.*, **70**(1993), 896.

[2] Hannu I. Miettinen and Jon Pumplin, "Diffraction Scattering and the Parton Structure of Hadrons," *Phys. Rev.*, **D18**(1978), 1696.

[3] L. Bertocchi and D. Treleani, "Glauber Theory, Unitarity, and the AGK Cancellation," *J. Phys.*, **G3**(1977), 147.

[4] M. Alvioli and M. Strikman, "Color fluctuation effects in proton-nucleus collisions," *Phys. Lett.*, **B722**(2013), 347, 1301.0728.

[5] The ATLAS collaboration (ATLAS), "Measurement of the centrality dependence of the charged particle pseudorapidity distribution in proton-lead collisions at $\sqrt{s_{NN}} = 5.02$ TeV with the ATLAS detector," (2013).

[6] L. L. Frankfurt and M. I. Strikman, "Point-like configurations in hadrons and nuclei and deep inelastic reactions with leptons:EMC and EMC like effects ," *Nucl. Phys.*, **B250**(1985), 143.

[7] Georges Aad *et al.* (ATLAS), "Centrality and rapidity dependence of inclusive jet production in $\sqrt{s_{\rm NN}} = 5.02$ TeV proton-lead collisions with the ATLAS detector," *Phys. Lett.*, **B748**(2015), 392, 1412.4092.

[8] Serguei Chatrchyan *et al.* (CMS), "Studies of dijet transverse momentum balance and pseudorapidity distributions in pPb collisions at $\sqrt{s_{\rm NN}} = 5.02$ TeV," *Eur. Phys. J.*, **C74**(2014) (7), 2951, 1401.4433.

[9] Massimiliano Alvioli, Brian A. Cole, Leonid Frankfurt, D. V. Perepelitsa, and Mark Strikman, "Evidence for x-dependent proton color fluctuations in pA collisions at the LHC," *Phys. Rev.*, **C93**(2016) (1), 011902, 1409.7381.

[10] Jaroslav Adam *et al.* (ALICE), "Coherent $?^0$ photoproduction in ultra-peripheral Pb-Pb collisions at $\sqrt{s_{\rm NN}} = 2.76$ TeV," *JHEP*, **09**(2015), 095, 1503.09177.

[11] L. Frankfurt, V. Guzey, M. Strikman, and M. Zhalov, "Nuclear shadowing in photoproduction of ρ mesons in ultraperipheral nucleus collisions at RHIC and the LHC," *Phys. Lett.*, **B752**(2016), 51, 1506.07150.

[12] A. J. Baltz, "The Physics of Ultraperipheral Collisions at the LHC," *Phys. Rept.*, **458**(2008), 1, 0706.3356.

[13] L. L. Frankfurt and M. I. Strikman, "Hard Nuclear Processes and Microscopic Nuclear Structure," *Phys. Rept.*, **160**(1988), 235.

[14] L. Frankfurt, V. Guzey, and M. Strikman, "Leading Twist Nuclear Shadowing Phenomena in Hard Processes with Nuclei," *Phys. Rept.*, **512**(2012), 255, 1106.2091.

Multi-particle production in small colliding systems from the Color Glass Condensate

Prithwish Tribedy[1]

[1]Physics Dept, Bdg. 510A, Brookhaven National Laboratory, Upton, NY-11973, USA

1 Introduction

Recent measurements of multi-particle correlations in high multiplicity events in small collisions systems such as p+p, p+A, d+A, ^{3}He+A resemble many features that are commonly observed in heavy ion collisions. Some of the observations are generally attributed to final state collective effects due to hydrodynamic flow. However alternative explanations can be obtained for a number of such phenomena using the framework of Color Glass Condensate effective field theory (CGC EFT) that includes *ab inito* treatment of multi-parton interactions (MPI) of QCD at high energies. We highlight some of the recent developments and challenges in this direction. In particular, we discuss on : 1) the origin of high multiplicity events and 2) the appearance of long-range azimuthal correlations in such events in small collision systems.

2 The CGC framework of multi-particle production

The fact that long-range ridge like correlations appear only in high multiplicity events in small colliding systems indicates the same underlying dynamics possibly drives these two phenomena. The first step is to understand the origin of high multiplicity events that populate the long tail of experimental multiplicity distributions. The probability distribution of multiplicity $P(n)$ contains the information of n-particle correlations, a first principle estimation of which is a challenging problem. This requires full treatment of different sources of initial state fluctuations of the wave functions of the colliding systems and a framework of multi-particle production. In the CGC EFT, the saturation scale (Q_S^2) is the natural scale controlling sub-nucleonic scale fluctuations which combined with the knowledge of nuclear geometry accounts for major sources of such initial-state fluctuations. Significant progress has been made in recent years to model these fluctuations using the framework of IP-Glasma model. Recently the importance of additional sources of initial state fluctuations have been realized, the origin of which is intrinsically non-perturbative and not captured in the conventional framework of CGC. Such fluctuations lead to a distribution of the intrinsic saturation scale of the hadron or nucleus as shown in Fig.1(left) and has to be introduced in the IP-Glasma model [1]. With the initial state including different sources of fluctuations constrained by the HERA data, the CGC EFT can be generalized to estimate n-particle production.

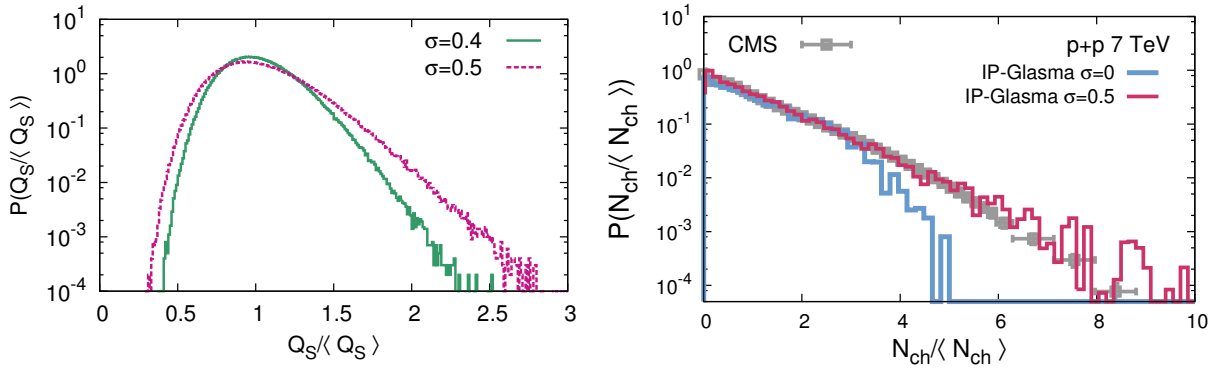

Figure 1: (left) Distribution of the saturation scale of proton driven by stochastic dipole splitting. (right) Effect of intrinsic fluctuation of proton saturation scale on the probability distribution of multiplicity ($\sigma = 0$ corresponds to no fluctuation of Q_S). The two figures are from Ref [1]

For a given configuration of initial color charge, the n-particle distribution is a negative binomial distribution (NBD) with mean and width related to the saturation scale. Due to fluctuation of impact parameter, a convolution of many such NBDs gives rise to the final probability distribution of multiplicity. However it has been demonstrated that such distribution is narrower compared to the data. Only after including the intrinsic fluctuations of the proton saturation scale one can describe the tails of the experimental multiplicity distributions (Fig.1(right)). Since multiplicity is dominated by low momentum ($p_T < 1$GeV) gluons, it is very challenging to implement a scheme of fragmentation for the production of soft hadrons. Therefore in this approach the number of produced charged particles are taken to be proportional to the number of gluons estimated in the IP-Glasma model. The results shown in Fig.1 indicate that the high multiplicity events that populate the tail of $P(n)$ distributions are generated due rare high color charge density configurations of the wave functions of the colliding systems.

3 Azimuthal correlations in CGC

CGC EFT predicts azimuthal collimation of the particles produced in the high multiplicity events. These collimations originate due to scatting of a parton from the projectile probing the color domains of size $\sim 1/Q_S$ in the target. These are microscopic correlations and suppressed by the number domains which are un-correlated with each other, therefore only dominate for smaller systems. This is quite a contrast to the picture of azimuthal correlations driven by hydrodynamic response to some global spacial geometric anisotropy. A number of processes lead to the emergence of azimuthal correlations in CGC. The Feynman diagrams describing the process of correlated two particle production are referred as "Glasma" graphs. Eight of such graphs give rise to non-factorizable two particle correlations that has symmetric structure in relative azimuthal angle $\Delta\phi$ around $\pi/2$ (see Fig.2). An additional diagram includes the contribution that can be factorized into the product of two single particle distributions, which is expected to have no modulation in $\Delta\phi$. However due to fluctuations leading to event-by-event breaking of the rotational invariance

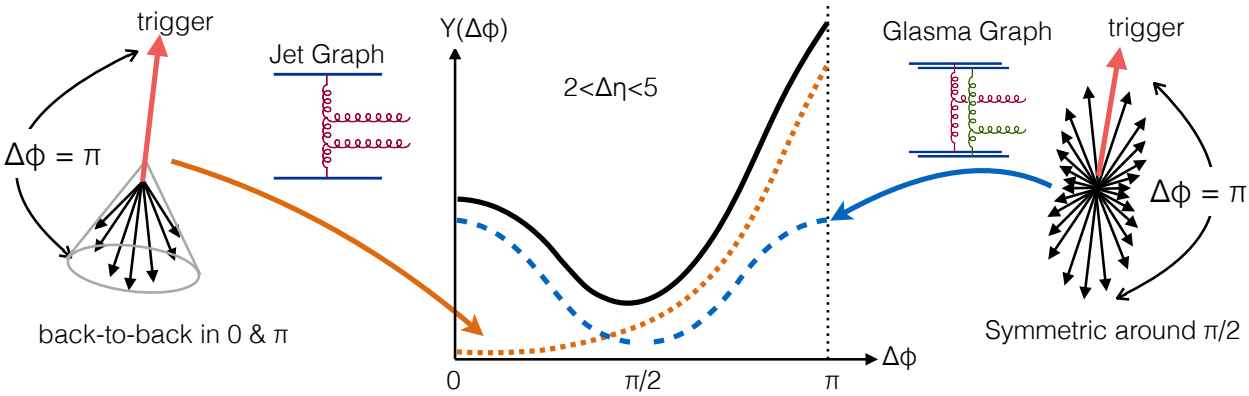

Figure 2: A cartoon showing the contributions of di-jet and glasma graphs in two particle correlation function $Y(\Delta\phi)$ integrated over a broad range of $|\Delta\eta|$.

of the color charge density, a momentum space anisotropy is introduced in the single particle distributions. Therefore all the "Glasma" graphs contribute to dominant two-particle correlations at early stages of collisions, they however produce collimations that are only symmetric around $\Delta\phi = \pi/2$. When decomposed in terms of the Fourier coefficients of the particle distributions, they give rise to non-zero even harmonics v_n. Further contributions to the azimuthal collimations come from the multiple scattering of partons during the space time evolution of the Glasma gluon fields after the collisions. These late time effects have been shown [2] to contribute to azimuthal correlations leading to both even and odd v_n. The boost invariant structure of the Glasma gluon fields extend the structure of azimuthal two particle correlations over a wide range in rapidity difference $\Delta\eta$.

The experimentally observed distribution of two-particle correlations when plotted in $\Delta\eta-\Delta\phi$ is also dominated by back-to-back di-jet productions. Such processes (also referred as "Mueller-Navelet" jets) are kinematically constrained to produce only away side (peaked at $\Delta\phi = \pi$) collimations. The relative strength of the di-jet production represented by the "Jet-Graph" and the "Glasma-Graphs" determines the features of the observed di-hadron correlations as shown in Fig.2. In high multiplicity events a relative enhancement of the Glasma graphs by α_S^{-4} compared to the "Jet-graphs" leads to a pronounced near side collimation at $\Delta\phi \sim 0$ that extends over a wide range of rapidity referred as "near side ridge". Since the near-side collimation is driven by the dynamics of gluon saturation, the strength of such correlations is determined by the saturation scale Q_S^2 that also determines the inclusive multiplicity. This results in an energy independent universal scaling of the near-side yield of ridge-like correlations when plotted against multiplicity in p+p collisions as shown in Fig.3 (left). This particular phenomenon observed in recent measurements confirms that multi-particle productions in small collision systems are driven by a single saturation scale as captured in the framework of the CGC EFT. Systematics of azimuthal correlations in both p+p and p+A collisions have been very well described both qualitatively and quantitatively in the CGC framework. Classical Yang-Mills simulations performed in [2] have recently demonstrated that the observation of non-zero positive odd v_n coefficients (Fig.3(right)) that are often attributed to collective hydrodynamic correlations can also be described from initial state

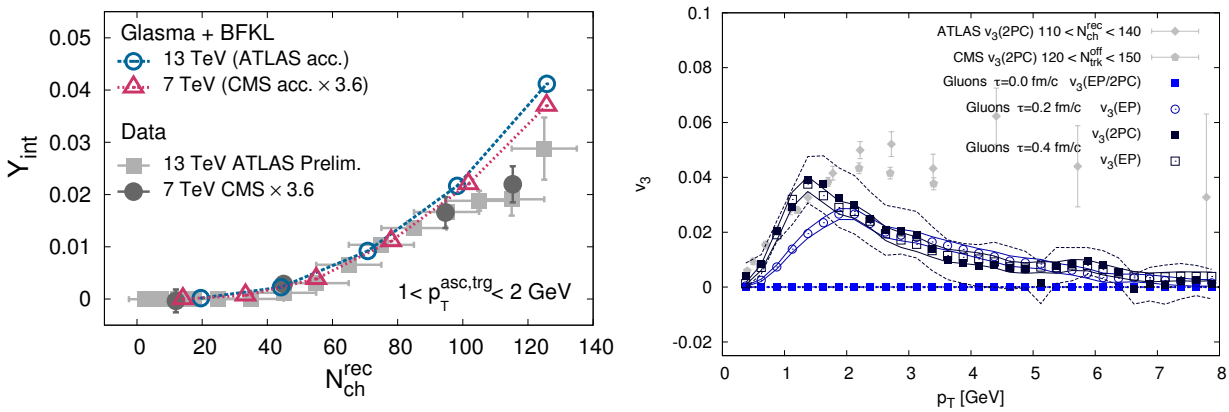

Figure 3: Left: The energy independence of the near side ridge yield in p+p collisions obtained from [3], Right: $v_3(p_T)$ in p+Pb collisions from Yang-Mills simulations, figure obtained from [2]

dynamics included in the CGC EFT.

4 Summary

We have argued how the dynamics of gluon saturation included in the CGC EFT provide consistent explanations to multi-particle production in small systems. A major challenge in this approach is to implement a scheme of fragmentation of produced gluons into hadrons, work in this direction is under progress.

Acknowledgements

We thank K. Dusling, L. McLerran, B. Schenke, S. Schlichting and R. Venugopalan for important discussions. This work was supported under Department of Energy Contract No. DE-SC0012704. We thank ICTP for hospitality and support during the MPI@LHC conference.

References

[1] Larry McLerran and Prithwish Tribedy, "Intrinsic Fluctuations of the Proton Saturation Momentum Scale in High Multiplicity p+p Collisions," *Nucl. Phys.*, **A945**(2016), 216, 1508.03292.

[2] Bjoern Schenke, Soeren Schlichting, and Raju Venugopalan, "Azimuthal anisotropies in p+Pb collisions from classical Yang? Mills dynamics," *Phys. Lett.*, **B747**(2015), 76, 1502.01331.

[3] Kevin Dusling, Prithwish Tribedy, and Raju Venugopalan, "Energy dependence of the ridge in high multiplicity proton-proton collisions," *Phys. Rev.*, **D93**(2016) (1), 014034, 1509.04410.

Preview from RHIC Run 15 pp and pAu Forward Neutral Pion Production from Transversely Polarized Protons

Steven Heppelmann[1]

[1]Penn State University(For STAR Collaboration)

1 STAR FMS Transverse Single Spin Asymmetries (TSSA)

The STAR collaboration has observed unexpected transverse momentum dependence in the forward single spin asymmetry of neutral pion production from pp collisions at center of mass energies of 200 GeV [1] and 500 GeV [2]. The transverse single spin asymmetry (TSSA) is defined by

$$A_N = \frac{\sigma^{\uparrow} - \sigma^{\downarrow}}{\sigma^{\uparrow} + \sigma^{\downarrow}}$$

with σ the observed cross section for pions scattering to the left and with transverse proton spin up $\uparrow$ or down $\downarrow$. The trends observed in these preliminary measurements stand in sharp contrast to a general argument that these asymmetries, as higher twist effects in a collinear fragmentation framework, should fall with transverse momentum p_T above a nominal p_T scale of about 1 or 2 GeV/c at fixed Feynman X_F. In conventional collinear Perturbative QCD (PQCD) models, the forward pions at large Feyman X_F and p_T >1 or 2 GeV/c are expected to come from the leading fragments of forward jets from hard parton interactions and should be observed above a background of soft jet fragments. With collinear factorization assumptions, the hard parton cross section does not significantly depend upon the transverse spin of the parton and neither would the forward pion cross section. Only by including the effects related to transverse components of parton momentum can significant asymmetries be modelled.

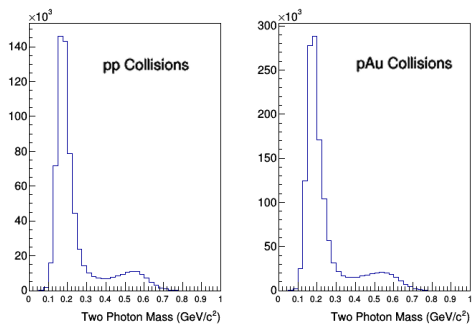

Figure 1: An example of the leading photon pair mass distributions used to select π^0 events is shown. For this sample, the π^0 energy range is 45 GeV<E<55 GeV and the transverse momentum range is 4 GeV/c < p_T <5 GeV/c. The same π^0 event selection, described in the text, is applied to proton-proton (left) and proton-gold (right) data. In this kinematic region, the selection criterion cuts off the mass distribution just above the η mass.

Characterizations of transverse parton momentum effects in the initial state are referred to as the Sivers effect [3,4] or in the final state fragmentation process are referred to as the Collins effect [5].

Many calculations have been done based on these ideas, focusing on the details of the role for parton transverse momentum [6–8]. However, the general argument about higher twist still should constrain the detailed predictions. Calculations have been done [9] that explore the parametriza tions of fragmentation that is required to push the p_T scale to larger values, as STAR has observed. It was also suggested in that analysis that at lower p_T the ratio of the TSSA asymmetry in pAu to pp is given by the ratio of the saturation scales in the pp and pAu systems.

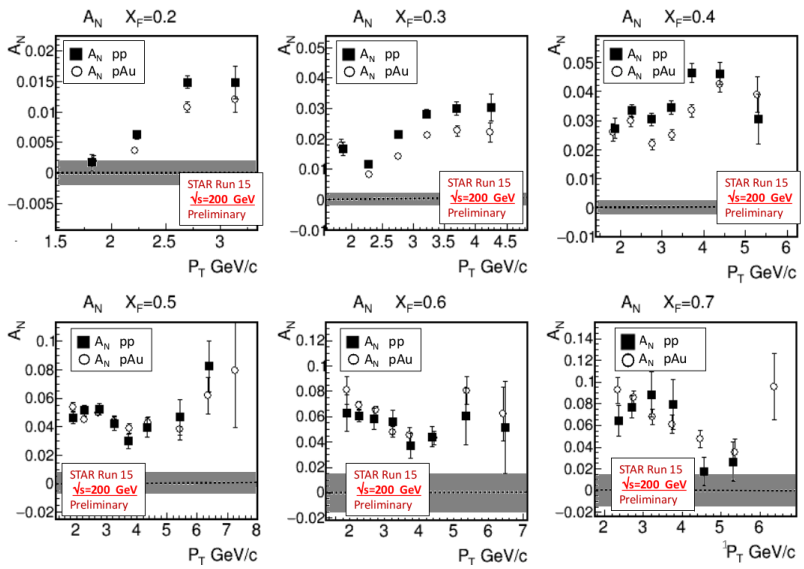

Figure 2: Comparison of TSSA A_N for forward π^0 production as a function of transverse momentum (p_T) for six Feynman x_F regions from 0.2 to 0.7 . The event selection is described in the text for both pp and pAu collisions at $\sqrt{s_{NN}} = 200$ GeV. The filled squares represent the asymmetries measured in pp and the open circles represent the asymmetries for pAu scattering. Systematic errors indicated by the bands at the bottom of each plot are dominated by variation in the asymmetry depending on Beam Beam Counter cuts, which could be an indication of centrality dependence.

2 TSSA Comparison Between pAu and pp Collisions

STAR has measured forward π^0 asymmetry A_N with the FMS electromagnetic calorimeter using data from the 2015 RHIC run from pp and pAu collisions. The data were collected from collisions with nucleon-nucleon center of mass energy of $\sqrt{s_{NN}} = 200$ GeV. The FMS detector covered the pseudo-rapidity range $2.6 < \eta < 4.0$, in the direction forward to the polarized proton. As in a jet analysis, the electromagnetic energy in each event is organized into clusters, where a cluster is defined by a cone radius of 0.035 radians and contains a minimum of 1 photon shower with energy > 3 GeV. The π^0 event sample is selected by finding the highest energy photon pair within the highest energy cone cluster in the event, with photon energies E_1 and E_2 each >3 GeV. We

further cut the sample based on the pion decay distribution with $|Z| < 0.7$ where $Z \equiv \frac{E_1 - E_2}{E_1 + E_2}$. The selected pion signal is obtained from the mass peak of the 2 photon distribution, selecting events with mass in the range $|M_{\gamma\gamma} - 0.135| < 0.12$ GeV/c^2. The pions are selected to satisfy an FMS p_T threshold trigger and a condition on the STAR Beam Beam counters [10], implying a real pp or pAu collision. For typical two photon mass distributions (Figure 1) the background under the π^0 mass peak is about 10% for the selected region. This selected event sample is then used to calculate the asymmetry A_N in Figures 2 and 3. In this kinematic region, this selection algorithm is nearly equivalent to inclusive event selection. In Figure 2, we show preliminary results, comparing A_N

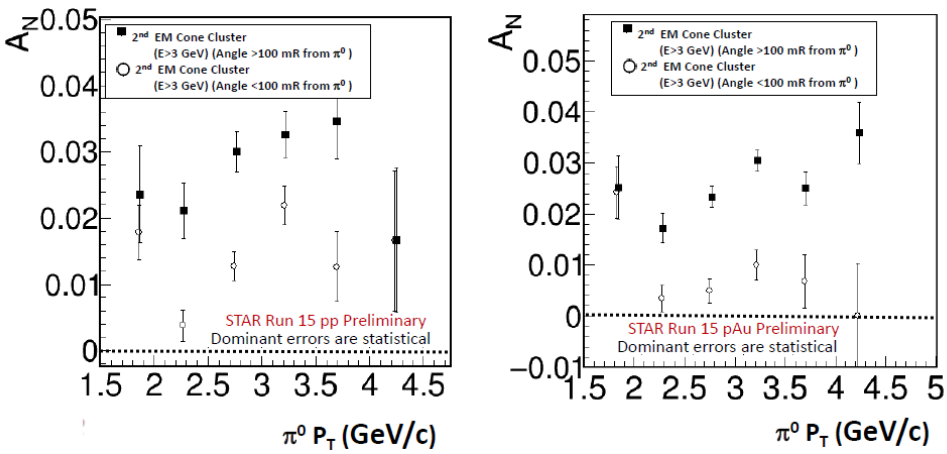

Figure 3: **This figure shows an enhancement of TSSA (A_N) for more isolated π^0 events in comparison to events with nearby fragments.** Transverse Momentum (P_T) dependence of π^0 A_N for events with an observed π^0 cluster and also a second cluster of EM energy (>3 GeV) within the FMS. This "two cluster" data set is from the 2015 pp and pAu STAR runs with nucleon-nucleon energy $\sqrt{s_{NN}}$=200 GeV. The π^0's were selected to have Feynman x_F in the range $0.25 < x_F < 0.35$. Open circles correspond to events where the second cluster is observed near the primary π^0, within an angle of 0.1 radians. The filled squares represent events with the direction of the second cluster at an angle of more than 0.1 radians from the π^0 direction. The left and right frames show this result for pp and pAu collisions, respectively.

for pp and pAu collisions from the RHIC 2015 data run. In Figure 3, we show that in the region $0.25 < x_F < 0.35$, the asymmetry is much reduced for events where a second cone is observed within 0.1 radians of the π^0 cone.

3 Conclusion

To summarize, STAR has made a preliminary analysis of data from 2015 comparing the TSSA of forward π^0 production in pp and pAu collisions. The general trend is that the asymmetry A_N for pAu collisions is nearly as large as that for pp collisions. For $x_F < 0.6$, the asymmetry generally rises with transverse momentum, up to transverse momentum as large as 7 GeV/c. As has been observed in pp measurements earlier, both pp and pAu measurements indicate that

the asymmetry is much larger for π^0 events that are produced in isolation than for events where the π^0 is observed with accompanying jet-like fragments. The scale of A_N asymmetries, the p_T dependence of asymmetries and finally the enhancement of A_N for events that are more isolated than for events that appear more jet-like are similar in pp and in pAu collisions.

References

[1] Steven Heppelmann (STAR), "Large p_T Forward Transverse Single Spin Asymmetries of $\pi 0$ Mesons at $\sqrt{s} = 200$ and 500 GeV from STAR," *PoS*, **DIS2013**(2013), 240.

[2] Mriganka Mouli Mondal (STAR), "Measurement of the Transverse Single-Spin Asymmetries for π^0 and Jet-like Events at Forward Rapidities at STAR in $p+p$ Collisions at $\sqrt{s}$ = 500 GeV," *PoS*, **DIS2014**(2014), 216, 1407.3715.

[3] Dennis W. Sivers, "Single Spin Production Asymmetries from the Hard Scattering of Point-Like Constituents," *Phys.Rev.*, **D41**(1990), 83.

[4] D. W. Sivers, "Hard scattering scaling laws for single spin production asymmetries," *Phys. Rev.*, **D43**(1991), 261.

[5] J. C. Collins, S. F. Heppelmann, and G. A. Ladinsky, "Measuring transversity densities in singly polarized hadron hadron and lepton - hadron collisions," *Nucl. Phys.*, **B420**(1994), 565, hep-ph/9305309.

[6] Alessandro Bacchetta, Cedran Bomhof, Umberto D'Alesio, P.J. Mulders, and F. Murgia, "The Sivers single-spin asymmetry in photon-jet production," *Phys.Rev.Lett.*, **99**(2007), 212002, hep-ph/0703153.

[7] M. Anselmino, *et al.*, "Sivers Effect for Pion and Kaon Production in Semi-Inclusive Deep Inelastic Scattering," *Eur.Phys.J.*, **A39**(2009), 89, 0805.2677.

[8] M.G. Alekseev *et al.* (COMPASS Collaboration), "Measurement of the Collins and Sivers asymmetries on transversely polarised protons," *Phys.Lett.*, **B692**(2010), 240, 1005.5609.

[9] Zhong-Bo Kang and Feng Yuan, "Single Spin Asymmetry Scaling in the Forward Rapidity Region at RHIC," *Phys. Rev.*, **D84**(2011), 034019, 1106.1375.

[10] J. Kiryluk (STAR), "Local polarimetry for proton beams with the STAR beam beam counters," in "Spin physics. Polarized electron sources and polarimeters. Proceedings, 16th International Symposium, SPIN 2004, Trieste, Italy, October 10-16, 2004, and Workshop, PESP 2004, Mainz, Germany, October 7-9, 2004," 718–721, 2005, hep-ex/0501072.

Multi-parton interactions in p-Pb collision at $\sqrt{s_{NN}}$ = 5.02 TeV with ALICE

C. Oppedisano for the ALICE Collaboration[1]

[1]INFN Sezione di Torino

1 Introduction

At LHC energies, the large number of initial hard parton-parton scatterings is a common feature of high-multiplicity pp and p-Pb collisions. In the Multi-Parton Interaction (MPI) model, high-multiplicity events in pp arise from low impact parameter collisions and statistical upward fluctuations of the number of MPI per event. Going from pp to p-A collisions, a larger number of MPI per event is accessible over an overlap reaction area similar to the one covered by the pp interaction. It is therefore crucial to understand MPI related effects in pp as a reference for p-A. While in A-A collisions the average number of initial parton-parton scatterings is largely determined by the collision centrality, in p-Pb collisions the proton-nucleon geometry becomes important [1].

In pp collisions, events characterized by a transverse momentum larger than average correspond to events where a multiplicity larger than average is measured [2]. Therefore selecting high p_T particles, more central collisions are selected. This observation must be properly taken into account especially when dealing with p-A collisions, where a selection based on multiplicity can bias the estimate of the number of hard scatterings per binary collision. Assuming that p-A collisions can be described as the independent superposition of pN collisions, the number of MPIs in p-A can be factorized as: $< n_{hard} >^{pA} = < N_{coll}^{MB} > \cdot < n_{hard} >^{pp}$. This implies that in general the scaling of particle yields from hard processes per binary collisions is unity when integrated over the whole centrality range but it can deviate from unity in centrality selected classes. In the following sections the centrality determination in p-A is discussed and results from jet-like two-particle correlations are presented.

2 Centrality in p-A collisions

Usually the Glauber model [3] is used to relate geometry quantities such as the impact parameter b, the number of participating nucleons N_{part} or the number of binary collisions N_{coll} to the experimental observables. A model to describe the observable distrbution is convoluted with Glauber in order to determine $< N_{part} >$, $< N_{coll} >$ values in classes of centrality selected from the observable distribution. The connection between the estimator and the geometry must be verified,

either comparing the calculations from a Glauber MC with experimental data for a known process or correlating observables from kinematic regions that are causally disconnected after the collision. In ALICE the centrality can be estimated by measuring the charged particle multiplicity at midrapidity (in the innermost silicon pixel layers of the Inner Tracking System, CL1 estimator) or at forward y (measuring the multiplicity in 2 scintillator odoscopes, V0A or V0C estimators). At very forward y the neutron Zero Degree Calorimeters (ZN) detect the energy carried by nucleons knocked out or emitted in de-excitation processes by the interacting nucleus. A detailed description of the centrality determination in ALICE can be found in [4]

2.1 Biases in centrality determination

In p-Pb collisions, the large relative fluctuations in particle multiplicity can induce a bias for a centrality estimator based on multiplicity. The bias can be quantified through the Glauber model convoluted with a Negative Binomial Distribution (NBD) to account for charged particle production. The left panel of Fig. 2.1, shows the ratio between the average multiplicity per participant and the average multiplicity from the NBD as a function of centrality. This ratio differs from unity over the whole centrality range, with large deviations for most central and most peripheral events. To study a baseline based on an incoherent and unconstrained superposition of nucleon-nucleon collisions, we coupled PYTHIA6 (Perugia 2011 tuning) [5] event generator to p-Pb Glauber MC calculation. For each N_{coll} value from the Glauber distribution, a corresponding number of independent PYTHIA pp events is summed (G-PYTHIA). In the right panel of fig. 3 the average number of hard scatterings per collision obatined from G-PYTHIA is plotted as a function of centrality. Deviation from the binary scaling are observed over the whole centrality range, with a behavior resembling the bias in multiplicity obtained from the Glauber MC.

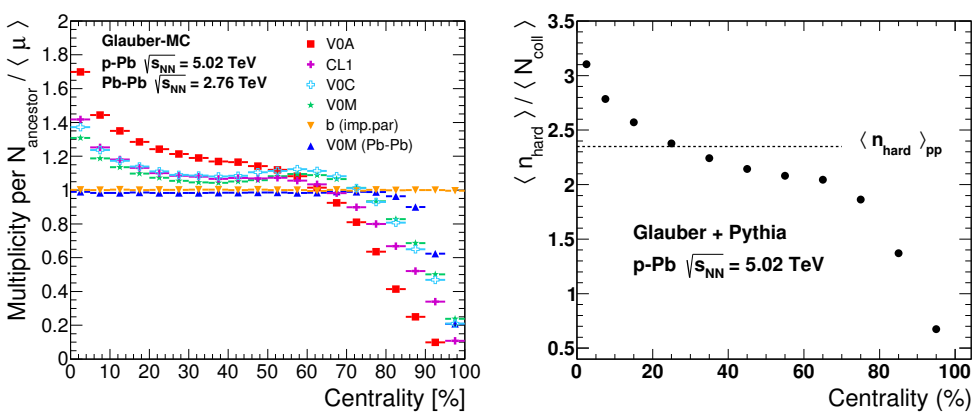

Figure 1: Left: multiplicity fluctuation bias calculated from NBD-Glauber MC as the ratio between mean multiplicity per ancestor and mean NBD multiplicity. Right: number of hard scatterings per N_{coll} as a function of centrality as calculated with GPYTHIA (see text).

A kinematic bias arises in events containing high p_T particles. These particles contribute to the overall event multiplicity and can thus introduce trivial auto-correlations between the centrality

estimator and the presence of a high p_T particle in the event.

Finally there is a purely geometrical, centrality estimator independent bias for peripheral p-Pb collisions. This is due to the fact that the mean impact parameter between two nucleons ($b_{\rm NN}$) is almost constant for central collisions, but rises significantly for peripheral interactions [6]. This reduces the average number of MPIs for most peripheral events, enhancing the effect of the bias leading to a nuclear modification factor less than (greater than) the one for peripheral (central) collisions.

In summary, these three sources of bias are expected to lead at high p_T to deviations from binary scaling both in peripheral and in central collisions. These expected deviations are present in the nuclear modification factor, that we denote as Q_{pPb} to remind that it is affected by biases due to the centrality selection. Therefore, as can be seen looking at Fig. 2.1, we have large deviations from unity when using particle multiplicity at midrapidity (CL1) as estimator. The bias is reduced increasing the rapidity gap between the estimator and the region where the tracks are measured. We assume therefore that the less biased estimator is the forward energy carried by nucleons detected by ZN. Then, based on experimental observations, we assume different scalings for particle production in different η regions and we determine the average N_{coll} values in each defined centrality class. With this approach the nuclear modification factors are compatible with unity over the whole centrality range.

3 Jet-like two-particle correlations

Two-particle angular correlations in azimuthal ($\Delta\phi$) and pseudo-rapidity ($\Delta\eta$) differences, after the subtraction of long range correlations, allow to study jet-like short range correlations [7]. These studies are of particular interest in this context since overlapping mini-jets are interpreted as due to MPIs. Therefore particle yields in the near side (NS, $\Delta\phi = 0$) and in the away side (AS, $\Delta\phi = \pi$) provide information about the fragmenting properties of the partons producing the jets. Another observable of interest is the number of uncorrelated seeds:

$$< N_{uncorrelated\ seeds} >= \frac{< N_{trigger} >}{< N_{correlated\ triggers} >} = \frac{< N_{trigger} >}{< N_{ass\ NS} > + < N_{ass\ AS} > +1} \qquad (1)$$

It provides the number of independent sources of particle production and contains information about the number of semi-hard scatterings in the events. PYTHIA predicts a strong correlation between the number of uncorrelated seeds and the number of MPIs.

The average number of associated particles in the NS and in the AS peaks in p-Pb collisions does not depend on centrality, implying that high multiplicity events are not built by a higher number of particles per trigger particle. The average number of uncorrelated seeds increases with multiplicity, indicating that the number of MPIs scales linearly with particle multiplicity (see Fig. 3). The same kind of analysis in pp collisions shows the onset of a saturation in the number of parton-parton scatterings. $< N_{uncorrelated\ seeds} >$ scales with the number of binary collisions at intermediate multiplicity. For most peripheral and most central collisions the multiplicity bias plays a role and deviations from the binary scaling are observed. An event selection based on ZN energy has a much flatter pattern as a function of centrality.

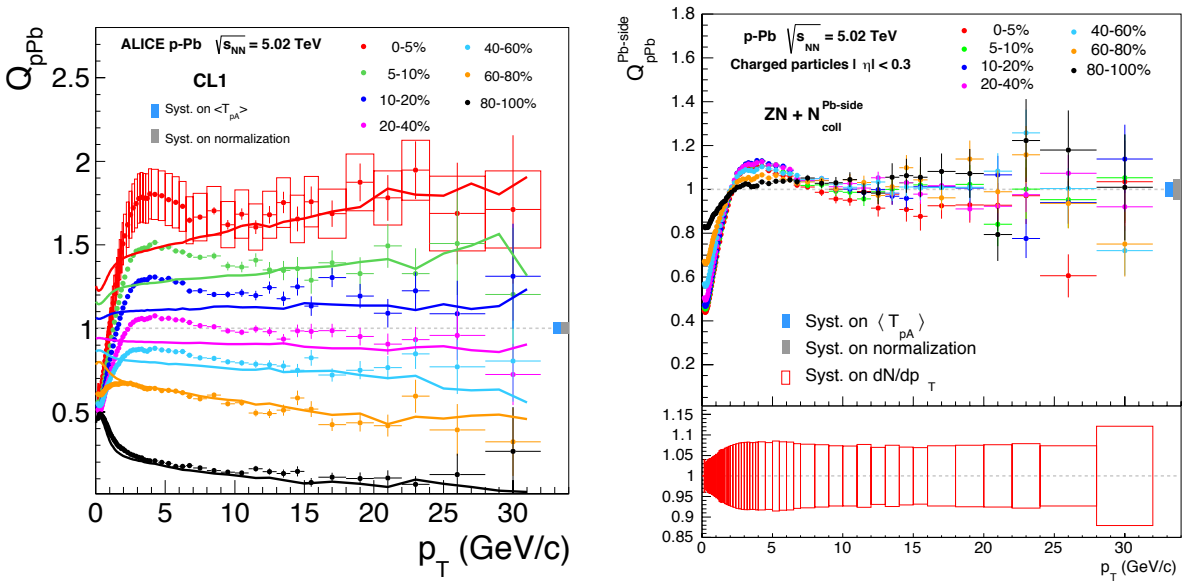

Figure 2: Left: Q_{pPb} based on CL1 estimator. Right: Q_{pPb} based on ZN event selection (see text for details).

4 Conclusions

The picture emerging from p-Pb collisions at $\sqrt{s_{NN}}$ = 5.02 TeV indicates that coherent effects are needed to explain some observations such as the rise of the average p_T as a function of centrality and the long range correlations. On the other hand, the per trigger yield in jet-like correlations are unmodified over a large centrality range, showing no coherence effects for MPIs. This finding is therefore consistent with a picture where independent parton-parton scatterings with consequent incoherent fragmentation produce the observed mini-jet yield. This imposes significant constraints on models which aim at describing p-Pb collisions.

References

[1] Andreas Morsch (ALICE), "Multiple Parton Interactions with ALICE: from pp to p-Pb," in "Proceedings, 30th Winter Workshop

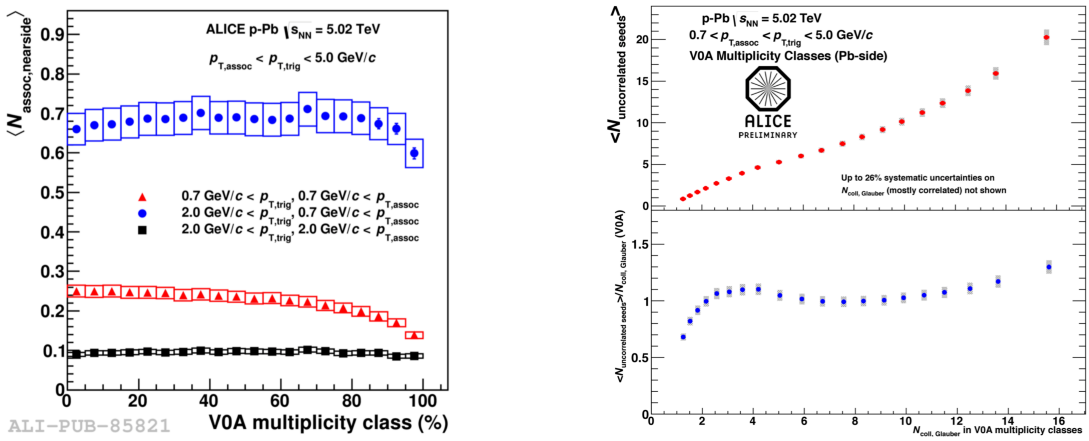

Figure 3: Left: Associate yield in the near side peak versus V0A multiplicity. Right: $< N_{uncorrelated\ seeds} >$ and $< N_{uncorrelated\ seeds} >$ per binary collision versus V0A multiplicity.

on Nuclear Dynamics (WWND 2014)," 2014, 1407.3628, URL http://inspirehep.net/record/1306293/files/arXiv:1407.3628.pdf.

[2] Jaroslav Adam *et al.* (ALICE), "Pseudorapidity and transverse-momentum distributions of charged particles in proton–proton collisions at $\sqrt{s} = 13$ TeV," *Phys. Lett.*, **B753**(2016), 319, 1509.08734.

[3] Michael L. Miller, Klaus Reygers, Stephen J. Sanders, and Peter Steinberg, "Glauber modeling in high energy nuclear collisions," *Ann. Rev. Nucl. Part. Sci.*, **57**(2007), 205, nucl-ex/0701025.

[4] Jaroslav Adam *et al.* (ALICE), "Centrality dependence of particle production in p-Pb collisions at $\sqrt{s_{\rm NN}}$= 5.02 TeV," *Phys. Rev.*, **C91**(2015) (6), 064905, 1412.6828.

[5] Peter Zeiler Skands, "Tuning Monte Carlo Generators: The Perugia Tunes," *Phys. Rev.*, **D82**(2010), 074018, 1005.3457.

[6] Jiangyong Jia, "Influence of the nucleon–nucleon collision geometry on the determination of the nuclear modification factor for nucleon–nucleus and nucleus–nucleus collisions," *Physics Letters B*, **681**(2009) (4), 320 , URL http://www.sciencedirect.com/science/article/pii/S0370269309012283.

[7] Betty Bezverkhny Abelev *et al.* (ALICE), "Multiplicity dependence of jet-like two-particle correlation structures in p–Pb collisions at $\sqrt{s_{NN}}$=5.02 TeV," *Phys. Lett.*, **B741**(2015), 38, 1406.5463.

Two Component model for hadroproduction in high energy collisions.

Alexander Bylinkin[1]

[1]Moscow Institute of Physics and Technology (MIPT), Moscow, Russia

1 Introduction

Recently a qualitative model considering two sources of hadroproduction has been introduced [1]. It was suggested to parametrize charged particle spectra by a sum of an exponential (Boltzmann-like) and a power-law p_T distributions:

$$\frac{d^2\sigma}{d\eta dp_T^2} = A_e \exp\left(-E_{Tkin}/T_e\right) + \frac{A}{(1+\frac{p_T^2}{T^2 \cdot N})^N}, \tag{1}$$

where $E_{Tkin} = \sqrt{p_T^2 + M^2} - M$ with M equal to the produced hadron mass. A_e, A, T_e, T, N are free parameters to be determined by a fit to the data. The detailed arguments for this particular choice are given in [1]. The exponential term in this model is associated with thermalized production of hadrons by valence quarks and a quark-gluon cloud coupled to them. The power-law term is related to the mini-jet fragmentation of the virtual partons (pomerons in pQCD) exchanged between two colliding partonic systems.

A typical charged particle spectrum as a function of transverse momentum fitted with this function (1) is shown in figure 1. As one can see, the exponential term dominates the particle spectrum at low p_T values.

Separating "soft" and "hard" contributions with this model allowed to calculate the predictions on the mean $< p_T >$ values as a function of multiplicity in a collision [2] and pseudorapidity distributions of charged particles. However, the major interest of many studies in QCD is the transverse momentum spectrum itself. Therefore, in this article it is discussed how its shape varies in different experiments under various conditions. In [1] it was shown that the parameters of the fit (1) show a strong dependence on the collision energy. Unfortunately, due to the fact that different collaborations measure charged particle production in their own phase space and under various experimental configurations, the dependences observed in [1] were smeared and did not allow to make strong predictions for further measurements. Thus, an approach to correct the measurements in order to allow an accurate combination of different experimental data is proposed here.

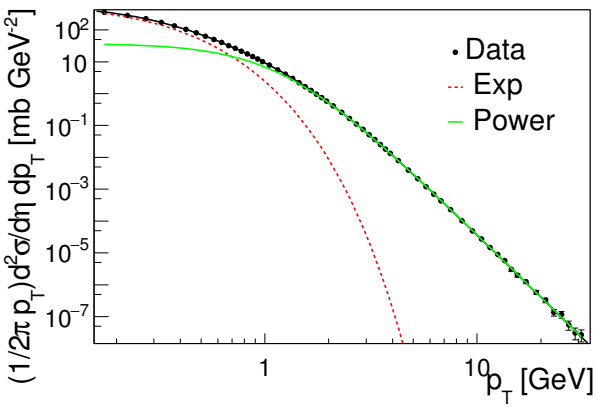

Figure 1: Charge particle differential cross section: the red (dashed) line shows the exponential term and the green (solid) line shows the power law term.

2 Parameter variations

In [3] it was shown that two sources of hadroproduction described above contribute to different pseudorapidity regions: while the power-law term of (1) prevails in the central rapidity region ($|\eta| \lesssim O(1)$), the exponential term dominates at high values of η. Since each collaboration presents measurements on transverse momentum spectra in various pseudorapidity intervals, these variations might explain the smearing of the dependences in [1]. The idea to study parameter variations as a function of both collision energy and pseudorapidity region has already been successfully tested in [4].

Let us now plot the parameter variations as a function of the rapidity interval between the incoming proton and the produced secondary hadron in the moving proton rest frame according to a simple formula:

$$\eta' = |\eta| - log(\sqrt{s}/2m_p), \;\; \eta'' = |\eta| + log(\sqrt{s}/2m_p), \tag{2}$$

where m_p is the mass of the incoming proton. The results of this procedure are shown in figure 2. Surprisingly, all the points came to a single line in this interpretation. To understand the origin of this universality one might use Monte Carlo(MC) generators: hard processes at large p_T are known to be described by MC generators pretty well, thus it is expected to get the value of the N-parameter from the fits of the MC-generated spectra rather close to the real data, but with a higher accuracy and in a wider collision energy range. To check this universality, we have produced the Monte Carlo samples for proton-proton collisions at different energies for inelastic(INEL) events with the PYTHIA 8.2 generator. Indeed, the values of the parameter N extracted from the fits to the MC-generated spectra are nicely placed at the same line. Thus, a universal parameter describing the shape of the transverse momentum spectra in pp-collisions has been found.

Remarkably, similarly to N, the T and T_e also show dependences as a function of both the collisions energy $\sqrt{s}$ and the measured pseudorapidity interval η. The variations of the T and T_e parameters were studied in [4]. The dependences are shown on figure 2 as well.

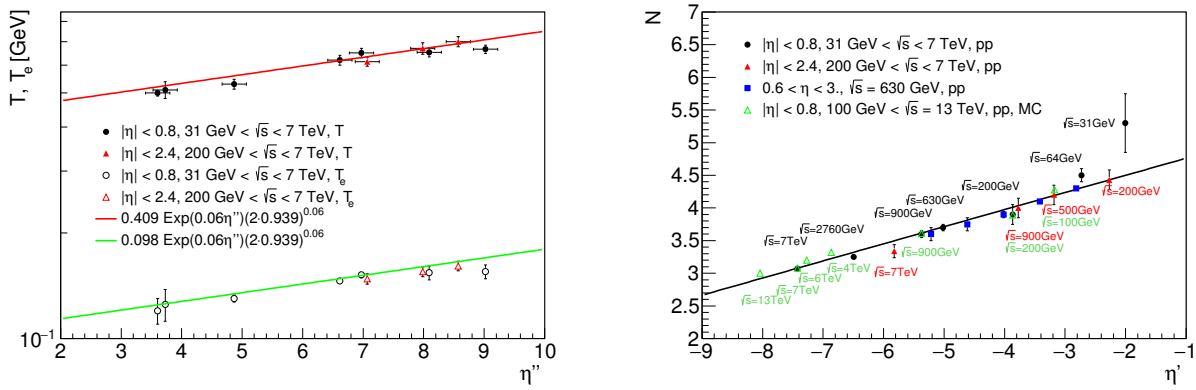

Figure 2: The dependence of the parameters on the pseudorapidity interval between the secondary hadron and the incoming proton.

3 Prediction for further measurements

Using the parameter dependences [5] extracted from figure 2, one can calculate double differential cross sections $d^2\sigma/(d\eta dp_T^2)$ of charged particle production in high energy collisions at different energies for NSD events. These predictions are shown in figure 3 for $|\eta| < 0.8$ and $|\eta| < 2.4$ pseudorapidity intervals together with the experimental data measured by CMS [6] and ALICE [7]. A good agreement of the prediction with the data can be observed. Thus, these results give us a powerful tool for predicting the spectral shapes in NSD events.

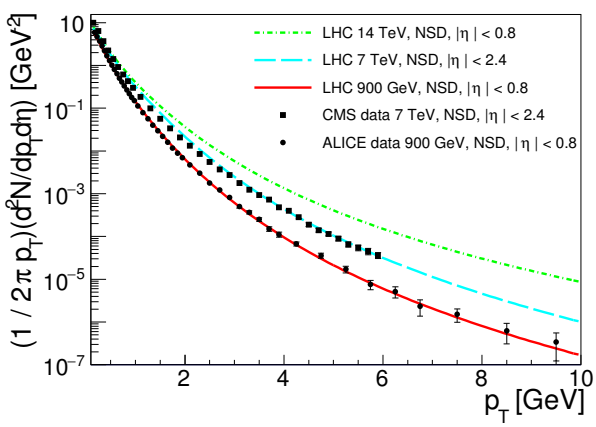

Figure 3: Predictions of the yield of charged particles $(1/2\pi p_T)d^2N/(d\eta dp_T)$ in high energy collisions in NSD events together with data points from the ALICE and CMS experiments.

4 Conclusion

In conclusion, transverse momentum spectra in pp-collisions have been considered using a two component model. Variations of the parameters obtained from the fit have been studied as a function of pseudorapidity η and c.m.s. energy $\sqrt{s}$ in the collision. A universal parameter describing a shape of the spectra in pp-collisions was found to be a preudorapidity of a secondary hadron in the moving proton rest frame. Finally, the observed dependences, together with previous investigations allowed to make predictions on double differential spectra $d^2\sigma/(dp_T^2 d\eta)$ at higher energies, successfully tested on the available experimental data.

References

[1] A. A. Bylinkin and A. A. Rostovtsev, Phys. Atom. Nucl. **75** (2012) 999 Yad. Fiz. **75** (2012) 1060; A. A. Bylinkin and A. A. Rostovtsev, arXiv:1008.0332 [hep-ph].

[2] A. A. Bylinkin, M. G. Ryskin, Phys. Rev. D **90** (2014) 1, 017501 [arXiv:1404.4739 [hep-ph]].

[3] A. A. Bylinkin and A. A. Rostovtsev, Nucl. Phys. B **888** (2014) 65 [arXiv:1404.7302 [hep-ph]].

[4] A. A. Bylinkin, D. E. Kharzeev and A. A. Rostovtsev, Int. J. Mod. Phys. E **23** (2014) 12, 1450083.

[5] A. Bylinkin, N. S. Chernyavskaya and A. A. Rostovtsev, Eur. Phys. J. C **75** (2015) 4, 166 doi:10.1140/epjc/s10052-015-3392-y

[6] V. Khachatryan *et al.* [CMS Collaboration], Phys. Rev. Lett. **105** (2010) 022002 [arXiv:1005.3299 [hep-ex]].

[7] K. Aamodt *et al.* [ALICE Collaboration], Phys. Lett. B **693** (2010) 53-68 [arXiv:1007.0719 [hep-ex]].

Leading particle spectra as a tool to tune the color reconnection models

E. Cuautle, S. Iga and G. Paić

Instituto de Ciencias Nucleares, Universidad Nacional Autónoma de México Apartado Postal 70-543, Ciudad de México 04510, México.

Abstract

Kinematic variables like average transverse momenta and multiplicity distributions in pp interactions at the LHC energies have been successfully described by phenomenological models which include color reconnection as part of the hadronisation processes. In the present work the transverse momentum distribution of the leading particles produced in pp interaction, are investigated using the PYTHIA 8 event generator with different color reconnection modes. The effect of the different modes is reported in function of the multiplicity of the events.

1 Introduction

A considerable amount of work has been dedicated by several groups, in the implementation of interactions among partons in the initial and final state, following the general idea of QCD. The color fields are modeled by strings interacting in the final state before hadronisation. Among them the color reconnection (CR) hadronisation mechanism has allowed to fit simultaneously the multiplicity and the p_t distributions in pp collisions. The attractive of the models implying multiparton interactions and color reconnection is that they consider plausible QCD mechanisms. In recent publications [1–4] the effects of the CR in producing flow-like effects in pp collisions has been investigated. The similarity with the predictions of hydrodynamics is striking and it would be very interesting to decide which approach is favored by nature. It was pointed out in Ref. [5] that it will be an important task for future experimental and phenomenological studies to find ways of disentangling color reconnection effects from hydrodynamics ones.

A key element in comparing color reconnection with hydrodynamics results might be to study the results for the two approaches in function of the transverse momentum range. Namely, the boost effect of the radial flow on transverse momentum diminishes at larger p_t values, getting rather small above p_t larges that 3 GeV/c. In the color reconnection modes, on the other hand, it is the probability to reconnect strings that gets smaller at higher transverse momenta.

Following the general idea exposed in [6,7] a Multiple Parton Interaction (MPI) system with a scale p_t of the hard interaction (normally happens in $2 \to 2$ QCD processes) can be merged with one of a harder scale with a probability that is $(R_{rec}P_{T0})^2/((R_{rec}P_{T0})^2 + P_T^2)$, where R_{rec} is the

color reconnection range and P_{T0} is the phase space cut of processes. The latter being the same energy-dependent dampening parameter as used for $MPI's$. Thus it is easy to merge a low-p_t system with any other, but difficult to merge two high-p_t ones with each other. However, for relatively hard transverse momenta of $\approx 10\ GeV/c$ the probability is still sizable so that we decided to investigate the behavior of the spectra at transverse momenta higher than the range where hydrodynamics and CR coincide in the qualitative description.
Our special interest is to see the effect of color reconnection at relatively high p_t values where we expect little influence of hydrodynamics. To see this effect we have chosen to study the leading particles in each event. By leading we mean the highest detected charged particle in the acceptance, for each event. We have studied the two cases of color reconnection: mode 0 - the original PYTHIA recipe, where the gluons of a lower-p_t MPI system are merged with the ones in a higher-p_t MPI; mode 1 - new scheme, where the gluons of a lower-p_t MPI system are merged with the ones in a higher-p_t. In both cases of color reconnection the QCD color rules are incorporated, and determine the probability that a reconnection is allowed.

2 Results and discussion

We have generated 100 million events for each CR mode, and for the no CR case for pp collisions at 7 TeV. Only the charged particles were taken into account excluding the weak decays, in a pseudorapidity interval of $|\eta| < 0.8$. All the PYTHIA parameters were set to the default values.

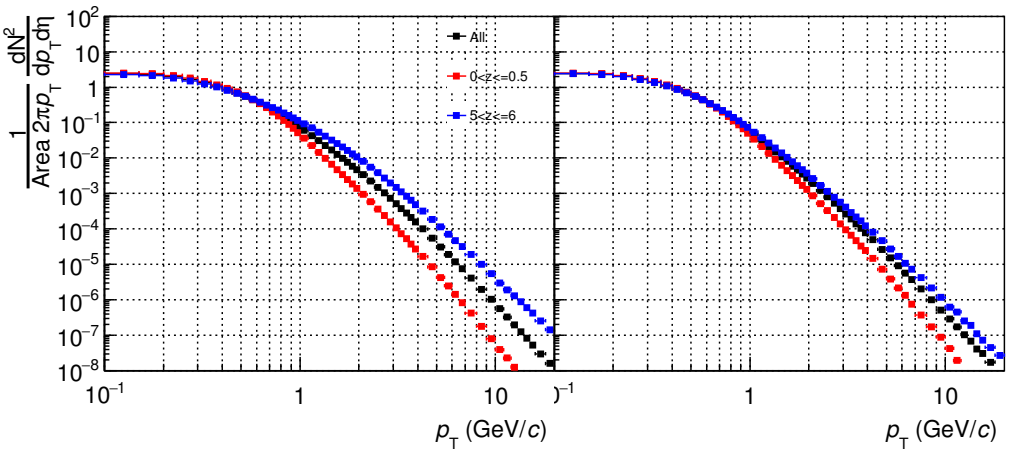

Figure 1: (Color online). Transverse momentum spectra for different multiplicities with CR mode 1 (left), and without CR (right)

In figure 1 we show the generated transverse momentum spectra obtained with CR mode 1 (left)

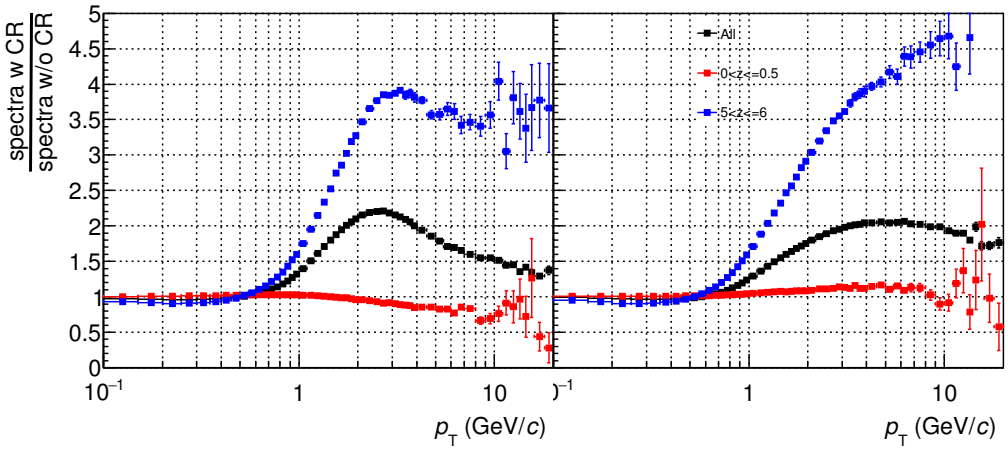

Figure 2: (Color online). Left panel: the ratio of the inclusive spectra with CR mode 1 to the spectra without CR. On the right one: the ratio for the case of the CR mode 0, as described in the text.

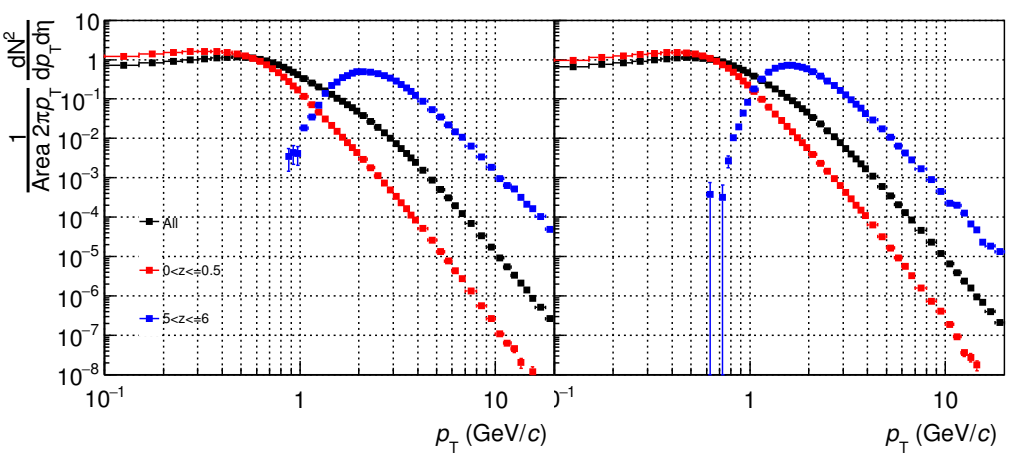

Figure 3: (Color online). Transverse momentum spectra of leading pions for three multiplicity ranges with (left) and without (right) CR mode 1.

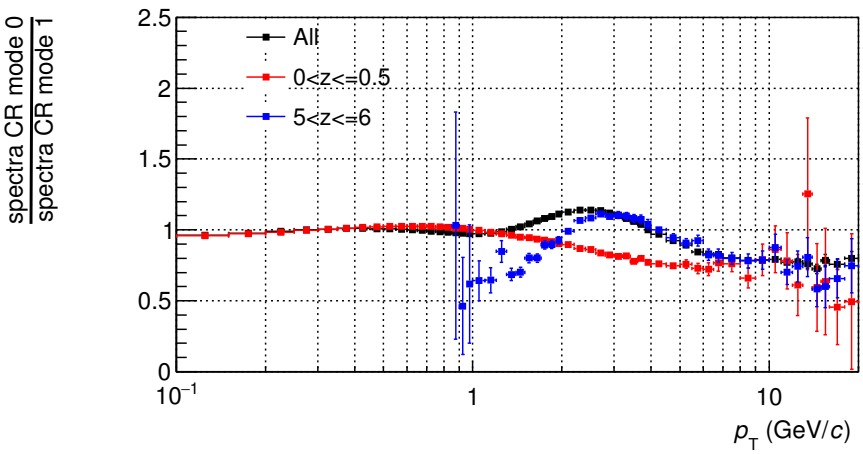

Figure 4: (Color online). Ratio of the leading particle p_t spectra for the case of CR mode 0 to the same spectra generated with mode 1.

and without CR (right) for the case of minimum bias events, and for two multiplicity ranges, defined in terms of the parameter $z = N_{ch}/ < N_{ch} >$: $0.0 < z < 0.5$ and $5 < z < 6$, which means low and high multiplicity events. Those distributions clearly show the p_t dependence with the multiplicity. We observe harder spectra when CR is included with respect to those without CR ones.

In Fig2, the ratio of the inclusive spectra with and without CR are shown for the same z bins as in the Fig.1. The left panel corresponds to the case CR mode 0, while the right side is for CR mode 1. From figure 2, we see that the spectra ratios show a very important dependence with the multiplicity, predominantly at high momenta, but significant differences are also observed for the CR modes used, especially, at high momenta. It is important to note that the effect of CR gets much more important at higher multiplicities which indicates that the lowest multiplicity range has a behavior very similar to no CR and could therefore be used for reference in the analysis of CR effects in experimental data.

In Fig. 3, we show the spectra for the leading pions, simulated in the same multiplicity ranges as in Figs. 1 and 2 for the CR mode 1(left) and without CR (right). It is visible that the peak of the high multiplicity distribution is shifted towards higher multiplicities by almost 1 GeV/c! Essentially the same behavior is observed for protons and other identified particles.

In the Fig. 4, we show the ratio of the leading particle spectra for the cases of CR mode 0 to the same spectra generated with CR mode 1. One observes that the high multiplicity events present the largest differences between the two modes.

In conclusion, we see that the color reconnection mechanisms have a very marked incidence on

transverse momentum spectra at high p_t. We have also demonstrated that the lowest multiplicity bins yields results very similar to the case with no color reconnection so that it may be used in experimental analysis to extract the ratios at high multiplicities instead of the no CR option used in this work. The ratio of the lowest multiplicity bin corresponding to events with less than half the mean multiplicity to the highest multiplicities renders possible an experimental check of the importance of color reconnection and a method to tune it. It is shown that different CR modes do produce slight differences among them, most significantly at highest p_t values, indicating possible studies on pQCD of this effects. A comparison with other hydrodynamics based generators like EPOS will allow an interesting comparison which could be composed to experimental data.

Acknowledgments

The authors acknowledge discussions with A. Ortiz. Support for this work has been received from CONACYT under the grant No. 270067; from DGAPA-UNAM under PAPIIT grants IN108414.

References

[1] Antonio Ortiz Velasquez, Peter Christiansen, Eleazar Cuautle Flores, Ivonne Maldonado Cervantes, and Guy Paić, "Color Reconnection and Flowlike Patterns in pp Collisions," *Phys. Rev. Lett.*, **111**(2013) (4), 042001.

[2] Eleazar Cuautle, Raúl Jiménez, Ivonne Maldonado, Antonio Ortiz, and Guy Paić, "Disentangling the soft and hard components of the pp collisions using the sphero(i)city approach," (2014), arXiv:1404.2372[hep-ph].

[3] Eleazar Cuautle, Antonio Ortiz, and Guy Paić, "Effects produced by multi-parton interactions and color reconnection in small systems ," (2015), arXiv:1512.09011[hep-ph].

[4] Eleazar Cuautle, Antonio Ortiz, and Guy Paić, "Mid-rapidity charged hadrons transverse spherocity in pp collisions simulated with PYTHIA ," *Nucl. Phys. A*, **941**(2015), 78, arXiv:1503.03129[hep-ph].

[5] Jesper. R. Christiansen and Peter Z. Skands, "String formation beyond leading colour," *JHEP*, **1508**(2015), 003.

[6] Torbjörn Sjöstrand, Stephen Mrenna, and Peter Skands, "A brief introduction to PYTHIA 8.1," *Comput. Phys. Commun.*, **178**(2008), 852.

[7] Torbjörn Sjöstrand, Stephen Mrenna, and Peter Skands, "PYTHIA 6.4 Physics and Manual," *JHEP*, **2005**(2006), 026.

Final State Hadrons in DIS.

B.Blok[1]

[1]Physics Department, Technion, Haifa 32000 Israel

The structure of final hadronic states in deep inelastic scattering (DIS) is important both from the point of view of deeper understanding of hadron structure, and for the understanding of ideas of coherence and angular ordering that play the crucial role in physics of lHC. Although there is a number of MC generators that describe the final hadronic states in DIS [1–4], it is of great interest to understand the structure of these states analytically, based on ideas of coherence and angular ordering. This is especially important since MC generators include fitting parameters, and the corresponding parametrisations may cover up new physical mechanisms. The MC approach is essentially classical and may miss important interference and correlation effects. In addition,such analysis may lead to better understanding of initial state radiation and underlying event (UE) in pp collisions at LHC.

The analytical picture of final hadronic states, based on DGLAP picture of DIS at small x , was developed in [5]. (For other studies, based on CCFM and BFKL pictures, see e.g. [6]). The authors of [5] considered however only the distribution of final states in energy of produced hadrons. Recently [7] a new data on distribution of final states in pseudorapidity in DIS at HERA had appeared. At the moment the data covers the entire current fragmentation region, and the recent measurements also touch the target fragmentation region, where the gluonic part of the ladder dominates. The purpose of the current letter is to apply the model [5] of final states in DIS to their distribution in pseudorapidity. We shall derive the distribution of final hadrons in pseudorapidity in the [5] framework, and compare this distribution to recent experimental measurements. Note that coherence and angular ordering are realised in ISR in a different way than in jets, and thus its study will shed additional light on color coherence effects in pQCD.

In this letter we shall calculate the soft gluon radiation in DIS and connect it to hadron final states via the concept of local parton hadron duality (LPHD) [8]. We shall calculate the pseudorapidity distribution of final hadrons $dN/d\eta$, and then compare it to experimental data, after averaging according to the corresponding experimental bins. We see good qualitative agreement with the experimental data. Quantitatively there is good agreement in the current fragmentation region in Breit frame $-\log(Q/\Lambda) < \eta < \log(Q/\Lambda)$, while the agreement sseems to worsen beyond this region. The possible reasons-rather low Q used for "penetration" in this properly target fragmentation region in HERA, inaccuracies in transition from c.m. to Breit frame for soft hadrons with $p_t \sim m$, m being their mass, or noneperturbative effects, are discussed below.

It was demonstrated in [5] that the DIS final state radiation originates from three basic contributions, each working in a different part of the phase space. For simplicity we shall work here in the Breit reference frame.

First contribution is due to the radiation from the ejected quark (current fragmentation), combined with the radiation from the virtual quark-antiquark pair. It was shown in ref. [5] that,due to color interference, in the Breit frame radiation from quarks is the same as for two quark-antiquark jets created in e^+e^- annihilation in their c.m.s. reference frame.

The second piece is the radiation and subsequent fragmentation of soft gluons with energies $l < Q$, where $-Q^2$ is the virtual photon virtuality, coming from the gluonic part of the ladder. The third part is the sum of structural and so called anomalous contributions. The structural contribution is the contribution from horizontal rungs of the ladder (see Fig. 1), while the anomalous is the radiation from the t-channel exchange gluons.

$$\frac{dN}{d\eta} = \frac{dN_1}{d\eta} + \frac{dN_2}{d\eta} + \frac{dN_3}{d\eta} \tag{1}$$

Consider first the current fragmentation region. In this region the multiplicity is described by a contribution of quark -antiquark dijet in its center of mass frame.

For the multiplicity inside the polar angle θ we shall use $N(Y_\theta = \log(2Q\sin(\theta/2)/Q_0)$, where N is the jet multiplicity in MLLA approximation, see ref. [9] for explicit expression in terms of modified Bessel functions. In actual curves we use distributions in pseudorapidity $\eta = -\log(\tan(\theta/2))$ so the rapidity distribution in the current fragmentation region is $dN(Y_{\theta(\eta)})/d\eta + dN(Y_{\theta(-\eta)})/d\eta$.

In the case of DIS energy of each jet is Q/2, so full multiplicity due to current fragmentation region is $2N(Q)$, while for pseudorapidity distribution we have:

$$\frac{dN_1}{d\eta} = (\frac{dN(Log(Q \times \sin(\theta(\eta)/2)}{dy} + \frac{dN(Log(Q/2 \times \sin(\theta(-\eta)/2)}{dy}) \cdot \frac{C_F}{N_c}. \tag{2}$$

where the connection between polar angle θ and pseudorapidity η is given by **??**.

The next contribution is due to the soft gluon radiation from inside ladder. Note that due to the color coherence the angle of radiation of soft gluon "l" (Fig.1) relative to beam axis is smaller than the quark angle i.e. this radiation is inside the quark cone:$Q > k_t, k_t > Q\sin(\theta)$, so we can obtain with double logarithmic accuracy

$$\frac{dN_2}{d\eta} = \frac{dN(Q\sin(\theta(\eta))}{d\eta} \frac{D_Q^h(x,Q) - D_Q^h(x, Q\sin(\theta(\eta))}{D_Q^h(x,Q)} \tag{3}$$

where $D_Q^h(x,Q)$ is the quark PDF. Note that gluon energy $l < Q$ both for first and second radiation types.

The third contribution is the structural and anomalous contributions, where by structural contribution we mean radiation from the ladder rungs, and anomalous is due to t-channel exchange

gluons. It is concentrated in the target fragmentation region.

$$\frac{dN_3}{d\eta} = \int_0^{\xi_Q} d\xi \int_Q^{kt/\theta} \frac{dl}{l} \frac{\alpha_s(l^2\theta^2)}{4\pi}$$

$$\times \quad D_h^q(l/P, k_t^2/Q_0^2) \frac{d^2 D_G^q(Q/l, Q^2/k_t^2)}{d^2\xi(Q^2, k_t^2)} N_g(l\sin(\theta)/Q_0)/(1+\exp(-y)) \tag{4}$$

This contribution includes fragmenting gluons with energy $P > l > Q$ and radiation in the cone or on larger angles than the angle of the radiated hard DGLAP gluon. Here $x = Q/(2P)$. While carrying the differentiation we use the approximate relation

$$\frac{dD_G^F(x,\xi)}{d\xi} = 2/3 D_G^G(x,\xi) \tag{5}$$

and next differentiate the DGLAP kernel D_G^G numerically. Note that this contribution is important only for sufficiently large rapidities, where we can use approximation $sin(\theta) \sim \theta$ without numerically influencing the results.

In our numerical calculations we take Λ_{QCD}=0.320 MeV, and use the limiting spectrum approximation, i.e. for soft partons the transverse cut off is $Q_0 = \Lambda_{QCD}$. This is the best fit from the analysis of LEP data on total quark jet multiplicities in MLLA [10]. Note that this is the value of Λ in the so called MC (Monte Carlo) scheme.

tIn structure functions G we use the GRV regularization scheme [12] which is actually a MC scheme with $\Lambda_{QCD} = 0.23$ GeV. The ratios of these two Λ obtained from best fit is 1.4 and is very close to the one obtained theoretically [11].

The comparison with experimental H1 data [7] is complicated by three considerations: first, the approach is strictly speaking, justified at $\alpha_s Log(1/x), \alpha_s \log(Q^2/\mu^2) \leq 1$, and these conditions are not fulfilled in the significant part of the bins. Second the experimental data is given in in c.m. reference frame, while theoretical calculations are performed in the Breit system, and the shift by $\log(1/x)/2$ is rather rude approximation, especially for massive particles. Third, the experimental data is presented after averaging in rather large bins, in Q^2, y, x. Nevertheless we have at Fig.2 qualitative agreement with HERA data, although further work must be done to make detailed comparison.

Consider first the transition from the Breit to c.m.s. system and vice versa. It is easy to see that nucleon momenta in Laboratory, Breit and c.m.s. systems are related as

$$P = (M, \vec{0}), (\frac{Q}{2\sqrt{x}}, \vec{0}, -\frac{Q}{2\sqrt{x}}), (\frac{Q}{2x}, \vec{0}, -\frac{Q}{2x}). \tag{6}$$

Hence the rapidity difference between the Breit and c.m. frame is

$$\Delta\eta = 1/2 \log(1/x) \tag{7}$$

for$x \sim 10^{-3}$ this rapidity difference is of order 3.4, i.e. the H1 data must be shifted by ~ 3.4 units. (and positive and negative directions interchanged).

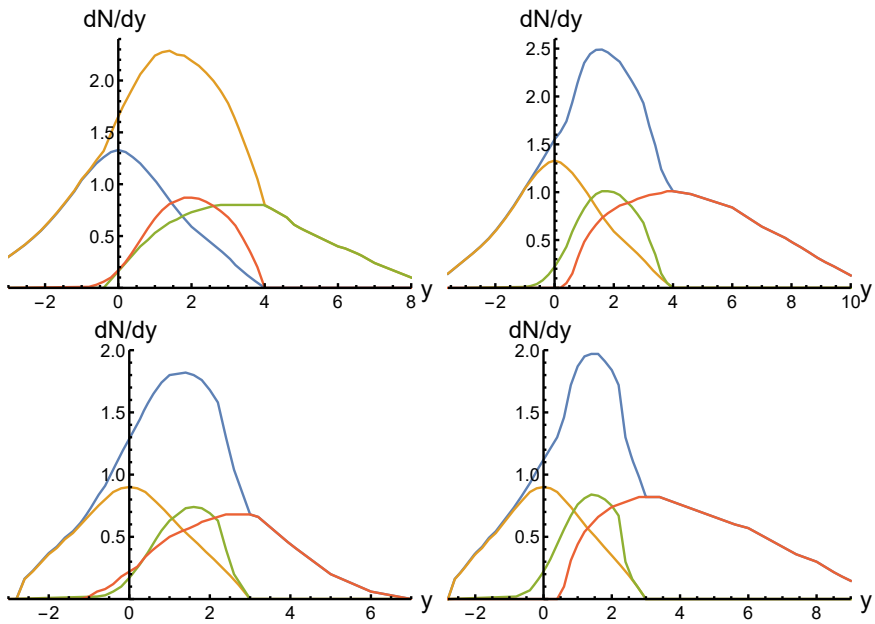

Figure 1: The pseudorapidity distribution of final hadronic states in DIS. Q=10 GeV, x=0.001 and x=0.0001, and Q=4.5 GeV, x=0.001,x=0.0001 (below). Here and in 3 subsequent pictures the four curves in the figure correspond to total, current (left), soft(middle) and structural plus anomalous (right) contributions to multiplicity. Note that here and in the following 3 pictures the graphs are in Breit frame the target fragmentation region corresponds to positive pseudorapidities.

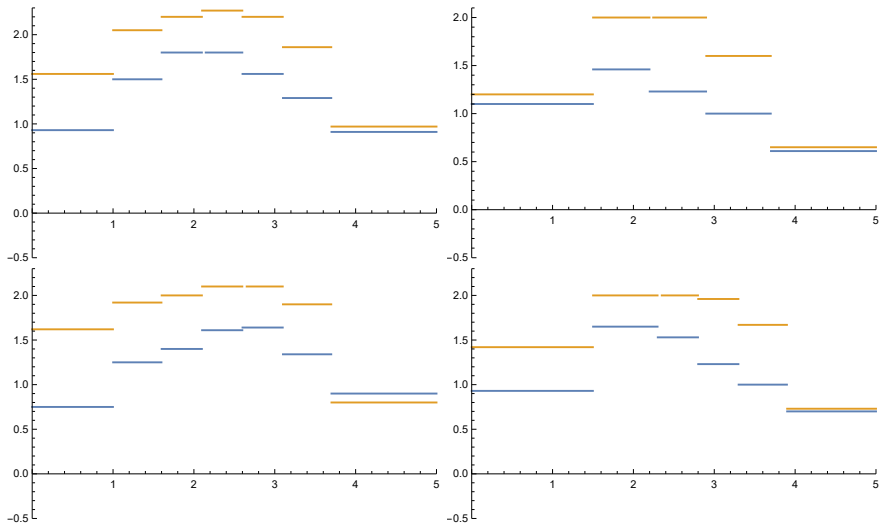

Figure 2: The averaged over bins pseudorapidity distribution $d\bar{N}/d\eta$: $20 < Q^2 < 100$ GeV^2,$0.0004 < x < 0.0017$ and and bin $10 < Q^2 < 20$ GeV^2,$0.0002 < x < 0.00052$,$0.00052 < x < 0.0017$. experiment versus pQCD. Note that the pictures are in c.m. frame of and the target fragmentation corresponds to negative values of pseudorapidities-opposite to Fig 1.

The average over bins is carried with the help of

$$\frac{d\bar{N}}{d\eta} = \frac{\int dxdQ^2dy\frac{d\sigma_{DIS}}{dxdQ^2}\frac{dN}{d\eta}(-\eta + \log(1/x)/2)}{\int dxdQ^2dy\frac{d\sigma_{DIS}}{dxdQ^2}} \tag{8}$$

where the limits of integration are determined by the bin boundaries. The deep inelastic cross section σ_{DIS} is given by

$$\frac{d\sigma_{DIS}}{dxdQ^2} = \frac{4\pi\alpha^2}{Q^4}((1+(1-y)^2)F_1 + (1-y)(F_2 - 2xF_1)/x) \tag{9}$$

and with current accuracy we use $F_2 = 2xF_1$, $F_2(x,Q^2(,F_!(x,Q^2)$ are standard electromagnetic structure functions, and $y = Q^2/(xs)$, where s is the invariant squared center of mass energy $s = 4 * 28 * 800$ GeV^2 for HERA. For F_2 we can use

$$F_2 = \frac{4}{9}x(u(x) + \bar{u}(x)) + \frac{1}{9}(d(x) + \bar{d}(x)) \tag{10}$$

where $u(x), d(x)$ are quark PDFs in nucleon [12]. The corresponding bins are detected in Fig. 2

Acknowledgements

This talk is based on joint work with M. Strikman and Yu. Dokshitzer (in preparation).

References

[1] S. Gieseke et al., Herwig++ 2.5, [arXiv:1102.1672].

[2] H. Jung, RAPGAP 3.1, Comput. Phys. Commun 86 (1995) 147.

[3] K. Charchula, G. A. Schuler and H. Spiesberger, DJANGOH 1.4, Comput. Phys. Commun. 81 (1994) 381.

[4] H. Jung, Comput. Phys. Commun. 143 (2002) 100; H. Jung et al., CASCADE 2.2.0, Eur. Phys. J. C70 (2010) 1237.

[5] L. V. Gribov, Y. L. Dokshitzer, S. I. Troian and V. A. Khoze, Sov. Phys. JETP **67** (1988) 1303 [Zh. Eksp. Teor. Fiz. **94** (1988) 12].

[6] H. Jung and G. P. Salam, Eur. Phys. J. C **19** (2001) 351 doi:10.1007/s100520100604 [hep-ph/0012143].

[7] C. Alexa *et al.* [H1 Collaboration], Eur. Phys. J. C **73** (2013) 4, 2406 [arXiv:1302.1321 [hep-ex]].

[8] Y. I. Azimov, Y. L. Dokshitzer, V. A. Khoze and S. I. Troyan, Z. Phys. C **27** (1985) 65.

[9] Y. L. Dokshitzer, V. A. Khoze, A. H. Mueller and S. I. Troian, "Basics of perturbative QCD," Gif-sur-Yvette, France: Ed. Frontieres (1991) 274 p.

[10] P. Abreu *et al.* [DELPHI Collaboration], Phys. Lett. B **449** (1999) 383. [hep-ex/9903073].

[11] S. Catani, B. R. Webber and G. Marchesini, Nucl. Phys. B **349** (1991) 635.

[12] M. Gluck, E. Reya and A. Vogt, Z. Phys. C **53** (1992) 127.